MESOSCALE BOUNDARIES AND STORM DEVELOPMENT IN SOUTHWESTERN ONTARIO DURING ELBOW 2001

LISA SUSAN ALEXANDER

A dissertation submitted to the Faculty of Graduate Studies
in partial fulfillment of the requirements
for the degree of

DOCTOR OF PHILOSOPHY

Graduate Programme in Earth and Space Science
York University
Toronto, Ontario

October 2012

© Lisa Susan Alexander, 2012

Abstract

The Effects of Lake Breezes on Weather (ELBOW) 2001 project was conducted in Southwestern Ontario, during summer 2001. Project goals included: understanding how lake breezes interact with one another, other mesoscale boundaries and synoptic fronts, understanding how lake breezes affect storm development, and helping to improve regional forecasts by transferring findings to forecasters.

Radar, Satellite, Mesonet and Integrated (considering all data sets) analyses were each used to identify the mesoscale boundaries that occurred during the study period. A contingency table approach, for lake breeze occurrence, was used to evaluate each of the analyses against a Final ‘Truth' Set. Findings showed that the Integrated analysis performed the best. Advantages and drawbacks of each analysis became apparent.

Evaluation of the analyses was also done by studying the inland penetration distances of the lake breeze fronts. This revealed that most the analyses had good correlation to the Final ‘Truth’ Set. The Mesonet analysis was the least accurate for pinpointing lake breeze fronts, due to lack of information between surface stations.

The boundary analysis showed that lake breeze fronts, originating from one or more of the surrounding lakes, occurred in the study area on 73 out of 86 days, or 85% of the days (for 1800 UTC).

Exeter radar data (CAPPI and MAXR) were run through URP cell identification and tracking algorithms. The locations of storm cells, when they reached a 40 dBZ level, were measured relative to the closest boundary. Considering study days without warm front influence, 70.4% of the 40 dBZ CAPPI cell initiations and 68.5% of the 40 dBZ MAXR cell initiations occurred at a distance of 20 km or less from a boundary. Cell distribution plots were created to show the locations of the 40 dBZ cell initiations in front or behind a specified boundary type or boundary classification.

Nowcasting techniques considering cumulus cloud development and Lifted Index values in the ‘lifting zone’ of the boundary, the convergence strength and updraft orientation along the boundary, and the boundary relative cell speed, were utilized in case studies. Reasons for the development, or the lack thereof, became apparent in cases presented.

Acknowledgements

I would like to thank my supervisor, Peter Taylor, for his guidance and encouragement during my graduate studies at York University. It has been a privilege to work with him and benefit from his counsel.

I would like to express my gratitude to David Sills, of the Cloud Physics and Severe Weather Research Section, Environment Canada, for his collaboration on certain analyses presented in this dissertation. The guidance he has provided, especially during my time at the King City Weather Radar Research Facility, has proven to be invaluable.

I would like to thank Patrick King, of MSC/MRB, for his guidance and collaboration, especially during the ELBOW 2001 field study.

Many thanks to my supervisory committee, including John McConnell, Donald Hastie and Ronald Stewart for their guidance and valuable suggestions on this work, as it evolved.

I would like to express my appreciation to the scientists at the King City Weather Radar Research Facility, Environment Canada, for their assistance and the use of their facilities. In particular, I would like to thank Brian Greaves, Norbert Driedger, Bob Paterson, Emma Hung and Janti Reid for their assistance in becoming familiar with and implementing the AURORA Research Tool for use with the ELBOW 2001 project data. I would also like to thank Sudesh Boodoo, Norman Donaldson, Paul Joe, Jim Young and Peter Rodriguez for their insight into and assistance with the radar products and algorithms. Sudesh Boodoo has

provided a large amount of assistance in obtaining the data/imagery needed for the ELBOW analyses presented in this work. Paul Joe has provided valuable insight into the cell identification and cell tracking algorithms, used to perform analyses in this study.

I would like to thank Jim Wilson, Cindy Mueller, Eric Nelson and Tom Saxen, from the National Center for Atmospheric Research (NCAR), for their insight into the NCAR Auto-Nowcaster and the nowcasting of storm development in association with mesoscale boundaries.

Last but not least, I would like to thank my family and friends for all the support and encouragement they have provided. Without them, this would not have been possible.

Dedicated to

my Friends and Family

especially

William and Susan Alexander

Table of Contents

List of Tables

List of Figures

1. Background

1.1 Low-Level Mesoscale Boundaries

The Great Lakes region is a unique area to observe the effects of low-level mesoscale boundaries on convective development. Low-level mesoscale boundaries are defined as the border or transition between two differing air masses, on a scale smaller than that of synoptic. These boundaries occur against the Earth's surface and can vary in depth, but generally are shallow. In Southwestern Ontario, these boundaries are so prevalent that they often interact during convective summer days. Low-level mesoscale boundaries which occur frequently in this area include lake breeze fronts, land breeze fronts and gust fronts. This chapter discusses the formation of these boundaries, identification methods, previous lake breeze occurrence studies, storm development associated with these boundaries and nowcasting techniques.

1.1.1 Lake Breeze Fronts and Land Breeze Fronts

Lake breeze fronts occur frequently in the Great Lakes area. Southwestern Ontario is surrounded by a number of lakes, including Lakes Ontario, Erie, St. Clair and Huron, each of which can act as a source of lake breeze fronts. These multiple sources often allow for interactions of lake breeze fronts in this region.

Lake breeze fronts (the leading edge on the land side of a lake breeze circulation) originate due to differential surface temperatures between land and lake. The land surface heats up more quickly in the daytime sun than the water

(which has a higher effective heat capacity). This temperature difference leads to the mesoscale circulation called a lake breeze. A number of papers and publications have offered detailed definitions of a lake breeze circulation, describing how it develops. A couple of these are noted following.

Simpson (1994) states that sea breezes (similar to lake breezes) are a result of modified low-level pressure caused by temperature differences between the land and sea. The air being heated over the warm land surface (via convection currents), up to a limited level (or stable layer), causes a low pressure area, as a result of the expansion of this air sideways (below the stable layer). He notes the air pressure over the sea stays relatively consistent, as there would be much less heating of this surface, therefore, a pressure gradient is created causing flow towards the lower pressure over land. Simpson (1994) mentions that a return flow (from the land side towards the sea) exists above the inland flow, in order to replace the air which has moved away from the sea.

Pearce (1955 & 1956) offers a further in depth explanation of sea breezes. Pearce notes that initially the daytime heated land surface, which heats more quickly than the water surface, warms the air and convection mixes it vertically into the atmosphere. A deep ‘tidal’ motion, or a weak flow from the land towards the sea, is the result as this warmed air over the land expands. Simultaneously the heating of the air over the land has caused a density difference. The warmed air over the land is now less dense than the colder air over the sea. This results in a low-level movement of the dense air pushing under the expanded air due to

gravity, or a flow from the sea towards the land. Due to the displacement of the air in the lower levels, a return flow occurs aloft from the land towards the sea completing the circulation (Pearce, 1955 & 1956).

Pearce (1956) also notes the general velocities of the motion in the different components of the sea breeze circulation. According to this paper, the tidal motion is in the order of 1 km/hr, the low-level flow from the sea towards the land is in the order of 10 km/hr, the return flow (aloft) has a velocity up to 5 km/hr (Pearce, 1956).

As for the depth of these circulations, Lyons (1972) specifies that the onshore flow layer (against the ground) is approximately 500 m in depth (as a mean value). However, lake breezes can differ in depth, and this onshore flow layer can be as deep as 1000 m or as shallow as 100 m (Lyons, 1972). Simpson (1994) notes that near the leading edge, the onshore flow layer will be deeper,

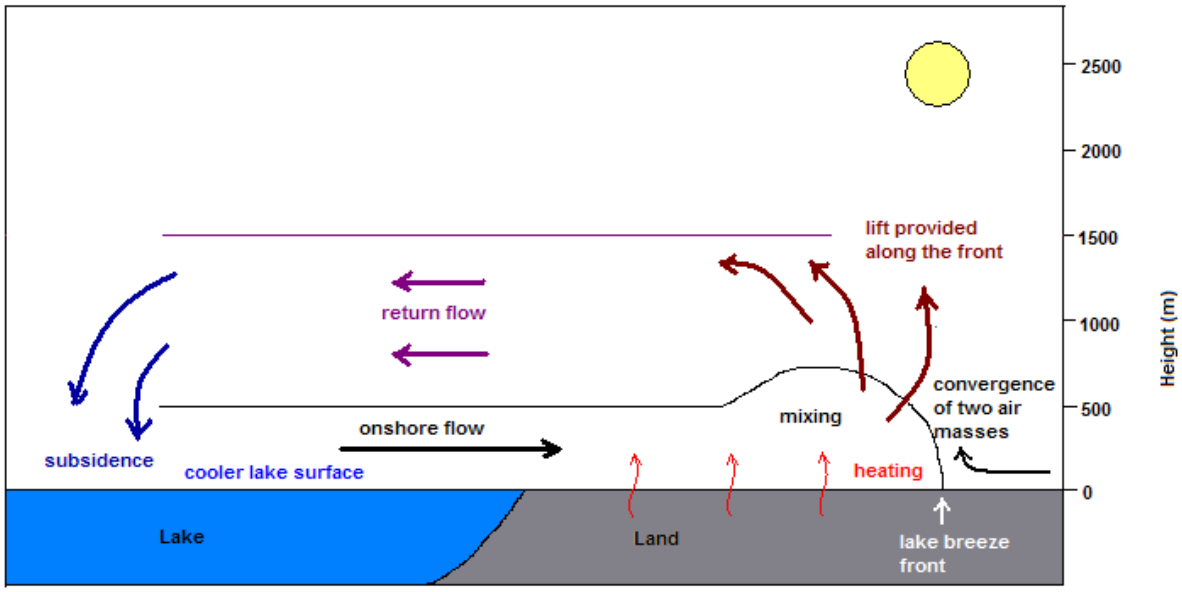

Figure 1.1. A visual representation of a typical lake breeze circulation of average depth.

due to mixing of the two air masses of different densities. Lyons (1972) specifies that the return flow (moving from land to lake) is deeper than the lower onshore flow layer. He noted it was generally observed to be approximately double the depth. See Figure 1.1 for a visual representation of a typical lake breeze circulation of average depth.

Land breeze fronts (the leading edge on the lake side of a land breeze circulation) also originate due to differential surface temperatures between land and lake. However, this circulation occurs during the evening and overnight hours, when no convective heating from the sun is occurring. Since the water has higher heat capacity compared to the land surface, it cools much slower than the land. This creates a temperature gradient similar to that causing the lake breeze circulation, but it is opposite due to the lake surface being warmer than the land surface. Against the surface, the cooler, dense land air pushes under the warmer lake air, causing a flow from the land towards the lake. Therefore, the land breeze front is the leading edge of the cooler, dense land air and generally progresses in an offshore direction. Aloft, a return flow occurs which flows from the lake towards the land to balance the circulation.

1.1.2 Gust Fronts

Another type of low-level mesoscale boundary that occurs frequently in the southwestern Ontario region is the gust front. These boundaries originate from storms forming in the area. Byers and Braham (1948) and Cotton (1990) note that they originate from the storm's downdraft which begins during the mature

stage of the storm's lifecycle. The downdraft starts when precipitation begins to fall from the storm along with dry external air being entrained. This downdraft flows down out of the storm and when it reaches the ground it spreads out and away from the storm base. The 'gust front' is the leading edge of this cool downdraft air, flowing along the ground. It is the boundary between two different air masses; the cool air originating from the storm and the warmer environmental air at the surface (Byers and Braham, 1948 and Cotton, 1990).

Cotton (1990) also mentioned that the downdraft, driving the gust front, could be intensified due to precipitation evaporation. This evaporation creates cool, dense air which strengthens the downward motion of the air (Cotton, 1990).

1.2 Previous Methods Used to Identify Low-Level Mesoscale Boundaries

A number of different data sets have been used in previous studies in order to identify a low-level mesoscale boundary. Commonly, the methods used for identification include viewing the cloud development through satellite imagery, using meteorological measurements (such as wind, temperature and humidity) and using radar (reflectivity and radial velocity). These common identification methods are covered in more detail in the subsections following.

It should be noted that other data sets have be used to identify or study the structure of low-level boundaries (such as radiosondes, aircraft measurements, sodar, etc.). However, in the following sections we look in more detail at the more common and widespread data sets (as noted above) as these will be used further in this study.

1.2.1 Identification Using Cloud Development

Simpson (1994) noted that the presence of a sea breeze could be seen through studying the clouds. Simpson noted that the sea breeze front could be seen both on clear days and days with a widespread cumulus cloud field. On a clear day the sea breeze front will appear as a single line of cumulus clouds. He notes that on a day with a cumulus cloud field present, the area behind the sea breeze front (in the circulation) will be clear and the environmental air (ahead of the sea breeze front) will show the cumulus clouds. Thus, the sea breeze front appears as the transition between the cloudy/clear zones, or the cumulus along the sea breeze front may have some vertical growth due to the convergence of the two air masses across the front. Simpson also mentions that this convergence area can show storm development in some cases. Another factor that helps to verify what is being seen is in fact a sea breeze front, is that it usually takes on a shape similar to the coastline of the lake it originated from, (Simpson, 1994). An example can be seen in Figure 1.2.

Some previous studies have used satellite imagery to observe lake breeze fronts and their movement inland. For example, Purdom (1976) used high resolution Geostationary Operational Environmental Satellite (GOES) imagery to observe low-level mesoscale boundaries such as sea breeze fronts and lake breeze fronts. Purdom was also able to view interacting boundaries and some of the associated storm development. King et al. (2003) used GOES satellite

imagery to observe lake breeze development in southern Ontario under varying strength and direction of environmental winds.

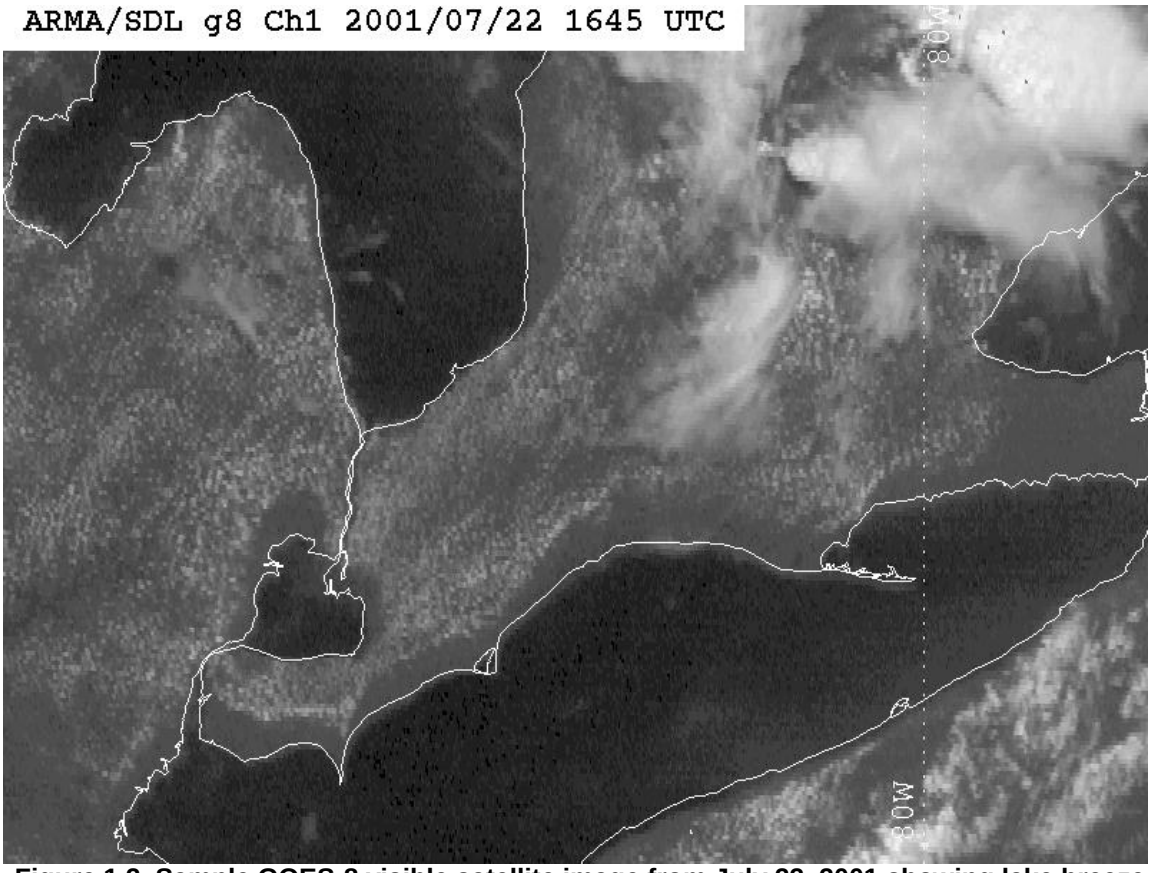

Figure 1.2. Sample GOES-8 visible satellite image from July 22, 2001 showing lake breeze development. Note the clearing between the lake and cumulus field.

1.2.2 Identification Using Wind, Temperature and Humidity Measurements

Simpson (1994) stated that sea breeze presence could be seen in wind, temperature and humidity measurements. Examples were shown by Simpson, displaying a strong change in wind direction and strength, a drop in temperature and rise in humidity with the passing of a sea breeze front.

If a number of monitoring stations exist surrounding a lake and at varying distances inland from the lake, one should be able to obtain an idea of how the lake breeze front is oriented and how quickly it penetrates inland from the lake.

Ryznar and Touma (1981) studied wind, temperature and humidity measurements on the eastern shore of Lake Michigan to identify lake breeze occurrence. Estoque, Gross and Lai (1976) did a study of the Lake Ontario lake breeze utilizing ten observing stations transecting inland from the southern shore, along with aircraft observations, cameras, soundings, etc.

Temperature and wind speed measurements have also been used to predict lake breeze circulations. Biggs and Graves (1962) developed a Lake Breeze Index in order to determine which days will allow for lake breeze development. They defined this Lake Breeze Index as:

$$\text{Lake Breeze Index} = U^2/(C_p \delta T)$$

where U is the wind speed (at an inland site not being affected by the lake breeze circulation), C_p is the specific heat capacity for dry air with a value of 1.003 J g^{-1} $^oK^{-1}$, and δT is the difference between the temperature over land (at an inland site not affected by the lake breeze circulation) and the surface temperature of the lake. Biggs and Graves (1962) used data from the west shore of Lake Erie to determine that the threshold for this index was 3. They noted that values equal to and below this threshold indicated a ‘lake breeze day’ and values above this threshold indicated a ‘non-lake breeze day’ (Biggs and Graves, 1962).

This Lake Breeze Index has been used in further studies. Comer and McKendry (1993) used the index to remove ‘non-lake breeze days’ from their study on the frequency of Lake Ontario breezes. Lyons (1972) used a modified version of the Lake Breeze Index as a predictor for the lake breezes occurring in the Chicago area.

1.2.3 Identification Using Radar

Wilson and Schreiber (1986) used Doppler radar to identify low-level lines of convergence (such as a lake breeze front, gust front, etc.). They noted that these boundaries could be identified through the radar by finding the lines of increased reflectivity or by finding signatures in the Doppler velocity depicting the convergence along these boundaries. These boundaries were often identified under clear air conditions (Wilson and Schreiber, 1986).

Atlas (1960) and Simpson (1994) both suggest two reasons why sea breeze fronts can be identified on the radar scans on a clear day. One suggestion was that there were targets such as insects, birds or particles swept up into the convergence zone, along the front, which creates the signature. The second suggestion was reflection due the change in air mass across the front (the warm, dry air over the land against the cold, moist air from the sea forcing landward).

Chapter 5 looks at low-level mesoscale boundary identification in the Great Lakes region using satellite, mesonet and radar analysis, as well as a combination of these data sets, in order to determine the best way to identify these boundaries.

1.2.4 Previous Lake Breeze Occurrence Studies

Wexler (1946) noted that the sea breeze occurrence rate is not consistent. Studying one coastal region compared to another will show different results. This is due to the fact that different regions have different climates which will affect development of these small-scale circulations. Studying a single coastal location will also show a difference in sea breeze occurrence from one summer to the next (Wexler, 1946).

A number of previous studies on lake breeze occurrence have been done in the Great Lakes area. A few of these studies and their findings are summarized below.

Lyons (1972) performed a study in the Chicago and Grand Haven areas in order to get a look at the climatology of Lake Michigan lake breeze. The study period, during 1966, 1967 and 1968, included a total of 10 months (all during the summer). They utilized reports from various airports, weather measurements from monitoring stations on the western and eastern shore of Lake Michigan, upper air data and visual observations including photographs taken by panoramic cameras and aircraft.

In order for Lyons (1972) to identify lake breeze development there were three set requirements. Initially, make sure that the feature being considered is not a synoptic front being mistaken for a lake breeze circulation. In other words, verify the scale of the feature being considered. Second, the circulation must be complete, that is not only should there be inland winds present at the surface, but

there should be a return flow above this to balance the circulation (winds from the land towards the lake, as seen in Figure 1.1). Finally, there must be a lake breeze front observed.

Following this set of three requirements, Lyons (1972) found that lake breezes occurred on 36% of the study days on the western shore of Lake Michigan (Chicago area). They occurred 25% of the study days on the eastern shore (Grand Haven area). 14% of the study days showed lake breezes occurring on both shores and 49% of the study days showed lake breeze development in the Chicago area and/or the Grand Haven area (Lyons, 1972).

Ryznar and Touma (1981) conducted a study on lake breeze occurrence on the Eastern shore of Lake Michigan during the years 1973 to 1978 and only between the months of March and November. Ryznar and Touma looked into development of a ‘true lake breeze’ (TLB). They defined a TLB to be a lake breeze circulation which develops against opposing background winds. That is the lake breeze circulation, which causes inland flow from the lake at the surface, must develop in conditions where the environmental winds are moving in a direction oriented offshore. Therefore, when the low-level environmental winds showed a similar direction to the low-level winds in the developing lake breeze circulation, these were not considered ‘true lake breezes’. In order for a day to have been considered for TLB development the conditions had to be cloud free or only partly cloudy, show conditions allowing for gradient winds moving in a

direction toward Lake Michigan, and there had to be no cold front influence on the study area (Ryznar and Touma, 1981).

Atmospheric measurements, taken on the eastern shore of Lake Michigan were studied to pinpoint sharp changes, indicating the movement of a TLB inland. In doing this, Ryznar and Touma (1981) determined that there were a total of 187 TLB occurrences during the study period (1973 to 1978). That means that every March to November period shows 31 true lake breezes (average). The months that showed the highest frequency of TLBs was July and August (Ryznar and Touma, 1981).

Comer and McKendry (1993) conducted a study on the lake breezes originating from Lake Ontario. They used data from 12 observation stations surrounding the lake. They considered the data from April 1 to September 30 for both 1988 and 1989. Three steps were taken in this analysis to identify the days with lake breeze development. Initially, the lake breeze index (LBI), as mentioned in section 1.2.2, was calculated for each of the study days. Any days that showed LBI values greater than 3.0 were eliminated as ‘non-lake breeze days’.

Secondly, days were removed which had synoptic fronts affecting the study area. This was done utilizing weather maps. Thirdly, the cloud cover was considered. The criteria for this third step was that elimination of the study day occurred if two full hours (during daylight) showed more than 3/10 cloud cover. After days were eliminated using these three criteria, 113 days remained which

were considered to show lake breeze development. This was approximately 30% of the days initially considered (Comer and McKendry, 1993).

Sills (1998) used surface station measurements, hodographs and satellite imagery to identify lake breeze fronts occurring in southwestern Ontario during the SOMOS project, which was conducted mid-July to mid-September 1993. Weather maps were used to ensure that the boundaries were mesoscale features and not synoptic scale. Satellite and Radar were used to ensure the identified boundaries were lake breeze fronts and not storm outflow boundaries. Sills found that lake breeze fronts occurred on 57% of the days during the study. Statistics for the specified lakes showed occurrence on 54% of study days for Lake Erie, 51% of study days for Lake Huron and 46% of study days for Lake St. Clair (Sills, 1998).

Recently, Sills et al. (2011) looked into lake breeze frequency during the Border Air Quality and Meteorology Study (BAQS-Met). The study period included June 1 through August 31, 2007. The study region included the southern Great Lakes area (including lakes Huron, Erie and St. Clair). They utilized radar, satellite and surface station data to identify lake breeze fronts. They found that 90% of the study days showed lake breeze development from one, if not more, of the lakes. It was also found that Lake Huron showed lake breeze development on 84% of the study days, Lake Erie showed development on 82% and Lake St. Clair showed development on 83% (Sills et al., 2011).

Curry (2012) studied June, July and August lake breeze development in southern Manitoba, including southern Lake Manitoba, Shoal Lake, and southern Lake Winnipeg. Using radar and surface station data for 2008 to 2010, it was found that lake breeze fronts occurred on 15.9% of the study days. Using radar, surface station data, satellite and synoptic maps for 2011, lake breeze fronts could be identified on 30.4% of the study days (Curry, 2012).

1.3 Storm Development in Proximity to Convergence Lines

Previous studies suggest that the convergence caused by lake breeze fronts and other low-level mesoscale boundaries provide a lifting mechanism which helps to trigger or strengthen storm activity.

Byers and Rodebush (1948) looked into the possible triggers for thunderstorm development in the Florida peninsula. The study period included the 1946 summer season. After studying the convergence in low-levels, they suggested that the frequent Florida thunderstorms (earlier thought to be caused by diurnal heating) were being triggered by the combination of two sea breezes (one from each shore) frequently affecting the area. It was noted to be possible that these sea breezes provided the convergence needed to trigger this activity (Byers and Rodebush, 1948).

Sills (1998) looked at case studies during the SOMOS and ELBOW 1997 projects where low-level mesoscale boundaries, mainly lake breeze fronts, had an effect on storm development in southwestern Ontario. These cases presented situations where storms formed along these boundaries and sometimes two

merging boundaries. Some of these cases, presented by Sills (1998), produced severe weather.

Purdom (1976) was able to observe storm development occurring in locations where low-level mesoscale boundaries, or ‘convective lines’ as he refers to them, were interacting. This was done through the use of GOES satellite imagery. Purdom (1976) concluded strengthening development may be anticipated by monitoring these boundaries to see where they will interact with one another and other convective activity.

Wilson and Schreiber (1986) conducted a study on convective initiation in proximity to low-level convergence lines occurring in Colorado, east of the Rocky Mountains. The study period was mid-May to mid-August, 1984. They identified convergence lines through Doppler radar (using the identification methods mentioned in subsection 1.2.3). Each convergence line (or boundary) was given a classification. The classifications included: “gust front, mountain outflow, synoptic front, Denver convergence line, unknown stationary, and unknown moving.” (Wilson and Schreiber, 1986).

During this study, Wilson and Schreiber (1986) considered ‘storms’ to be cells initiating to an intensity of 30dBZ or greater. This is the reflectivity that must be seen at an altitude, above the ground, of 1 km. They then measured the distance from these storms to the closest boundary. From the results they found that many of the storms formed within close proximity of these low-level convergence lines (boundaries). In fact, 79% of the 30dBZ or greater storms that

initiated in the study area were initiated by the low-level convergence lines. This increased to 92% looking at cells which initiated in the study area at 60dBZ or greater. Wilson and Schreiber (1986) also found that storms showed different results in how close they developed to boundaries, depending on whether the boundaries were moving, stationary or colliding. In the case of a moving boundary, the storms generally formed right over top and up to 20 km behind it. For stationary boundaries, the storms usually developed from 0 to 15 km from it. Colliding boundaries showed that storms associated with them generally trigger in very close proximity; a range of 0 to 5 km. It was also apparent during the study that these boundaries could also strengthen older storms if they moved into close proximity of one of these boundaries (Wilson and Schreiber, 1986).

In order to see if storm cells are related similarly to lake breeze fronts and other boundaries occurring in the Great Lakes region, a similar study to Wilson and Schreiber (1986) was done in Southwestern Ontario. Chapter 6 covers the details of this analysis and the results.

1.4 Nowcasting Techniques

This section takes a look at nowcasting (short-term forecasting) techniques used to help determine where storm activity, or the lack there of, will occur in proximity to low-level mesoscale boundaries. The techniques have been noted in a number of references by research scientists at the National Center for Atmospheric Research (NCAR) in Boulder, Colorado. These have been used as some of the basic ideas behind software to produce convective nowcasts, known

as the NCAR Auto-Nowcast System (Mueller et al., 2003). These include assessing the cumulus development and lifted index values in the environment surrounding the boundaries, the strength of the convergence associated with the boundaries, the updraft orientation caused by the low level shear in relation to the boundary movement, and the speed of the developing cells in comparison to the boundary movement.

The following subsections cover a general description of these nowcasting indicators. These are then used to look at case studies in the Great Lakes region in Chapter 7.

1.4.1 Cumulus Development In the Lifting Zone

Wilson et al. (2000) note the cumulus clouds within the boundary's lifting zone (the area where the boundary has the ability to affect the cell development) can be a good indicator of instability in association with the boundary, and the boundary can add to its development. Therefore, it is important to observe the cloud vertical growth in this zone (Mueller et al., 2003 and Wilson et al., 2000).

If cumulus cloud development begins to grow vertically (becoming cumulus congestus) this may be an indicator that the environment is favourable for further development of the cells in this area. If this growth is occurring along the boundary, this could be an indication that this boundary is modifying the environment enough to aid in further development.

1.4.2 Lifted Index in the Lifting Zone

Wilson et al. (2000) note that one of the nowcasting indicators, for boundary interaction to initiate storm development, is the Lifted Index (LI). They note that generally the Lifted Index will be less than zero, within the lifting zone of the boundary, to trigger storm development.

The Lifted Index is an indicator of thunderstorm development potential and is calculated from atmospheric soundings. As defined by Galway (1956) the Lifted Index can be found by initially modifying the lower 3000 feet of the sounding. The average mixing ratio for the lower 3000 feet and the dry adiabatic lapse rate drawn through the predicted peak temperature for the day (or the average measured temperature in the lowest 3000 feet) are used to find the lifted condensation level (LCL). From the LCL the resulting moist adiabatic lapse rate is followed up to 500 mb. The 500 mb temperature value found by doing this is subtracted from the actual environmental temperature displayed on the sounding at 500 mb, therefore giving the value of the lifted index (Galway, 1956).

The Environmental Research Services (2002) notes that potential for storm development is weak if this index is greater than -3, moderate for values of -3 to -5 and strong for values less than -5.

1.4.3 Convergence Strength

Wilson et al. (2000) noted that with substantial low-level convergence in association with a boundary, in combination with a deeper updraft, the better chance there is for stronger storm development. We can see a visual

representation of convergence strength in Figure 1.3. For example, when the environmental winds and the winds driving the boundary are more directly colliding with one another then the convergence is stronger. If both environmental winds and boundary winds show the same or similar direction and similar magnitude, then convergence would be weak. Wilson et al. (2000) used 200 m winds derived from Doppler radar to look at convergence strength.

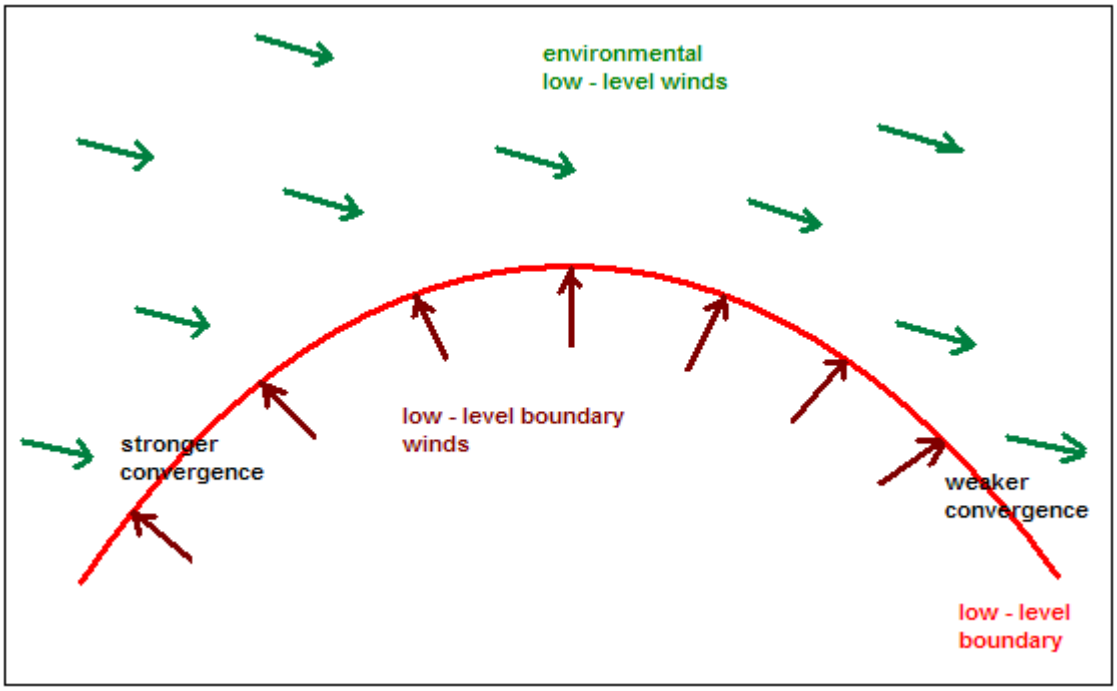

Figure 1.3. A visual representation of weak and strong convergence along a low-level mesoscale boundary in relation to the environmental winds.

1.4.4 Updraft Orientation

Rotunno et al. (1988) studied the environmental wind shear in relation to examples with and without 'cold pool' (such as storm outflow) influence. They found that in cases with 'cold pool' influence, low-level shear actually aided in

creating an erect updraft, and without the environmental shear the updrafts tended to be tilted (Rotunno et al., 1988).

Wilson et al. (1998) and Wilson et al. (2000) note that the tilt of an updraft at the boundary layer convergence line is a factor which helps to determine if storms will initiate and mature into a stronger cell (or continue development in the case of pre-existing cells). They looked at the low-level shear in relation to the boundary. Specifically, what was considered was “the vector difference, normal to the boundary, of the surface wind minus the 2.5 km wind” (Wilson et al., 2000). Wilson et al. (2000) notes that the threshold for this difference is -8 m/s. Anything less than this threshold will show an erect updraft which is more conducive to development. See Figure 1.4 for a visual representation of tilted and erect updraft cases. Wilson et al. (1998) also note that the upper winds (steering the storms) show to be similar to the boundary movement, in the case where erect updrafts develop. The upper winds show to be opposite in motion to the boundary, in the tilted updraft case (Wilson et al., 1998).

1.4.5 Boundary Relative Cell Speed

The speed of a cell, relative to the movement of a low-level boundary can determine if the cell will be enhanced by the boundary and continue to develop, or if it will dissipate (Wilson et al., 2000). Weisman and Klemp (1986) stated that a cell developing will continue to do so if its propagation is similar to that of the low-level boundary associated with the development (they used a gust front as an example); in this case the convergence along the front will continue to supply the

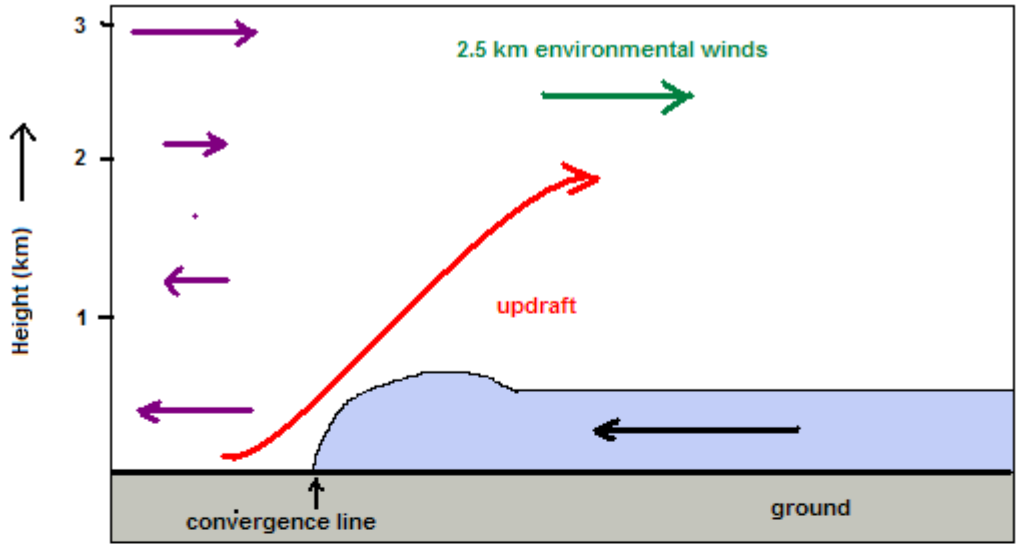

Case 1. Not conducive to storm development. The low-level shear in orientation to the convergence line cause the updraft to be very tilted.

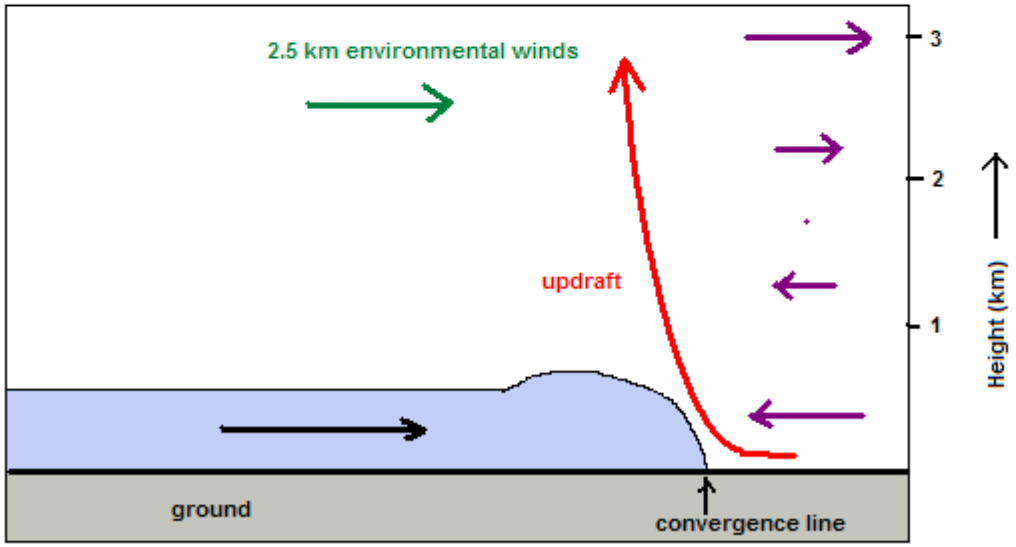

Case 2. Conducive to storm development. The low-level shear in orientation to the convergence line cause the updraft to be erect.

Diagram adapted from Wilson et al. (1998) and Wilson et al. (2000)

<u>Figure 1.4.</u> A visual representation of updraft orientation by looking at the low-level shear in relation to the boundary. The blue area represents the cool moist air pushing under the warmer environmental air. This blue area could be due to a storm outflow boundary, a lake breeze circulation, a land breeze circulation, etc. The winds in purple, at the sides, represent the environmental winds.

developing mechanism to the storm. Wilson and Megenhardt (1997) define the boundary relative cell speed (Ub) as:

$$Ub = Sb - Sc(\cos A)$$

where Sb is the boundary speed, Sc is the cell speed, and A is the angle between the boundary and cell trajectories (or the angle between their directions). Wilson et al. (2000) notes that the threshold for boundary relative cell speed is 4 m/s. The cell will progress away from the boundary if Ub is greater than this threshold value (meaning cell dissipation is probable). However, for values smaller than this, cells may develop further because they will stay in close proximity to the boundary. Wilson et al. (2000) estimated the motion of the cells using the mean wind at a height between 2 to 4 km (steering winds).

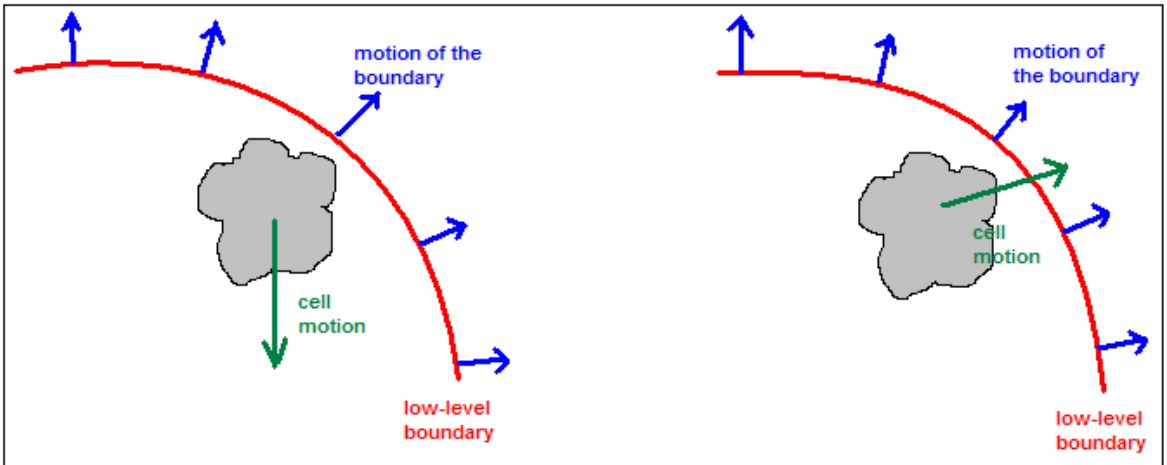

Case 1. Boundary relative cell speed (Ub) is large. The cell will proceed on a trajectory diverging from the boundary. Dissipation of this cell is a probable outcome.

Case 2. Boundary relative cell speed (Ub) is small. The cell will proceed on a trajectory similar to that of the boundary, keeping it close to the boundary. The result is continued development of the cell.

Diagram adapted from Wilson et. al. (2000)

Figure 1.5. A visual representation of 'Boundary Relative Cell Speed'. Case 1 shows large boundary relative cell speed and Case 2 shows small boundary relative cell speed.

2. The ELBOW 2001 Project

The Effects of Lake Breezes On Weather (ELBOW) 2001 project was run from May to August, 2001. The study was conducted in Southwestern Ontario, a unique mesoscale weather region surrounded by the Great Lakes. Specifically, the study region was based on the area depicted by the Exeter radar Doppler range ring (as seen in Figure 2.1). The project was led by David Sills (MSC-MRB), Patrick King (MSC-MRB), and Peter Taylor (York University). A number of organizations and institutions were involved in the project. These included The Meteorological Service of Canada (MSC), York University, University of Western Ontario, The University of Guelph, The Weather Network, NAE/NRC, and Zephyr North. Funding for the project was provided by the Canadian Weather Research Program (CWRP) and the Canadian Foundation for Climate and Atmospheric Sciences (CFCAS).

This chapter is intended to give an overview of the ELBOW project and the instrumentation used. In order to get more detailed information on equipment and data archives, refer to the ELBOW 2001 Final Data Report (Alexander et al., 2003).

2.1 Project Goals

The ELBOW 2001 project had three major goals:

- To understand how lake breezes interact with one another, other low-level mesoscale boundaries and synoptic fronts.
- To understand how lake breezes can affect storm development.

- To help improve forecasts in the Great Lakes region by transferring findings to forecasters.

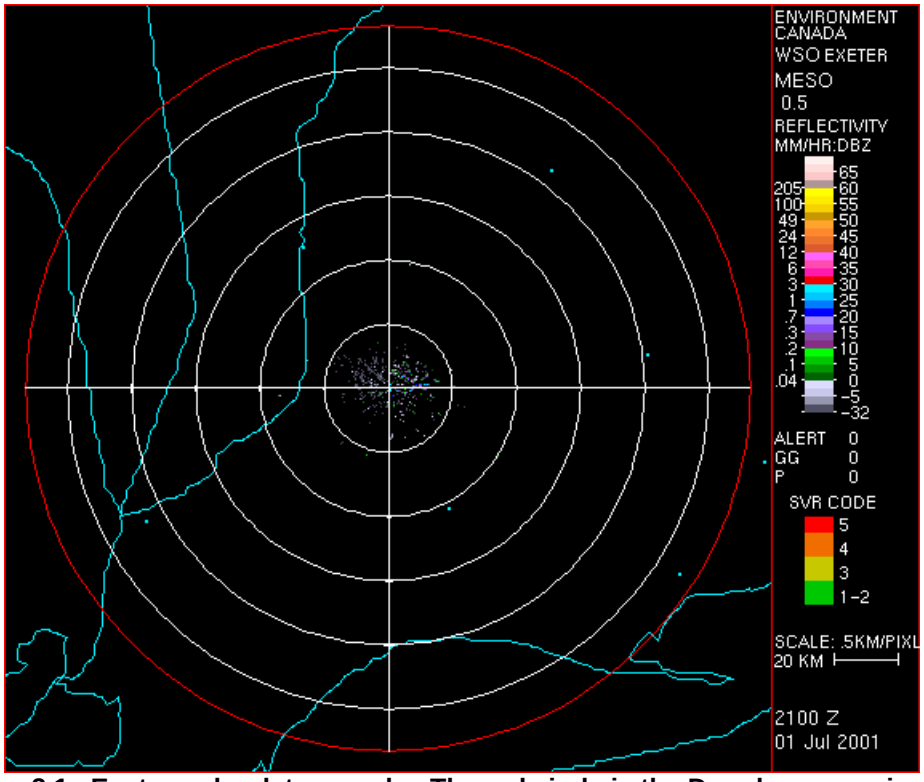

Figure 2.1. Exeter radar data sample. The red circle is the Doppler range ring and represents the ELBOW 2001 study area.

2.2 Intensive Observation Days

Intensive Observation Days (IODs) were days in which lake breeze development was expected and storm development, associated with lake breeze fronts, was possible. David Sills and/or Patrick King assessed the potential for an IOD each day before 1200 UTC. They used the regional GEM model to determine if the environment was suitable for convective development, and the experimental GEM 2.5 to determine where lake breeze fronts may develop. Early in the day, radar, satellite and sounding data were compared against the models to ensure the models were showing accurate conditions. Status messages were

written to summarize the potential for lake breeze and associated storm development. If conditions were favourable, the status message declared an IOD.

With the declaration of an IOD a meeting was held at Huron Park Airfield (just southwest of Exeter radar) at 1200 UTC. During this meeting it was decided which data were to be collected. Field team members were assigned their locations and tasks for the day.

On a standard IOD, radiosondes were launched at the three fixed radiosonde stations at 1500, 1800 and 2100 UTC (more details about these stations can be found in the following sections). The team members from two of these stations performed mobile surveys between radiosonde launches. The Mobile Jeep Unit was sent out to a specified area, within the study region, which was forecast to have the most likely storm development along the lake breeze fronts. Depending on the conditions, the X-Band Doppler Radar may have been

Table 2.1. The ELBOW 2001 Intensive Observation Days (IODs)

ELBOW 2001 IODs			
June	5	**July**	3
	8		4
	11		7
	12		9
	13		10
	14		16
	15		17
	18		18
	19		19
	21		20
	26		21
	27		22
	28		23
	29		24
	30		

run and an aircraft may have been used to take measurements transecting inland from the lakes at different levels.

Over the ELBOW 2001 study period there were a total of 29 IODs. The IODs are listed in Table 2.1.

2.3 ELBOW Instrumentation and Data Sets

A number of instruments and data collection stations were set up specifically for the ELBOW 2001 project. These included 14 mesonet stations, 3 radiosonde stations, mobile survey routes, X-band Doppler radar, 2 wind profilers, a Mobile Jeep Unit and aircraft. Special QPF discussions were created and the GEM 2.5 model was run for the project. The location of many of the instruments during ELBOW 2001 can be seen in Figure 2.2. Sections 2.3.1 to 2.3.9 explain these instruments and data sets in more detail.

2.3.1 Mesonet Stations

Mesonet stations can play an important role in identifying the location of low-level mesoscale boundaries. As a lake breeze front passes a station the wind direction usually changes to show onshore flow from the lake. The temperature and dewpoint values recorded by mesonet stations can also help to pinpoint the location of lake breeze fronts, from the strong changes seen in these values. For example, as long as the lake air has not been modified by surface heating (usually when the lake breeze front is still close to the lake shore), a drop in temperature can be seen with the passing of a lake breeze front. Refer to

section 1.2.2 for further discussion of how lake breeze fronts can be identified through these data.

A number of mesonet stations were set up specifically for the ELBOW 2001 project. A total of 14 stations were set up on paths transecting inland from Lake Erie and Lake Huron. The names and locations of the stations can be seen in Table 2.2. A visual representation of the station locations can be seen in Figure 2.2 (referred to as surface stations). Stations recorded measurements of

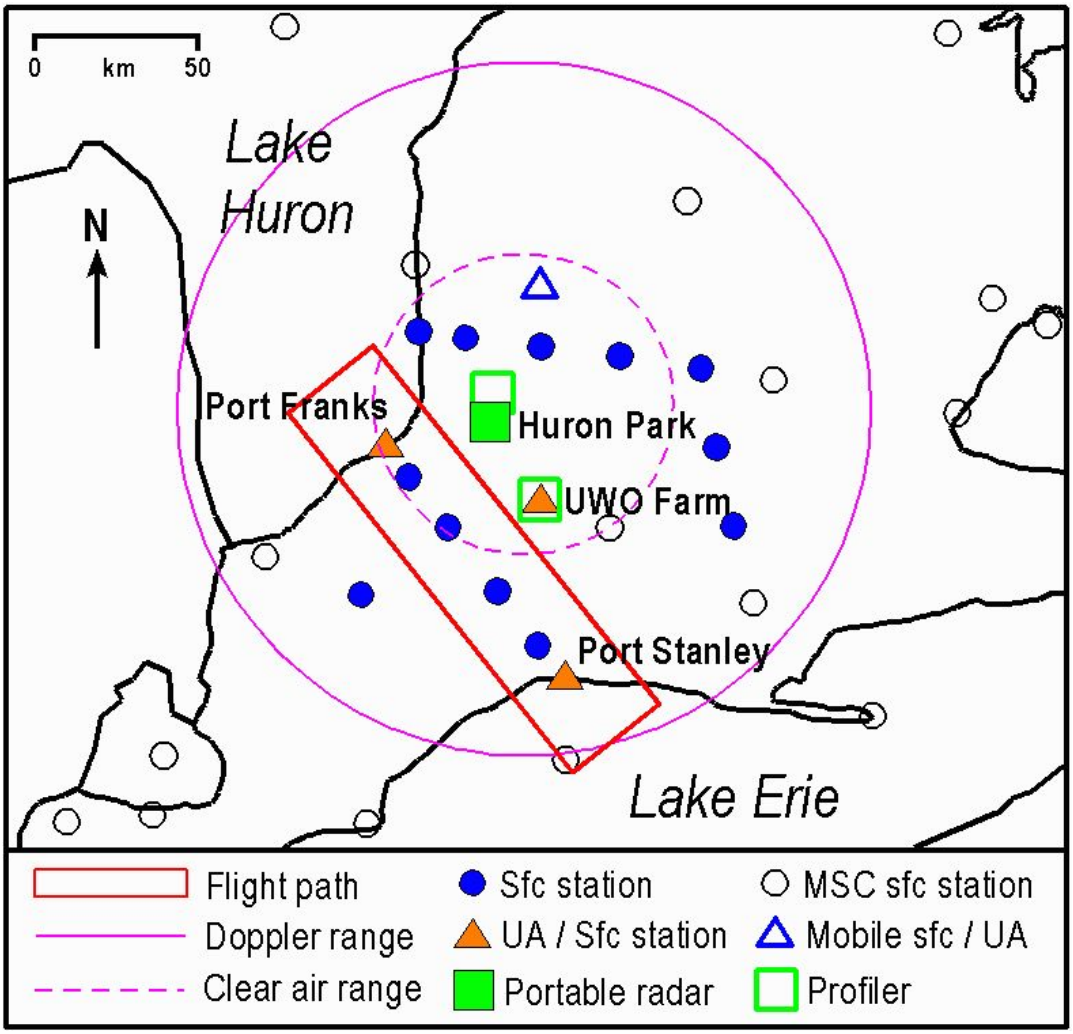

Figure 2.2. Locations of the ELBOW 2001 instrumentation. Instruments shown include radiosonde (upper air) stations, surface stations, X-band portable radar, and wind profilers.

Table 2.2. ELBOW 2001 mesonet station names and locations.

ELBOW Surface Mesonet Stations		
Station #	**Station Name**	**Location**
1	Port Franks	43.230722 °N, 81.902638 °W
2	Thedford	43.162500 °N, 81.838722 °W
3	Springbank	43.045861 °N, 81.692861 °W
4	Delaware	42.854194 °N, 81.429777 °W
5	Middlemarch	42.740166 °N, 81.244555 °W
6	Port Stanley	42.664972 °N, 81.163472 °W
7	Walnut	42.878722 °N, 81.862500 °W
9	Bayfield	43.571583 °N, 81.708722 °W
10	Varna	43.529861 °N, 81.576083 °W
11	Brodhagen	43.538111 °N, 81.259027 °W
12	Brunner	43.527972 °N, 80.942388 °W
13	Bamberg	43.489916 °N, 80.721555 °W
14	Bright	43.273750 °N, 80.673250 °W
15	New Durham	43.054166 °N, 80.539361 °W

temperature, dewpoint, wind speed, wind direction and gust wind speed. At some stations, precipitation, relative humidity and difference in temperature between 1.5 m and 9.5 m heights were also recorded. The specific availability of data can be found in the ELBOW 2001 Final Data Report (Alexander et al., 2003).

All towers were installed by June 19, 2001 and were dismantled on September 4 and 5, 2001. Specific installation dates can be seen in Appendix A. Data from existing stations in the Great Lakes region were also collected to be used in further study. These included Coastwatch, MSC, Ridgetown, and OME stations.

2.3.2 Radiosondes

It was important to obtain a vertical profile of the atmospheric conditions during the IODs. Radiosonde measurements allowed for an assessment of the

atmospheric stability. Indices such as Convective Available Potential Energy (CAPE), Lifted Index (LI), Total Totals (TT) and so forth, allowed us to look into the potential for severe weather to develop in the study region.

Radiosonde profiles can also show the presence of a lake breeze circulation. If the radiosonde was launched in lake air (after a lake breeze front had passed the station) a temperature inversion and onshore winds were seen in the low levels of the profile (near the surface).

There were three fixed radiosonde (upper air) stations during the ELBOW 2001 project (as seen in Figure 2.2). These were located at:

- Port Franks on the shore of Lake Huron (43.21° N, 81.86° W, 180 m above sea level)
- Port Stanley on the shore of Lake Erie (42.66° N, 81.16° W, 175 m above sea level)
- The University of Western Ontario (UWO) Farm

A fourth, mobile radiosonde station, was added to the Mobile Jeep Unit (more details on this unit can be seen in section 2.3.6). The radiosonde systems located at Port Franks, Port Stanley and the Mobile Jeep Unit were LORAN-C systems with DigiCORA II MW15s. The UWO Farm had an NCAR CLASS radiosonde system.

a. LORAN-C/DigiCORA II MW15 Radiosondes

The LORAN-C radiosonde systems reported a number of variables every ten seconds. These included: Time (minutes and seconds), Pressure (hPa),

Height (gpm), Temperature (°C), Dewpoint (°C), Relative Humidity (%), Wind Speed (m/s), and Wind Direction (degrees). In order to make sure that radiosonde signals were not interfering when launches were occurring at different stations simultaneously, each station was assigned its own frequency range. The Mobile Jeep Unit was assigned a frequency of 400.0 to 401.0 MHz. The Port Stanley location was assigned a frequency of 401.5 to 402.5 MHz. Port Franks was assigned 404.5 to 405.5 MHz. A frequency of 405.96 MHz was used in an emergency (usually when soundings had to be relaunched). Each launch team made sure that each radiosonde reached a pressure level of 500 mb before going out to perform mobile surveys (as seen in section 2.3.3). These soundings were usually allowed to reach a pressure level of 100 mb before being completed. See Figure 2.3 for a sample sounding. Figure 2.3 shows an Emagram plot of the temperature and dewpoint temperature. The temperature is represented by the solid red line (to the right), and the dewpoint temperature is represented by the dashed red line (to the left). The table to the upper right of the plot shows a list of sounding indices and levels computed by the RAOB program. To the right side of the Emagram plot, a vertical profile of the winds can also be found. These are depicted by wind barbs showing the wind speed and direction. The shaft points in the direction the winds are originating from (at the specified level), and the barbs along the shaft indicate the wind speed.

These radiosonde launches were performed between May 24 and August 3, 2001. The specific launch times can be seen in Appendix A. The data

collected from these radiosondes have been formatted to be viewed through the Rawinsonde Observation Program (RAOB). Specific details on what has been done with these data can be seen in Chapter 3.

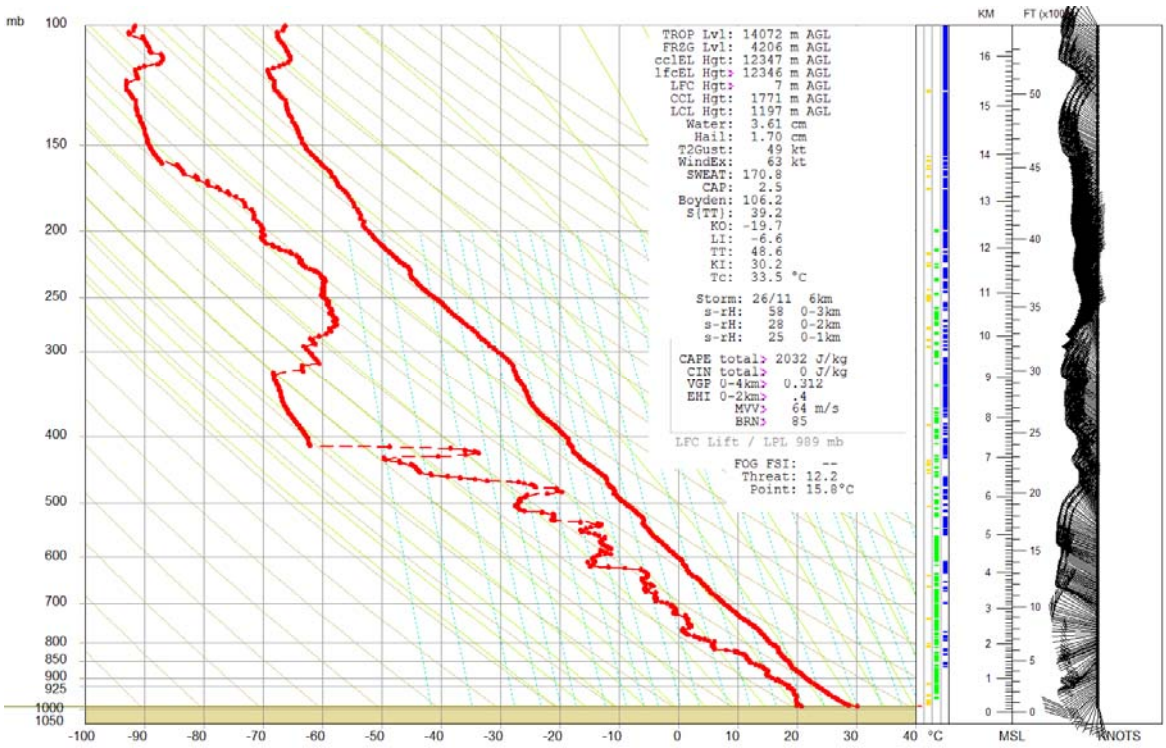

Figure 2.3. Port Franks radiosonde for July 22, 2001 as seen through RAOB. This radiosonde was launched at 1801 UTC.

b. NCAR CLASS Radiosondes

The NCAR CLASS Radiosonde system also recorded a number of variables once every ten seconds during its ascent. These variables included: Time (s), Pressure (mb), Temperature (°C), Dewpoint (°C), Relative Humidity (%), U and V component winds (m/s), Wind speed (m/s), Wind direction (degrees), dZ (m/s), Longitude and Latitude (degrees), Range (km), Az (degrees), Altitude (m), as well as a number of data flags (quality indicators). The radiosonde station at the UWO Farm was assigned the frequency range of 403.0

to 404.0 MHz. Again, the emergency frequency was 405.96 MHz in case there was a problem with the first radiosonde launch. See Figure 2.4 for a sample sounding.

These radiosondes were launched by the University of Western Ontario. All of the radiosondes from this station were launched between June 5 and July 24, 2001. Specific launch times can be seen in Appendix A. These data were quality checked and reformatted for RAOB. See Chapter 3 for more details on the changes that were made to these data.

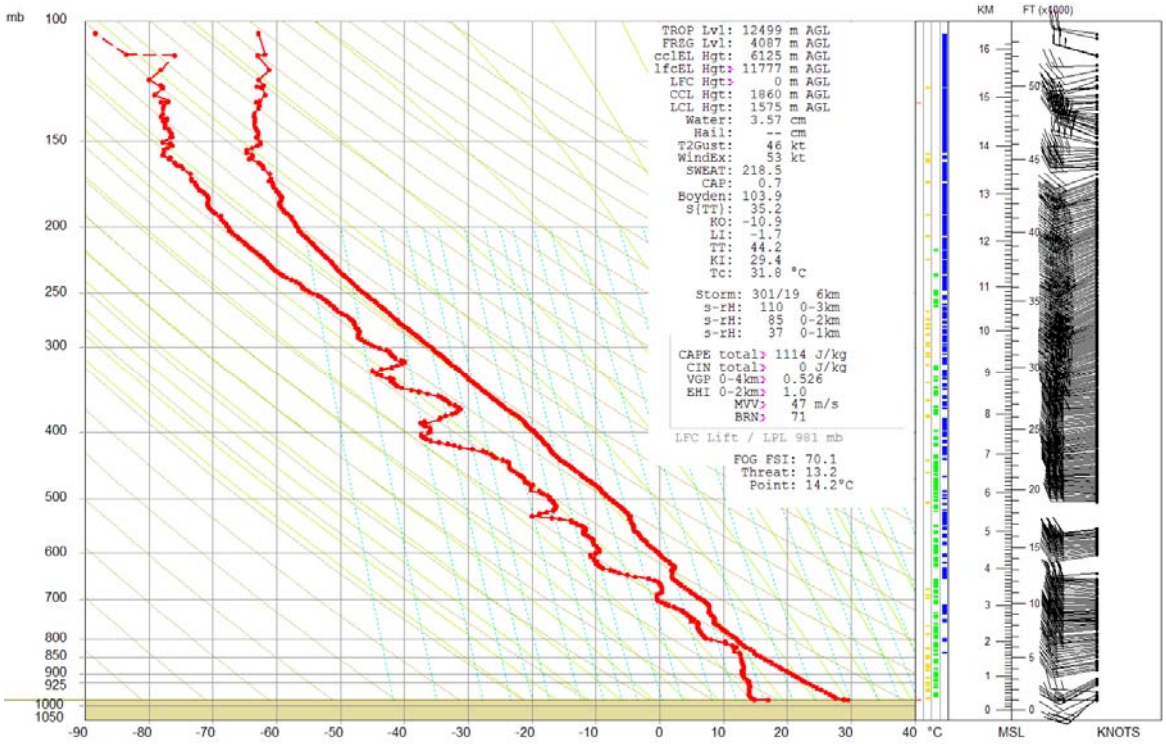

Figure 2.4. UWO Farm radiosonde for June 30, 2001 as seen through RAOB. This radiosonde was launched at 1803 UTC.

2.3.3 Mobile Surveys

Mobile surveys were conducted by the team members running the Port Franks and Port Stanley radiosonde stations. Mobile surveys were done

between radiosonde launches. Measurements were taken at 7 set locations transecting inland from the shoreline of Lake Huron and the shoreline of Lake Erie. A third mobile survey route was set up to the east of Lake Huron, transecting inland. This route was used if there were the appropriate weather conditions. Mobile surveys were also performed by the Mobile Jeep Unit (see section 2.3.6).

Each mobile survey kit was equipped with a handheld GPS, a handheld anemometer, bubbles or a string and dowling to measure wind direction, sling psychrometer and distilled water, a camera and/or a camcorder, and a compass. Rainguages were also set up at many of the stations.

The measurements recorded included:

- *Time* – the time measurements were taken at each station was recorded.
- *Location* – latitude, longitude and height above sea level were recorded if measurements were not being taken at a fixed station.
- *Wind Speed*
- *Wind Direction*
- *Temperature and Wet Bulb Temperature*
- *Precipitation Amounts* – rain readings were taken during the first mobile survey of the day to keep evaporation to a minimum.
- *Cloud Description* – cloud descriptions were taken from the observer's viewpoint. The amount of overall cloud cover was taken and sometimes

that of each cloud type. Sky diagrams were also drawn to assist in descriptions.

- *General Descriptions* – any observations such as haze, fallen limbs, or storm damage was also recorded.
- *Photos* – pictures were taken of significant development along the lake breeze fronts. Where the pictures were taken and what direction the observer was facing was also recorded.

2.3.4 X-Band Doppler Radar

The portable X-Band Doppler Radar was located on the control tower at Huron Park Airfield (see Figure 2.2). As can be seen from Appendix A, the X-Band radar was run on IODs with storm development, as long as it occurred within range of the radar. Scans were therefore conducted between June 15 and July 23, 2001. Scans were done to get a closer look at storm locations in the study region, specific vertical storm structure and horizontal storm structure. For example, Plan Projection Indicator (PPI) scans could be done for the full area surrounding the radar at set elevation angles, and Range Height Indicator (RHI) scans could be used to get vertical images of a storm. The types of scans performed on each day are listed in Appendix A and Alexander et al. (2003). Firanski (2002) covers more detail on how the scans were conducted along with a number of case studies. See Figure 2.5 for a sample of the radar data.

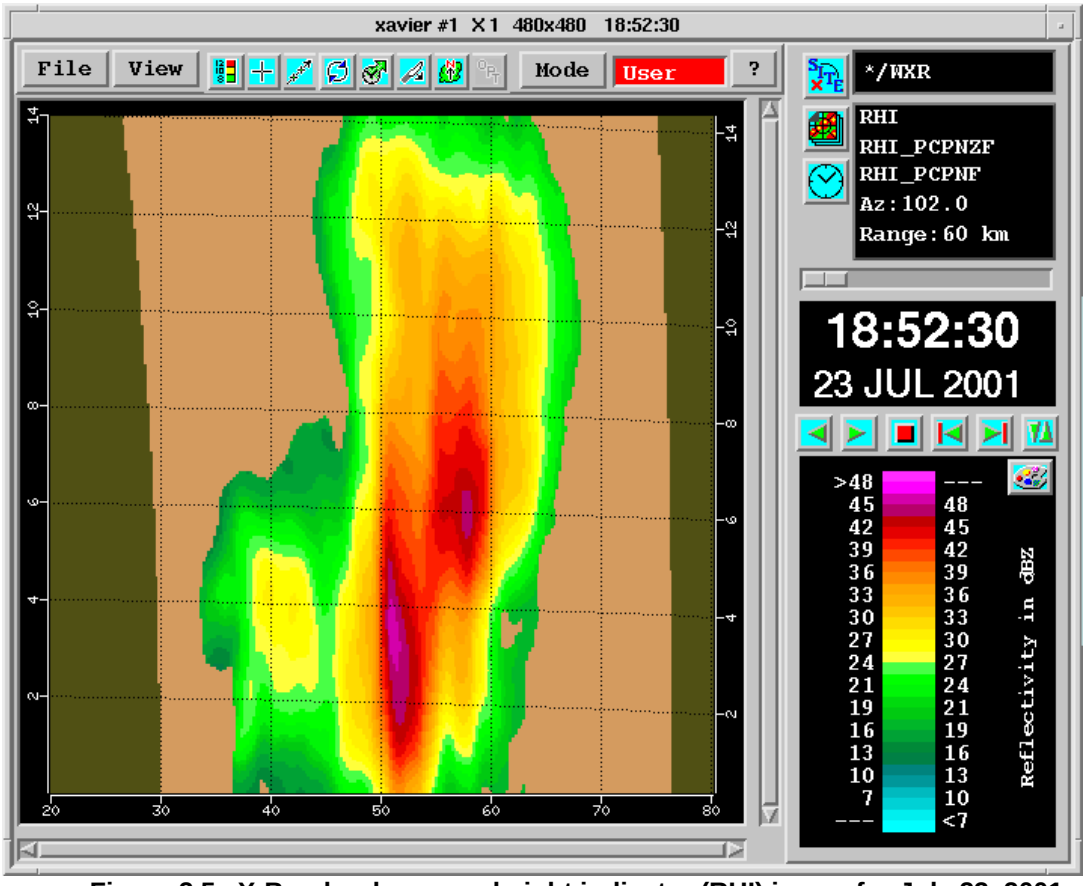

Figure 2.5. X-Band radar range height indicator (RHI) image for July 23, 2001.

2.3.5 Wind Profilers

There were two wind profilers used during the ELBOW 2001 study period. The CLOVAR wind profiler is located at the University of Western Ontario Farm. The second was located just north of Huron Park Airfield (see Figure 2.2), run by Environment Canada. These profilers were mainly used to obtain vertical profiles of horizontal wind speed and direction. However these profilers also have the ability to measure other variables such as precipitation fall speeds and reflectivity (Alexander et al., 2003).

Again, it was important to get a profile of the vertical wind field especially when lake breeze circulations were present. These data allowed for a more

detailed look into the structure of the circulation. See Figure 2.6 for a sample of the wind profiler data.

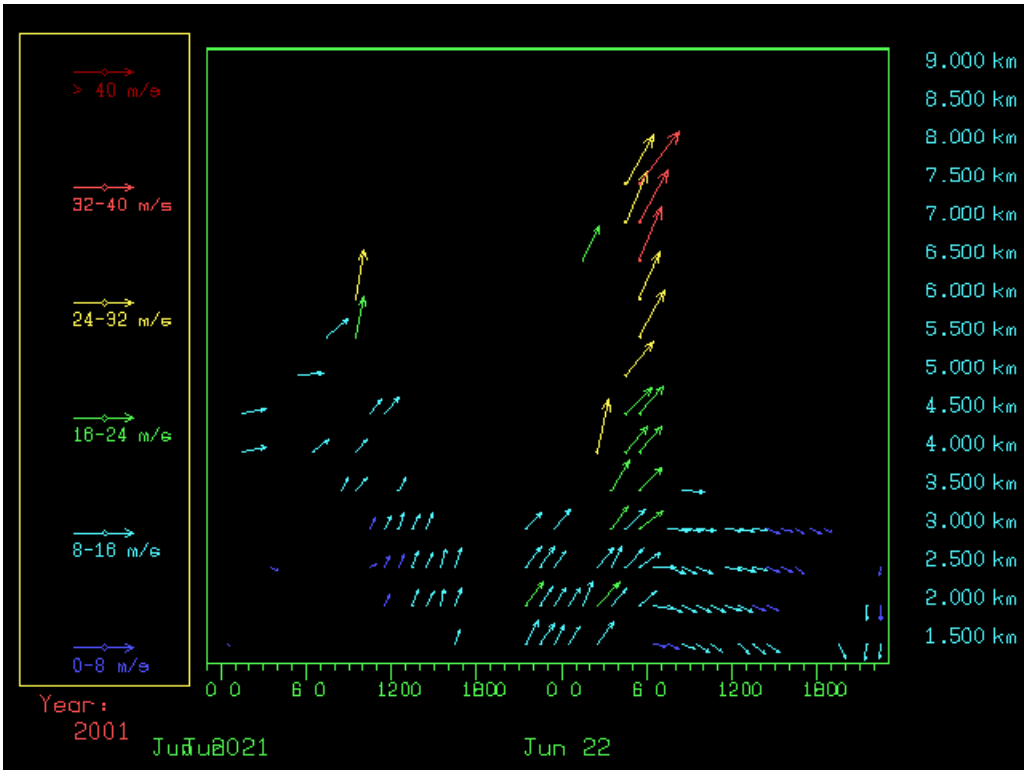

Figure 2.6. Sample image of CLOVAR wind profiler data.

2.3.6 Mobile Jeep Unit

The Mobile Jeep Unit had the ability to travel to the places where storm development, associated with lake breezes, was most likely to occur. The route driven by the unit was recorded. Observations were taken by a passenger while driving to a location of interest; this included sky observations and any storm damage. The location and direction of the observations were taken with a handheld GPS. When conditions of interest were present, the unit was often stopped to take mobile survey measurements (see section 2.3.3) along with pictures.

The Mobile Jeep Unit was also equipped with a LORAN-C radiosonde system with a DigiCORA II MW15, as well as instrumentation on the roof to record wind direction, wind speed and temperature. Therefore, radiosonde profiles and measurements could be taken in appropriate locations. As we can see in Appendix A, there were 10 'Mobile' radiosonde launches done at locations other than the three fixed stations.

2.3.7 Aircraft

Two aircraft were used to take measurements during the ELBOW project: the National Research Council (NRC) Twin Otter and an Aventech Cessna. As can be seen from Appendix A, flights were conducted between June 15 and July 24, 2001. There were ten Twin Otter flights and seven Cessna flights. A wide range of measurements were made during the flights. As can be seen in the Final Data Report (Alexander et al., 2003) these included location, temperature, dewpoint, pressure, wind speed and direction, particle size, concentrations (of CO_2, H_20, and ozone), etc. Instrumentation varied between aircraft.

Flight plans were drawn up depending on the daily lake breeze conditions expected. Flight paths usually occurred on transects between Lake Huron and Lake Erie and concentrated on the transitions from lake to land. The flights were usually done at a number of levels, to not only get a view of measurement profiles horizontally, but also vertically. These measurements would be important in studying features such as the depth of the lake breeze circulations.

There was usually an ELBOW 2001 team member present on each flight. This gave them the ability to record visual observations from the sky and take photos. Cameras were also mounted to the Twin Otter aircraft to create a video of each flight.

2.3.8 QPF Discussions

As noted in Alexander et al. (2003), QPF discussions were created by MSC forecasters, when needed for condition assessment, starting June 18, 2001. These messages discussed the synoptic weather conditions and the potential for rainfall over the next 24 hours. They also showed exceedence probabilities for 6 hour periods during the day. These experimental discussions assisted the team leaders in their daily assessment of the weather conditions and decision for an IOD status.

2.3.9 GEM 2.5

The Global Environment Multiscale (GEM) model was run with a 2.5 km resolution for the ELBOW 2001 project. As noted in Alexander et al. (2003), the model was run daily (started at 0600 UTC) and was initialized with the 6 hour forecast GEM regional data. The model gave hourly output and was run from June 9 to the end of August, 2001.

2.4 Data Collected from Operational Systems

A number of GOES-8 GIF images were archived on CD (at the King City Radar Facility) for June, July and August, 2001. Visible (channel 1), Infrared (channel 4) and Water Vapour (channel 3) images for every 30 minutes (15

minutes and 45 minutes past the hour) were archived for the Eastern Canada sector. Visible images for a smaller Great Lakes sector were also collected. These images are archived for approximately every 15 minutes. An even smaller sector, looking at southwestern Ontario was also archived for every 15 minutes. See Figure 2.7 for a sample GOES-8 satellite image.

These data are also archived regularly on DAT tapes. More data have been extracted to be used with the AURORA Research Tool, which will be discussed further in Chapter 4.

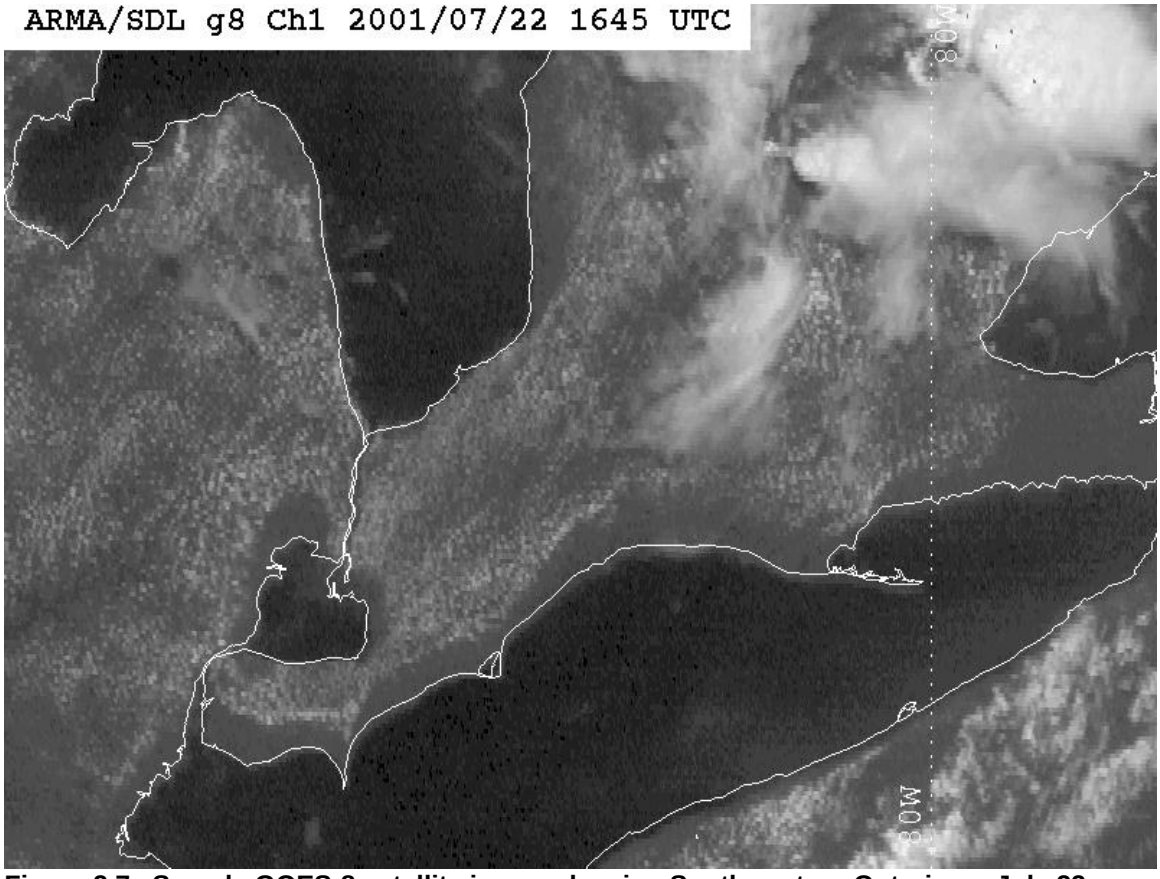

Figure 2.7. Sample GOES-8 satellite image showing Southwestern Ontario on July 22, 2001 at 1645 UTC.

A number of Exeter Conventional and Doppler Radar GIF images were stored on CD (at the King Radar Facility) for June, July and August, 2001. These included: 0.5 degree Conventional PPI, 2.0 km MAXR, 1.5 km CAPPI, RFAs, ECHOTOPS, PRECIP, SVRWX, VIL, WDRAFT, 0.3 (long range), 0.5, 1.5 and 3.5 degree radial velocity and reflectivity scans, MESO, MICROBURST and VAD. All scans and products are archived for every 10 minutes except for the RFAs which are available every hour. See Figure 2.8 for a sample Exeter radar image.

Raw IRIS files are also stored on CDs at the King City Radar Facility. More data has been extracted and used to create other data sets for further study. This will be discussed further in Chapter 4.

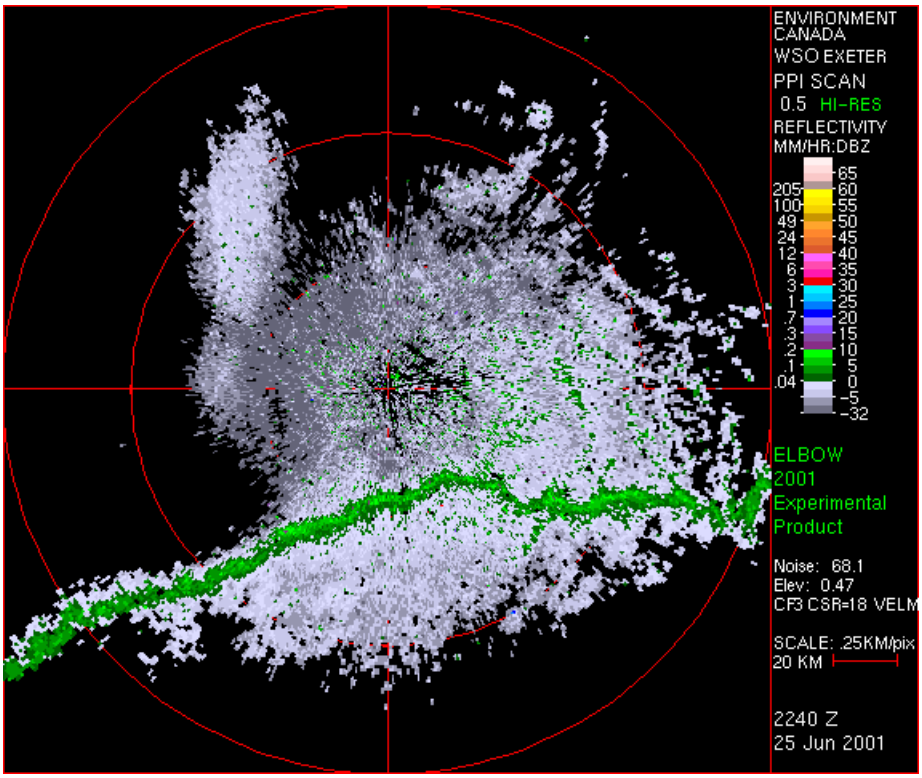

Figure 2.8. Exeter radar 0.5 degree reflectivity image for June 25, 2001 at 2240 UTC.

3. Data Quality Checking

It was important to perform quality checks to all of the sounding data, collected in the ELBOW 2001 project, in order to make sure that they were in the most accurate and usable form for further analysis (as was done for case studies in Chapter 7). Sections 3.2 to 3.4 discuss the quality checks and/or formatting performed on the Loran-C radiosondes, CLASS radiosondes, and the measurements taken in ascent and descent during aircraft flights.

3.1 Rawinsonde Observation Program

It was desirable to get these data into a format which could be read by the Complete RAwinsonde Observation Program (RAOB). This program was produced by Environmental Research Services (ERS) and can display the data in a Tephigram, Skew-T or Emagram format and allow the user a number of display options, including a Hodograph display. RAOB also calculates a number of atmospheric indices such as convective available potential energy (CAPE), lifted index (LI) and Total Totals (TT), just to name a few (Environmental Research Services, 2002).

With this information the user gets a better idea of the stability of the atmosphere and the potential for convective development. During the ELBOW project, ERS has come out with a number of versions of the RAOB program with many upgrades. For example, RAOB 4.0 was the initial version being used during ELBOW, which was an MS-DOS version that plotted significant levels (accepting up to 50 data levels). Later, a Windows version (RAOB 5.0 and

greater) was released which allowed for hundreds of data levels to be plotted allowing for a much more detailed look at the vertical structure of the atmosphere.

3.2 LORAN-C Radiosondes

A Fortran 77 program called ‘Vaisal.for’ was written for the LORAN-C (Vaisala DigiCORA II MW15) soundings. This was used to format the radiosonde data into a ‘raw data’ format that is accepted by the RAOB program. This allowed RAOB to ingest the pressure, temperature, dew point, height, wind direction and wind speed.

The sounding system performed quality control on the radiosonde data as they were being collected (Vaisala, 1996). However, just to make sure everything was checked and recorded properly, the ‘Vaisal.for’ program performed a quick check for unrealistic data. Specifically the ‘Vaisal.for’ program checked:

- that the wind and temperature data sets corresponded to one another. They should be taken at the same time, pressure and altitude.
- the pressure was not greater than 1200 hPa
- the temperature was not greater than 80 ºC and less than -100 ºC
- the dew point was not greater than 80 ºC and less than -120 ºC
- the altitude was not greater than 18000 m
- wind direction is not greater than 360 degrees and not less than 0 degrees
- wind speed is not greater than 300 m/s

It is obvious that these values are very unrealistic; however this was the first version of the program which allowed the observer to determine if further, more detailed, quality checks were required. The soundings were viewed in RAOB after this first run and all data appeared to be realistic, meaning the sounding system had no problem with quality control. Therefore, no further modifications to 'Vaisal.for' in terms of quality checks were required. See Figure 3.1 for a sample sounding from a LORAN-C system equipped with a Vaisala DigiCORA II MW15, plotted using the RAOB program.

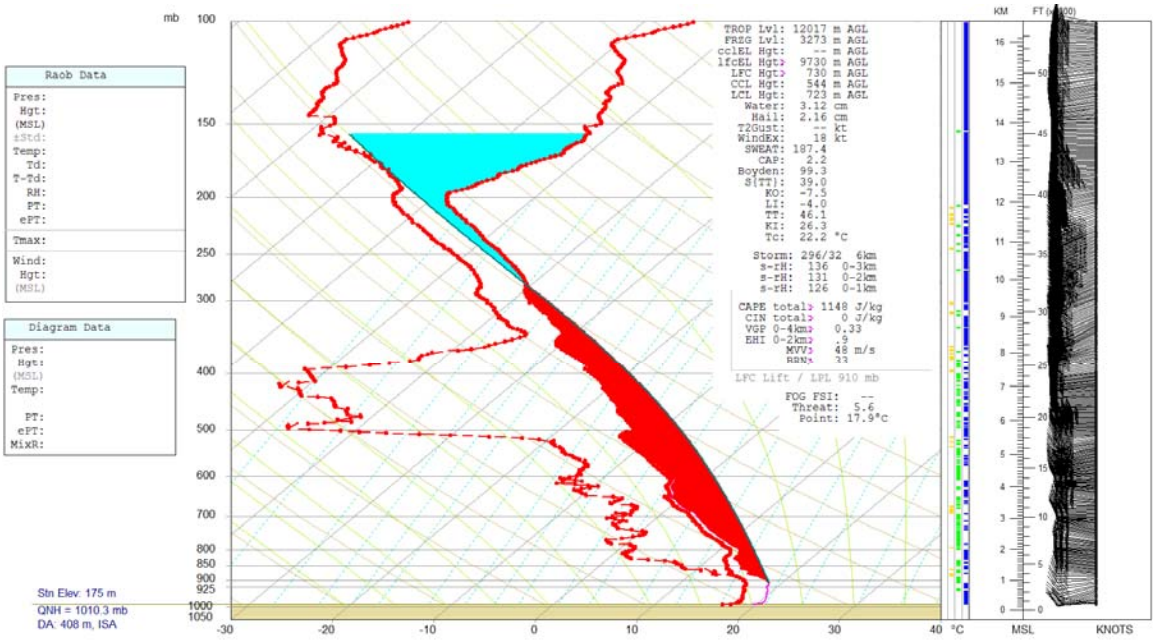

Figure 3.1. Data from a radiosonde launched at Port Stanley on July 4, 2001 at 1800 UTC as seen through RAOB. This sounding was performed with a Loran-C system equipped with a Vaisala DigiCORA II MW15.

3.3 NCAR CLASS Radiosondes

A Fortran program, written for the NCAR CLASS radiosondes, was used to format the data for RAOB (in a raw data format) and perform detailed quality

control. By looking at the unedited CLASS data, some data points were obviously unrealistic. For example, when the radiosonde became delimited or the signal was lost, data were recorded as '99999'. Some of the information surrounding these delimited data points was also unrealistic.

The data were run through a number of trial programs in order to edit out unrealistic data. Initially there was a program written to the remove the '99999' values and format the data for RAOB. It also performed basic quality checks such as those done on the LORAN-C soundings. The program checked for unrealistic values of pressure, temperature, dewpoint, altitude, wind speed and wind direction, as well as performing a check for vertical consistency in pressure and altitude. The data, output from the Fortran program, were then opened in RAOB to determine how accurate the plots were. It was found that these basic quality checks failed to eliminate all of the inaccurate data. Observing the data in the RAOB program showed that many unrealistic spikes in the profiles remained. These included strong changes in the temperature and dewpoint for just one data level.

Progressively, more quality checks were added into the Fortran program and the output was studied for accuracy. After a number of trials, a final version of the fortran program was written called 'MRS.for' (modified radiosonde). This program not only checked for realistic data values, it also checked for realistic changes in these values between the data sampling times. Through this method,

strong, unrealistic spikes in the profiles could be eliminated. This new and final program specifically checked:

- that the pressure was not greater than 1100 mb
- that the temperature was not greater than 40 ºC or less than -80 ºC
- that the dew point was not greater than 40 ºC or less than -110 ºC
- that there were no unusual temperature/dew point values that spike more than 3 ºC for a pressure change of equal or less than 10 mb
- if the temperature change was greater than 10 ºC in 30 mb then the data level was removed
- the ascent rate (change in pressure divided by change in time) must not be higher than 10 mb/s
- for vertical consistency in pressure (any vertically inconsistent data were removed - one level was removed near the surface and two levels were removed if inconsistency occurred aloft). If the pressures were the same then one was removed
- the altitude was not greater than 31000 m
- wind direction was not greater than 360 degrees or less than 0 degrees
- wind speed was not greater than 80 m/s
- the u component and the v component winds were not greater than the wind speed
- the absolute change in v component wind divided by the change in time was less than 4.0 m/s^2

- the absolute change in u component wind divided by the change in time was less than 4.0 m/s^2
- the absolute change in wind speed divided by the change in time was less than 4.0 m/s^2
- the absolute change in latitude divided by the change in time was less than 0.0005 deg/s
- the absolute change in longitude divided by the change in time was less than 0.001 deg/s
- the absolute ascent rate (change in height divided by change in time) was less than 50 m/s
- for vertical consistency in altitude (any vertically inconsistent data were removed – one level was removed near the surface and two levels were removed if inconsistency occurred aloft). If the altitudes were the same, one was removed

Many of these values (such as the absolute change in longitude divided by the change in time) were found by creating excel plots using data from five or six of the CLASS soundings. A variety of soundings were used in the plots: soundings which had many inaccuracy problems in earlier quality checks and soundings which appeared fairly accurate. Each sounding had hundreds of data points, so the excel plots contained approximately two thousand data points. An example of one of these plots can be seen in Figure 3.2 showing a change in longitude over change in time (dlong/dt) plotted against altitude. More examples

of the excel plots can be seen in Appendix D. By viewing these excel plots and assigning different trial values in the 'MRS.for' program, the most realistic plots were produced. We can see the obvious outliers in Figure 3.2. The Fortran program used a limit of 0.001 deg/s or less for a change in longitude over a change in time. The 'MRS.for' Fortran code can be seen in Appendix B.

In order to prevent accurate data from being removed, it was important to refrain from making the limits too restrictive. The 'MRS.for' program not only output the quality checked RAOB raw data file, it also output an error file which contained the data lines removed from the original sounding (through quality

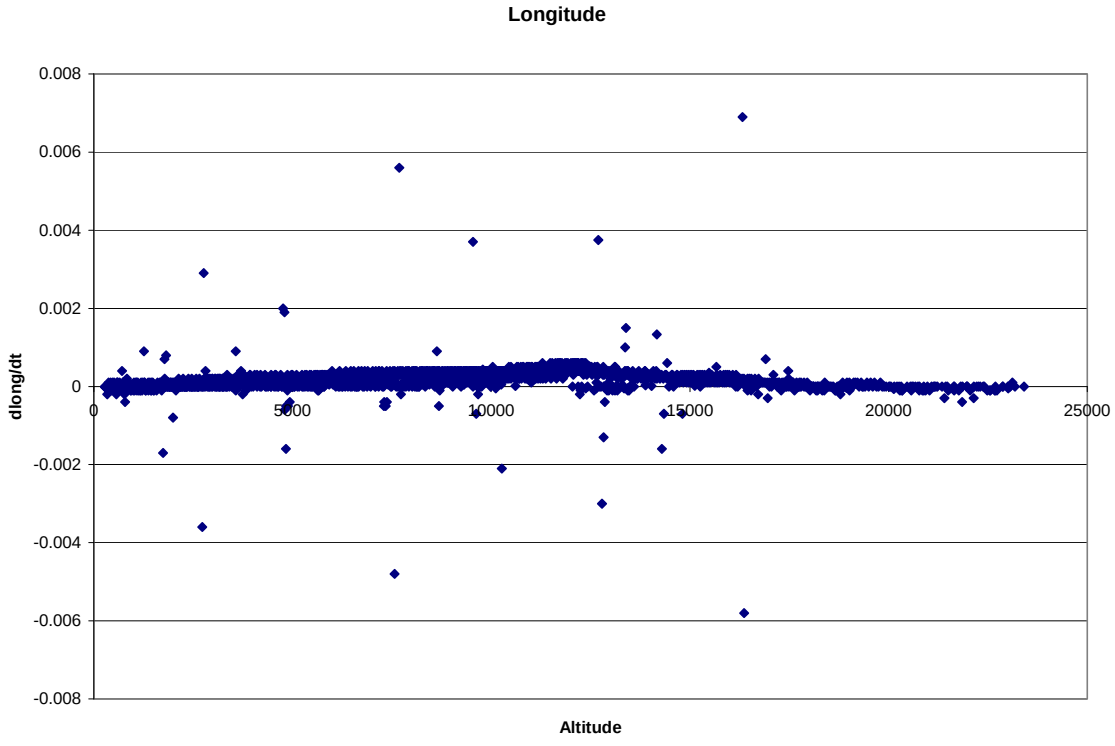

Figure 3.2. Excel plot showing the change in longitude over change in time (dlong/dt) versus altitude. CLASS soundings from the ELBOW 2001 project were used for this plot. Outliers can be seen clearly. Note that dlong/dt is in deg/s and Altitude is in m.

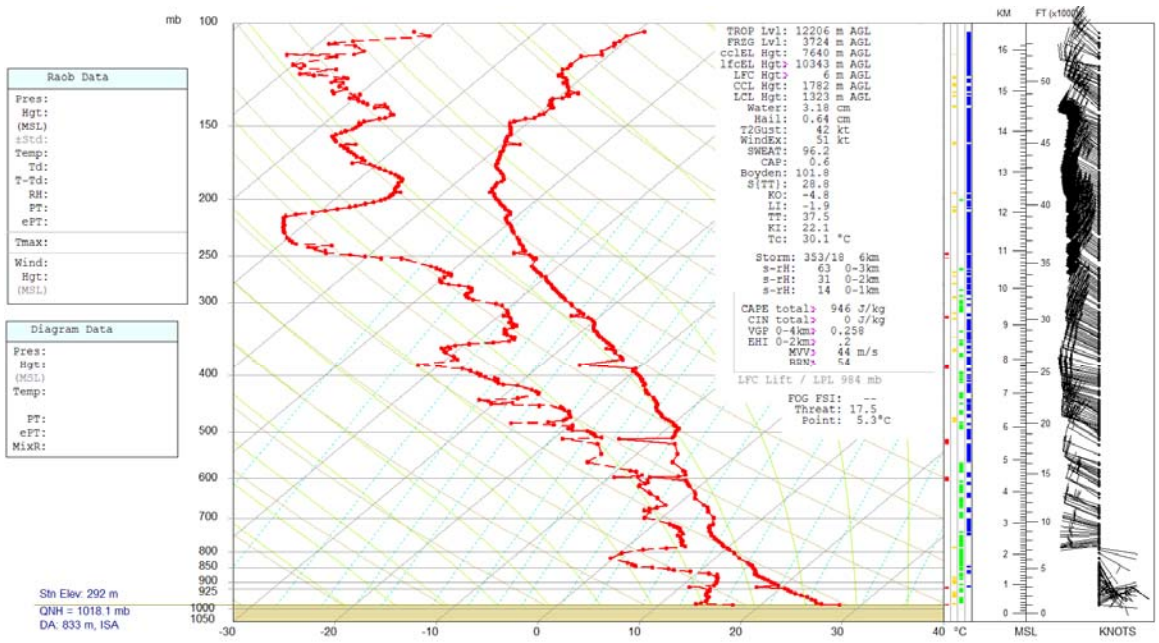

<u>Figure 3.3(a) and 3.3(b).</u> UWO Farm sounding for July 18, 2001 at 1800 UTC. Above (a) shows the sounding with the few unrealistic data spikes remaining after quality checking. Below (b) shows the sounding after the unrealistic spikes have been removed.

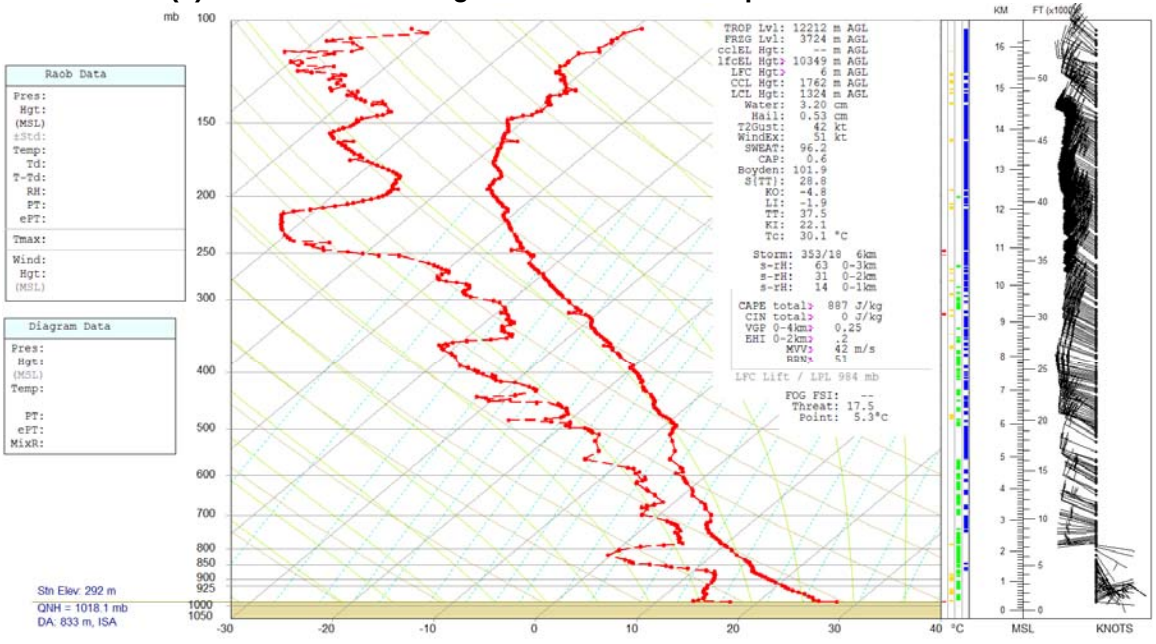

checking) and the reason why each was removed. The new profiles were viewed in RAOB and any of the few unrealistic spikes left in the data were removed by manually deleting the data in the raw data file. These manually 'modified' RAOB files were then saved as final radiosonde plots for further analysis. Twenty out of fifty four CLASS radiosondes were manually modified; sometimes only one or two data levels were removed manually. See Figure 3.3a and 3.3b for RAOB plots before and after remaining unrealistic data spikes were removed.

While working with these data, a sample CLASS sounding was sent to ERS. Shortly after, RAOB version 5.3 was released. This version ingested and quality checked the original CLASS data.

3.4 Aircraft Ascents and Descents

The aircraft measurements taken in flight during an ascent or descent, were also put into a raw data format in order to be displayed in RAOB. By doing this, the vertical structure of the atmosphere could be displayed for the heights covered by the aircraft. The program 'Aircraft.for' was written to:

- Check for vertical consistency in pressure and altitude
- Check the temperature is not less than the dewpoint
- Check if the 'sounding' begins at ground level or an elevated level
- Make height corrections to get the ground height above sea level and use the height above ground level for the data points in the sounding
- Write the data into the raw data format accepted by the RAOB program

It should be noted that there were some problems plotting the elevated measurements (flight measurements starting at a height above the ground) in the RAOB version being used at the time. RAOB required a surface station reference and assumed that the first data point in the profile (even if it was elevated) represented the surface location. This resulted in the mean sea level being shown at a level higher than it should be (comparing the data and sounding profile).

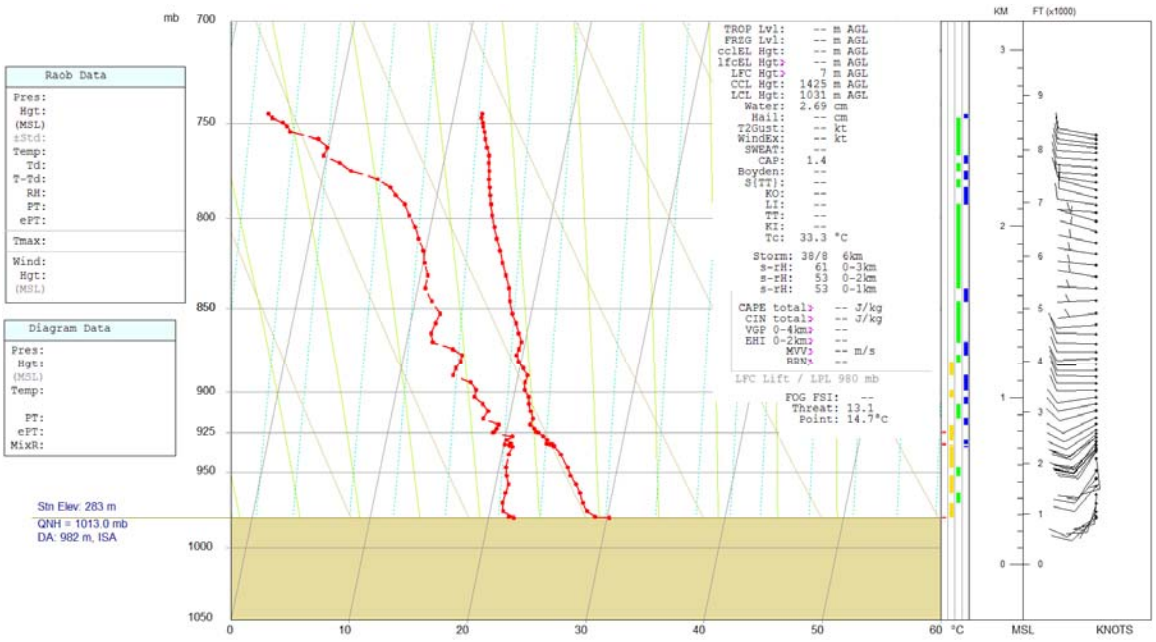

Figure 3.4. RAOB plot of data taken during aircraft descent on July 22, 2001 at 1947 UTC.

These profiles were simply meant to give a visual vertical plot of the variables. Anyone using the data for further analysis should be aware of these height problems especially if sounding indices are being calculated. For the purposes of plotting, it was assumed that RALT (from the original data) was the height above the ground and LALT was the height above sea level. A value of

-9999 was assumed to be an RALT value of zero. See Figure 3.4 for a sample plot of the aircraft data.

4. AURORA

Developed by Environment Canada, the Forecast Production Assistant (FPA) is a tool designed to provide assistance to forecasters in operational weather forecasting. As noted by Paterson et al. (1993), this software, which creates a workstation based on graphical images, has been distributed to a number of government and non-government meteorological offices. Environment Canada has also developed AURORA which is a research version of the FPA. This research tool has been designed to aid in research analysis. As noted by Greaves et al. (2001), it is geared towards nowcasting (or short term forecasting) research in order to develop new procedures to improve forecasts. AURORA has been used to conduct the ELBOW 2001 research, such as the low-level mesoscale boundary analysis (Chapter 5), cell initiation analysis (Chapter 6) and a more in depth view of specific case studies (Chapter 7).

By reference to a geographic map, with boundaries defined by the user, AURORA gives the user the ability to view, loop, interpolate, modify and overlay different sets of data and images. It also allows the user to manually draw in any type of boundary, such as synoptic fronts, lake breeze fronts, gust fronts, or whatever type of boundary the user chooses. Once these boundaries have been drawn into AURORA, they are automatically saved into an object database. For example, during the ELBOW 2001 low-level boundary analysis (conducted through AURORA) the scientists were able to visually overlay radar, satellite, and mesonet station data in order to pinpoint where the low-level boundaries (such as

lake breeze fronts) existed. They were then able to draw these boundaries on the workstation screen within AURORA, and these were saved into the database for further analysis.

One of the advantages of AURORA is that it is fully configurable. The ELBOW 2001 data could be ingested and displayed in an appropriate way. Patterns could be created for different types of low-level mesoscale boundaries. This is the first time that AURORA has played a major role in a research project and the present project provided an opportunity for an evaluation of this research tool.

This Chapter summarizes how AURORA has been set up in order to aid in research for ELBOW 2001. The following sections provide a look at the AURORA configuration and setup, the data ingested into AURORA for analysis and the low-level boundary patterns utilized.

4.1 AURORA Configuration and Setup

AURORA has a number of main files that were used to ingest and display the ELBOW 2001 data in order for further analysis:

- The *configuration* file is used to declare fields available for AURORA. This is where the data available were declared. The configuration file, for the ELBOW 2001 data, was called ‘Config.elbow’.
- The *presentation* file allows the user to specify the way the data should be displayed. For the ELBOW 2001 data this was called ‘Presentation.elbow’.

- The *setup* file allows the user to indicate the location of the files containing the new data, so that AURORA knows where to access them (a basic directories list). It also allows the user to define the target map area (see Figure 4.1) and the colour of the background to be viewed through AURORA. The user can also declare which data fields are to be edited. There were a number of setup files, which were modified for ELBOW so that more than one person could work with the data at a time. All depictions (down to 5 min intervals) or just hourly depictions could be viewed. These modified files included: 'Setup.elbow', 'Setup.elbow_hourly', 'Setup.elbow_lisa' and 'Setup.elbow_dave'.
- The *image* file allows the user to specify the image metafiles, such as radar and satellite, to be ingested into AURORA. It also allows the user to specify the colour tables to be used to display these data. The image file, for the ELBOW data, was called 'Image.elbow'.

Appendix E includes a list of the data sets/fields for which AURORA has been configured and setup to ingest. The main files, listed above, have been modified for an appropriate display of these data. For example, the modifications made to the AURORA files for the 1.0 km CAPPI metafiles can be seen in Appendix F. Also, the modifications made to the AURORA files for some of the cell tracking data can be seen in Appendix G. Modifications similar to these have been made for each of the data fields listed in Appendix E.

The configuration and setup of AURORA was a collaborative effort of the ELBOW 2001 researchers that were using the tool for further analysis. These researchers included the author and Dr. David Sills of the Cloud Physics and Severe Weather Research Section, Environment Canada. Help needed in becoming familiar with AURORA or the configuration/setup was provided by the FPA/AURORA Technical Support team at King City Radar.

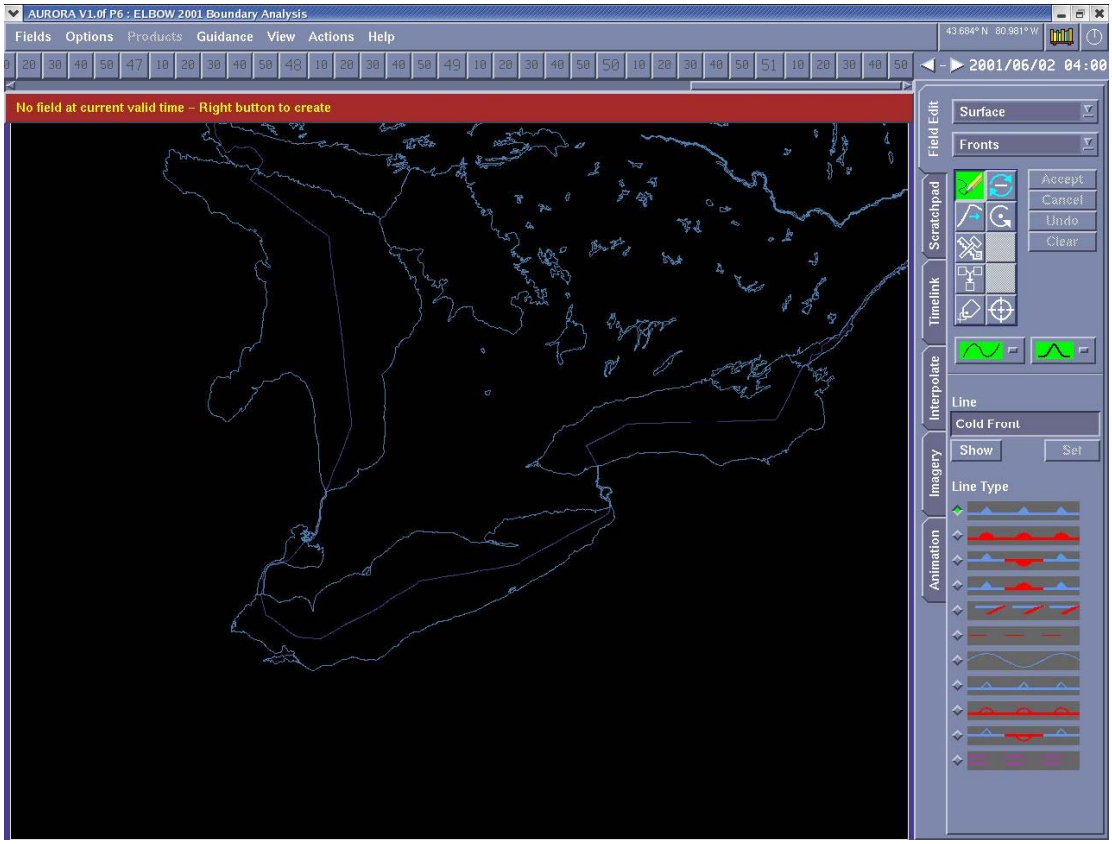

Figure 4.1 AURORA image showing the target map area covered by the ELBOW 2001 setup.

4.2 ELBOW Data Sets and AURORA

4.2.1 Satellite Data

GOES-8 EA sector water vapour, GL and EA sector infrared, and GL and LB sector visible satellite data were extracted from DAT tapes and ingested into

AURORA through the setup and configuration files. The EA sector shows Eastern Canada, the GL sector shows the area containing the Great Lakes and the LB sector shows a closer look at the Great Lakes (making this particular sector useful in identifying lake breeze fronts, as Southwestern Ontario is depicted in great detail). See Figure 4.2 for a sample image of the GOES-8 visible satellite as seen through AURORA.

Different colour tables were made, through AURORA, to enhance the images as needed. For the visible, brighter images allowed the user to see the lake outline and cumulus development clearly. These bright colour tables were useful for the early or late daylight hours when sunlight was not at its peak.

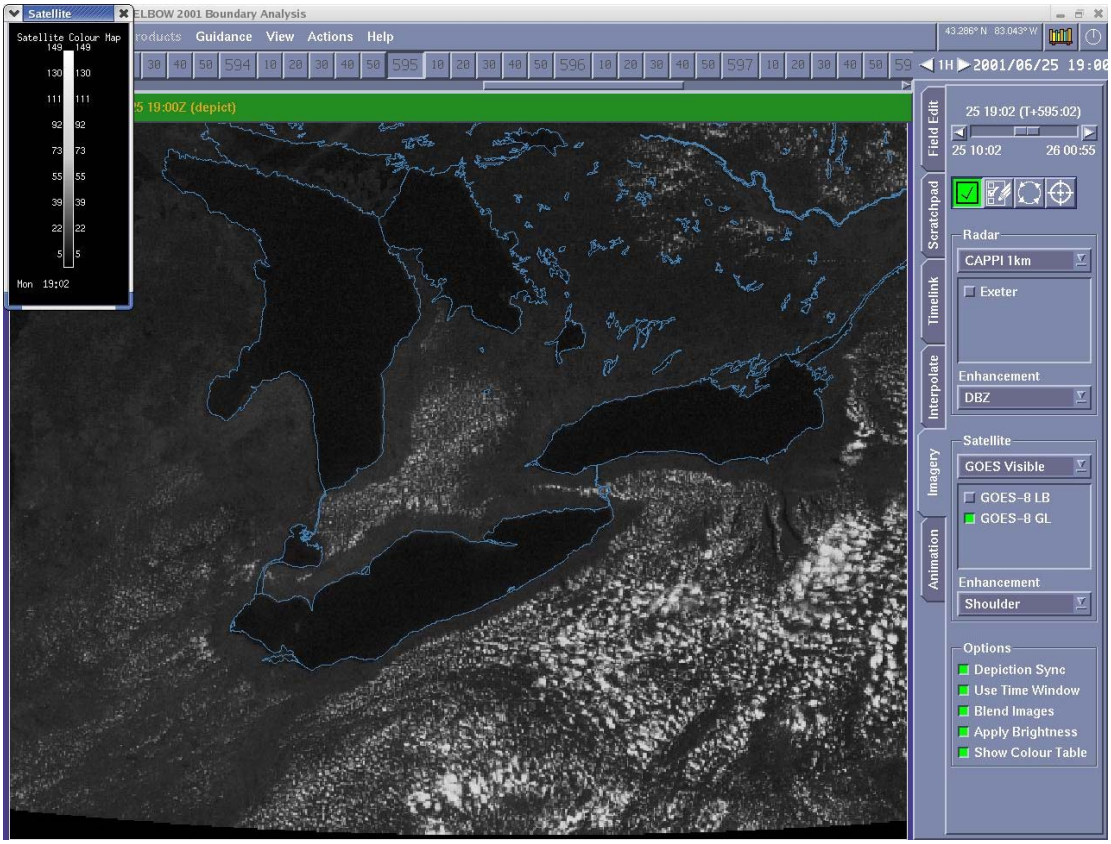

Figure 4.2 A sample of the GOES-8 visible satellite as seen through AURORA.

Colour tables which were dimmer allowed the user to see detail in the convective regions in the middle of the day.

4.2.2 Radar Data

Raw data files (IRIS files) for Exeter radar were taken from CDs stored at the King City Radar Facility. Metafiles for the Exeter radar reflectivity and radial velocity were created by running the raw IRIS files through the Unified Radar Processor (URP). Aurora was configured to accept these data.

Again, images could be enhanced by different colour tables. A wider range of colours would allow the user to see more detail in the radar data. Colour tables could also be made to highlight areas of stronger convection. For example

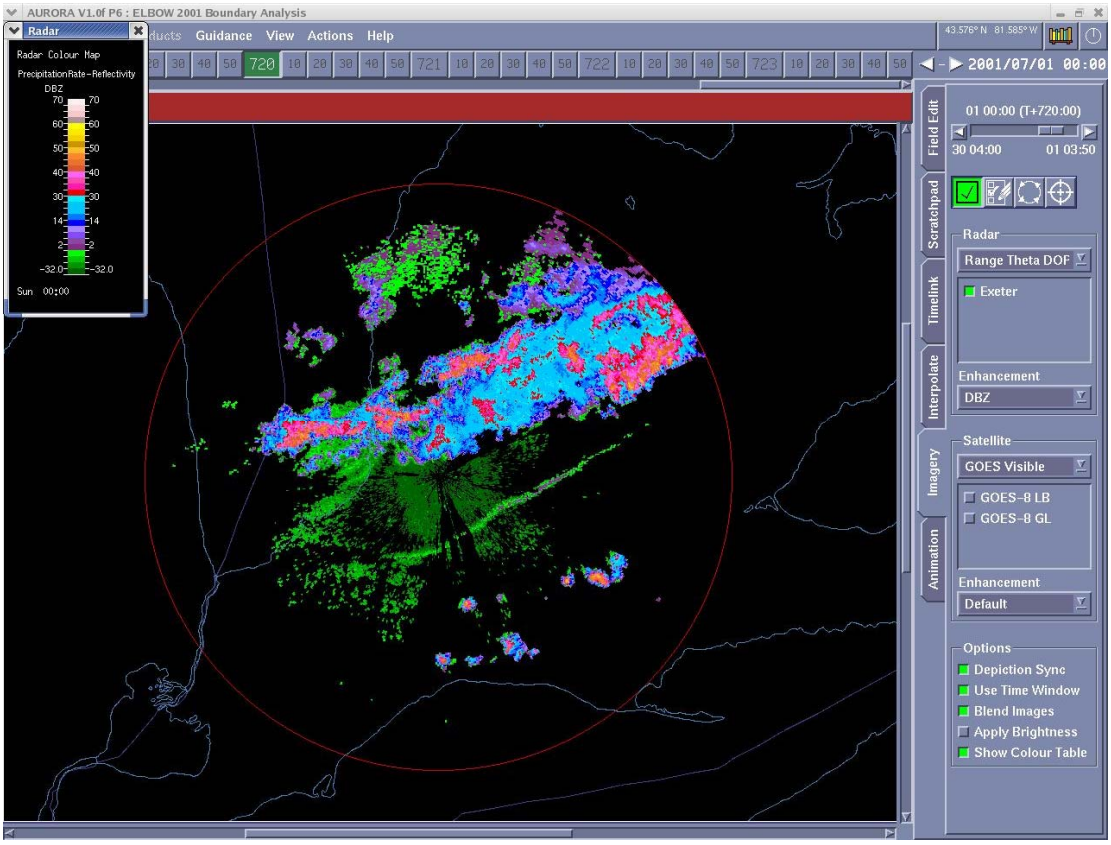

Figure 4.3 A sample image of the Exeter 0.5 degree reflectivity for July 1, 2001 at 0000 UTC as seen through AURORA. Notice the colour table displayed in the upper left corner.

one colour table allowed the reflectivity bins to be grey below 40 dBZ and brighter colours above 40 dBZ. This made it clear which cells were well developed.

Figure 4.3 shows the Exeter radar reflectivity as seen through AURORA. Figure 4.4 shows the Exeter radar radial velocity. The corresponding colour tables, for these images, can be seen in the upper left hand side of the figure.

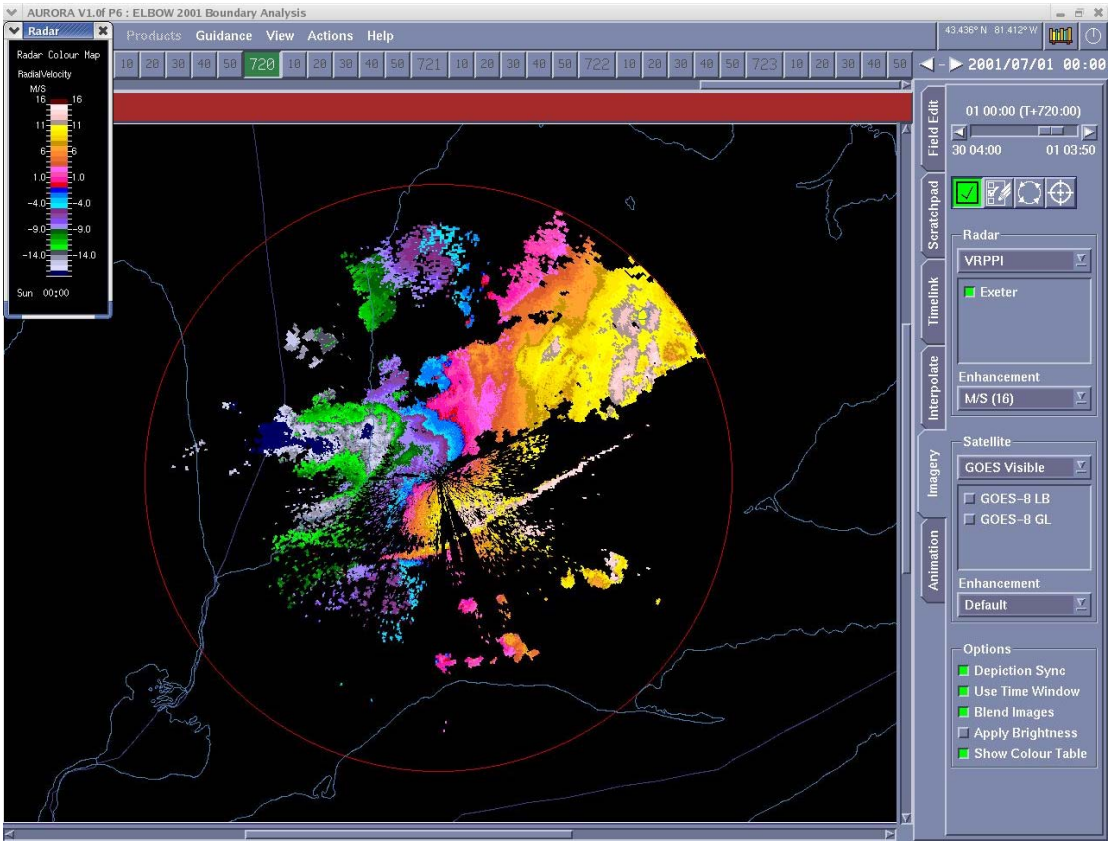

Figure 4.4 A sample image of the Exeter radial velocity for July 1, 2001 at 0000 UTC as seen through AURORA. Notice the colour table in the upper left corner.

4.2.3 Mesonet Data

Mesonet data, from stations within the study region and the area surrounding, were formatted into a 'metafile' format which was accepted by AURORA. Formatting was done through the use of the FORTRAN programming

language. The mesonet stations included: Coastwatch, Ridgetown, OME, MSC and 14 stations set up specifically for the ELBOW 2001 project by York University (approximate locations can be seen in Figure 2.2). Separate files were created for each of these mesonet station types. Data files were created for the frequency at which the data were taken. ELBOW mesonet stations collected data every 5 or 10 minutes, therefore, data files for these time intervals were created.

AURORA was configured to accept the Coastwatch, Ridgetown, OME, MSC and York mesonet metafiles as 'scattered field' data. This means that these data were plotted with markers on the target map area. The presentation file was modified to mark the locations of the stations with circles. It was also modified to display wind barbs, and the temperature and dewpoint data to the upper right and bottom right of the circle respectively.

All these data were displayed in shades of yellow. See Figure 4.5 for a display of the mesonet station data as seen in AURORA. Depending on the type or set of stations, the shade of yellow was slightly different. This made the user aware of the different data sets when viewing all these mesonet data together.

Some data were displayed beside the mesonet station markers (temperature and dewpoint), but in order to see values that were not displayed, the field could be sampled. See Figure 4.6 to see the sample box (upper left) that appears when a station is sampled in AURORA. All the station data that

have been ingested into AURORA could be configured to be displayed in this box.

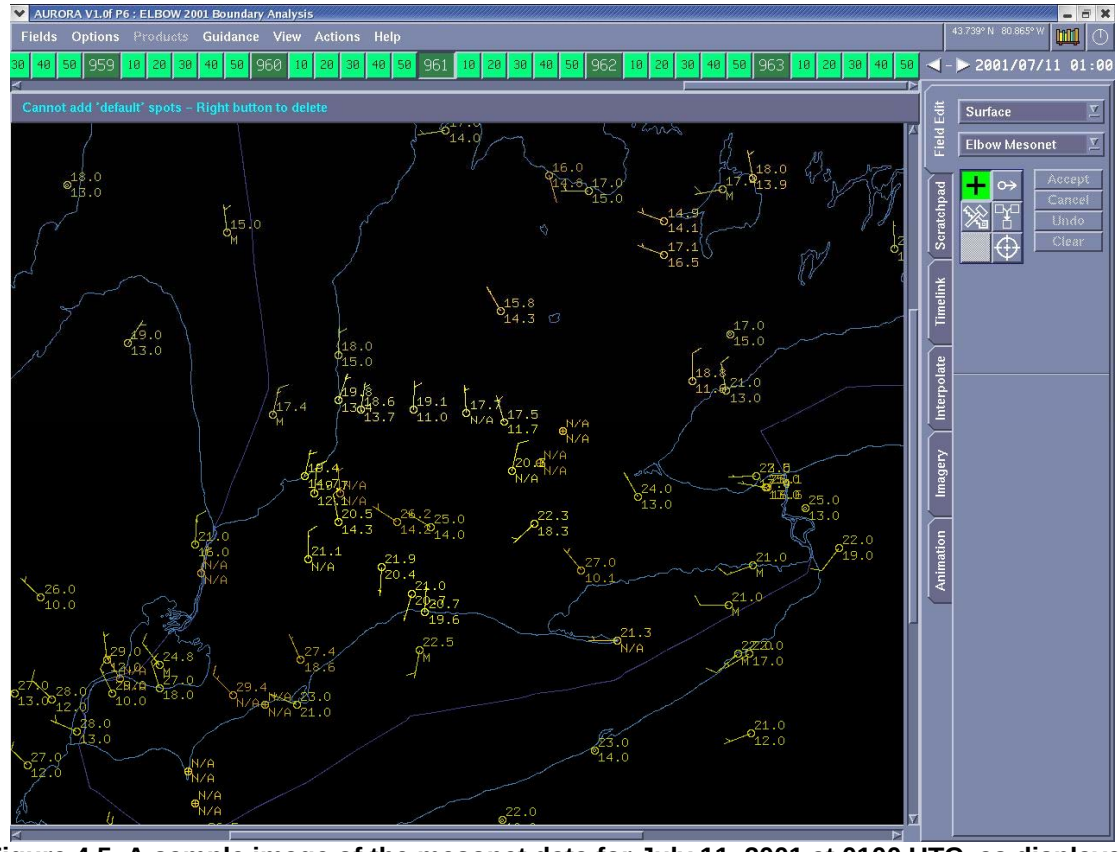

Figure 4.5 A sample image of the mesonet data for July 11, 2001 at 0100 UTC, as displayed in AURORA. Notice the wind barbs from each circle (representing a station) and the temperature and dewpoint displayed to the upper right and lower right respectively.

4.2.4 Mesoscale Boundary Patterns

A number of patterns were created in order to mark the boundary identifications specified in Chapter 5. Patterns were created for a Lake Erie lake breeze front, a Lake Huron lake breeze front, a Lake Ontario lake breeze front, a Lake St. Clair lake breeze front, an outflow boundary (or a gust front originating from a storm), other boundaries (including horizontal convective rolls, synoptic boundaries and boundaries of unknown origin), a land breeze front, etc.

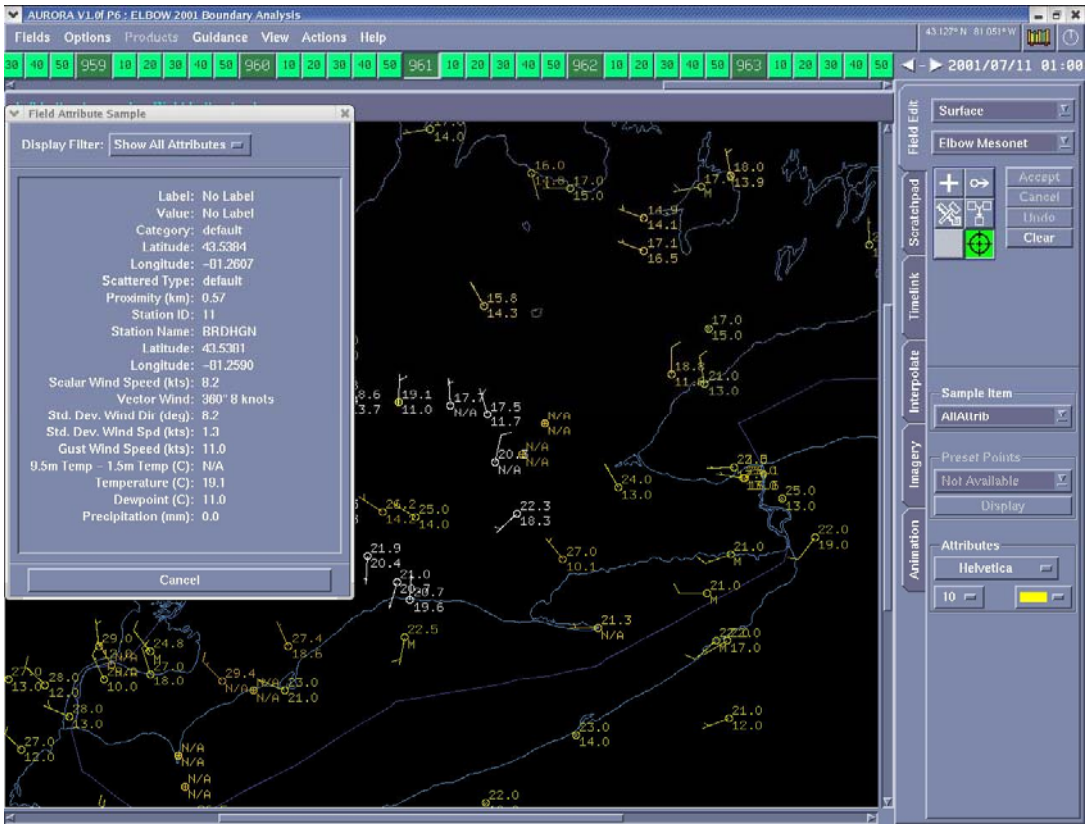

Figure 4.6 A sample image of one of the York University mesonet stations being sampled in AURORA. Notice the data corresponding to the station in the 'Field Attribute Sample' box to the upper left.

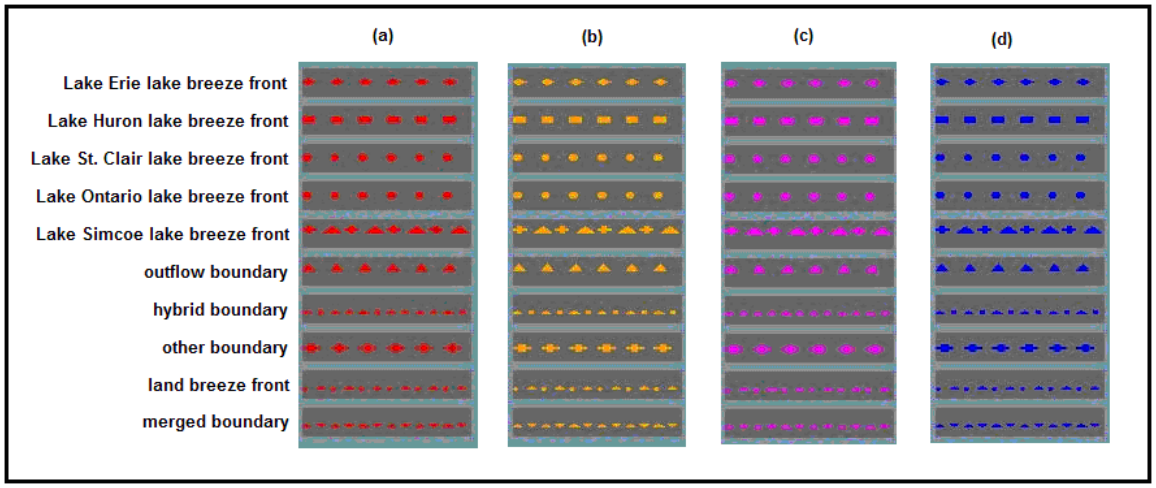

Figure 4.7. Shown from left to right: boundary pattern used for (a) the mesonet analysis, (b) the radar analysis, (c) the satellite analysis and (d) the integrated analysis. Notice each boundary type has the same pattern for each analysis but are in red, orange, magenta and blue corresponding to the mesonet, radar, satellite and integrated analyses respectively. Boundaries are shown here as they can be seen in AURORA.

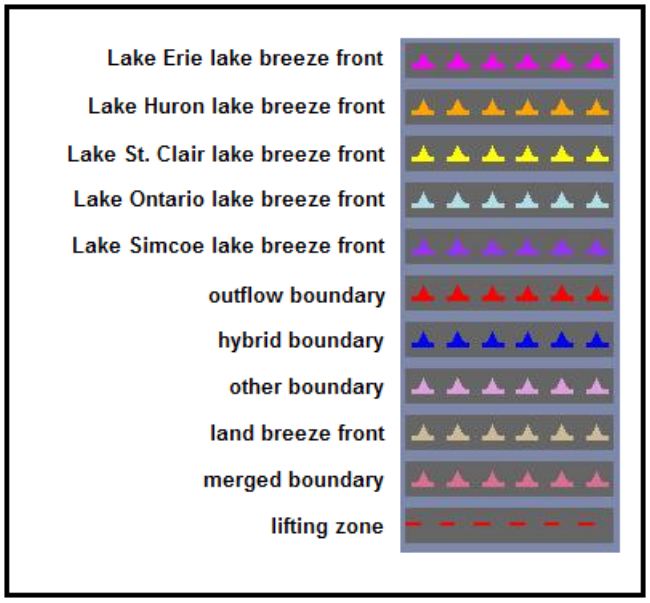

Figure 4.8. Boundary patterns for the Final 'truth' set. Notice that all boundary types have the same pattern but are different colours. Boundaries are shown here as they are seen in AURORA.

See Figure 4.7a, b, c and d for boundaries corresponding to the Mesonet, Radar, Satellite and Integrated analyses respectively. As can be seen, these all have the same patterns for each boundary type, but different colours depending on the analysis being done. See Figure 4.8 for the boundaries corresponding to the Final 'truth' set. Notice all of the boundaries have the same pattern but are different colours depending on the boundary type. A pattern used to identify a lifting zone is also shown in this set and is only occasionally used for case studies, as will be shown in Chapter 7.

To see an example of how these boundaries have been used on an ELBOW study day, see Figures 5.1 to 5.4 which show the mesonet, radar,

satellite and integrated boundaries respectively, for June 25, 2001 at 1800 UTC. Figure 5.5 shows the Final boundaries for the same time.

4.2.5 Cell Identification and Cell Tracking

In order to study storm development in relation to low-level mesoscale boundaries, as in Chapter 6, a number of data sets had to be created. First the Conventional Scan Exeter radar raw IRIS files were extracted from the CDs, at Environment Canada's King City Research Facility, by using a pre-existing extraction program called URPRadarEx.jar. This was done for the full study period: June 1 to August 31, 2001.

A file called 'CAPMAX.pl' was used to obtain 1.0 km CAPPI and 1.0 km MAXR metafiles through URP. This program was slightly modified from a pre-existing program called 'sfeed_CAPPI_MAXR.pl' obtained from Sudesh Boodoo at the King City Research Facility.

These metafiles were then used to obtain cell identification data for specific threshold values. Again, pre-existing PERL scripts (obtained at King City Research Facility) were modified in order to obtain these data. The PERL scripts ran the metafiles through the URP cell identification algorithm, and then ran the cell identification data through the URP cell tracking algorithm. Note that these URP algorithms have been based on the concepts and methodology behind the Thunderstorm Identification, Tracking, Analysis and Nowcasting (TITAN) algorithm, developed by the National Center for Atmospheric Research (NCAR). Details on TITAN are covered by Dixon and Wiener (1993).

Cell identification and tracking was collected for thresholds of 30, 40 and 60 dBZ for both the 1.0 km CAPPI and 1.0 km MAXR metafiles. The 1.0 km CAPPI is the reflectivity at a height of 1.0 km and the 1.0 km MAXR displays the maximum reflectivity found from a height of 1.0 km and up. These cell identification and tracking data were collected for every 10 minutes, since there were radar metafiles available for this time interval.

The cell identification and tracking data were initially collected for all 3 thresholds, requiring a minimum of two pattern vectors for the cell to be identified. Pattern vectors are specified trajectories or vectors that the radar is sampling, containing at least two consecutive bins of the dBZ threshold (or greater) in question. After viewing a few days worth of data through AURORA, the minimum pattern vector requirement was changed to 6 for 30 dBZ, 4 for 40 dBZ and 1 for 60 dBZ. These data were found to be more accurate, therefore the data for the full period were collected with these settings. A more detailed explanation of pattern vectors and how the URP cell identification works will be covered in Chapter 6.

Once these data were collected, there were new PERL scripts written to format these data for AURORA. See Appendix H for a sample metafile, resulting from these PERL scripts, for the 40 dBZ, 4 pattern vector (minimum) cell tracking corresponding to the 1.0 km CAPPI radar data. AURORA was then configured to accept these new data. Fields which could be displayed in AURORA included: Cell identification, full cell tracks (showing the location of the cell at displayed

times) and the present cell (showing the present location of the cell and its track number). See Appendix G for the modification to the configuration and setup files in order for AURORA to accept the data displayed in Appendix H.

Appendix F includes the modifications to the configuration and setup files in order for AURORA to accept the 1.0 km CAPPI data. This was done similarly for the 1.0 km MAXR data. Colour tables were created for the 1.0 km CAPPI and 1.0 km MAXR data. Basic colour tables highlighting dBZ levels, which were already used for the reflectivity and radial velocity, were applied here. See Figures 4.9 and 4.10 for a sample image of the 1.0 km CAPPI and 1.0 km MAXR data respectively. New colour tables were also created in order to highlight 30,

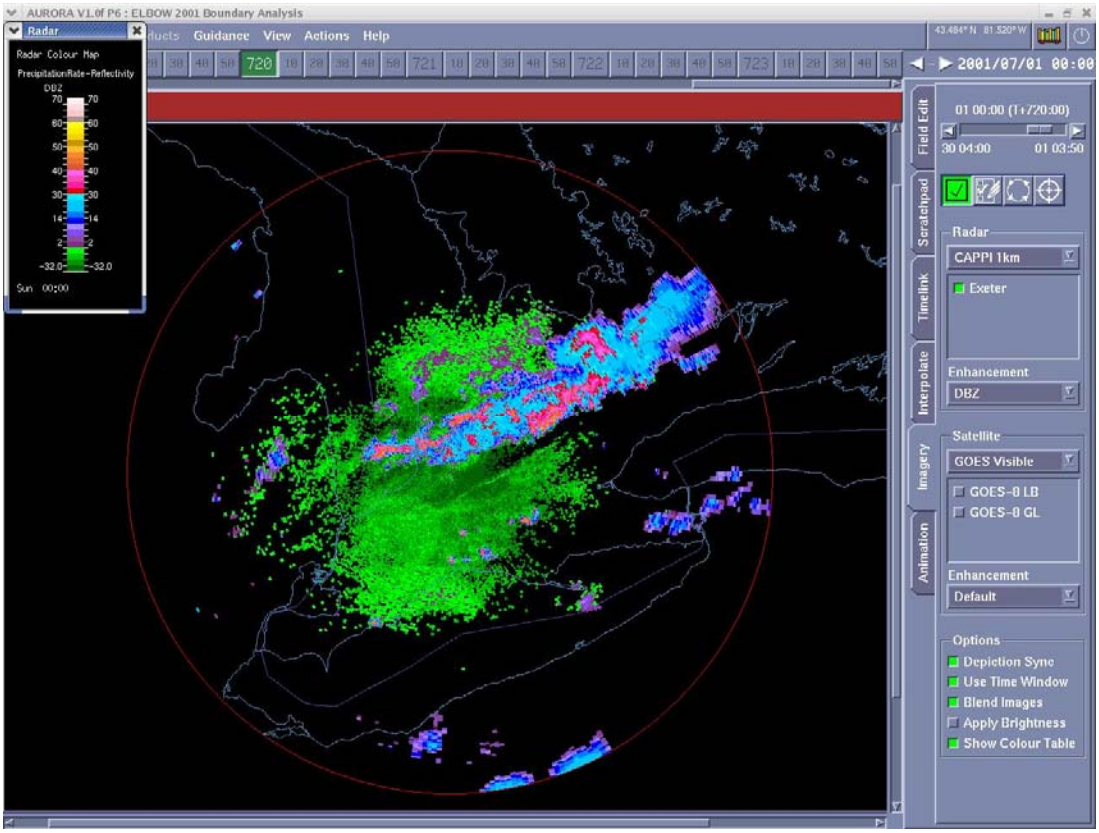

Figure 4.9. A sample image of the Exeter 1.0 km CAPPI for July 1, 2001 at 0000 UTC, as viewed through AURORA. Notice the colour table to the upper left corner.

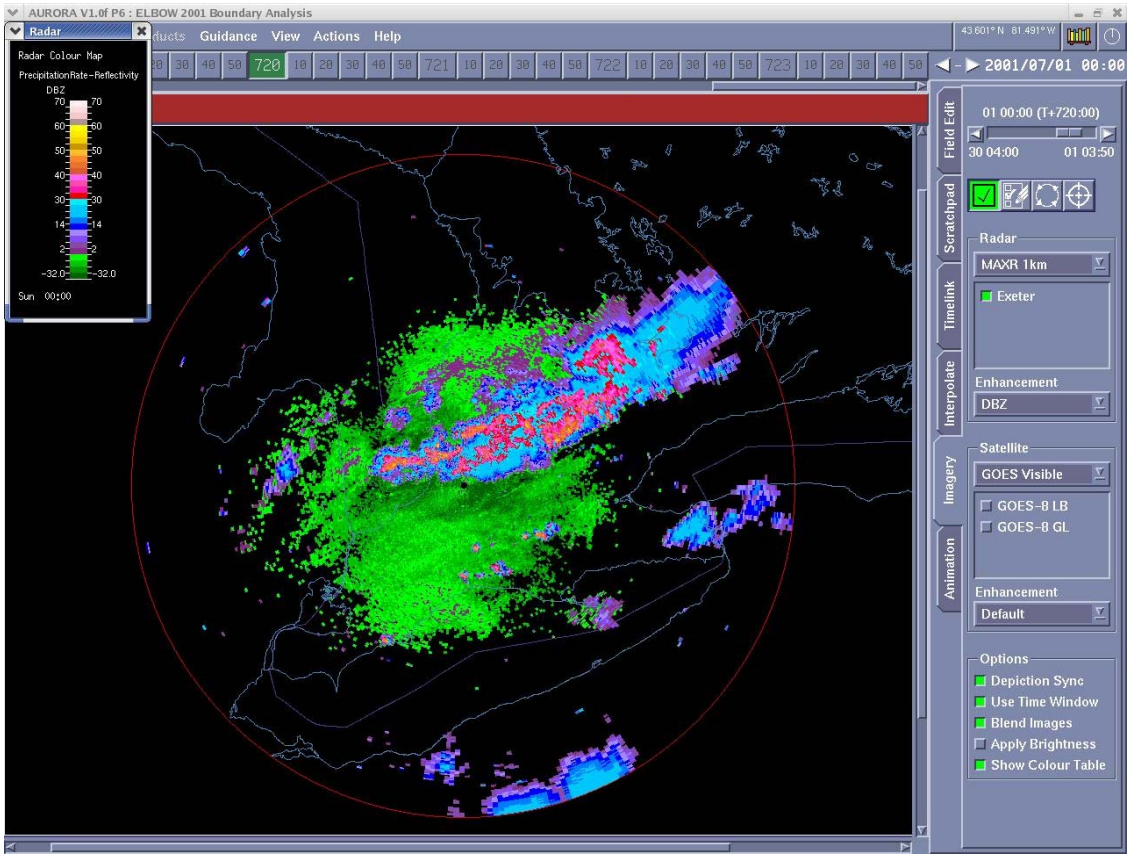

Figure 4.10. A sample image of the Exeter 1.0 km MAXR for July 1, 2001 at 0000 UTC, as viewed through AURORA. Notice the colour table in the upper left corner.

40 and 60 dBZ data. For example, the colour table to highlight the 40 dBZ data showed all the bins below a value of 40 dBZ to be grey and all the bins with a value of 40 dBZ or greater to be blue. This made it easier to see how the cell identification algorithm produced the numbered cells that were being viewed through AURORA. See Figure 4.11, showing the 1.0 km CAPPI image with reflectivity values 40 dBZ or greater highlighted. The colour table can be seen the in upper left side of the image.

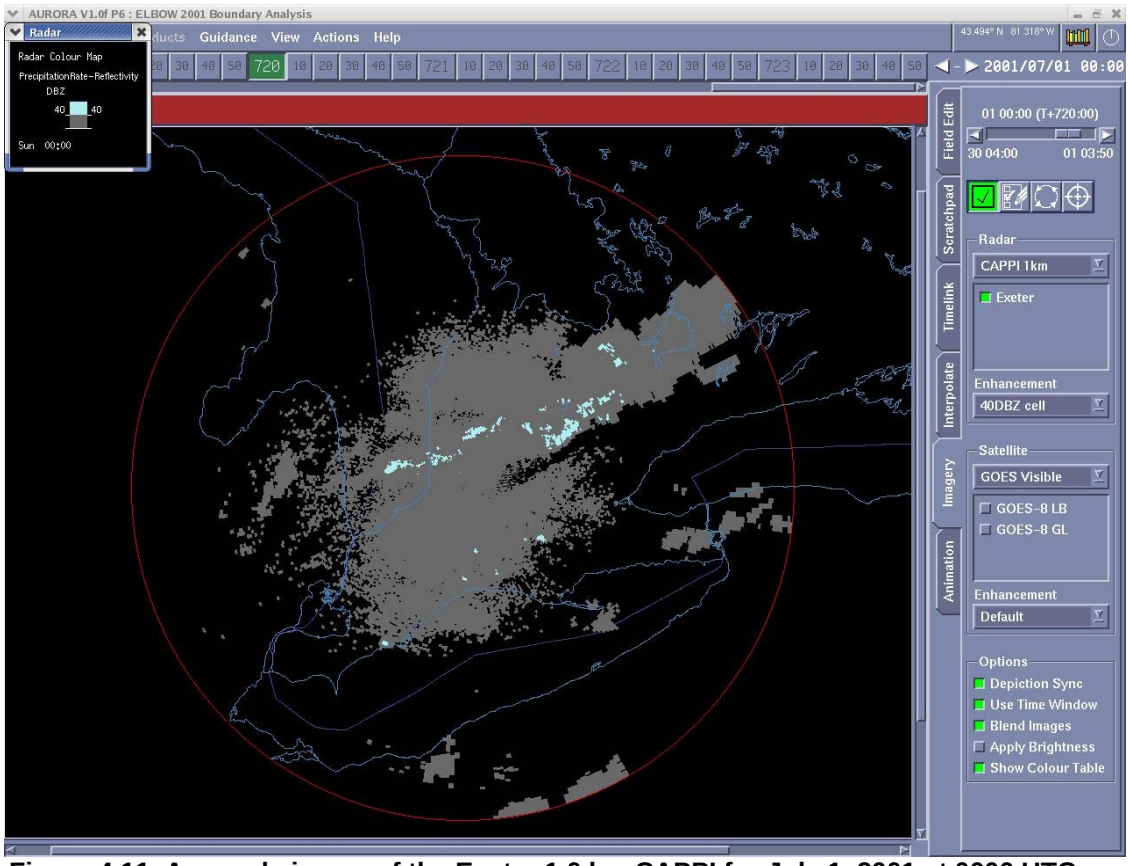

Figure 4.11 A sample image of the Exeter 1.0 km CAPPI for July 1, 2001 at 0000 UTC, as viewed in AURORA. This image has had a colour table applied to make all bins below 40 dBZ to be grey and all bins with a value of 40 dBZ or higher to be blue. See the colour table in the upper left corner.

4.2.6 Other Data and Applications

A 'map setting' option was added to display the fixed radiosonde station locations in green (see Figure 4.12). This was useful when looking at case studies in Chapter 7. It was very useful to know the exact location of the radiosonde launches in respect to the low-level mesoscale boundaries.

An option to display the mobile radiosonde locations was also added. These were displayed as blue circles. The date and time the radiosonde was

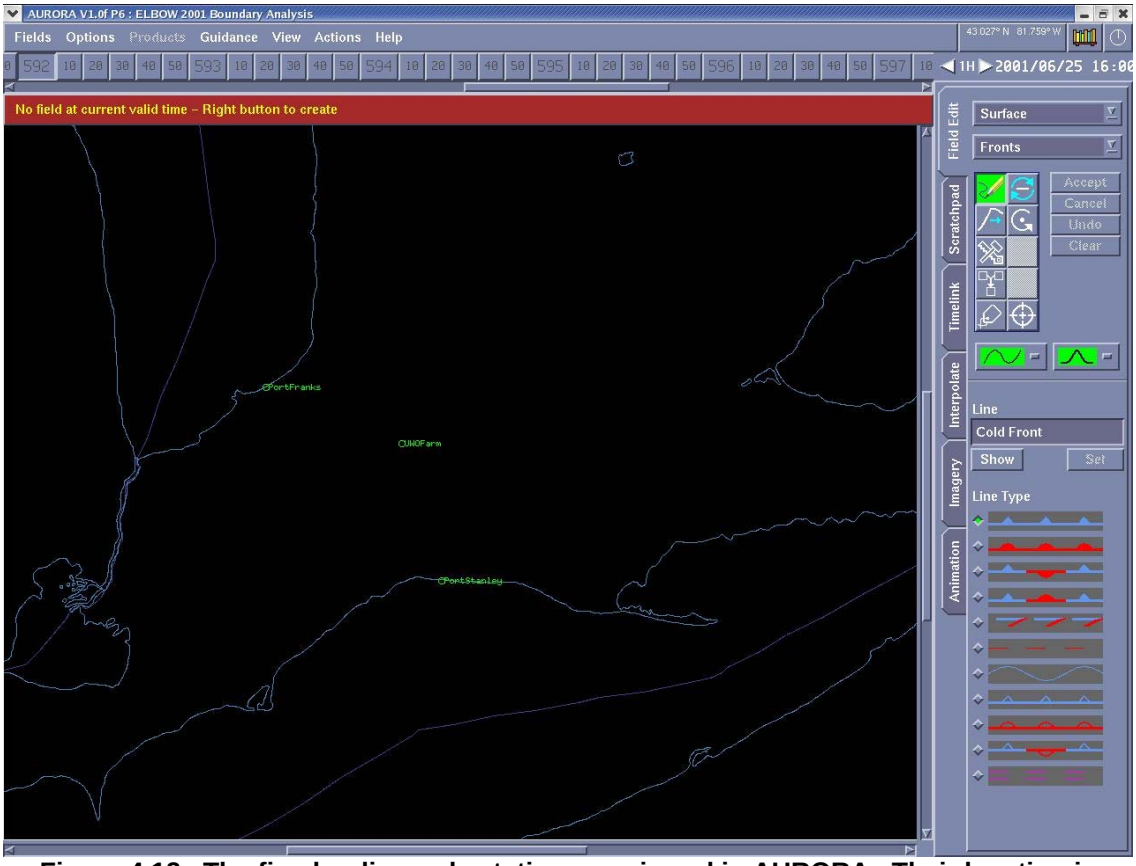

Figure 4.12. The fixed radiosonde stations as viewed in AURORA. Their location is marked with a green circle. The station name is also displayed to the right of the circle.

launched was displayed to the right side of the circles (see Figure 4.13). Again, it was useful to visualize where these were launched in relation to the mesoscale boundaries.

The tornado data from the TOP database produced by Dr. David Sills was also added as a display option in AURORA. The strength of past tornadoes, from F0 to F5, were shown depending on the size of the marker displaying the location.

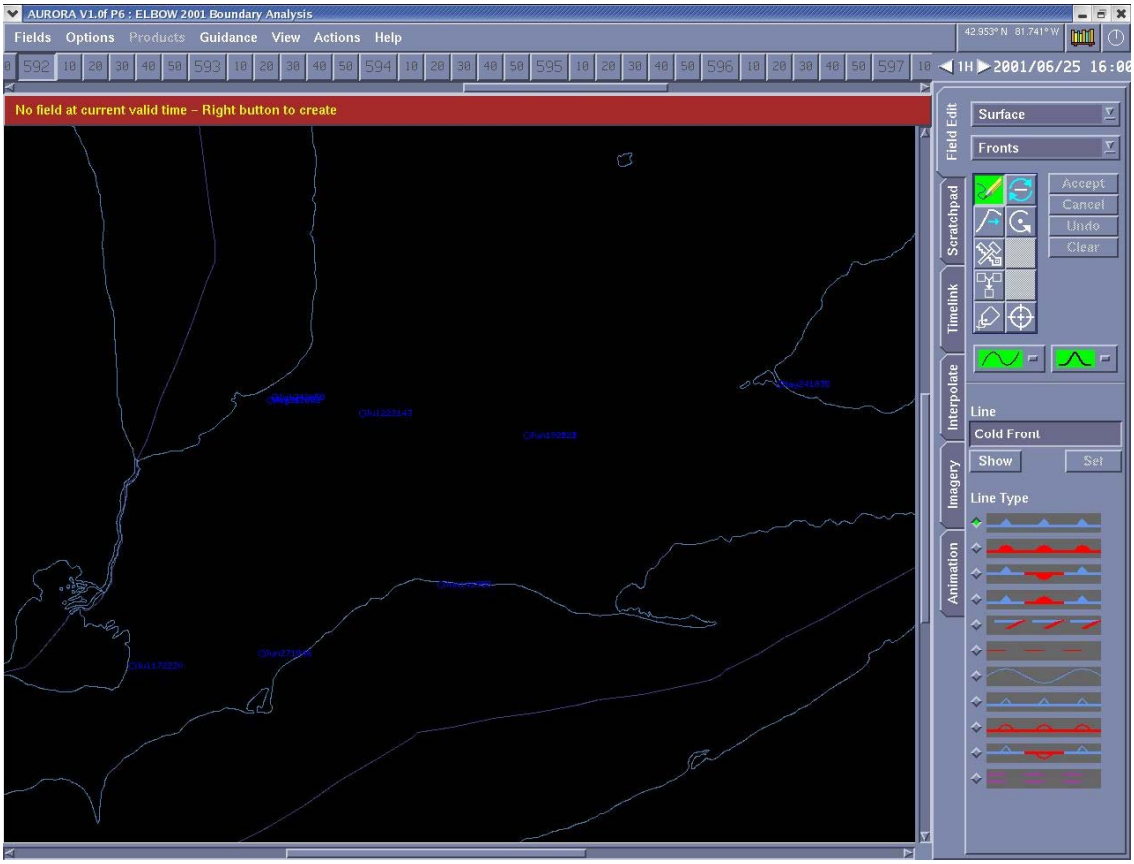

Figure 4.13. The locations where the Mobile Jeep unit launched radiosondes as viewed through AURORA. The locations the radiosondes were launched from are marked by blue circles. The date and time of the radiosonde launch is also displayed to the right of the markers.

It should be noted that some of the configurations for AURORA from ELBOW 2001 have also been used for the Research Support Desk (RSD) at Environment Canada (Downsview location). To be more specific, the patterns used to identify low-level mesoscale boundaries have been used, operationally, at the RSD. Methods to identify low-level mesoscale boundaries (to be discussed in Chapter 5) have also been applied by researchers at the RSD.

AURORA is a research version of the FPA and many of the features added to each version were being tested by the author doing the research discussed in this thesis. When AURORA was initially being used for ELBOW

2001, the imagery (such as radar and satellite) had just been added. In using AURORA, bugs or problems found by the author and Dr. David Sills were reported to the FPA/AURORA developers. Suggestions were also made for additional changes/functions to the program which would be useful to users of later versions.

4.3 Summary

Overall AURORA has proven to be an excellent research tool for the ELBOW 2001 project analysis. Specifically, it has been very useful as a tool for viewing and comparing data fields, drawing and storing low-level mesoscale boundaries and synoptic fronts, and analysing full data sets and case studies. It has the potential to be very useful in future research projects and in the development of new nowcasting techniques to improve operational forecasts.

5. Low-Level Mesoscale Boundary Identification and Evaluation

In order to perform further analysis of the ELBOW 2001 data from a nowcasting and severe weather viewpoint, the low-level mesoscale boundaries had to be identified. A number of analysis methods, using different data sets, were applied in order to distinguish which was the most accurate and useful for further studies. Statistical techniques, including a contingency table approach and a correlation approach, were used to evaluate these methods.

5.1 Analysis Methods

The low-level mesoscale boundary identification exercise was a collaborative effort with Dr. David Sills, from the Cloud Physics and Severe Weather Research Section, Environment Canada. Low-level boundaries were identified for each hour of June 1 to August 31, 2001. The boundaries were identified over the full three month period using the AURORA research tool and four different analysis methods. These were:

- ***Mesonet Analysis:*** The boundaries were identified using only the mesonet station data (see Figure 5.1). These included information from Coastwatch, OME, Ridgetown, and MSC, as well as 14 stations set up for the ELBOW 2001 project.
- ***Radar Analysis:*** The boundaries were identified using only the reflectivity and radial velocity images from Exeter radar (see Figure 5.2).
- ***Satellite Analysis:*** The boundaries were identified using only the GOES-8 visible satellite images (see Figure 5.3).

- ***Integrated Analysis:*** The boundaries were identified by viewing all the data sets above simultaneously (including mesonet, radar and satellite). See Figure 5.4 for an example.

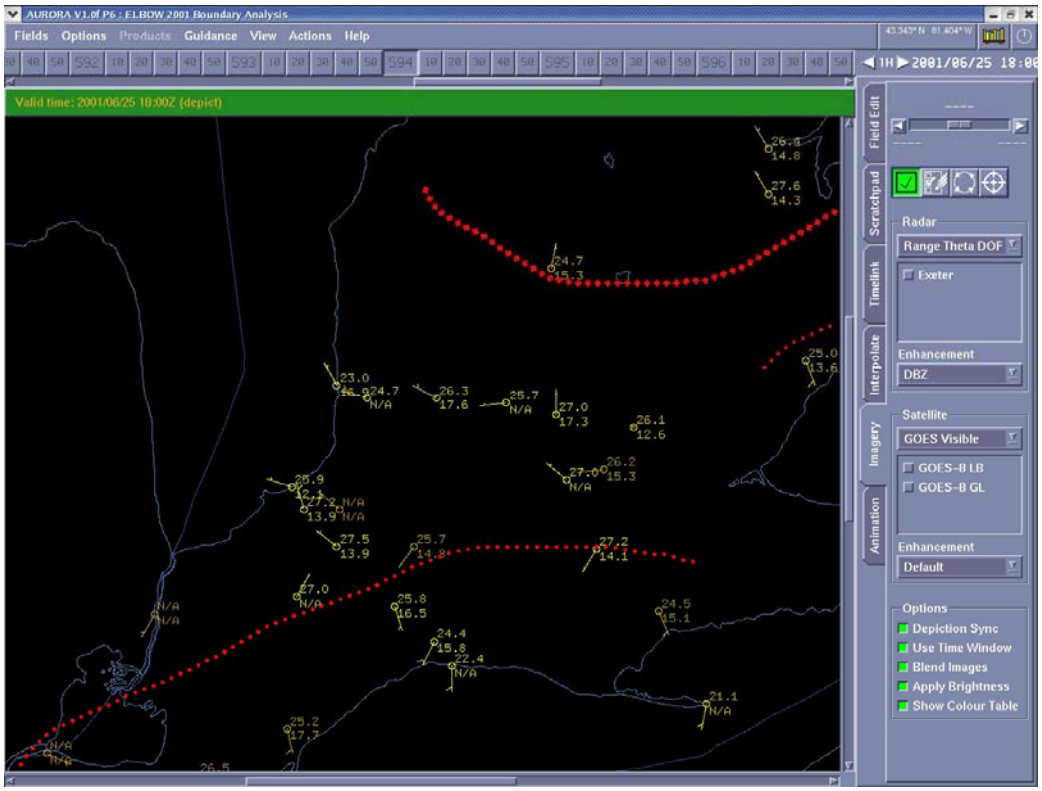

Figure 5.1. An example of the mesoscale boundaries identified using the Mesonet analysis for June 25, 2001 at 1800 UTC. Note these boundaries were all identified using red patterns.

All mesoscale boundary types were identified. These types included:

- *lake breeze fronts*
- *land breeze fronts*
- *'merged' boundaries* (the result of two lake breeze fronts interacting)
- *'hybrid' boundaries* (the result of a lake breeze front interacting with another boundary type)

- *'outflow' boundaries* (storm gust front)
- *'other' boundaries* (this included well developed horizontal convective rolls and boundaries in which the origin was unknown).

Semi-objective criteria were used to identify the boundaries in each analysis. Criteria were written for each data type and included positive, negative and ambiguous factors contributing to boundary identification. See Table 5.1 for the criteria to identify lake breeze fronts. The criteria used to identify all the different types of low-level mesoscale boundaries can be found in Appendix I. The criteria were laid out by Dr. David Sills with some input/modifications by the author.

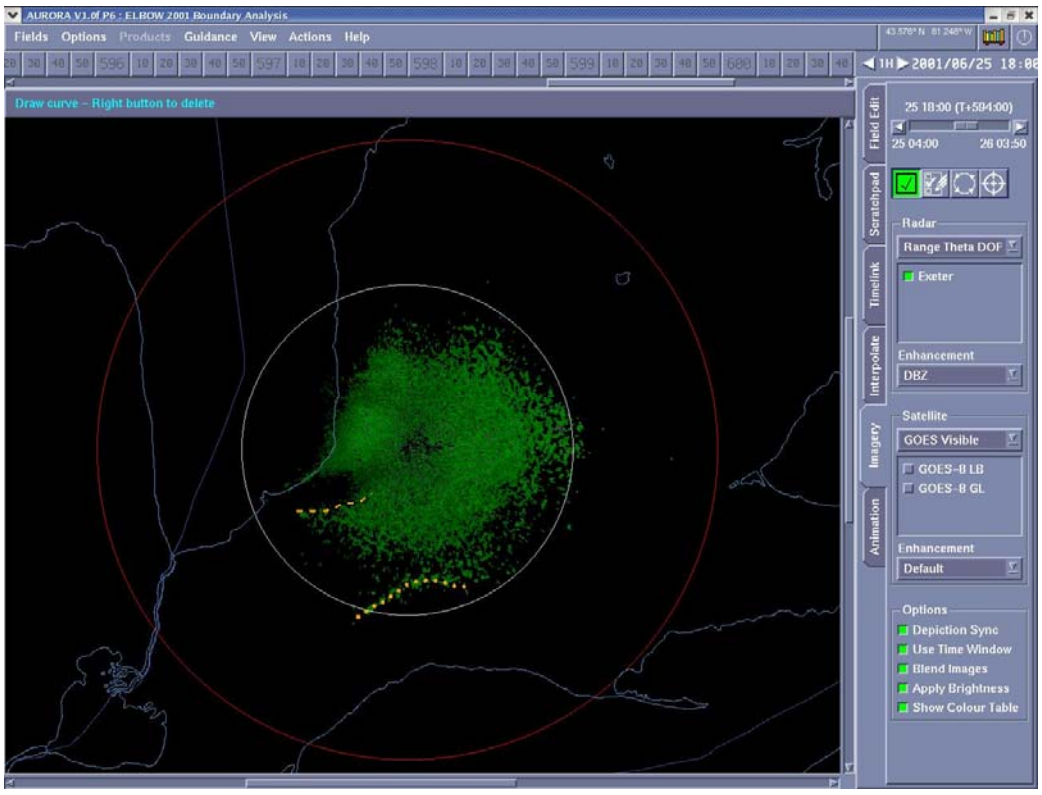

Figure 5.2. An example of the mesoscale boundaries identified using the Radar analysis for June 25, 2001 at 1800 UTC. Note these boundaries were all identified using orange patterns.

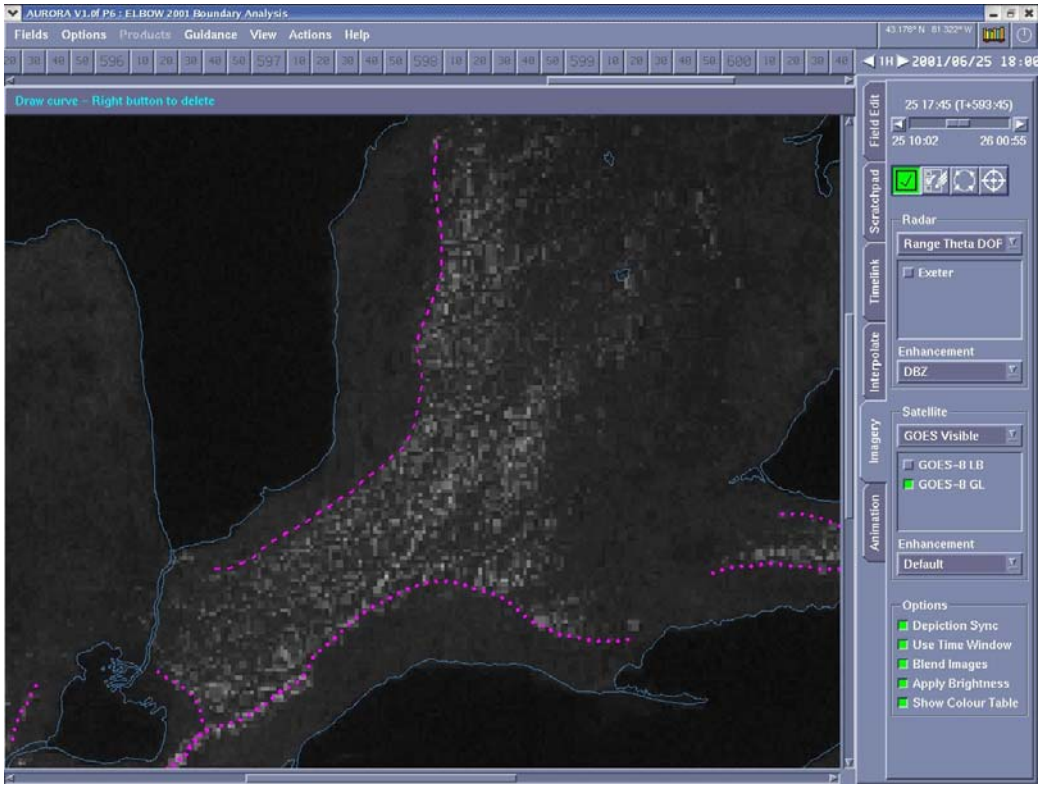

Figure 5.3. An example of the mesoscale boundaries identified using the Satellite analysis for June 25, 2001 at 1800 UTC. Note these boundaries were all identified using magenta patterns.

5.2 Using Aurora for the Boundary Analysis

Aurora is a research version of the Forecast Production Assistant (FPA), developed by the Meteorological Service of Canada. A significant effort was needed to become familiar with the Aurora research tool and to collect and format data sets for use with Aurora. Time was spent configuring Aurora to ingest and display the specified data. Patterns were created within the program to depict the different mesoscale boundary types. See Chapter 4 for more details about data collection and Aurora's setup for ELBOW 2001.

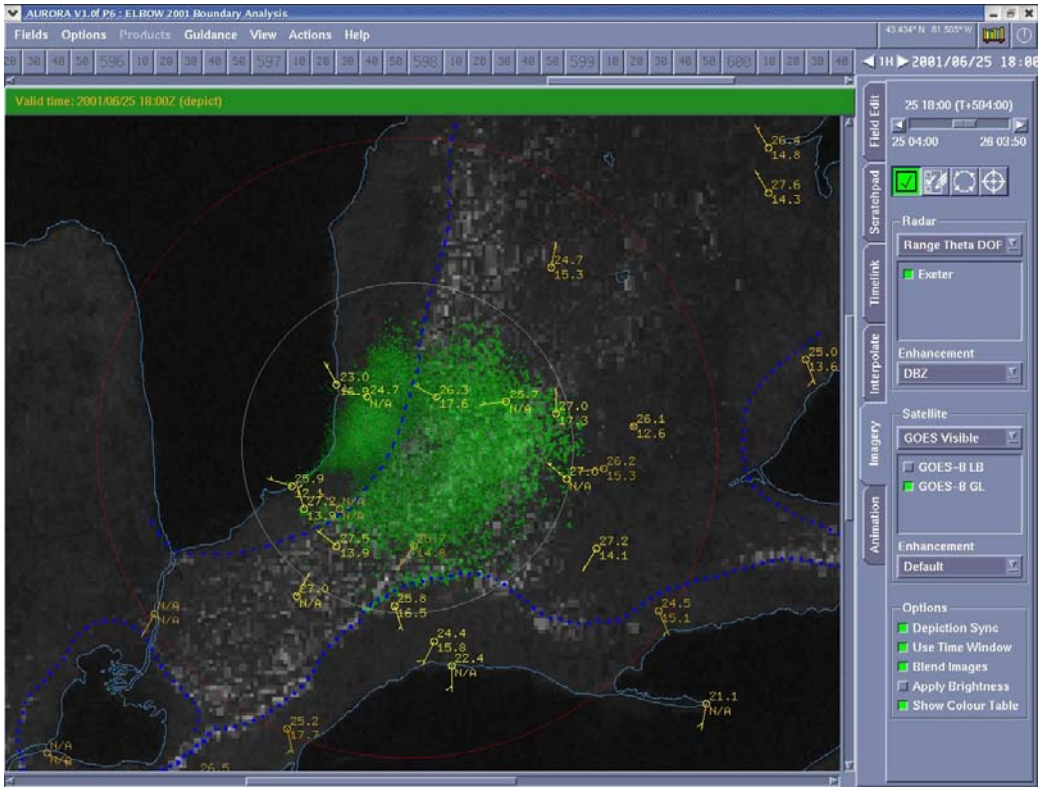

Figure 5.4. An example of the mesoscale boundaries identified using the Integrated analysis for June 25, 2001 at 1800 UTC. Note these boundaries were all identified using blue patterns.

5.3 Advantages and Drawbacks of Analyses

Each analysis showed specific traits which made it more or less difficult to detect and pinpoint the low-level mesoscale boundaries. In this section some the advantages and drawbacks of each analysis, as noticed by the identifier, are described.

5.3.1 Mesonet Analysis

The mesonet analysis usually showed a strong change in wind direction with a passing boundary. After the passing of a lake breeze front, strong changes in temperature and dew point were sometimes seen. However, this temperature

Table 5.1. Semi-objective criteria for identifying lake breeze fronts.

Platform	Positive Factors	Negative Factors	Ambiguous
Satellite (visible)	► line of cumulus clouds or sharp gradient in cumulus cloudiness quasi-parallel to shoreline ► gradual inland penetration of above	► persistent thick cloudiness over most or all of lake ► gradual change in the depth of cumulus clouds inland from lake (gradually deepening CBL)	► no cloud visible ► thin cirrostratus or broken mid-level clouds prevents seeing cumulus clouds
Radar (LogZ, Vr)	► fine line or sharp gradient in clear air reflectivity quasi-parallel to shoreline ► shift in radial velocity along fine line ► gradual inland penetration of above	► large area of persistent precipitation over region	► no clear air echoes ► fine line or gradient in clear air echoes not well defined
Surface (Stn plots, time series)	► rapid shift in wind direction to onshore wind (may be accompanied by rapid change in wind speed, sharp decrease in temperature and dew point within ~20 km of shore), ► gradual inland penetration of onshore winds ► elongated area of convergence quasi-parallel to shoreline Note: an area of broad divergence over the lake and the adjacent lake shore indicates a lake breeze circulation is present and may be used to support the presence of a lake breeze front	► no onshore winds	► often very subtle surface gradients at boundaries in moderate / high low-level wind regimes

change became less apparent as the lake air moved further inland and was modified due to surface heating.

In order to get a detailed picture of where the boundaries were located there had to be a high density of stations covering the study region. In areas where there were few stations it was hard to identify the location of the boundaries accurately. As the boundaries moved between stations it was not possible to pinpoint their exact location. If the boundary sped up or slowed down between stations this would not be apparent. For example, the stations were very sparse on the east side of Lake St. Clair, so it was difficult to identify a lake breeze front on this side of the lake. This study assumed that the boundaries were moving uniformly between stations if there was no data to show the exact location.

Also, the location and movement of a boundary was not apparent if background winds were similar to the motion of winds driving the boundary. Here a strong change in wind direction would not be observed. Light and variable winds also caused some confusion because there was no consistent speed and direction to the background flow. This made it hard to tell if changes in wind direction were due to the variable background winds or the passing of a boundary.

Another factor that made boundary identification difficult, using the mesonet analysis, was the lack of convective information. In the radar or satellite analysis, well developed convection could be seen. In the mesonet analysis, the

identifier had to rely on the station information. However if stations were sparse there was not always an indication of convection (or the lack of) occurring nearby a boundary. This could make it difficult to distinguish the type of boundary, such as a gust front which required an origin from a convective area.

5.3.2 Radar Analysis

The radar analysis depicted all low-level mesoscale boundaries very clearly in the clear air region of Exeter radar. They could be seen as a fine line in the Exeter 0.5 degree reflectivity and radial velocity images. However, further from the radar location, the boundaries were less apparent. This was due to the radar beam overshooting these boundaries at extended distances. Since the radar was located close to the Lake Huron lake shore, the Lake Huron lake breeze front was identified most often, using this analysis method. For the other boundaries to be identified they had to form in the clear air region or move into it. The lake breeze fronts created by Lake Ontario and Lake St. Clair usually had to move well into the range ring before they could be identified. The detection distance from the radar would depend on the depth of the lake breeze circulation.

By performing the boundary identification using this analysis, it was noticed that a number of ‘other’ or unknown boundaries could be identified by looping the radar. In some cases, variations and lines in the radar only became apparent by viewing the images in sequence.

5.3.3 Satellite Analysis

The satellite analysis used the visible GOES-8 images and therefore only allowed for the identification of boundaries during the daylight hours. However, on days with cumulus cloud development, the lake breeze fronts could be seen clearly over the entire study region. These boundaries appeared as lines of cumulus clouds with clear air on the lake side of the boundary and cumulus clouds in front of the boundary (see Figure 5.3). In most cases, cumulus clouds did not become well developed until the afternoon. Within the peak heating hours, these lake breeze fronts would often become well defined in the satellite imagery.

In some cases, increasing cloudiness inland from the lakeshore could be deceiving. This sometimes appeared to show a cloud line depicting a lake breeze front. However, by looping the data and looking for *sharp* cloud lines these cases can usually be discerned from mesoscale boundary cases.

5.3.4 Integrated Analysis

The integrated analysis was performed using the visible GOES-8 images, the Exeter radar reflectivity and radial velocity images, and the mesonet data. In order to identify a boundary it had to be visible in at least one of the data sets. This method has proven to be useful because the data sets would often agree with each other in terms of boundary location. For example, if a boundary was sitting between two mesonet stations and the exact location was not apparent, then it could also be seen in the satellite and/or radar data in order to get a more accurate location.

5.3.5. Differences Between Analyses

It should be noted that the identifier performing the integrated analysis, Dr. David Sills, had more experience in low-level mesoscale boundaries and identifying them. The author (less experienced at identifying mesoscale boundaries previous to this study), performed the mesonet, radar and satellite analyses. Each person's approach was different, yet followed the same criteria. For example, the identifier doing the integrated analysis felt it was more useful to zoom in on the radar and other data sets in order to find small or detailed boundaries, while the identifier doing the radar analysis (and other analyses) felt it was more useful to loop the radar to see the small variations over time.

5.4 Accuracy of Boundary Locations

The accuracy of the boundary location could have been affected by a number of different factors. When viewed through Aurora, it was apparent the satellite images shifted slightly and did not always sit on the accurate location of the lake outline map. This could often be compensated for by the identifier, however this would still contribute some error to the location. Also, cloud development, as seen on the satellite images, was offset due to parallax. When finding lake breeze fronts using satellite, it was more accurate to view the shallow cumulus (cloud patterns before strong vertical development). Deep development was offset the most by parallax, therefore the error was minimized by looking at the shallow development.

Again, if the boundaries were identified using only the mesonet data, then it was difficult to get an exact location of the boundary between stations. As noted previously, the boundary was assumed to have uniform motion in these cases, however, it could not be expected that the boundaries would move in this 'ideal' fashion. If the boundary sped up or slowed down the location would be slightly different, contributing some inaccuracy.

The angle of the boundary vertically must also be taken into account. Perhaps the boundary was not perfectly vertical, yet the cloud line or radar line was elevated from the ground. The location of the boundary at the surface level as compared to the elevated level may have been different.

The resolution used for the boundaries in Aurora also contributed an error range. The resolution used in Aurora, at this point of the project, allowed for plus or minus 0.71 kilometers.

The exact image time, as compared to the depiction time in Aurora, varied due to the availability of the data. For example, GOES-8 visible satellite images, of the Great Lakes region, were available approximately every 15 minutes. If the image was not taken at the exact time being analyzed, Aurora would simply substitute the closest image. If the difference was a couple minutes then there would be a small error, and would increase with a faster moving boundary.

Another factor which could influence the accuracy of the boundaries was the vertical wind environment. As seen in the satellite images, vertical development of the cloud lines, depicting the lake breeze fronts, may have been

shifted due to wind shear. In this situation these clouds may be shifted towards the lake side of the front. This made it difficult to identify the exact location of the boundary. In this case the lake breeze front would appear to be closer to the shore than it actually was.

Overall, the error in boundary location would have been somewhat larger when only looking at one data set. It was easier to find a more accurate location of a mesoscale boundary when there were other data sets to compare and help correct obvious problems with the data. For example, for offset satellite images, or parallax issues it was useful to compare the locations against the radar reflectivity since these seemed to show more accurate locations for boundaries in these cases. After considering all the factors, it was concluded that the integrated boundary set (as well as the final 'truth' set mentioned in the following section) be assigned an error range of approximately +/- 2.0 kilometers.

5.5 Identifying the Final 'truth' Boundary Set

Once the four boundary analyses were completed, a final 'truth' boundary set was created. The idea of creating a final boundary set was to come up with an inventory of the most realistic boundaries present in the study region during the summer of 2001; hence a 'truth' set.

This final 'truth' boundary set was identified (by Dr. David Sills) by considering all of the boundaries from the four analysis methods and all of the data sets. The boundaries were made uniform, in a single display, so that the type of analysis used to find each boundary was not apparent. As each boundary

was considered, all the data was viewed in order to get an idea of which boundaries were correct, incorrect or needed modification. Analyses using single data sets may have caught some small details that the integrated analysis missed but mainly the integrated analysis showed a better overall picture. The final 'truth' boundary set is considered to be the best representation of the boundaries that were present. See Figure 5.5 for an example of these boundaries.

The final boundary set is the set of boundaries that was used in further analysis of the ELBOW 2001 project (such as nowcasting and convective initiation). The four initial analysis (mesonet, satellite, radar and integrated) were

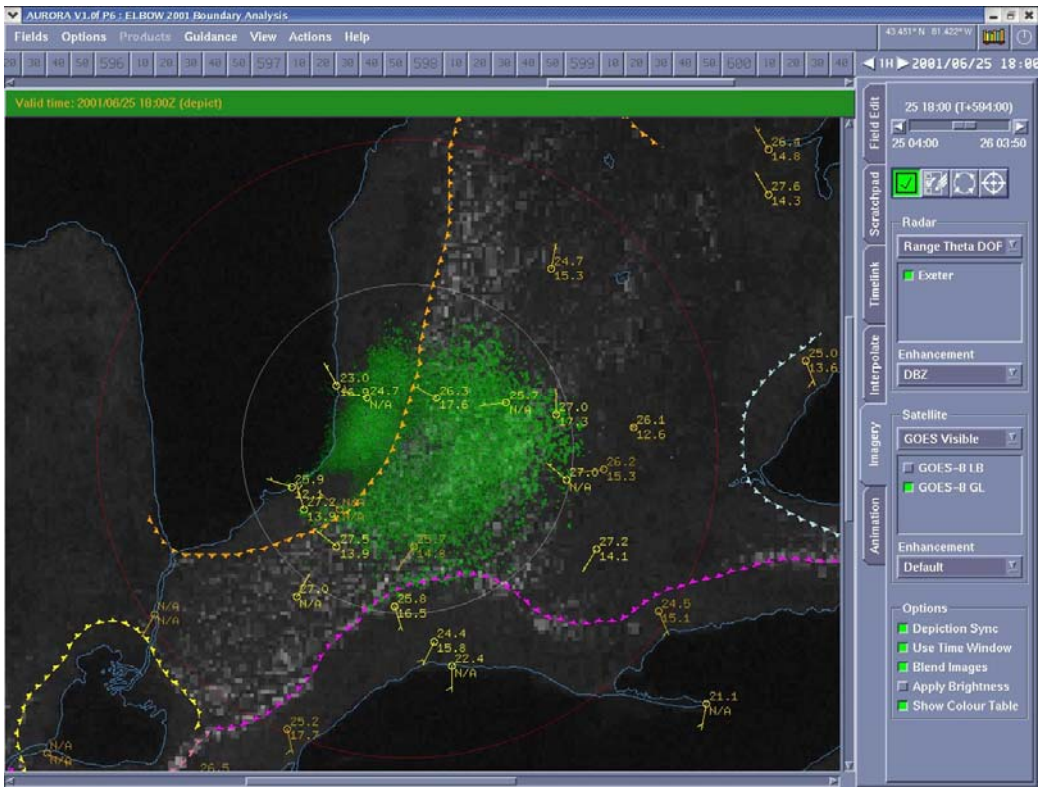

Figure 5.5. An example of the mesoscale boundaries identified by the Final 'truth' set for June 25, 2001 at 1800 UTC. Each boundary type has its own colour.

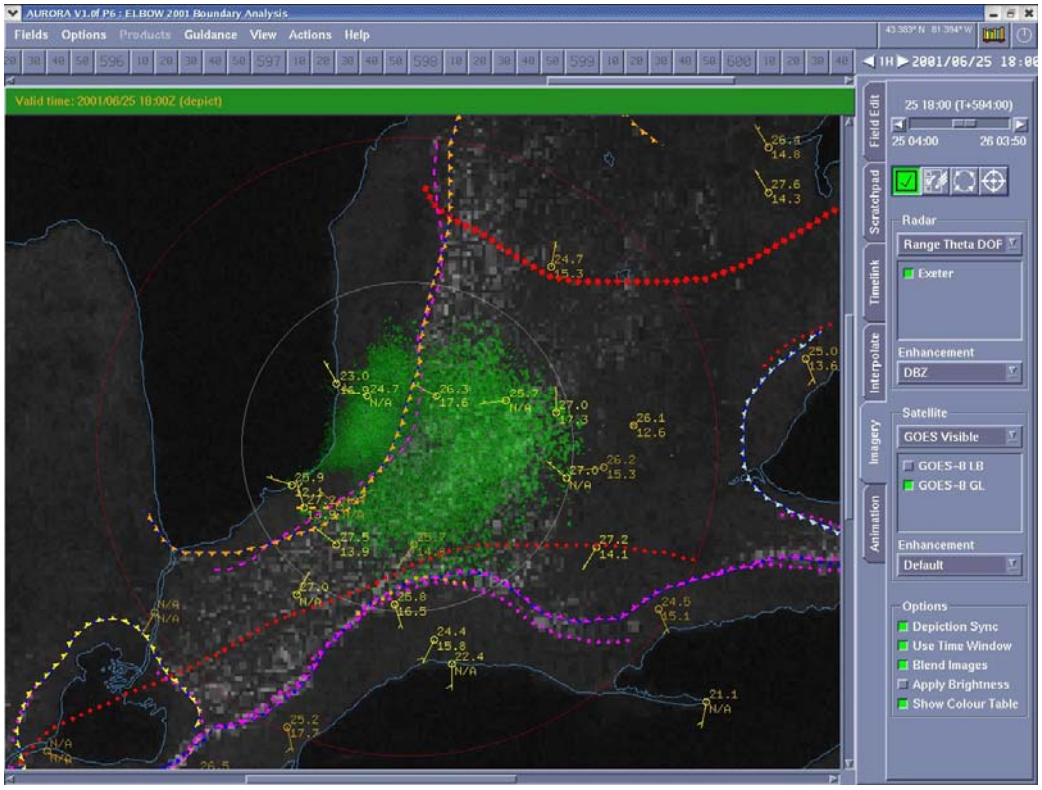

Figure 5.6. An example of the mesoscale boundaries identified by all the analyses for June 25, 2001 at 1800 UTC.

also evaluated against this final 'truth' set to determine which was the most accurate. By evaluating this we can see which boundary analysis is the best to use in future low-level mesoscale boundary studies. See Figure 5.6 for a visual comparison of the boundaries (from all the analyses) for June 25 at 1800 UTC.

5.6 Statistical Evaluation of Analyses using Lake Breeze Front Identification

5.6.1 Contingency Table Approach

After the boundary analyses had been performed, each day from June 1 to August 31 was viewed in order to evaluate the analyses. A 'yes' was recorded for each specific lake if a lake breeze front (originating from that lake) was

present in the study region (Exeter Doppler range ring as seen in Figure 2.1) at the specified time of day (entry appears as a 'Y' in the Tables in Appendix J). If the lake breeze front was not present during the time of concern, then a 'no' was recorded (appear as the blank spaces in the Tables in Appendix J). This was done for each analysis type: mesonet, radar, satellite, integrated and the final 'truth' set. It was also done for three specified times: 1500, 1800 and 2100 UTC.

Once the tables of lake breeze front presence were completed (as in Appendix J) the four analyses were compared to the final 'truth' boundary set using a contingency table approach. This was done similar to a method looking at 'forecast' against 'observed' by Wilks (1995). For our purposes, the final 'truth' set was used in place of the 'observed' and the other four analyses were used in place of the 'forecast' (see Figure 5.7).

Figure 5.7. Contingency tables from Wilks (1995) and that used for the ELBOW 2001 boundary analysis.

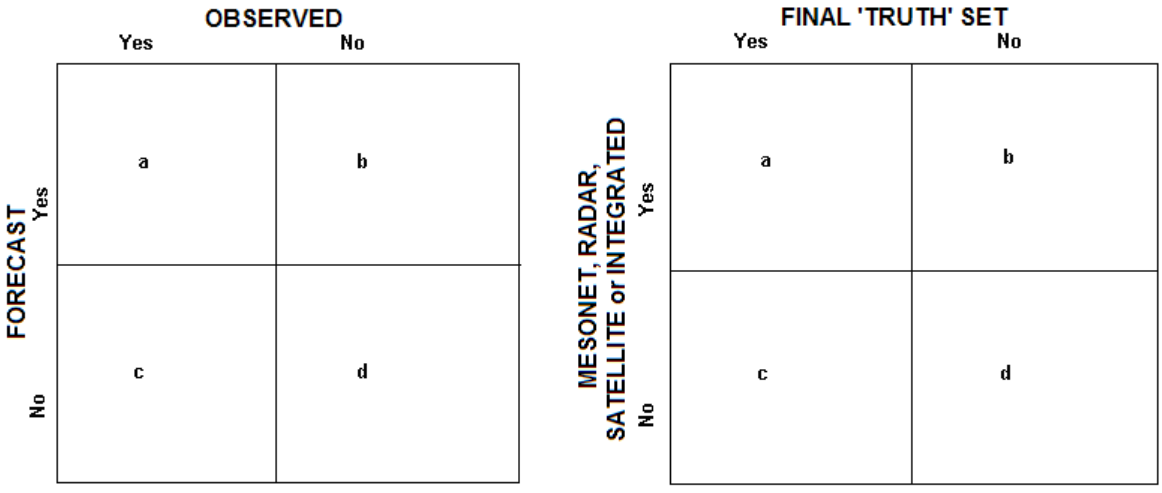

Contingency Table from Wilks (1995), p. 239.

Contingency Table used to evaluate the lake breeze analyses.

As can be seen from Figure 5.7, ‘a’ is the sum of the cases where both the final ‘truth’ set and analysis being compared found the specified lake breeze front was present in the study region at the specified time. ‘b’ is the sum of the cases where the final ‘truth’ set found the specified lake breeze front was not present and the analysis being compared found it was present. ‘c’ is the sum of cases where the final ‘truth’ set found the lake breeze front was present and the compared analysis found it was not. Finally, ‘d’ is the sum of cases where both the analyses found that the lake breeze front was not present during the specified time. These four values were then used to calculate the indices found in Wilks (1995) equations 7.5 to 7.9:

Hit Rate = H = (a+d)/n

Threat Score or **Critical Success Index** = TS = CSI = a/(a+b+c)

Probability of Detection = POD = a/(a+c)

False-alarm Rate = FAR = b/(a+b)

Bias = B = (a+b)/(a+c)

where n is the sample size or total number of days considered. When data were missing critical to the analyses in question, the day was eliminated from the statistical evaluation. The results of this contingency table evaluation will be considered in section 5.7.1.

5.6.2 Correlation of Inland Penetration Distances

A second statistical method was used to look at the inland penetration distances of the lake breeze fronts. The final ‘truth’ set was compared to each of

the four analyses. The inland penetration distance from the shore was measured for Lake Erie and Lake Huron. Port Stanley was the shore reference location for Lake Erie and Port Franks was the shore reference location for Lake Huron. Inland penetration of the lake breeze fronts were measured from the shoreline location closest to these stations. Inland penetration distances were found using the Aurora research tool (which allows for measurement to the nearest km) and measured perpendicular to the shoreline. Positive distances represented the lake breeze front over land, and negative distances were recorded when the fronts were still over the lake. The distance was recorded as zero if the front was directly over the lake shore. This was done for 1800 and 2100 UTC. 1500 UTC did not show enough lake breeze front detection perpendicular to these locations to get accurate correlations for the analysis comparisons.

For example, if the Final 'truth' set was being compared to the Mesonet boundaries, then we would need both sets showing boundary occurrence at a location approximately perpendicular to the corresponding lake shore location. These two distances, for each lake breeze front location, can then be added to the data set. If the lake breeze front did not occur for one or both of the analyses, at the given time and location, then the data could not be included in the correlation data set.

In order to see if there was a significant correlation in the data set, equation 3.17 from Wilks (1995) was used:

$$r_{xy} = (\sum_{i=1}^{n} [x_i' y_i']) / ([\sum_{i=1}^{n} (x_i')^2]^{1/2} [\sum_{i=1}^{n} (y_i')^2]^{1/2})$$

This was calculated with the actual distances to find the Pearson correlation coefficient, and with the ranks of the distances to find the Spearman rank correlation coefficient. The results can be seen in section 5.7.2.

5.7 Results and Discussion

5.7.1 Contingency Table Results

Contingency table results were calculated for 1500, 1800 and 2100 UTC. The results for these times for Lake Huron and Lake Erie are presented in the following subsections. It should be noted that Lake Ontario and Lake St. Clair were included in the boundary analysis but are not included in the statistical study. The statistics resulting from these lakes were found to not accurately represent the lake breeze activity related to them due to their shorelines lying outside of the study region. The existence of lake breeze fronts resulting from these lakes would not be recorded in this study unless they penetrated into the study region during the time in question, therefore making the lake breeze front occurrence appear less than was realistic.

a. 1500 UTC Results

Table 5.2 shows the results of the contingency table indices for 1500 UTC. Indices have been calculated for Lake Huron and Lake Erie lake breeze fronts. The period includes June 1, 2001 through August 31, 2001. Note that a total of 84 days were considered for 1500 UTC, as 8 days were eliminated due to unavailable satellite or radar images during this time.

The hit rate (HR), as seen in section 5.6.1, shows how well the analysis in question did as compared to the final ‘truth’ boundaries. If the outcome of the two analyses were exactly the same, the HR value would be 1. The less the analysis in question was like the final ‘truth’ set, the closer the HR value was to zero. As we can see, the Integrated has the best HR value for Lake Huron. The Mesonet/Radar/Satellite combination has the best HR value for Lake Erie. Note that the Mesonet/Radar/Satellite combination numbers are simply the three analyses combined; any one (or more) of the Mesonet, Radar or Satellite analyses must detect the lake breeze front to be counted in these ‘combination’ statistics.

The Threat Score or Critical Success Index (TS or CSI), as seen in section 5.6.1, is the number of times both analyses had a ‘yes’ for lake breeze presence (a), divided by the number of times that the final set and/or the analysis in question had a ‘yes’ for lake breeze presence (a+b+c). The best value for TS is 1. The worse the analysis in question did in comparison to the final set, the closer the value was to zero. As we can see, the Integrated shows the best TS value for Lake Huron. The Mesonet/Radar/Satellite combination has the best TS value for Lake Erie.

The Probability of Detection (POD), as seen in section 5.6.1, is the number of times that both the analysis in question and the final ‘truth’ set detected the lake breeze front presence (a), divided by the number of times that the final ‘truth’ set detected the lake breeze presence whether the analysis in question showed a

'yes' or 'no' (a+c). Again, the best POD value would be 1, meaning that the analysis in question is showing the same as the final 'truth' set. The smallest value for POD would be zero showing the greatest difference between the two analyses. The values at 1500 UTC show that the Mesonet/Radar/Satellite combination has the best POD value for both Lake Huron and Lake Erie at 0.8 and 0.714 respectively. Note that the Radar POD value (and TS value for that matter) is zero for Lake Erie. This is due to the fact that the lake breeze fronts did not have enough time to penetrate into the clear air region of Exeter radar in order to be detected by the analysis.

The False-alarm Rate (FAR), as seen in section 5.6.1, is the number of times that the final 'truth' set showed no lake breeze front presence during the times that the analysis in question did (b), divided by the total number of times that the analysis in question showed lake breeze front presence (a+b), as seen in Wilks (1995). We hope to get a small false-alarm rate, meaning that the analysis in question correctly detected lake breeze front presence. The smallest and best value for this index is zero, and it becomes worse as it approaches 1. Both the Integrated and Satellite analyses show a value of zero for Lake Huron. The Integrated analysis also shows a zero value for Lake Erie. Notice that the FAR cannot be calculated for the Radar analysis on Lake Erie. This is again due to the fact that the lake breeze fronts have not penetrated into the clear air region of the Doppler range ring.

Table 5.2. 1500 UTC Contingency Table Results. Note the best values for each index are in bold. The study period includes June 1, 2001 through August 31, 2001.

Results for 1500 UTC		
Mesonet Analysis vs. Final 'truth' Boundary Set		
	Lake Huron	**Lake Erie**
HR	0.798	0.786
TS or CSI	0.528	0.526
POD	0.543	0.571
FAR	0.050	0.130
B	0.571	0.657
Radar Analysis vs. Final 'truth' Boundary Set		
	Lake Huron	**Lake Erie**
HR	0.655	0.583
TS or CSI	0.194	0
POD	0.200	0
FAR	0.125	N/A
B	0.229	0
Satellite Analysis vs. Final 'truth' Boundary Set		
	Lake Huron	**Lake Erie**
HR	0.690	0.643
TS or CSI	0.257	0.189
POD	0.257	0.200
FAR	**0**	0.222
B	0.257	0.257
Integrated Analysis vs. Final 'truth' Boundary Set		
	Lake Huron	**Lake Erie**
HR	**0.905**	0.798
TS or CSI	**0.771**	0.514
POD	0.771	0.514
FAR	**0**	**0**
B	0.771	0.514
Mesonet/Radar/Satellite Analyses vs. Final 'truth' Boundary Set		
	Lake Huron	**Lake Erie**
HR	0.893	**0.833**
TS or CSI	0.757	**0.641**
POD	**0.800**	**0.714**
FAR	0.067	0.138
B	**0.857**	**0.829**

The Bias (B), as seen in section 5.6.1, is the total number of times that the analysis in question detected the lake breeze front presence (a+b), divided by the total number of times that the final 'truth' set detected the lake breeze front presence (a+c). If B is greater than 1, then the analysis in question detected the presence more than the final 'truth' set. If B is less than 1, then the analysis in question detected the presence less than the final 'truth' set. B equals 1 if the analysis in question detected the same number of lake breeze fronts as the final 'truth' set. In our 1500 UTC results, we can see that the final 'truth' set was detecting more lake breeze fronts than the analysis in question for Lake Huron and Lake Erie. Notice the value for Lake Erie, for the Radar analysis, is zero because of the lack of penetration into the clear air region of Exeter.

b. 1800 UTC Results

Table 5.3 shows the contingency table results for 1800 UTC. Note that a total of 86 days were considered for 1800 UTC, as 6 days were eliminated due to unavailable satellite or radar images during this time. The Integrated analysis shows the highest HR values and TS values for both the lakes.

Both the Integrated analysis and the Mesonet/Radar/Satellite combination show the highest POD value for Lake Huron at 0.971. However, the Integrated analysis has the highest POD value for Lake Erie, at 0.895.

The smallest FAR values can be seen for the Mesonet analysis and the Integrated analysis, for Lake Huron. The smallest FAR value for Lake Erie was

Table 5.3. 1800 UTC Contingency Table Results. Note the best values for each index are in bold. The study period includes June 1, 2001 through August 31, 2001.

Results for 1800 UTC		
Mesonet Analysis vs. Final 'truth' Boundary Set		
	Lake Huron	**Lake Erie**
HR	0.686	0.721
TS or CSI	0.603	0.593
POD	0.603	0.614
FAR	**0**	0.054
B	0.603	0.649
Radar Analysis vs. Final 'truth' Boundary Set		
	Lake Huron	**Lake Erie**
HR	0.558	0.465
TS or CSI	0.449	0.193
POD	0.456	0.193
FAR	0.031	**0**
B	0.471	0.193
Satellite Analysis vs. Final 'truth' Boundary Set		
	Lake Huron	**Lake Erie**
HR	0.744	0.744
TS or CSI	0.681	0.627
POD	0.691	0.649
FAR	0.021	0.051
B	0.706	0.684
Integrated Analysis vs. Final 'truth Boundary Set		
	Lake Huron	**Lake Erie**
HR	**0.977**	**0.895**
TS or CSI	**0.971**	**0.850**
POD	**0.971**	**0.895**
FAR	**0**	0.056
B	0.971	**0.947**
Mesonet/Radar/Satellite Analyses vs. Final 'truth' Boundary Set		
	Lake Huron	**Lake Erie**
HR	0.953	0.860
TS or CSI	0.943	0.800
POD	**0.971**	0.842
FAR	0.029	0.059
B	**1**	0.895

found using the Radar Analysis. All FAR values for Lake Huron and Lake Erie were below 0.06.

The B values are all below a value of 1, except the Mesonet/Radar/Satellite combination comes up with a score of 1 for Lake Huron. The B values for the Radar analysis are consistently low for both the lakes. This means the final 'truth' set detected the lake breeze fronts, at this time, much more frequently than the Radar analysis. The B values for the Integrated analysis are greater than 0.94 for both lakes. Lake Huron and Lake Erie have values of 0.971 and 0.947 respectively.

c. 2100 UTC Results

The contingency table results for 2100 UTC can be seen in Table 5.4. Note that a total of 87 days were considered for 2100 UTC, as 5 days were eliminated due to unavailable satellite or radar images during this time. The highest HR values for Lake Huron and Lake Erie are found using the Integrated analysis. Both lakes showed a value of 0.92. The highest TS values for Lake Huron and Lake Erie were also shown by the Integrated Analysis; both showing to be greater than 0.87.

The Integrated analysis also shows the best POD values for Lake Huron and Lake Erie with values of 0.935 and 0.877 respectively. The Satellite, Radar and Integrated analysis show the best FAR value for Lake Erie. Notice the best FAR value for Lake Huron is given by the Radar analysis. This is due to the radar being so close to the Huron shoreline, putting the lake breeze development in

Table 5.4. 2100 UTC Contingency Table Results. Note the best values for each index are in bold. The study period includes June 1, 2001 through August 31, 2001.

Results for 2100 UTC		
Mesonet Analysis vs. Final 'truth' Boundary Set		
	Lake Huron	**Lake Erie**
HR	0.586	0.724
TS or CSI	0.438	0.586
POD	0.452	0.596
FAR	0.067	0.029
B	0.484	0.614
Radar Analysis vs. Final 'truth' Boundary Set		
	Lake Huron	**Lake Erie**
HR	0.598	0.586
TS or CSI	0.444	0.368
POD	0.452	0.368
FAR	**0.034**	**0**
B	0.468	0.368
Satellite Analysis vs. Final 'truth' Boundary Set		
	Lake Huron	**Lake Erie**
HR	0.655	0.724
TS or CSI	0.531	0.579
POD	0.548	0.579
FAR	0.056	**0**
B	0.581	0.579
Integrated Analysis vs. Final 'truth Boundary Set		
	Lake Huron	**Lake Erie**
HR	**0.920**	**0.920**
TS or CSI	**0.892**	**0.877**
POD	**0.935**	**0.877**
FAR	0.049	**0**
B	**0.984**	**0.877**
Mesonet/Radar/Satellite Analyses vs. Final 'truth' Boundary Set		
	Lake Huron	**Lake Erie**
HR	0.828	0.874
TS or CSI	0.776	0.810
POD	0.839	0.825
FAR	0.088	0.021
B	0.919	0.842

range of the clear air region of the radar. It is possible, as noted in section 1.2.3, that the strength of the circulations and surface heating at this time of the day would have caused many bugs/particles to get caught in the upward motion along the lake breeze fronts, or there may have been a stronger contrast in the properties of the two air masses (lake air and environmental air). When the radar detected these they very clearly depicted the boundary. This allowed for fewer inaccurate identifications.

The B values are closest to 1 by using the Integrated analysis for Lake Huron and Lake Erie, showing values of 0.984 and 0.877 respectively.

d. Overview of Contingency Table Results

The Mesonet/Radar/Satellite analysis showed some better results than the Integrated analysis for 1500 UTC. This suggests that it may be useful to concentrate on the data sets individually during the earlier hours of the day. Perhaps the lack of lake breeze front presence in majority of the data sets allowed the identifier to miss some of the small details seen in one single data set. For example, the lake breeze front for Lake Erie would usually not be present in the radar data by 1500 UTC. It would not have penetrated inland far enough to reach the clear air region of the radar. Also, the satellite analysis would not always detect lake breeze fronts by 1500 UTC because cumulus clouds were often not very well developed by this time. So, the lake breeze front may have only been obvious in the mesonet analysis. The identifier who performed the mesonet analysis would have easily identified it if it were present. However, it is

possible that the identifier who performed the integrated analysis, looking at the overall data set, may have missed small details in the mesonet when other data sets were showing no presence. Therefore, this may have allowed the Mesonet/Radar/Satellite combination to perform better than the Integrated at 1500 UTC.

The Integrated analysis shows even better results for 1800 UTC and 2100 UTC, which outperforms the Mesonet/Radar/Satellite combination and other analyses most of the time. The Mesonet/Radar/Satellite combination often comes in a close second in the results. Looking at the bold results in Tables 5.3 and 5.4, the Integrated analysis performs best overall when compared to the Final 'truth' Set. The Mesonet/Radar/Satellite combination performs very well in comparison to the Final 'truth' Set as well, however this method is significantly more time consuming than the Integrated analysis and most of the time does not perform quite as well. The Integrated analysis allows the identifier to look at all the data together and make a clear identification on the location of the lake breeze fronts. The Mesonet/Radar/Satellite combination requires the identifier to go through the days studied three separate times in order to identify the lake breeze fronts for each data set.

The single Mesonet analysis, Radar analysis and Satellite analysis rarely outperform the Integrated analysis. However, after having performed each of these single analyses, it is apparent where their strengths in identification exist when other analyses may fail. The Mesonet analysis allows for identification of

the lake breeze circulations when they first develop. At earlier times of the day when convective development of cumulus clouds have not commenced or signatures are not strong enough to be caught in the clear air region of the radar or have not moved into this clear air region, the Mesonet analysis may still show lake breeze front identification.

The Radar analysis allows for lake breeze front identification when the front is within the clear air region of the radar. On days where there is little or no cumulus cloud development, the presence of a lake breeze front is still apparent. The Radar analysis also allows the identifier to be very accurate in the location of the lake breeze front. The Mesonet analysis lacks this accuracy when fronts are between stations, and strong vertical cumulus cloud development can obscure the exact location in the Satellite analysis.

The Satellite analysis allows for lake breeze front identification over the whole region as long and cumulus cloud development is present. Lake breeze fronts will be identified using this analysis even when mesonet stations are sparse over the area or the lake breeze fronts have not moved into the clear air region of the radar. It is consistent over the whole study area.

Considering all the contingency table results, the Integrated analysis generally outperforms the other analyses as compared to the Final ‘truth’ set.

5.7.2 Correlation Results

a. 1800 UTC Correlation Results

Appendix C shows scatterplots of the Final ‘truth’ set versus each of the other analyses for both lake Erie and Lake Huron lake breeze front distances from the shore. Visually it looks like the data have a fairly good linear correlation, however we can see that there are a couple of outliers, such as in the 1800 UTC Final ‘truth’ set versus the Radar analysis for Lake Huron and the 2100 UTC Final ‘truth’ set versus Mesonet analysis for Lake Huron.

The Pearson correlation coefficient values, for 1800 UTC, can be seen in Table 5.5. The data used to calculate these values can be seen in Appendix K and a sample calculation can be seen in Appendix L. As noted by Wilks (1995), The Pearson correlation coefficient can have values from -1 to 1. A value of 1 represents positive linear correlation and a value of -1 represents a negative linear correlation (Wilks, 1995). In our case we hope the outcome will be 1 because this would mean that both analyses showed the same penetration distance results.

As we can see, all the Lake Erie Pearson correlation coefficients are showing values just below 1. This means there is good positive linear correlation between the analyses compared. For lake Erie, the Final ‘truth’ set versus the Radar analysis distances are most closely correlated. This means that these two analyses had very similar distances for the inland penetration of the Lake Erie lake breeze at 1800 UTC on each day. However, it should be noted that this

correlation did not have many points to compare (only 9) since it is fairly hard for the Exeter radar to detect the Lake Erie lake breeze front because it is usually closer to the edge of the detection area (outside the clear air range). The radar would most likely overshoot this shallow circulation until it moved closer to the radar.

Table 5.5. Pearson Correlation Coefficient Results for 1800 UTC. Note the best correlation values are shown in bold.

Results for 1800 UTC			
		Pearson Correlation Coefficient	**Sample Size**
Lake Erie	**Final/Mesonet**	0.884	31
	Final/Radar	**0.999**	9
	Final/Satellite	0.934	23
	Final/Integrated	0.986	44
Lake Huron	**Final/Mesonet**	0.980	18
	Final/Radar	0.512	20
	Final/Satellite	0.868	18
	Final/Integrated	**0.993**	46

We can also see that most of the Lake Huron Pearson correlation coefficients are very close to perfect positive correlation. The Final 'truth' set versus the Integrated analysis shows the best correlation. However, the Final 'truth' set versus the Radar analysis only had a coefficient value of 0.512. This is most likely due to the outlier (which can be seen in the scatterplot in Appendix C) on August 8, 2001 when the Final 'truth' set picked up a Lake Huron lake breeze front distance of 57 km inland and the Radar analysis only picked up a distance of 7 km for the same front. Most of the other points are very well correlated. Obviously the Pearson correlation method is not very 'resistant' to

these outliers. That is why we now consider the Spearman rank correlation which is more ‘resistant’ to outliers (Wilks, 1995).

Table 5.6 shows the Spearman rank correlation coefficients. A Spearman value of 1 would represent a perfect correlation. The closer the value is to zero the less similar the values are. As we can see, all the lake breeze front distances for Lake Erie are very well correlated. The Final ‘truth’ set versus the Radar analysis is showing a perfect correlation of 1. But it should be noted again that this correlation only had 9 distances to compare.

Table 5.6. Spearman Rank Correlation Coefficient Results for 1800 UTC. Note the best correlation values are shown in bold.

Results for 1800 UTC			
		Spearman Rank Correlation Coefficient	**Sample Size**
Lake Erie	**Final/Mesonet**	0.939	31
	Final/Radar	**1**	9
	Final/Satellite	0.965	23
	Final/Integrated	0.976	44
Lake Huron	**Final/Mesonet**	0.790	18
	Final/Radar	0.830	20
	Final/Satellite	0.823	18
	Final/Integrated	**0.990**	46

The Lake Huron coefficients show values between 0.790 and 0.990. The Final ‘truth’ set versus the Integrated analysis shows a very close correlation of 0.990. The others are somewhat less than the Lake Erie values. We can see that the Final ‘truth’ set versus the Radar analysis shows a much better correlation for the Spearman method than the Pearson method. This is due to the Spearman ‘resistance’ to outliers as mentioned in Wilks (1995).

b. 2100 UTC Correlation Results

Table 5.7 shows the Pearson correlation coefficient results for 2100 UTC. As we can see, all the values for Lake Erie show very good correlations. All values are above 0.91. The Final 'truth' set versus the Radar analysis shows the best correlation with a value of 0.998. The Final 'truth' set versus the Integrated analysis has a coefficient value of 0.995.

Table 5.7. Pearson Correlation Coefficient Results for 2100 UTC. Note the best correlation values are shown in bold.

Results for 2100 UTC			
		Pearson Correlation Coefficient	**Sample Size**
Lake Erie	**Final/Mesonet**	0.912	31
	Final/Radar	**0.998**	17
	Final/Satellite	0.965	16
	Final/Integrated	0.995	47
Lake Huron	**Final/Mesonet**	0.694	16
	Final/Radar	**0.999**	16
	Final/Satellite	0.954	14
	Final/Integrated	0.990	36

Lake Huron shows very good correlation values for the Final 'truth' set versus the Radar, Satellite and Integrated analyses with values of 0.999, 0.954 and 0.990 respectively. However, the Final 'truth' set versus the Mesonet analysis only has a value of 0.694, which is significantly less than the rest. Again, this could be due to an outlier found in the data. On July 10, the Final 'truth' set found a lake breeze front inland penetration distance of 34 km for Lake Huron. The Mesonet analysis only found it to be 5 km. In order to remove the outlier effects, the Spearman rank correlation coefficient values were calculated and can be seen in Table 5.8.

Table 5.8. Spearman Rank Correlation Coefficient Results for 2100 UTC. Note the best correlation values are shown in bold.

Results for 2100 UTC			
		Spearman Rank Correlation Coefficient	**Sample Size**
Lake Erie	**Final/Mesonet**	0.888	31
	Final/Radar	0.991	17
	Final/Satellite	0.898	16
	Final/Integrated	**0.996**	47
Lake Huron	**Final/Mesonet**	0.649	16
	Final/Radar	**0.992**	16
	Final/Satellite	0.955	14
	Final/Integrated	0.984	36

The Spearman Rank values show good correlation for Lake Erie although some are less than those for the Pearson technique. The Final 'truth' set versus the Integrated analysis shows a similar value of 0.996.

The Spearman rank values for Lake Huron are very good for the Final 'truth' set versus the Radar, Satellite or Integrated analysis with values of 0.992, 0.955 and 0.984 respectively. However, the Final 'truth' set versus the Mesonet analysis has a lower value than the Pearson correlation coefficient. This could be due to a few factors since it is obviously not the outlier. First, it should be noted that there are only 16 data points for this correlation. Second, the lake air in the circulation can easily become modified by surface heating by 2100 UTC. Therefore, the identifier would not necessarily see a strong change in temperature when a lake breeze front passed. Third, boundary interactions can become very complex late in the day and it is hard to determine what type of boundary is being identified by looking solely at the mesonet data, so there could be some discrepancy in the identification here. Fourth, it is possible that many of

the days showed the same penetration distance by 2100 UTC (or slightly different), which would make ranking the values very inaccurate when the km values were so similar for these data points. This in combination with not knowing the exact location of the lake breeze between mesonet stations could cause the data to show poor correlation.

5.8 Other Interesting Results

The number of days in which lake breezes were detected in the study region (the Exeter Doppler range ring), as determined by the Final 'truth' set, are given in Table 5.9. Note that there are a different number of total days depending on the time of day. There were a total of 92 days during the June 1 to August 31, 2001 period for boundary analysis, however if any data were missing at the specified time, then the day was removed due to a lack of accuracy. As can be seen there were more data missing at 1500 UTC than at the other analysis times.

It is also obvious that the lake breeze front occurrence numbers for Lake St. Clair and Lake Ontario are significantly less than the other two lakes. This is because the lake breeze fronts had to penetrate into the Exeter Doppler range ring (the study region) before they would be counted. Therefore these numbers are not a good indicator of the lake breeze front occurrence from these lakes, and only show the observed occurrence in the study region.

The 1500 UTC results show significantly less occurrence than those at 1800 UTC and 2100 UTC. This is due to the fact that it was still early (11:00 EDT) in the day. Perhaps lake breezes did not develop by this time, or the signature

was not strong enough to be detected at this hour. Cumulus clouds had not always developed early in the day, creating a lack of detection in the satellite data. Lake breeze fronts also had to penetrate into the clear air region to be detected by the radar.

Table 5.9. Number of days in which lake breeze fronts (LBF) were present in the study region (as determined by the Final 'truth' Set). Numbers are given for 1500 UTC, 1800 UTC and 2100 UTC.

	Time					
	1500 UTC		1800 UTC		2100 UTC	
Lake	LBF days	Total Days	LBF days	Total Days	LBF days	Total Days
Lake Huron	35	84	68	86	62	87
Lake Erie	35	84	57	86	57	87
Lake St. Clair	2	84	20	86	19	87
Lake Ontario	2	84	13	86	19	87

The number of days which had lake breeze front occurrence greatly increased for 1800 UTC. In fact 68 days out of 86 days had lake breeze front occurrence corresponding to Lake Huron at this time. That is 79% of the days during the study period. With no consideration as to which lake the lake breeze front originated from, the number of days with lake breeze front occurrence in the study region increases to 73 out of 86 days for 1800 UTC. That is 85% of the days during the study period. The results for 2100 UTC are also very close to those for 1800 UTC. Note that the number of days showing Lake Ontario lake breeze front occurrence have increased from 1800 UTC to 2100 UTC, suggesting that the front has had more time to penetrate into the study region.

The overall results of 85% occurrence at 1800 UTC (originating from one or more lake) shows to be higher than was found in previous lake breeze

occurrence studies in the Great Lakes area (as noted in section 1.2.4), but is verified by the recent study done by Sills et al. (2011) during BAQS-Met in summer 2007. Sills et al. (2011) showed similar overall results, noting 90% of the study days showed lake breeze development (from one or more of the Great Lakes in the study region).

5.9 Conclusion

In looking at the results for the contingency table indices, we can see that the accuracy of the mesonet analysis was highly dependent on the density of the stations, as well as the environmental or background flow affecting the region.

The Radar analysis had good values for the detection of lake breezes that occurred close to the radar (such as Lake Huron), but was less effective in the detection of lake breezes that occurred at a distance from the radar location.

The Satellite analysis showed fairly consistent results. It often showed comparable or better index values than those for the Radar and Mesonet analysis at 1800 and 2100 UTC. Results for 1500 UTC had the poorest values for this analysis. The afternoon surface heating allowed for optimum conditions for cumulus cloud development which allowed for a clear picture of the lake breeze front location. If other low-level boundaries, occurring in the overnight hours, were being analysed here, the visible satellite image would not be available.

The Integrated analysis showed the most accurate and correct results overall, as compared to the Final ‘truth’ set. The combination of the results from the Mesonet/Radar/Satellite analyses were sometimes better than the Integrated

analysis but usually showed to be second best. This combination of analyses turned out to be very accurate compared to the Final 'truth' set, however it was *very* time consuming.

Correlation coefficients (both Pearson and Spearman Rank) were calculated based on the inland penetration distances of lake breeze fronts, in order to evaluate the different analyses further. The 1800 UTC Pearson correlation coefficients all had values over 0.86 except for the Final 'truth' set versus the Radar analysis which had a value of 0.512 for Lake Huron. This shows that the Pearson method is not very 'resistant' to outliers. The 2100 UTC Pearson correlation coefficients all had values over 0.91, however, the Final 'truth' set versus the Mesonet analysis had a value of 0.694 for Lake Huron.

The Spearman rank correlation coefficient was found to be more 'resistant' to outliers. All 1800 UTC analysis comparisons had fairly good correlations according to this coefficient. The correlations for Lake Erie were all greater than 0.93 and the correlations for Lake Huron were equal to or greater than 0.790. The 2100 UTC results showed very good correlation values accept for the Lake Huron Final 'truth' set versus Mesonet analysis comparison having a value of 0.649. This could be due to lake air modification by daytime heating over land, mesoscale boundary type/identification errors due to the lack of a clear picture of complex interactions later in the day, or due to the lack of information as to the exact location of the lake breeze front between mesonet stations.

6. Storms Associated with Mesoscale Boundaries

6.1 Background

As described more fully in Chapter 1, subsection 1.3, Wilson and Schreiber (1986) did a study on convective initiation in proximity to low-level convergence lines occurring in Colorado, east of the Rocky Mountains. The study period was May to August, 1984. They identified boundary layer convergence lines through Doppler radar. Each boundary was classified. These classifications included: “gust front, mountain outflow, synoptic front, Denver convergence line, unknown stationary, and unknown moving” (Wilson and Schreiber, 1986). They looked at storms initiating to 30dBZ at a 1 km altitude and measured the distance from these to the closest boundary. From the results they found that many storms occurred within close proximity of these low-level convergence lines. Storms seemed to form at or up to 20 km behind a moving boundary, usually from 0 to 15 km from a stationary boundary and 0 to 5 km from a colliding boundary (Wilson and Schreiber, 1986).

In order to determine if lake breeze fronts, and other low-level mesoscale boundaries in the Great Lakes region, have similar results to the convergence lines in Colorado, analyses were performed on the ELBOW 2001 data, similar to those done by Wilson and Schreiber (1986). The following sections describe the details of these analyses and discuss the results.

6.2 AURORA Setup

In order to conduct this analysis, AURORA needed to be set up with the required data. Since Wilson and Schreiber (1986) studied cells initiating at a 1.0 km altitude, AURORA was set up to ingest 1.0 km CAPPI metafiles, as well as 1.0 km MAXR metafiles for comparison. The 1.0 km CAPPI files show the reflectivity at approximately 1 km altitude and the 1.0 km MAXR files show the maximum reflectivity for a column starting from 1 km and up. AURORA was also set up to ingest both the Unified Radar Processor (URP) cell identification and URP cell tracking files. The details on data collection and AURORA set up have already been covered in Chapter 4 (subsection 4.2.5).

6.3 Specifics on Cell Identification and Tracking

The CAPPI and MAXR Metafiles were analysed, in turn, by the URP cell identification and URP cell tracking algorithms. These algorithms were developed by Environment Canada and were based on the concepts and methodology behind the TITAN algorithm, developed by the National Center for Atmospheric Research (as noted in Chapter 4).

The URP cell identification algorithm looks at these radar data in range, theta coordinates. It searches for elements (or bins) which have a value equal to or greater than the threshold value set for identification. The elements then form ‘pattern vectors’ or a number of consecutive elements along the vector in question (there must be at least two to be considered a ‘pattern vector’). The

algorithm has an adjustable consecutive pattern vector number, required for cell identification.

Looking at Figure 6.1 as a rough example, the blue area of the cell represents a reflectivity of 30 to 40 dBZ while the red area represents a reflectivity of 40 dBZ and greater. Each of the black lines represent the vectors being sampled. If we have a threshold of 30 dBZ set for cell identification and a minimum of 4 consecutive pattern vectors are required, we can see that there are 5 consecutive vectors which lie through an area (or a number of elements) of 30 dBZ or greater, meaning there are 5 'pattern vectors' (assuming that each of these pattern vectors have at least two consecutive bins showing the threshold value or greater). If a threshold of 40 dBZ was set and 4 pattern vectors required, then the cell in Figure 6.1 would not be identified since it only has 3 pattern vectors showing 40 dBZ or greater.

During the initial collection of these data, the cells were identified for:

- 30 dBZ threshold and a minimum of 2 pattern vectors
- 40 dBZ threshold and a minimum of 2 pattern vectors
- 60 dBZ threshold and a minimum of 2 pattern vectors

These data were collected for both the CAPPI and MAXR metafiles (for every 10 min). They were then run through the URP cell tracking algorithm, which matched up the most likely cell tracks through a weighting system and numbered them accordingly. A PERL script was then written to format these data into a 'scattered field' listing for AURORA (similar to those created for the mesonet

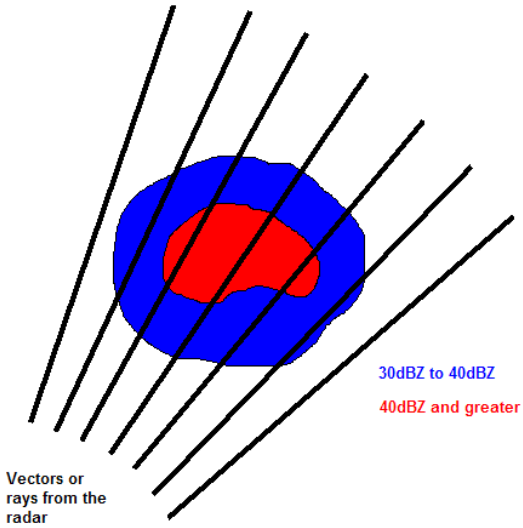

Figure 6.1. An example of a cell (shown in colour ranges representing radar reflectivity) and the vectors which are sampled for cell identification. The blue area depicts a reflectivity of 30 to 40 dBZ and the red area depicts a reflectivity of 40 dBZ and greater.

data). The AURORA configuration, setup and presentation files were modified in order to ingest these new data.

By viewing these new data in AURORA, it was found that the threshold and number of pattern vector settings were not resulting in the most accurate data. A cluster of cells were often being identified close to the radar, especially for the 30 dBZ data (see Figure 6.2). This was mainly due to the fact that only 2 pattern vectors were required. Closer to the radar, the elements, or bins, become much narrower, so only a very small area of the threshold value was required for identification. The cell tracking algorithm was also having trouble in these situations since the cells were unrealistic. Cell tracking numbers would often jump from one cell to another. These data were collected again. This time the cell identification data were collected for:

- 30 dBZ threshold and a minimum of 6 pattern vectors

- 40 dBZ threshold and a minimum of 4 pattern vectors
- 60 dBZ threshold and a minimum of 1 pattern vector

These were collected for a couple days, for both the CAPPI and MAXR metafiles (for every 10 min), and were then run through the cell tracking algorithm. Once formatted and configured for AURORA, these data appeared to be more accurate than the previous. These data were then collected for the rest of the study period using the same thresholds and minimum pattern vector settings.

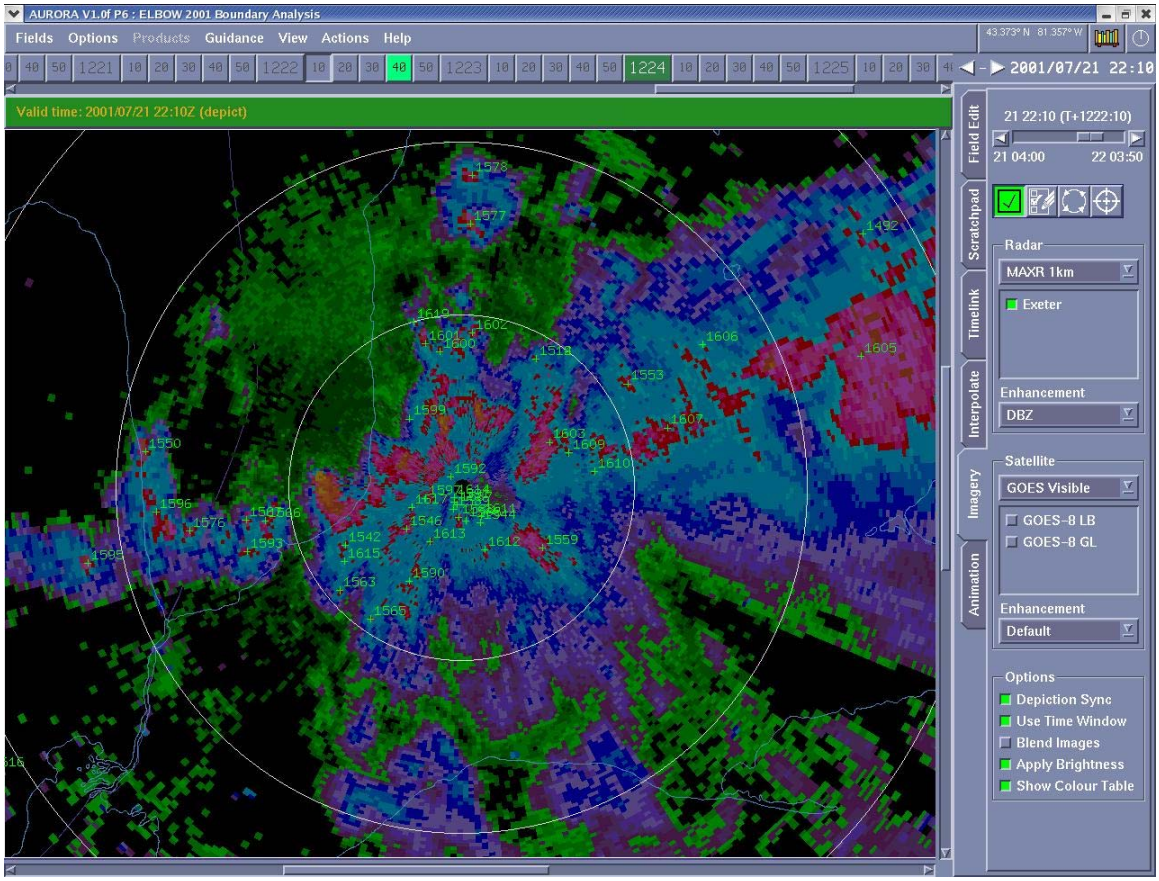

Figure 6.2. AURORA Image showing the MAXR 1.0 km and 30dBZ cell tracking data (minimum 2 pattern vectors) for July 21, 2001 at 2210 UTC. Notice the cells (labelled in green) clustered around the radar.

6.4 Cell Initiation Analysis

6.4.1 Choice of Reflectivity Threshold Level

The second collection of cell identification and tracking data were studied more closely, revealing that they seemed to be more accurate with higher dBZ thresholds. The 30 dBZ threshold appeared to be the least accurate. On cloudy days, there seemed to be identifications of large areas of 30 dBZ (which may have actually contained more than one cell since they may have been connected by 30 dBZ reflectivity); this made tracking difficult. Even though the minimum pattern vector setting was increased, there were still some cases in which many cells were shown to be clustered around the radar (though not as drastic as with a pattern vector setting of 2). A minimum number of pattern vectors of 6 were used to try to minimize this problem, but in some cases it also allowed the identification algorithm to miss some cells further from the radar. See Figure 6.3 for a visual explanation. For example, if a minimum of 5 pattern vectors and 30 dBZ threshold were required in the case in Figure 6.3, the cell closer to the radar would be identified but the cell further from the radar would not (even though they are the same size). This is due to the bins being wider further from the radar and very narrow close to the radar. In future studies, this may be able to be corrected by making a pattern vector limit based on the distance from the radar. Perhaps there could be a higher number of pattern vectors required for identification closer to the radar, and less required at a large distance.

Wilson and Schreiber (1986) looked at convective initiation, considering cells reaching a 30 dBZ level. In this study, the URP cell identification and tracking algorithms are being used, so cells reaching a 40 dBZ level will be considered since these data seem to be more accurate. So, for the purposes of this study, cell 'initiation' means cells which initially reach a level of 40 dBZ.

Figures 6.4a and 6.4b show a sample of these cell data for a threshold of 30 dBZ. There are fewer cells identified here because large areas are above 30 dBZ and considered as one cell. Figures 6.4c and 6.4d show a sample of the cells obtained using a threshold of 40 dBZ. Here it can be seen that the individual cells are identified more accurately.

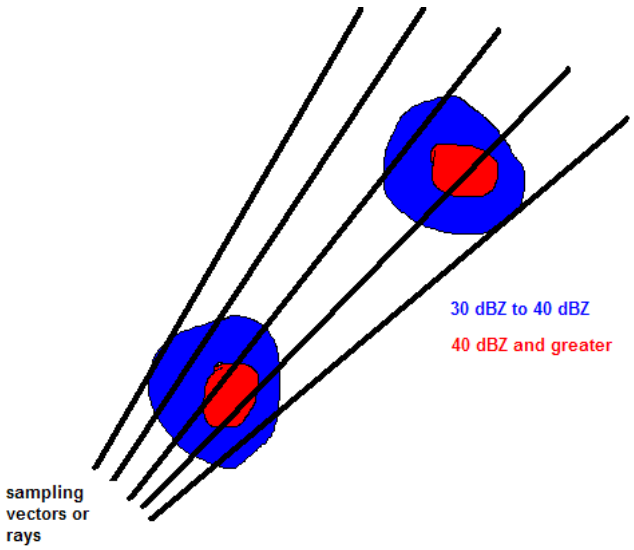

Figure 6.3. Example of two similar sized cells at two different distances from the radar location. The cell closer to the radar has more pattern vectors than the cell further from the radar.

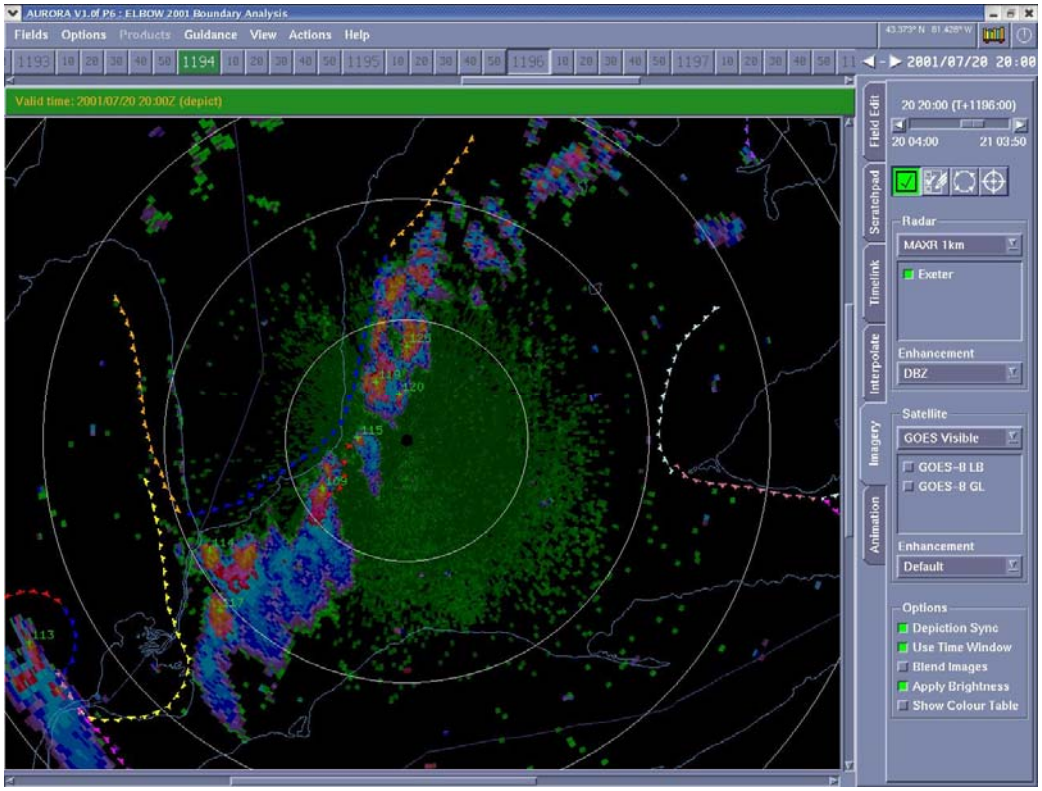

<u>Figure 6.4a (above) and 6.4b (below)</u>. Above shows the MAXR image and 30 dBZ cells for July 20, 2001 at 2000 UTC. Below shows the areas greater than or equal to 30 dBZ (in blue) for the same time.

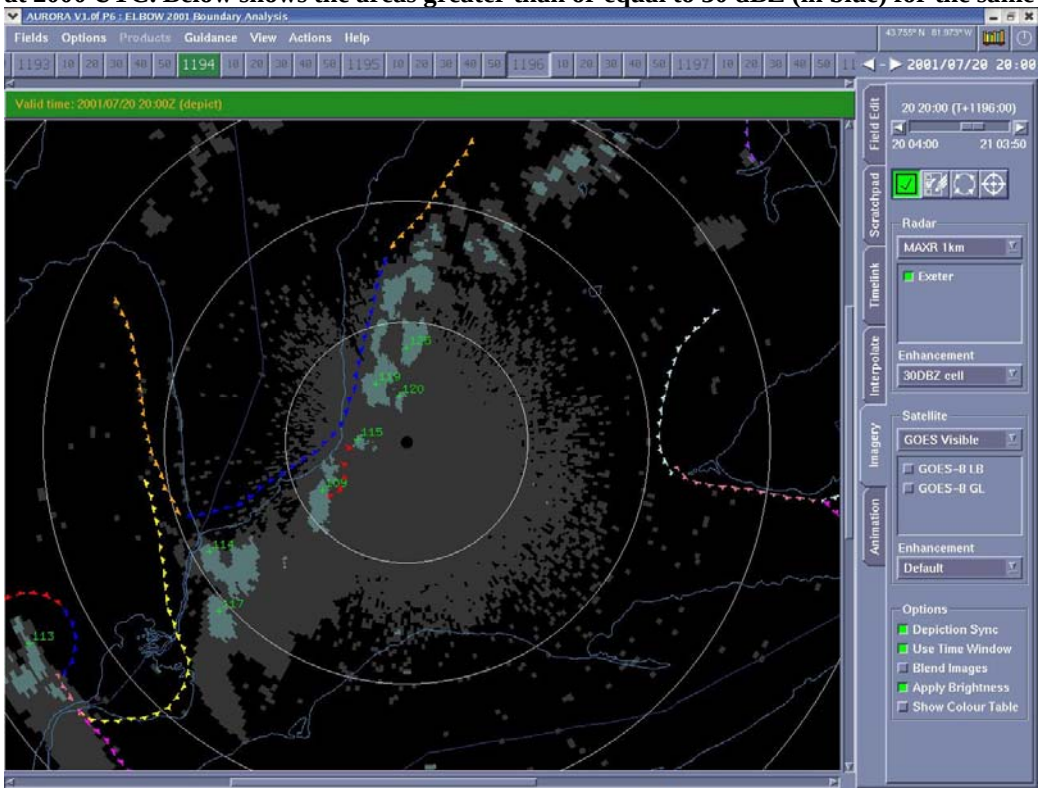

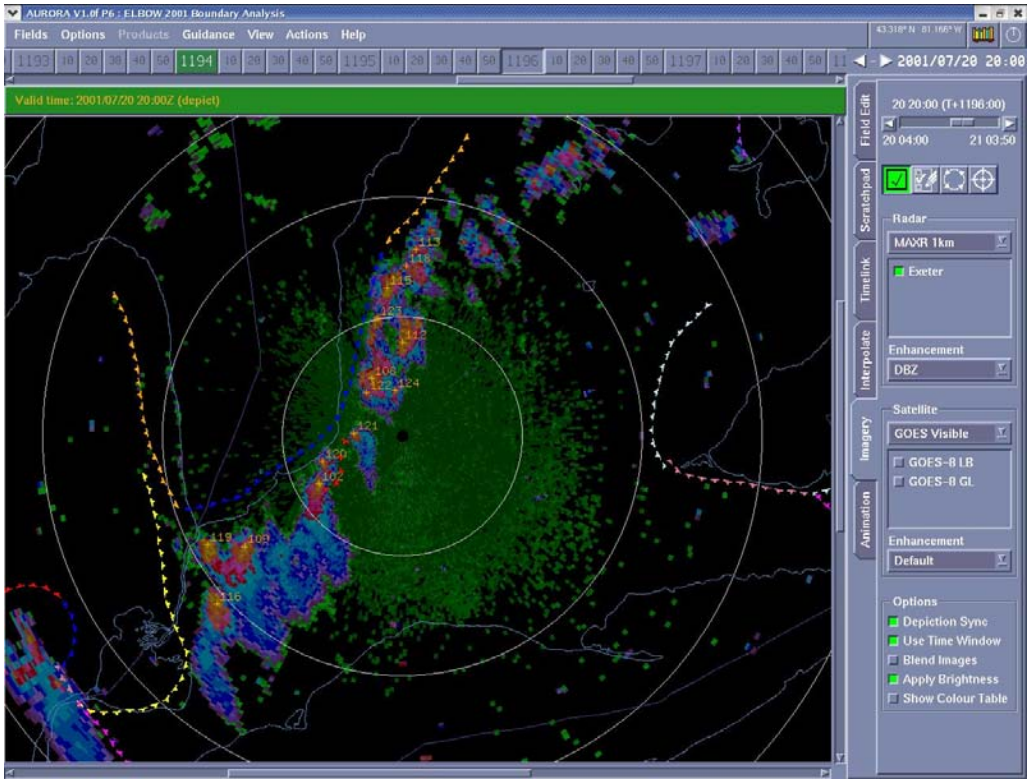

<u>Figure 6.4c(above) and 6.4d (below)</u>. Above shows the MAXR image and 40 dBZ cells for July 20, 2001 at 2000 UTC. Below shows the areas greater than or equal to 40 dBZ (in blue) for the same time.

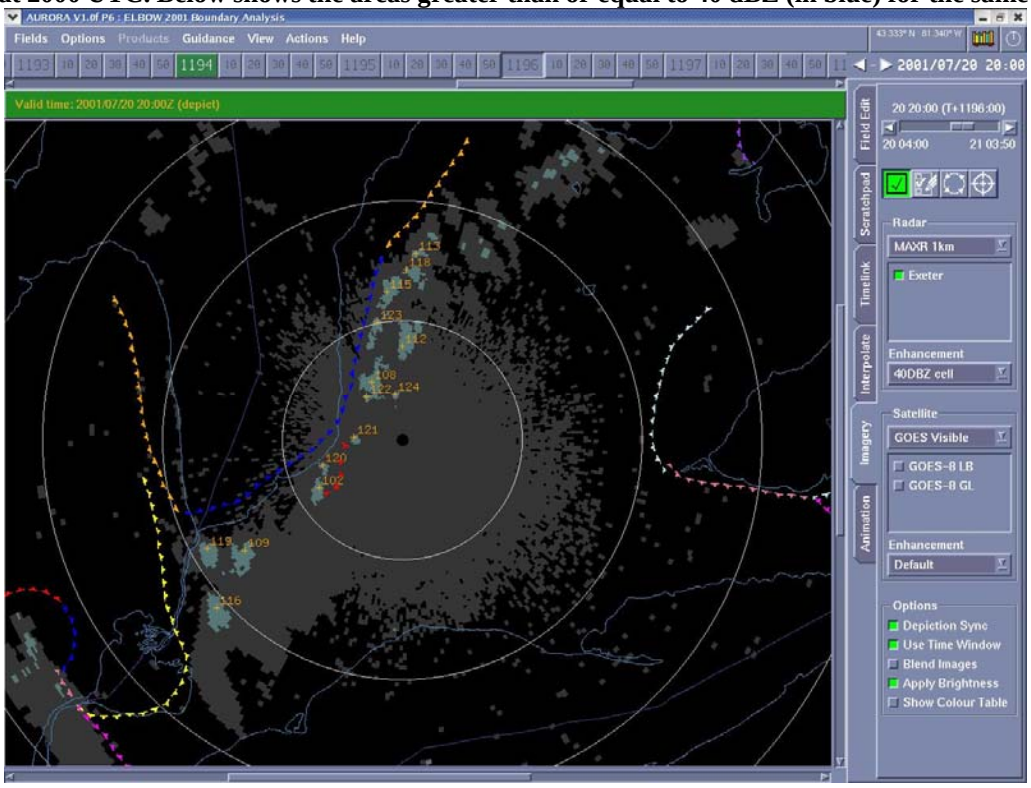

6.4.2 First Analysis

In order to make sure all boundaries were identified in the area surrounding each cell, only the cells (which reached the 40 dBZ threshold) within a distance of 50 km of the radar were considered. The Final 'truth' set of boundaries were used for this analysis (boundaries identified included lake breeze fronts, land breeze fronts, gust fronts, hybrid boundaries, merged boundaries and 'other' boundaries which included boundaries of unknown origin, horizontal convective rolls and synoptic boundaries, as noted in Chapter 5). Since these boundaries were identified for each hour, cells which reached a 40 dBZ level on the hour or 10 min after were considered. Both these times were considered because the radar scans for each were conducted very close to the hour. Conventional scans for the radar image on the hour are actually started 5 min before the hour, and conventional scans for the radar image 10 min past the hour are actually started 5 min past the hour.

When a cell initially reached a 40 dBZ level, the distance from the cell to the closest boundary (as found in the Final 'truth' set of boundaries) was measured. In other words, if this cell had not been identified for the previous identification time (10 minutes before), it was considered in this analysis. Cells identified on the hour and 10 minutes past were measured to the closest boundary on the hour. AURORA allowed for this since it had a tool to measure from one chosen location to another. AURORA gave the distance to the closest km and the direction (see Figure 6.5). Specifically, distances were measured

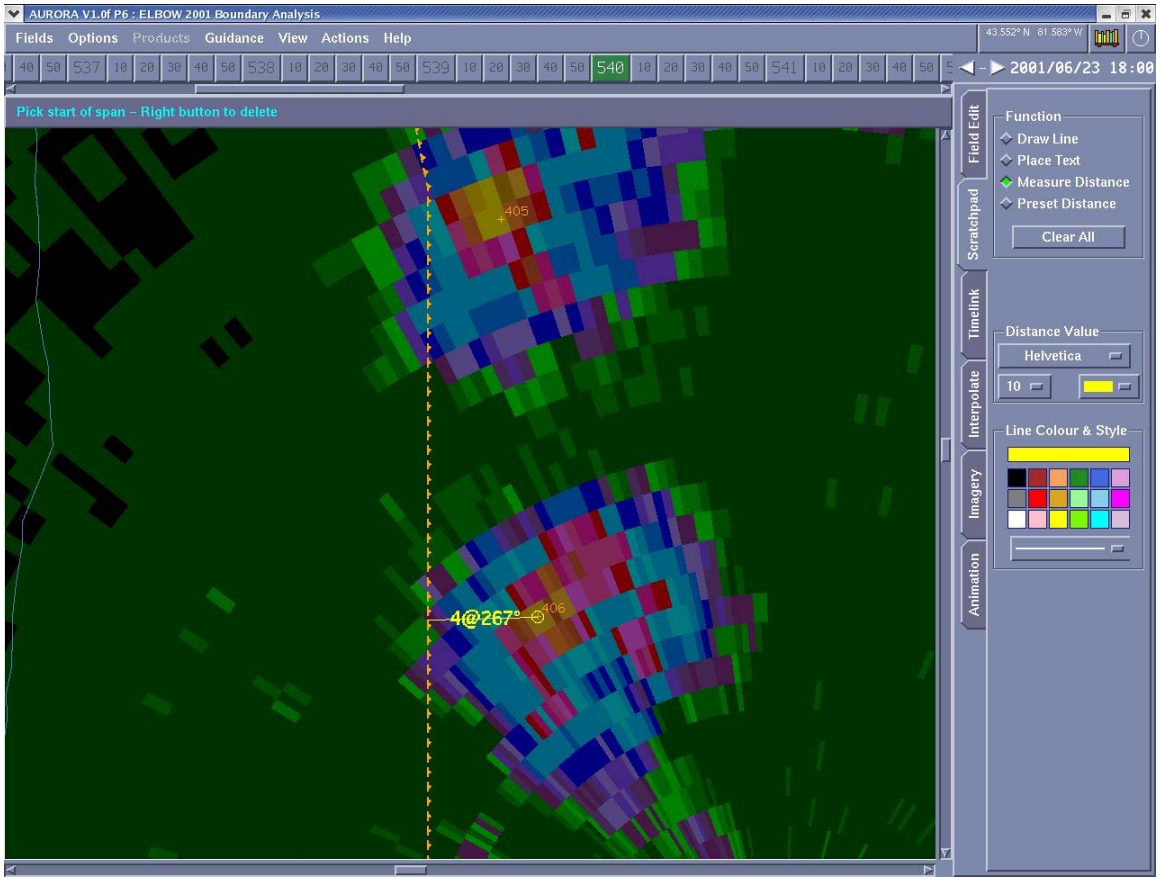

Figure 6.5. Showing the distance and direction measured (in yellow) from the maximum reflectivity of a cell to the closest boundary. As can be seen from this image, this was done in AURORA.

from the storm's highest reflectivity to the closest boundary. This was done for both the CAPPI and MAXR cell information. Each day, from June 1 to August 31, 2001, was analysed from 1600 to 0000 UTC. The initial results can be seen in Figure 6.6a and 6.6b.

In this first analysis, the cell tracking was assumed to be consistently evaluating the data correctly. So, when a new track number started at the times in question (on the hour and 10 minutes past) they were considered to be cells which have initially reached 40 dBZ.

The CAPPI 1.0 km data showed 153 cells reaching a 40 dBZ level within 50 km of the Exeter radar, during the period of June 1 to August 31, 2001. The MAXR 1.0 km data showed significantly more cells. 264 cells reached a 40 dBZ level within 50 km of the Exeter radar. The results of the first analysis can be seen in Appendix M. Figure 6.6a and 6.6b show that many cells occur close to a boundary that has been identified in the Final 'truth' set of the boundary analysis. In fact, 62.7 percent of the CAPPI cells reached a 40 dBZ level at a distance of 20 km or less from a boundary and 57.2 percent of the MAXR cells reached a 40 dBZ level at a distance of 20 km or less from a boundary. Notice from Figures 6.6a and 6.6b the peak number of CAPPI cells occurred at 5 to 9 km and the peak number of MAXR cells occurred at 0 to 4 km (for those which occurred in close proximity to a boundary). This suggests that the MAXR may have detected the cells at a 40 dBZ level before the CAPPI. Figures 6.6a and 6.6b also show peaks at the '100 kilometers and greater or none' interval. This column represents the cells that reached a 40 dBZ level at 100 km or more from an identified boundary, or there was no existing boundary to measure to. The number of MAXR cells, in this column, is much higher than the number of CAPPI cells. Since these MAXR data represent the greatest reflectivity in a column from 1.0 km and above, it is possible that many of these cells represent elevated convection which was not associated with low-level mesoscale boundaries or cold fronts identified in the Final 'truth' set. These cells may have often occurred

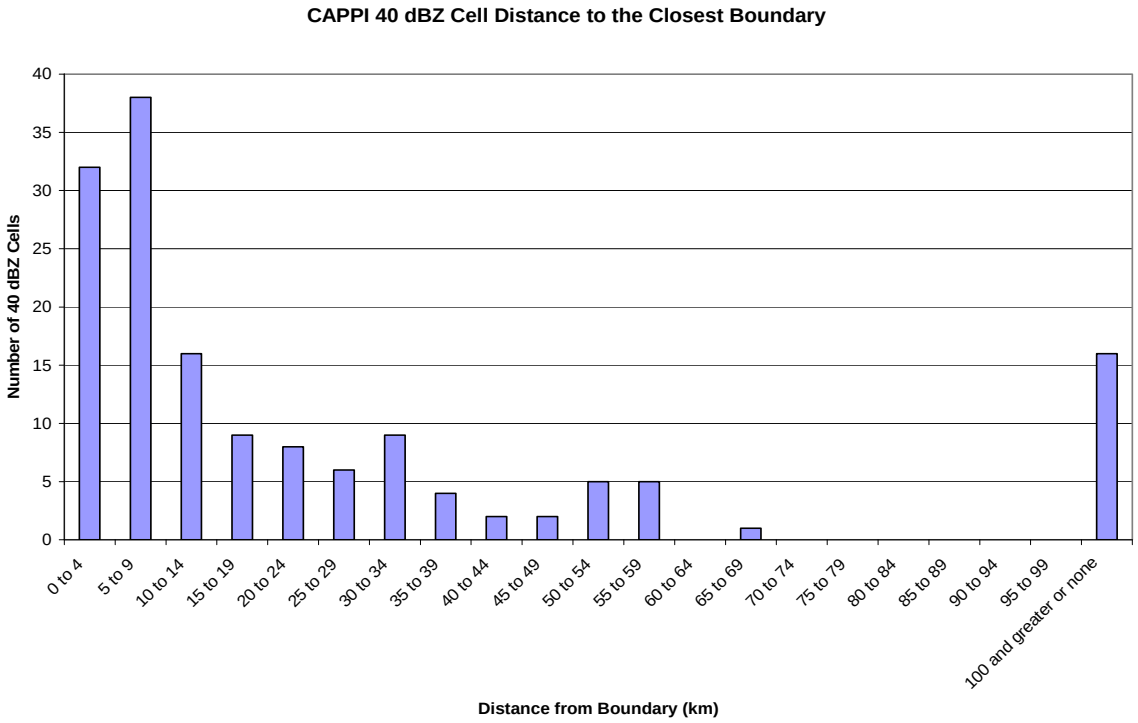

Figure 6.6a (above) and 6.6b (below). Bar charts showing the distance from the cells (reaching a 40dBZ level) to the closest boundary, for both CAPPI (above) and MAXR (below). These results correspond to the first analysis.

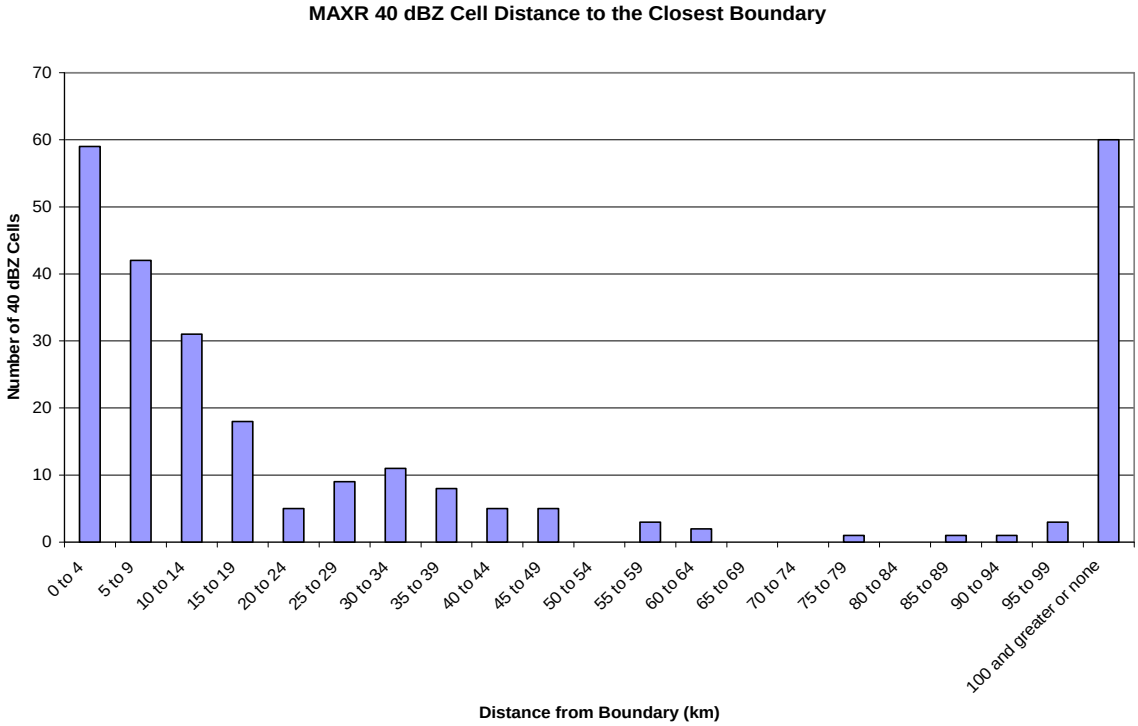

in warm front cases (where elevated convection has a tendency to occur). Warm fronts would not have been identified in the mesoscale boundary identification (so cells could not be measured to these warm fronts), therefore the large distances would represent distances to a mesoscale boundary the cell was not associated with.

In order to test this theory, the data on days which had warm front influence in the study region were separated from the data on the days with no warm front influence. Surface Analysis charts for 0000, 0600, 1200 and 1800 UTC, from the Meteorological Service of Canada, were studied to reveal if there was warm front influence in the study area for each day from June 1 to August 31, 2001. After visually interpolating between the map times, if the warm front was present in the ELBOW 2001 study region or the cloud formations associated with a warm front were affecting the study region, then the day was considered a 'Warm Front Day'. The Warm Front days were as follows:

June: 1, 5, 6, 9, 10, 11, 12, 18, 20, 21

July: 3, 4, 7, 15, 16, 17, 19, 20, 21, 25, 28

August: 1, 2, 8, 12, 16, 18, 22, 25, 27, 30

The bar charts in Figures 6.7a and 6.7b show the 40 dBZ cell distance to the closest boundary on Warm Front days. The plots in Figures 6.8a and 6.8b show the 40 dBZ cell distance to the closest boundary on Non-Warm Front days.

As can be seen from Figures 6.7a and 6.7b, the Warm Front days include many of the cell initiations that are 100 km and greater from a boundary, or have

no boundary present to measure to. For the CAPPI results, 81.2 percent of the 100 km or greater/none category for all days are shown in these warm front results. As expected, the MAXR results show 91.7 percent of these cells in the 6.7b Warm Front day bar chart.

As can be seen, there are still 40 dBZ cell initiations which are close to boundaries in both the CAPPI and MAXR Warm Front day results. Many of these may be due to the fact that full days which had warm front influence were considered in this category. For example, a warm front may have only affected the study area in the morning, so all the boundaries and cells that formed after its passing (on the same day) are also considered in these statistics.

Looking at Figures 6.8a and 6.8b, representing days with no warm front influence, we can see that many of the cells initially reaching 40 dBZ occur close to a boundary. In the CAPPI results, 72.3 percent of the cells reached 40 dBZ at a distance of 20 km or less from a boundary. Only 3 cells were found to reach 40 dBZ at a distance of 100 km or greater (or no boundary present). In the MAXR results 79.4 percent of the cells reached 40 dBZ at a distance of 20 km or less from a boundary. Only 5 cells were found to reach 40 dBZ at a distance of 100 km or greater (or no boundary present).

Clearly, the cells which reach 40 dBZ on days with no warm front influence are more closely related to the boundaries such as lake breeze fronts, land breeze fronts, gust fronts, hybrid boundaries, merged boundaries, and other boundaries (including boundaries of unknown origin, horizontal convective rolls

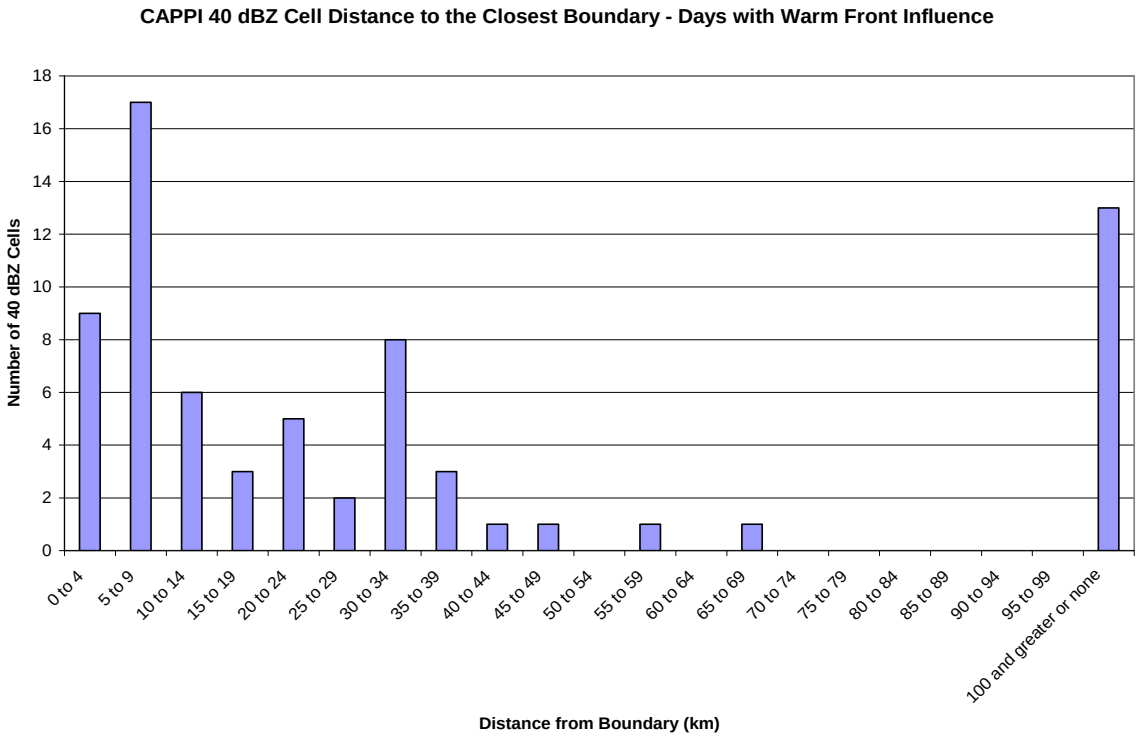

Figure 6.7a (above) and 6.7b (below). Bar charts showing the distance from the cells (reaching a 40dBZ level) to the closest boundary, for both CAPPI (above) and MAXR (below) on days with warm front influence.

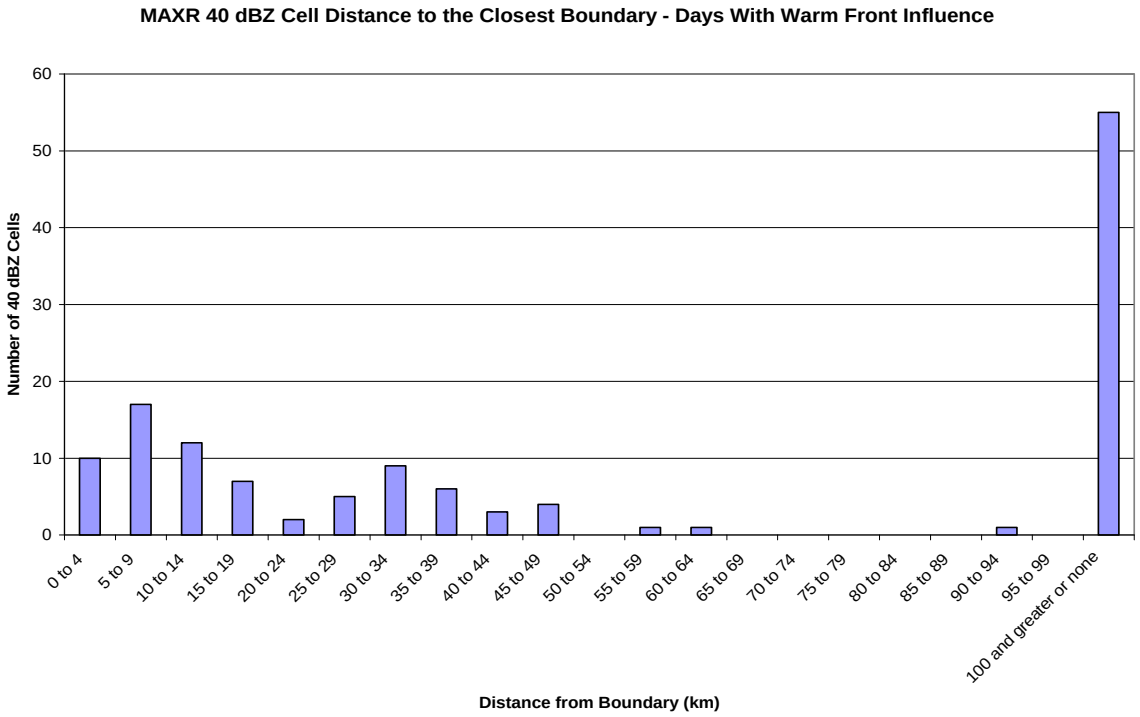

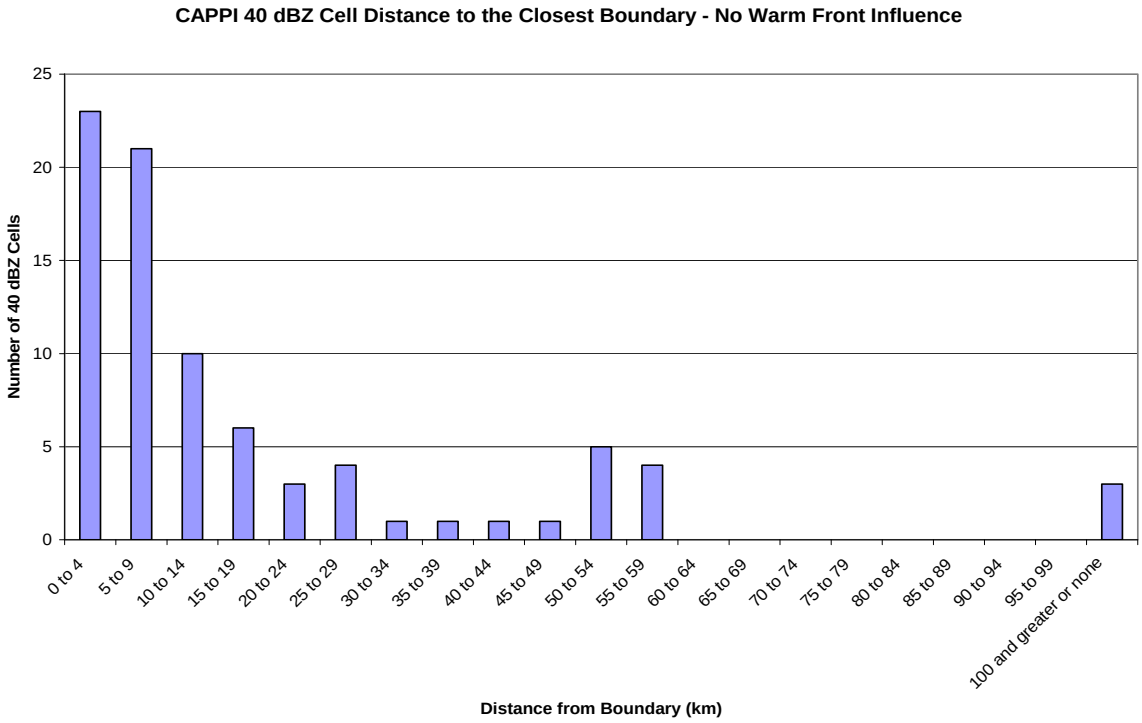

Figure 6.8a (above) and 6.8b (below). Bar charts showing the distance from the cells (reaching a 40dBZ level) to the closest boundary, for both CAPPI (above) and MAXR (below) on days without warm front influence.

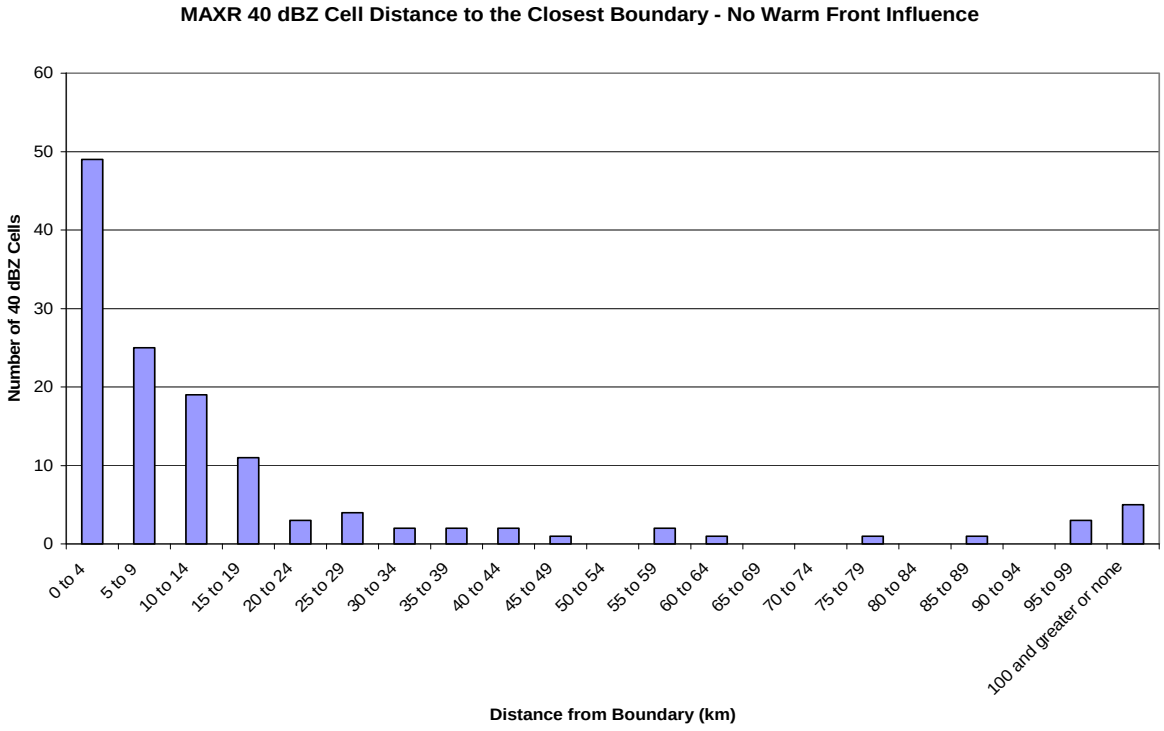

and cold fronts). A second analysis was done on the 40 dBZ cell data, looking more in depth at the days with no warm front influence. This analysis is covered in the following section.

6.4.3 Second Analysis Methodology

A second analysis again looked at the cells initially reaching 40 dBZ for both 1.0 km CAPPI and 1.0 km MAXR data. This analysis only looked at days *without* warm front influence and only considered cells between 1600 and 0000 UTC on the hour and 10 minutes after the hour. The cells within 80 km of the radar were considered in this analysis (up from 50 km in the previous) in order to increase the size of the data set. In this analysis the URP cell tracking data was only used as a *suggestion*. From looking closely at these data in the previous analysis, it was clear that when many small cells occurred in a small area, the tracking numbers are not always consistent, or the numbers would jump from one cell to another. The URP cell identification was still considered to be correct. So, if a cell showed to have a reflectivity level of 40 dBZ but was not present in the 40 dBZ identification data 10 minutes before, it was considered in this analysis (after judging the track visually).

The distance to the closest boundary (in the Final 'truth' set) was then measured for each of these initiating cells. However, if the closest boundary was a gust front, the previous identification times were observed to make sure the gust front did not originate from this cell. If the gust front did appear to originate from the cell in question, then the cell distance was measured to the second

closest boundary. This was done because the purpose of this study was to look at cell development possibly caused by boundaries, not the other way around.

In order to get a better understanding of the development in the Great Lakes region, more details about these cells (and their related boundaries) were collected in this analysis. It was important to track these cells visually after they reached 40 dBZ. The following data were collected for each cell:

- Month
- Day
- Cell Number (tracking numbers)
- Time (UTC)
- Noted if there was more than one identification of the cell (consecutively following)
- Distance to the Closest Boundary (to the nearest kilometer)
- Direction from the Cell to the Boundary
- Boundary Type
- Boundary Classification
- Noted if the Cell was ahead, behind or to the side of the boundary (if applicable)
- Noted if the Cell reached 60 dBZ
- Boundary Speed
- Direction of the Boundary
- Latitude of the Cell

- Longitude of the Cell
- Distance the Cell was from the radar location
- Direction to the radar from the cell
- Speed of the Cell
- Direction of the Cell

Some of the data that were collected in this second analysis will now be explained in more detail as to how they were collected and why. This is done for the data that are not simply self explanatory.

a. New 40 dBZ Cells

To identify a 40 dBZ cell initiation the cell must be shown in the 40 dBZ URP cell identification and tracking data. The tracking numbers are taken as a suggestion for the actual track of the cell. In this second analysis the tracks for the cells and the new 40 dBZ cells are found visually. If the cell did not appear in the previous 10 minute identification then the cell is considered in this analysis. Therefore, it may be possible for a cell to be at 40 dBZ, drop below this threshold for a time and then re-intensify to 40 dBZ again (in this case a cell would be considered twice).

If there was a large 40 dBZ area identified at the previous time, which included a number of different cells, then the cells included in this area cannot be counted at the present time (time being considered). Also, since tracking numbers are taken as a suggestion, new numbers do not always mean there is a new 40 dBZ cell. Old numbers can often be found to be new 40 dBZ cells if the

tracking numbers have jumped from one cell to another, especially with many cells in a small area. The numbers of the new 40 dBZ cells can be found by looping the radar to see how the cells have progressed and if they were identified at the previous 10 minute identification.

b. Boundary Type

The 'boundary type' is the type of boundary that the initiated cell was closest to (as long as it was not a gust front formed by the cell itself). These boundary 'types' were simply the boundary type found from the Final 'truth' set boundaries being used for this analysis. This could be a lake breeze front (which lake it originated from was also noted), a land breeze front, a gust front, a merged boundary, a hybrid boundary, or an 'other' boundary (their definitions can be found in Chapter 5).

c. Boundary Classification

Boundaries were 'classified' similarly to those in Wilson and Schreiber (1986). The classifications included: Moving, Stationary, Merger, Intersection, Collision, and Synoptic. Moving or Stationary boundaries had to show fairly consistent motion or a lack of motion, respectively. Stationary boundaries may shift back and fourth slightly (due to small variations in the boundary identification) but generally stay in the same area. Synoptic boundaries could be synoptic scale fronts (cold fronts were the only boundaries that seem to be identifiable using the boundary analysis).

Merger, Intersection and Collision were all Intersecting boundaries, such as Merged or Hybrid boundary types. In order to find which classification these boundaries lie under, it was necessary to look at previous times when the two boundaries start to collide at the closest location to the cell in question. If it was impossible to see the interaction at this point, the next closest point along the boundary was viewed. If it was still difficult to see the initial interaction, satellite, radar and mesonet data were studied at times between the hours to get an idea of how the boundaries were oriented when they started to interact.

If the boundaries were moving in a similar direction when they came together (less than 90 degrees difference), they were classified as a *Merger*. If the boundaries were moving towards each other they could be one of two classifications. If the boundaries were interacting at an angle of greater than 30 degrees they were classified as an *Intersection*, however, if the boundaries came together closer to a head-on orientation, at an angle of less than 30 degrees, they were classified as a *Collision*. Figure 6.9 shows how the boundaries may be

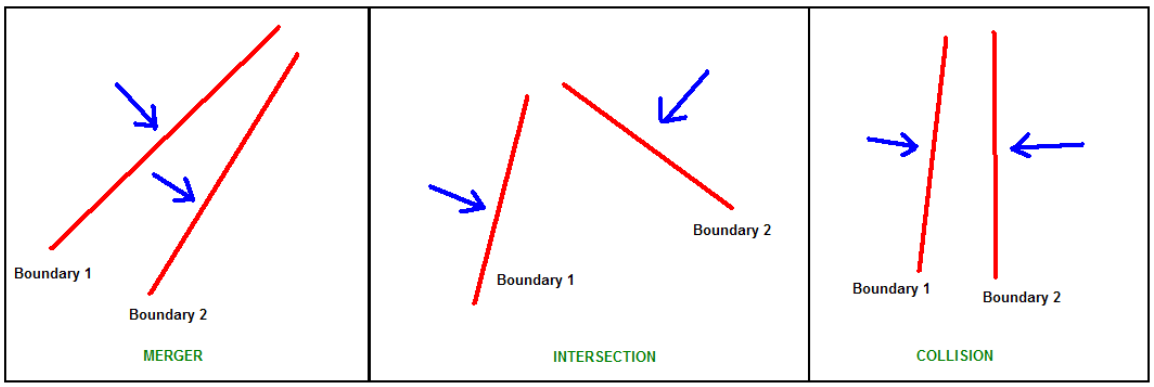

Figure 6.9. Showing an example of how two boundaries may be oriented before they interact in a Merger, Intersection or Collision case. The red lines represent the mesoscale boundaries and the blue arrows represent their motion.

oriented previous to a Merger, Intersection or Collision (as long as the movement is consistent).

d. Cells Ahead, Behind or to the Side of a Boundary

In order to look at the locations where the cells initiated relative to the boundary, it was noted if the cell occurred ahead, behind or to the side of a boundary. Figure 6.10 shows an example of a boundary (shown in red) with motion shown by the blue arrows. This could be a gust front, for example. Here we can see that the area around the boundary has been split into 4 areas. At the end of the boundary, two lines have been drawn 45 degrees to the perpendicular orientation of the boundary. The areas at the end of the boundary, outlined by these lines (in aquamarine), is the area where cells occurring are considered to be to the side of the boundary. If the cell occurs in the white area it is considered to be behind the boundary. If the cell occurs in the yellow area it is considered to be ahead of the boundary. It is significant to consider these in the final results for reasons pertaining to the boundary identification criteria. The boundary identification criteria (as mentioned in Chapter 5) stated generally that boundaries must be identified by fine lines in the radar, cumulus cloud lines in the satellite, or sharp changes in wind direction in the mesonet. However, it notes that these boundaries cannot simply be identified by lines of strong convective development. Since these boundary criteria were going to be used to show that convective development occurs from effects of these boundaries, the convective development could not be assumed to show the presence of a boundary. It is

possible that when convective development occurred along these boundaries, they may not have been fully identified due to obscurity caused by this development. It is also possible that in the identification, especially using the mesonet, it may have been hard to determine where the end of the boundary was. So, if these boundaries extended further than identified, there is a 'to the side' category created, so that larger distances from the boundary were not contributed to the statistics for the cells which occurred ahead or behind the boundary. Figure 6.11 shows a case where anomalous distances may be contributed. The red line represents a boundary, and the blue dotted line represents where the boundary could possibly extend (if it could not be fully identified). Notice that distance 1 (distance to the boundary if it did not extend) is

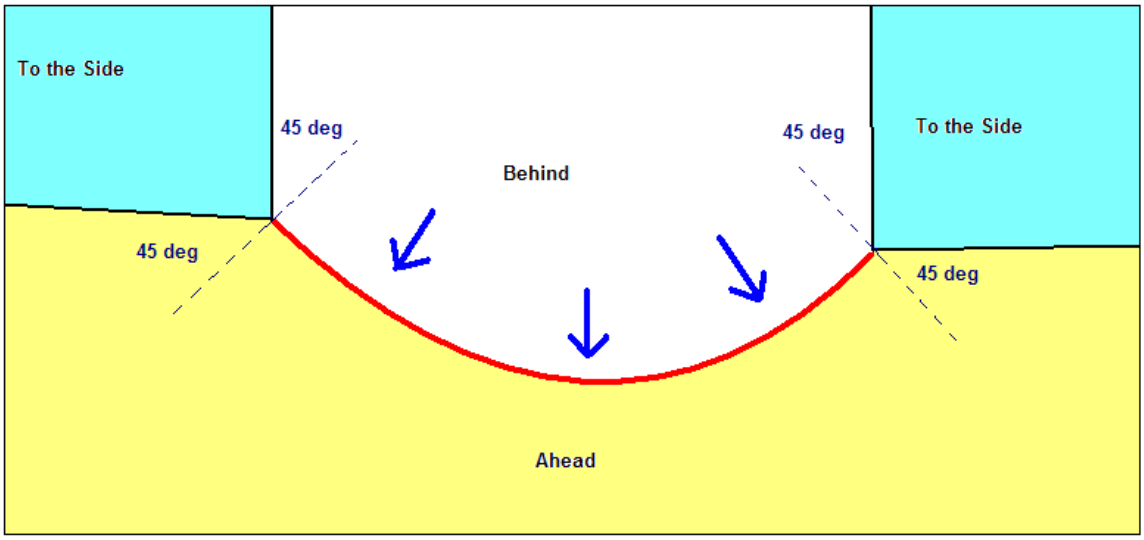

Figure 6.10. Diagram showing the areas where cell locations would be considered to be ahead, behind or to the side of a boundary. The red line is the boundary and the blue arrows show its motion.

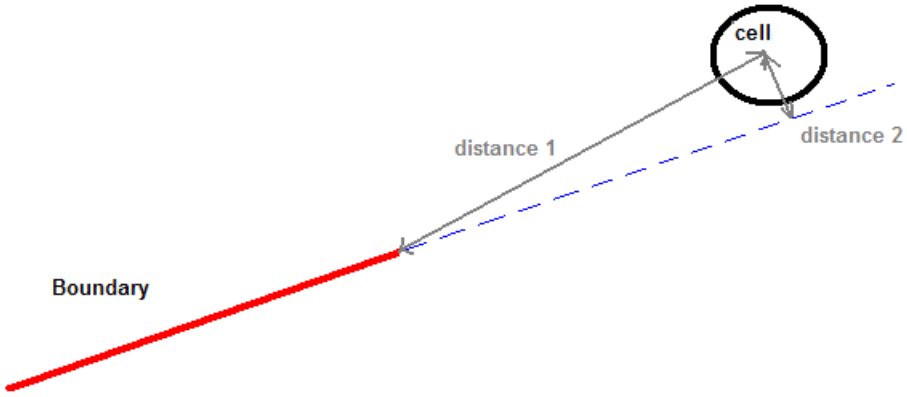

Figure 6.11. A diagram showing how the distance of a cell from a boundary may be larger than is accurate, if a boundary was not fully identified. The red line represents the boundary and the blue dotted line represents where it may extend, if the presence was obscured by convective development.

significantly larger than distance 2 (if the boundary did extend and could not be identified here). So, in order to get a clear look at the data it was split into the ahead, behind and to the side categories.

It should also be noted that what is considered ahead, or behind was dependent highly on the boundary type. Gust fronts always moved away from the storm which caused them, so the side towards the storm they originate from is considered 'behind' the boundary and 'ahead' is the side away from the storm of origin. Lake breeze fronts were *always* considered to have the land side 'ahead' of the boundary and the lake side is 'behind' the boundary. Sometimes the lake breeze fronts could be seen to retreat (backwards) towards the lake, but generally they moved inland. For the 'Other' boundaries, which were moving, we simply look at motion: 'ahead' is the side the boundary is moving towards. Merged, Hybrid, and boundaries which are stationary did not have their data split

into ahead or behind because there was no way to distinguish. However, it was noted if the cells occurred to the side of these boundaries.

e. Cells reaching 60 dBZ

URP Cell identification and tracking was also done for a 60 dBZ threshold. Therefore the 40 dBZ cells were visually tracked through their lifetime to see if they reached the 60 dBZ threshold. It was noted if they did or did not reach this threshold.

f. Boundary Speed and Direction

It is very difficult to get the exact motion of the boundaries in question. In this analysis the speed and direction of the boundary were always measured perpendicular from the boundary at the time the cell reached 40 dBZ (using the measurement tool in AURORA). The speed and direction for each case was always measured at the boundary location closest to the cell. In the ideal case the speed and direction was measured for the hour before the cell reached 40 dBZ. If the boundary was not identified the hour before, then it could be measured to a time less than an hour before. If no boundary identifications were done then, then this could be measured for the hour following or to a time less than an hour following, as long as the boundaries were identified for these times. If there was no perpendicular boundary location to the point of the boundary closest to the cell, then the next closest point along the boundary with a perpendicular location was chosen to estimate the movement of the boundary.

In the case of interacting boundaries, such as a merged boundary, the boundary must be measured to the same boundary type (merged boundary) an hour before. If the boundary did not yet interact (merge) by this time, then it must be measured to the next time option, as explained earlier. In other words, the motion of the interacting boundary cannot be measured using the location of the single boundaries which eventually interact to create it.

g. Cell Latitude and Longitude

In AURORA, the cells identified/tracked could be sampled. In this study, the locations of the cells were marked by their point of maximum reflectivity. When this point was sampled, AURORA displayed the latitude and the longitude of the cell location. This was noted for further analysis, such as the cell plots in section 6.4.5.

h. Cell Speed and Direction

The speed and direction of a cell were measured if the cell had more than one identification (consecutive time identification). That is, if the cell was still identified 10 minutes after it is initially identified for 40 dBZ. The AURORA measurement tool was used to measure from the first location cell reflectivity maximum to the maximum reflectivity of the same cell 10 minutes later. Again, this cell has been tracked through a visual judgement. It should be noted that the distance and direction the cell moves (found in this manner) may not be the most accurate, since the reflectivity maximums within a cell may change over time, but this allows for a general estimate of the motion.

6.4.4 Second Analysis Results

We can see the results for the second analysis for both CAPPI and MAXR in Figures 6.12a and 6.12b. The distance scale is different in these charts (as compared to the first analysis charts) due to the change in study area size for this analysis, as compared to the area the boundaries were identified for. The results from the second analysis are considered to be the most accurate results, since more precautions were taken in tracking (done visually) and measuring distance to a boundary which was not caused by the cell in question.

The analysis of the CAPPI data showed a total of 169 initiating 40 dBZ cells. 70.4 percent of the cell initiations occurred at a distance of 20 km or less from a boundary. The MAXR analysis captured considerably more cells, showing a total of 260 initiating 40 dBZ cells. Similar to the CAPPI results, the MAXR showed 68.5 percent of the cell initiations occurred at a distance of 20 km or less from a boundary.

Both Figures 6.12a and 6.12b show the peak number of initiating 40 dBZ cells to be located at the 0 to 4 km interval from the boundary. However, 24.9 percent of the initiating 40 dBZ cells occur in the 0 to 4 km interval for the CAPPI results, and the MAXR shows a higher percentage of 30.8. Again, this suggests that these 1.0 km MAXR data show a better lead time in cell detection than the 1.0 km CAPPI data. The final interval shows a peak in the data (more distinct for MAXR than for the CAPPI). This could partly be due to the fact that this interval

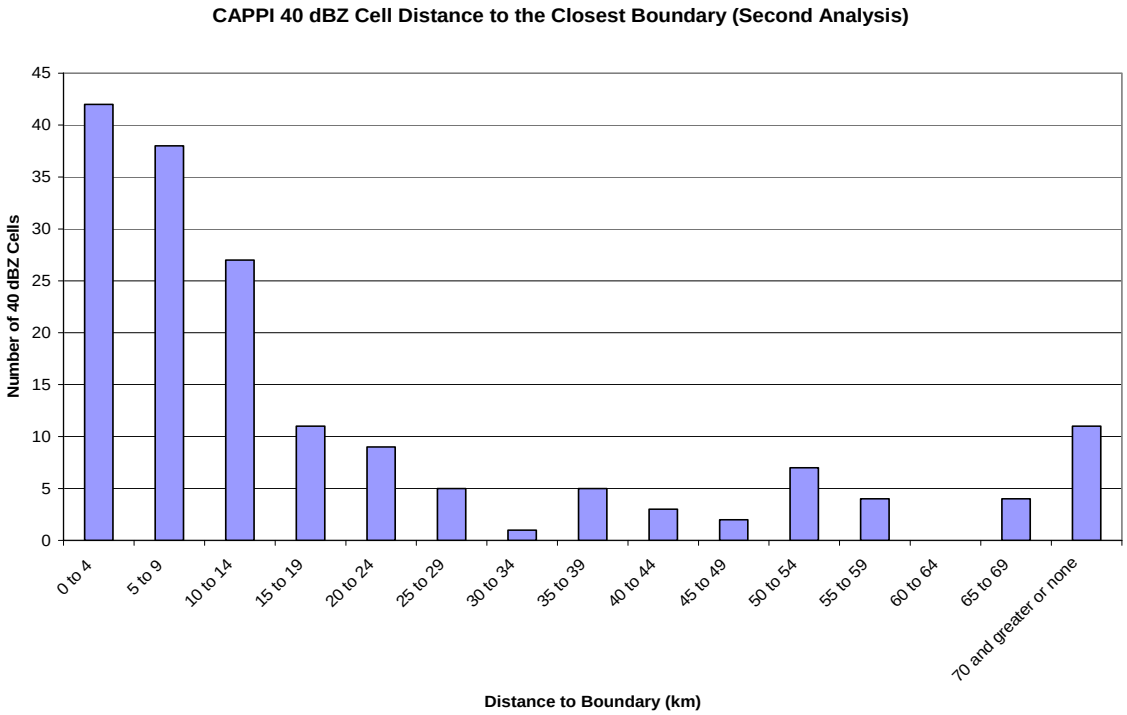

Figures 6.12a (above) and 6.12b (below). Bar charts showing the distance from the cells (reaching a 40dBZ level) to the closest boundary, for both CAPPI (above) and MAXR (below) on days without warm front influence. These charts show the results for the second analysis.

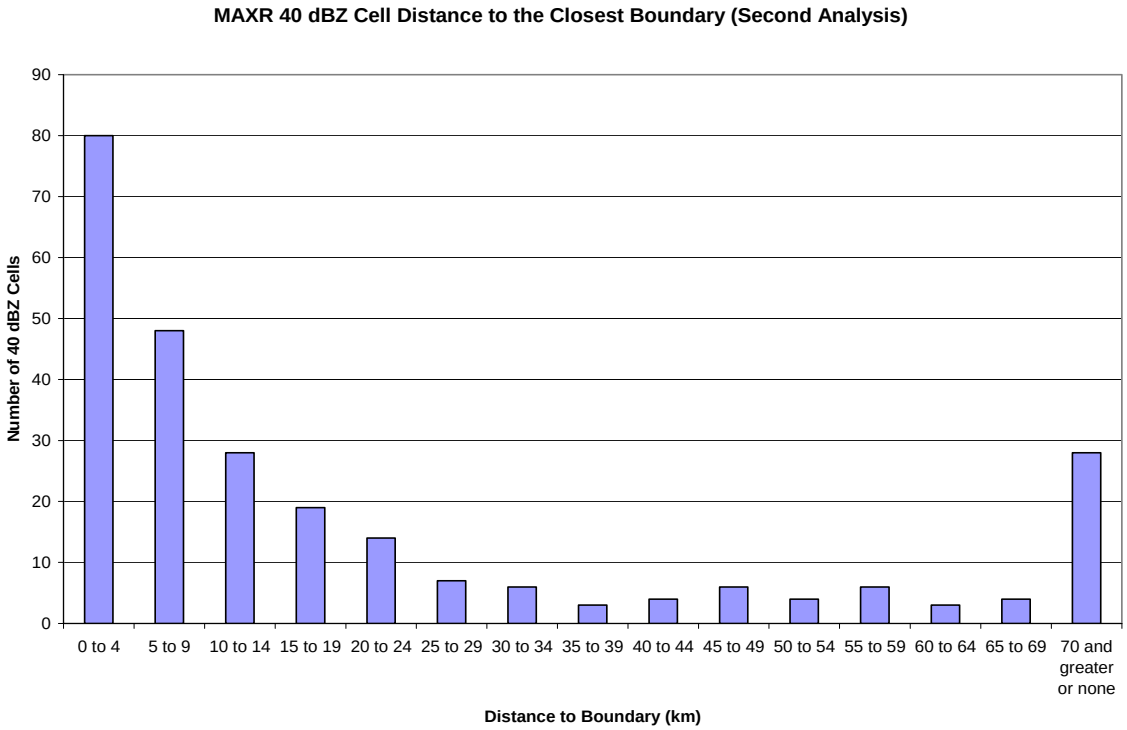

is 70 km and greater, or no boundary to measure to, instead of from 100 km and greater for the previous analysis.

Table 6.1 shows the percentage and number of the initiating cells that are pertaining to each boundary type, for the CAPPI results. The similar MAXR results are shown in Table 6.2. Notice that for both tables the Gust Fronts show the largest number of cell initiations. Lake Breeze Fronts show to have the second highest results. For the CAPPI results, the Merged Boundaries show the fewest cell initiations and for the MAXR the Merged and Joint Between Boundaries show the fewest cell initiations. This is most likely due to the fact that lake breeze fronts have to be well developed and have moved inland far enough to form a merged boundary so occurrences are not as frequent as that of other boundaries in the ELBOW study region. Joints are where two boundaries appear to be linked (end to end) without actually becoming a hybrid or merged boundary. Therefore, these 'Joints' also require some boundary interactions, again suggesting that their occurrences are not as frequent in the ELBOW study region.

The number of 40 dBZ cell initiations measuring closest to a gust front is significant. In theory, something needs to be triggering the initial cell which subsequently causes gust front development. By looking at the CAPPI cell data (as can be seen in Appendix N), 10 days had 40 dBZ cell initiations measuring closest to gust fronts or boundaries with gust fronts involved (such as Hybrid boundaries). Of these 10 days there were 6 days which found cell initiations measuring closest to a boundary, which was not a gust front or involving a gust

front, first. In fact, the first boundary type an initiated cell measured closest to on these days was a lake breeze front. This suggests that lake breeze fronts may tend to trigger the first storms of the day which in turn can form gust fronts.

Looking at the MAXR data (in Appendix N) we can see that of 11 days that showed 40 dBZ cell initiations measuring closest to a gust front or a boundary involving a gust front, 7 days showed cell initiations measuring closest to another type of boundary first; 6 of these days showed the first boundary type to be a lake breeze front.

Table 6.1. CAPPI results split into Boundary Type. Showing the number and percentage of cells (initiating to 40 dBZ) which measured closest to each boundary type.

	# of Cells (initially reaching 40 dBZ)	Percentage of Total
Total Cells	169	
Lake Breeze Front	22	13.0
Gust Front	99	58.6
Merged Boundary	3	1.8
Hybrid Boundary	18	10.7
Joint Between Boundaries	5	3.0
Other Boundary	16	9.5
No Boundary to Measure to	6	3.6

Table 6.2. MAXR results split into Boundary Type. Showing the number and percentage of cells (initiating to 40 dBZ) which measured closest to each boundary type.

	# of Cells (initially reaching 40 dBZ)	Percentage of Total
Total Cells	260	
Lake Breeze Front	53	20.4
Gust Front	142	54.6
Merged Boundary	4	1.5
Hybrid Boundary	21	8.1
Joint Between Boundaries	4	1.5
Other Boundary	24	9.2
No Boundary to Measure to	12	4.6

So do lake breeze fronts tend to initiate the storm activity for the convective day? This would be clearer if the full day and every 10 minutes of data were studied, instead of every hour. However, we can see from the CAPPI data in Appendix N that 58.3 percent of the days which had cell initiations detected showed the first cell initiation, of the 1600 to 0000 UTC period, to measure closest to a lake breeze front. The MAXR data in Appendix N shows that 55.6 percent of the days which had cell initiations detected showed the first cell initiation of the period to measure closest to a lake breeze front. So, the majority of the first 40 dBZ cells initiate closest to a Lake Breeze Front.

These 40 dBZ cell initiation data can also be split up into boundary classifications, which are similar to those used by Wilson and Schreiber (1986). Table 6.3 shows the CAPPI results split into boundary classifications and Table 6.4 shows the MAXR results split the same way. As we can see, 78.1 of the CAPPI 40 dBZ cell initiations and 79.6 of the MAXR 40 dBZ cell initiations measured closest to a moving boundary. The Great Lakes region is a very unique mesoscale boundary region in the summer, which has a large number of lake breeze fronts and gust fronts occurring. These boundary types would be included in the moving boundary classification. Therefore these results seem very suitable for this region.

Table 6.3. CAPPI results split into Boundary Classification. Showing the number and percentage of cells (initiating to 40 dBZ) which measured closest to each boundary classification.

	# of Cells (initially reaching 40 dBZ)	Percentage of Total
Total Cells	169	
Moving Boundaries	132	78.1
Colliding Boundaries	11	6.5
Intersecting Boundaries	3	1.8
Merger Boundaries	12	7.1
Stationary Boundaries	2	1.2
Synoptic Boundaries	3	1.8
No Boundary to Measure to	6	3.6

Table 6.4. MAXR results split into Boundary Classification. Showing the number and percentage of cells (initiating to 40 dBZ) which measured closest to each boundary classification.

	# of Cells (initially reaching 40 dBZ)	Percentage of Total
Total Cells	260	
Moving Boundaries	207	79.6
Colliding Boundaries	15	5.8
Intersecting Boundaries	5	1.9
Merger Boundaries	8	3.1
Stationary Boundaries	5	1.9
Synoptic Boundaries	8	3.1
No Boundary to Measure to	12	4.6

Tables 6.5 and 6.6 show the results of the CAPPI 40 dBZ cells for the distance they were measured to the closest boundary, split into boundary types and boundary classification, respectively. It should be noted that the cells which had no boundary to measure to were not considered in either of these tables.

In Table 6.5, the Merged Boundaries and Joint Between Boundaries showed to have 100 percent of the initiating cells to be 20 km or less from the boundary. However, it should be noted that these were a very small data set. The data set of considerate size was that of the Gust Front which showed that out of 99 initiating cells, which showed to measure closest to this boundary type,

63.6 percent of the cells were 20 km or less from the gust front when they reached 40 dBZ.

In Table 6.6, the Colliding, Intersecting and Stationary Boundaries showed that 100 percent of the 40 dBZ cells occurred 20 km or less from a boundary. But again, these boundaries have a very small data set, as seen from the cell totals. The data set of considerate size is the Moving Boundaries classification. This boundary classification showed a total of 132 initiating cells and 68.2 percent of the cells occurred at a distance of 20 km or less from a moving boundary.

Table 6.5. Distribution of 1.0 km CAPPI 40 dBZ Results for each Boundary Type.

	Number of 40 dBZ Cell Initiations Pertaining to Boundary Type					
Distance to Closest Boundary	**Lake Breeze Front**	**Gust Front**	**Merged Boundary**	**Hybrid Boundary**	**Joint Between Boundaries**	**Other Boundary**
0 to 4 km	2	24	1	7	2	6
5 to 9 km	7	18	2	6	2	3
10 to 14 km	8	12	0	3	0	4
15 to 19 km	0	8	0	1	1	1
20 to 24 km	0	7	0	1	0	1
25 to 29 km	2	3	0	0	0	0
30 to 34 km	0	1	0	0	0	0
35 to 39 km	1	4	0	0	0	0
40 to 44 km	1	2	0	0	0	0
45 to 49 km	0	2	0	0	0	0
50 to 54 km	0	7	0	0	0	0
55 to 59 km	0	4	0	0	0	0
60 to 64 km	0	0	0	0	0	0
65 to 69 km	0	3	0	0	0	1
70 km and greater	1	4	0	0	0	0
TOTAL	22	99	3	18	5	16
Percent of cells 20 km or less from boundary	77.3	63.6	100	94.4	100	87.5

Table 6.6. Distribution of 1.0 km CAPPI 40 dBZ Results for each Boundary Classification.

	Number of 40 dBZ Cell Initiations Pertaining to Boundary Classification					
Distance to Closest Boundary	**Moving**	**Colliding**	**Intersecting**	**Merger**	**Stationary**	**Synoptic**
0 to 4 km	32	6	1	3	0	0
5 to 9 km	25	4	1	5	2	1
10 to 14 km	23	0	0	3	0	1
15 to 19 km	9	1	1	0	0	0
20 to 24 km	8	0	0	1	0	0
25 to 29 km	5	0	0	0	0	0
30 to 34 km	1	0	0	0	0	0
35 to 39 km	5	0	0	0	0	0
40 to 44 km	3	0	0	0	0	0
45 to 49 km	2	0	0	0	0	0
50 to 54 km	7	0	0	0	0	0
55 to 59 km	4	0	0	0	0	0
60 to 64 km	0	0	0	0	0	0
65 to 69 km	3	0	0	0	0	1
70 km and greater	5	0	0	0	0	0
TOTAL	132	11	3	12	2	3
Percent of cells 20 km or less from boundary	68.2	100	100	91.7	100	66.7

The larger sized data sets can be graphed by not only the distances, but whether the cells occurred ahead, behind or to the side of the boundary type or boundary classification. Figures 6.13a and 6.13b show the CAPPI results for the Gust Front boundary type. Figures 6.14a and 6.14b show the CAPPI results for the Moving Boundary classification. As can be seen from Figure 6.13a, the peak of 40 dBZ cells occur 1 to 5 km behind the gust fronts. A second smaller peak occurs 6 to 10 km ahead of the gust fronts. Initiating cells appear to have a tendency to form 11 to 15 km ahead of a gust front to 11 to 15 km behind a gust from with the majority of these forming behind. Figure 6.13b shows initiating 40

dBZ cells to be fairly scattered across the graph, but with a peak at 11 to 15 km. It is a possibility that the gust front could not be fully identified due to cell development obscuring the view of the small scale effects. This could have potentially caused some of the closer cells.

Figure 6.14a shows very similar results for Moving Boundaries. Peaks are seen in the same place as for Figure 6.13a. Cells also appear to form in the same region in front and behind these boundaries as well. This may be partly due to the fact that majority of these boundaries are the same gust fronts, but other moving boundaries such as lake breezes and 'other' boundaries are also included here. Wilson and Schreiber (1986) found, from their results (mentioned in Chapter 1), that many of the 30 dBZ cells formed 0 to 20 km behind a moving boundary. From the ELBOW data we can see that there also appears to be a tendency for some storms to form ahead of a moving boundary as well. This could be due to the fact that the cells in this analysis are being considered at 40 dBZ instead of 30 dBZ. It is possible if the moving boundary is moving slowly, that the cells could have formed closer to the boundary at 30 dBZ but by the time they reached the 40 dBZ level they may have moved ahead of the boundary (depending on their motion as compared to that of the boundary). This statistical difference could also partly be due to the unique moving boundary types in this particular study region, such as lake breeze fronts.

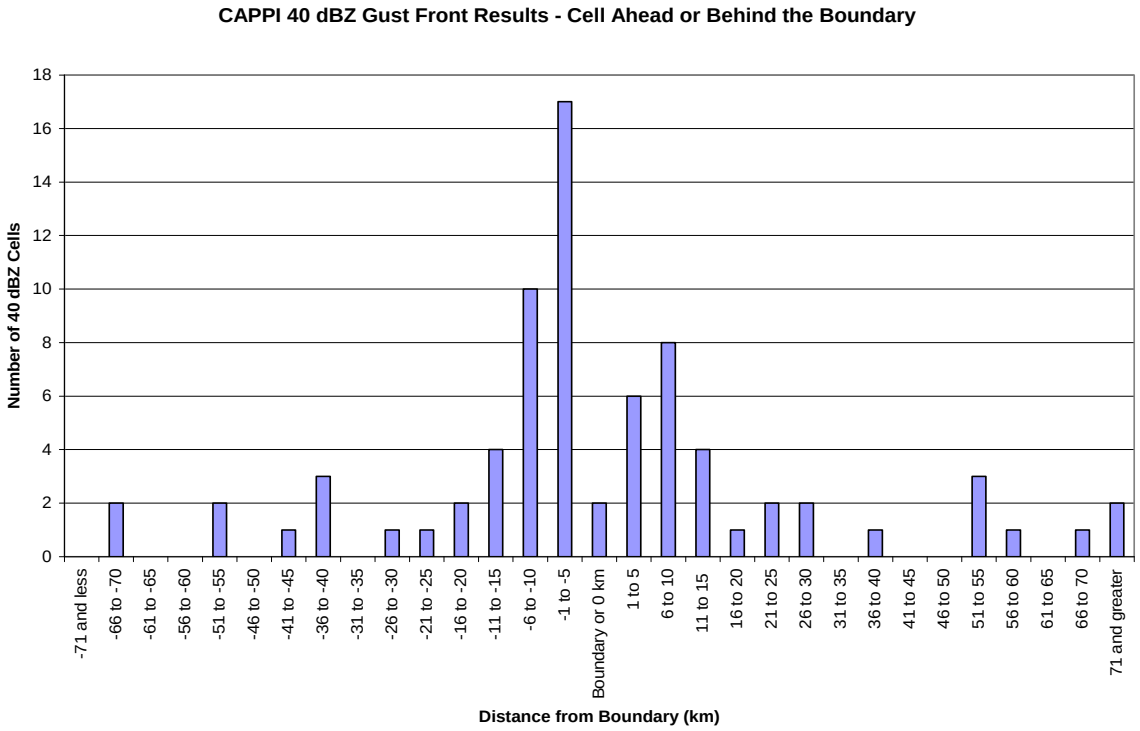

<u>Figure 6.13a (above) and 6.13b (below)</u>. 1.0 km CAPPI Gust Front Results for cells (initially reaching 40 dBZ) which occurred ahead or behind a gust front (above) and to the side of a gust front (below). In 6.13a negative km values are distances behind the boundary and the positive are distances ahead.

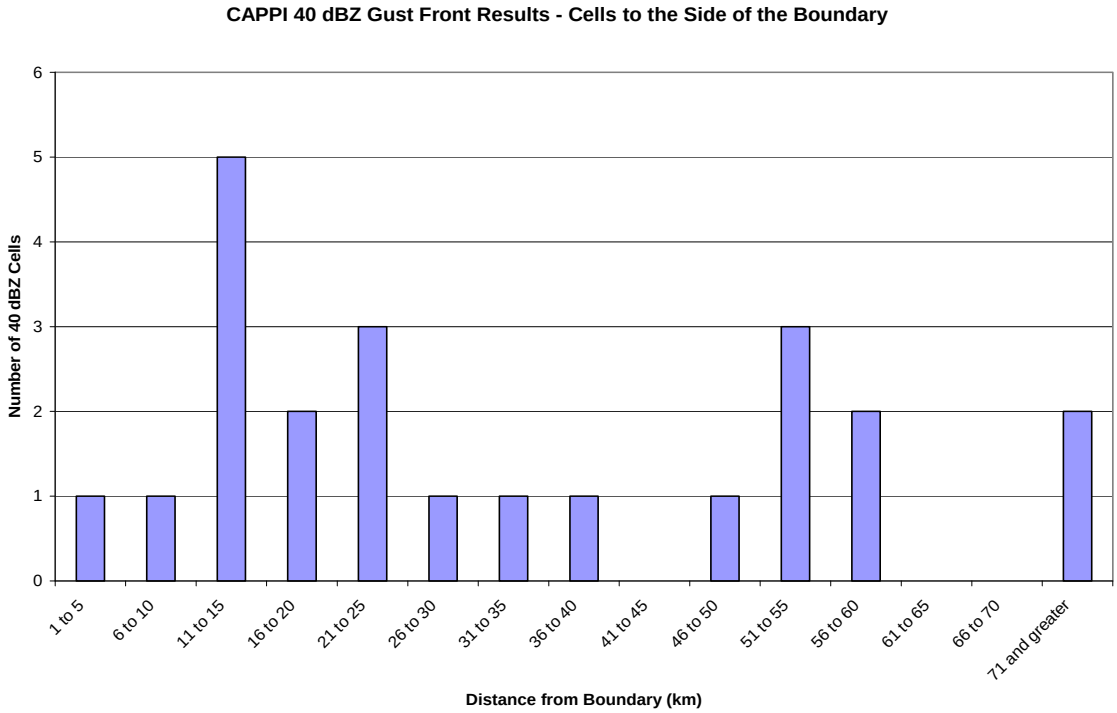

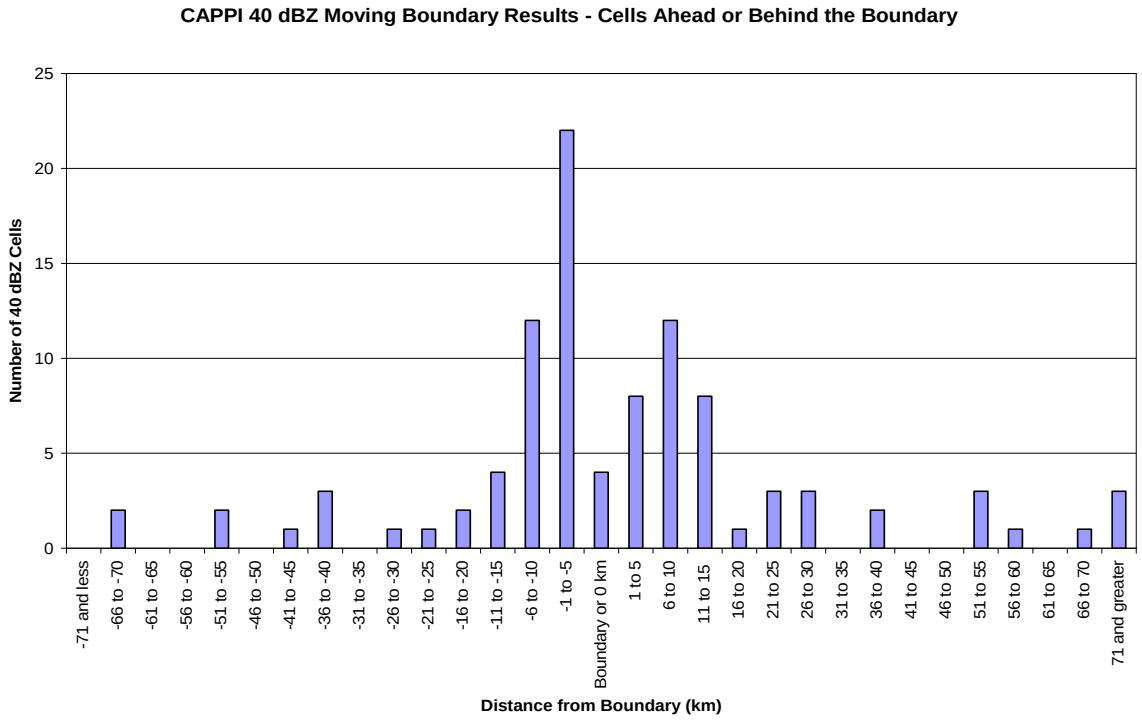

Figure 6.14a (above) and 6.14b (below). 1.0 km CAPPI Moving Boundary Results for cells (initially reaching 40 dBZ) which occurred ahead or behind a moving boundary (above) and to the side of a moving boundary (below). In 6.14a negative km values represent distances behind the boundary and the positive represent distances ahead.

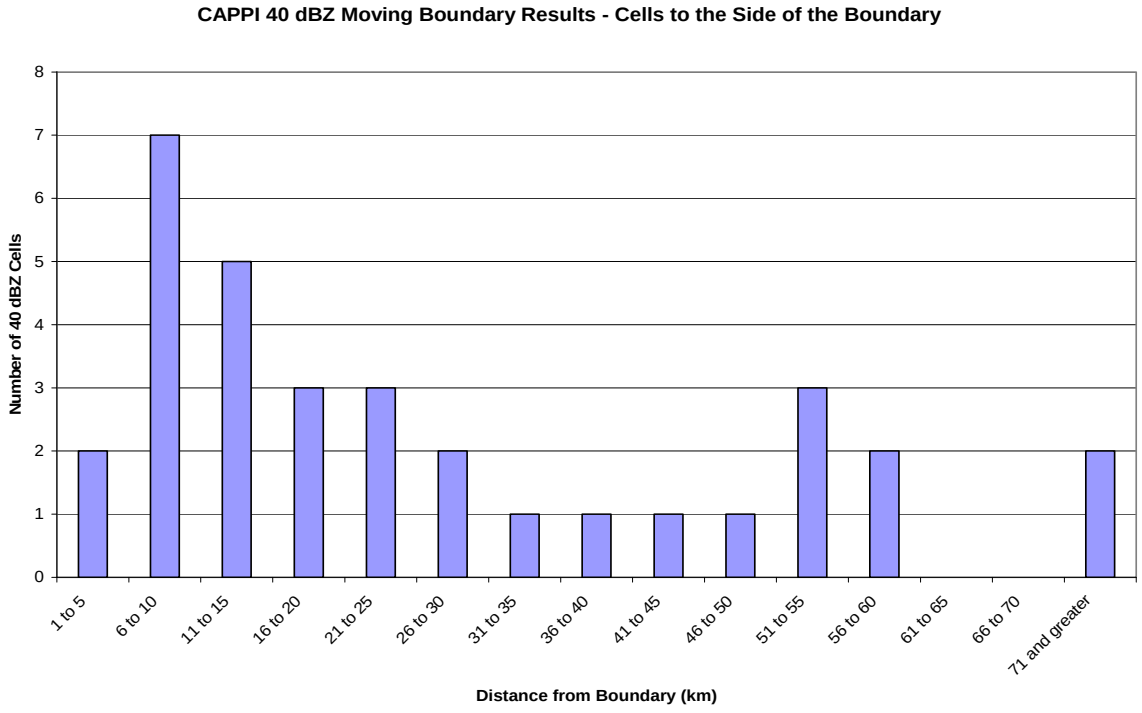

Figure 6.14b shows a peak, similar to Figure 6.13b, but at 6 to 10 km to the side of the Moving boundary. Again, it is possible that the boundary may have extended further but was not able to be identified due to development obscuring the mesoscale effects. Perhaps it is also possible that the end of the moving boundary may have some effect on development at a distance to the side.

Tables 6.7 and 6.8 show the MAXR 40 dBZ cell initiation results corresponding to boundary type and boundary classification, respectively. Again, cells which had no boundary present to measure to were not considered in these tables. As can be seen for Table 6.7, the Merged Boundary and Joint Between Boundaries show all the initiating cells to have occurred 20 km or less from the boundary but the data set is very small. For data sets with 50 or more cells, we can see that the Lake Breeze Front Type shows 75.5 percent of the 40 dBZ cells occurring 20 km or less from the boundary. The Gust Front Type showed 65.5 percent of the 40 dBZ cells occurring at a distance of 20 km or less.

Table 6.8 shows the Colliding and Intersecting Boundary Classifications to have all the cells reaching 40 dBZ at a distance of 20 km or less. However, these results come from very small data sets. The substantial data set shown by the Moving Boundary Classification shows that 68.6 percent of the cells reaching 40 dBZ occur at a distance of 20 km or less.

Boundary Types and Classifications that showed 50 or more cells (as seen in Tables 6.7 and 6.8) were plotted. These were plotted to show the distances

ahead, behind and to the side of the corresponding boundary. Figures 6.15a and 6.15b show the results for the initiating MAXR 40 dBZ cells corresponding to Lake Breeze Fronts. Figures 6.16a and 6.16b show the initiating MAXR 40 dBZ cells measuring closest to a Gust Front. Figures 6.17a and 6.17b show the initiating MAXR 40 dBZ cells related to the Moving Boundaries.

Figure 6.15a shows no cells initiating right at the lake breeze front (0 km distance); however it does show a peak at a distance of 1 to 5 km ahead of the lake breeze front. The cells appear to be mainly initiating 11 to 15 km ahead to 6 to 10 km behind. Figure 6.15b does not show many 40 dBZ cells occurring to the

Table 6.7. Distribution of 1.0 km MAXR 40 dBZ Results for each Boundary Type.

	Number of 40 dBZ Cell Initiations Pertaining to Boundary Type					
Distance to Closest Boundary	**Lake Breeze Front**	**Gust Front**	**Merged Boundary**	**Hybrid Boundary**	**Joint Between Boundaries**	**Other Boundary**
0 to 4 km	16	40	3	9	1	11
5 to 9 km	13	24	1	4	2	4
10 to 14 km	8	12	0	7	0	1
15 to 19 km	3	14	0	0	1	1
20 to 24 km	3	10	0	1	0	0
25 to 29 km	1	4	0	0	0	2
30 to 34 km	0	4	0	0	0	2
35 to 39 km	1	1	0	0	0	1
40 to 44 km	0	4	0	0	0	0
45 to 49 km	0	6	0	0	0	0
50 to 54 km	0	4	0	0	0	0
55 to 59 km	0	6	0	0	0	0
60 to 64 km	1	2	0	0	0	0
65 to 69 km	0	3	0	0	0	1
70 km and greater	7	8	0	0	0	1
TOTAL	53	142	4	21	4	24
Percent of cells 20 km or less from boundary	75.5	65.5	100	95.2	100	70.8

Table 6.8. Distribution of 1.0 km MAXR 40 dBZ Results for each Boundary Classification.

	Number of 40 dBZ Cell Initiations Pertaining to Boundary Classification					
Distance to Closest Boundary	**Moving**	**Colliding**	**Intersecting**	**Merger**	**Stationary**	**Synoptic**
0 to 4 km	63	8	2	3	2	2
5 to 9 km	38	2	1	3	1	3
10 to 14 km	20	5	1	1	1	0
15 to 19 km	18	0	1	0	0	0
20 to 24 km	12	0	0	1	1	0
25 to 29 km	6	0	0	0	0	1
30 to 34 km	6	0	0	0	0	0
35 to 39 km	3	0	0	0	0	0
40 to 44 km	4	0	0	0	0	0
45 to 49 km	6	0	0	0	0	0
50 to 54 km	4	0	0	0	0	0
55 to 59 km	6	0	0	0	0	0
60 to 64 km	3	0	0	0	0	0
65 to 69 km	3	0	0	0	0	1
70 km and greater	15	0	0	0	0	1
TOTAL	207	15	5	8	5	8
Percent of cells 20 km or less from boundary	68.6	100	100	87.5	80	62.5

side of a lake breeze front, but there is a peak at 11 to 15 km. Again, this could be due to development obscurities.

Figure 6.16a shows a peak at a distance of 1 to 5 km behind a gust front. The 40 dBZ cells tend to be initiating in the 6 to 10 km ahead of a gust front to 16 to 20 km behind. Figure 6.16b shows that 62.2 percent of the 40 dBZ cells occurring to the side of a gust front occur within 25 km of the boundary. Again, this could be due to mesoscale boundary obscurity by convective development.

Figure 6.17a shows a peak at a distance of 1 to 5 km behind a moving boundary. Initiating 40 dBZ cells appear to have a tendency to occur 11 to 15 km

ahead of the moving boundary to 16 to 20 km behind. Compared to Wilson and Schreiber's (1986) results there appears to be cells developing in the 0 to 20 km behind the boundary, which is consistent with their results, but there are also cells developing ahead of the moving boundary. The lake breeze results had showed a peak ahead of the lake breeze front, and many of these results would be included in the moving boundaries so this may be contributing to some of this difference. Also, this study looked at 40 dBZ cells and Wilson and Schreiber's (1986) work studied cells initiating to a level of 30 dBZ. The time it took for a cell to intensify from 30 dBZ to 40 dBZ may have meant the cell could have moved ahead of a boundary it formed closest to (depending on its movement). Another factor that could have contributed to this difference was that Wilson and Schreiber's (1986) work considered cells at a 1.0 km height, while in the MAXR data, cell maximum reflectivity from a level 1.0 km and up is being considered.

Figure 6.17b shows the cells which occurred to the side of a moving boundary. There appears to be a peak at 6 to 10 km from the boundary and decreases, fairly consistently, with further distance from the boundary. This again suggests that the full extent of the boundary was not identified due to obscurity from convective development. It is also possible that the moving boundary has some effect on convective development at a distance to the side.

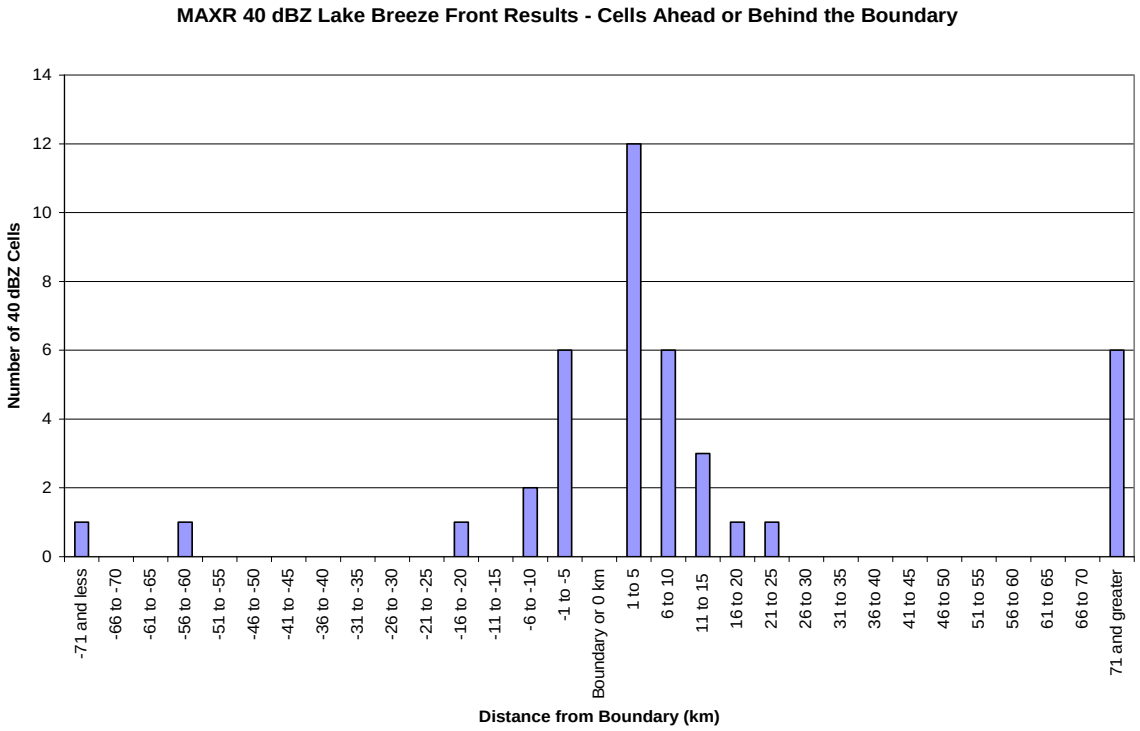

<u>Figure 6.15a (above) and 6.15b (below)</u>. 1.0 km MAXR Lake Breeze Front Results for cells (initially reaching 40 dBZ) which occurred ahead or behind a lake breeze front (above) and to the side of a lake breeze front (below). In 6.15a negative km values represent distances behind the boundary and the positive represent distances ahead.

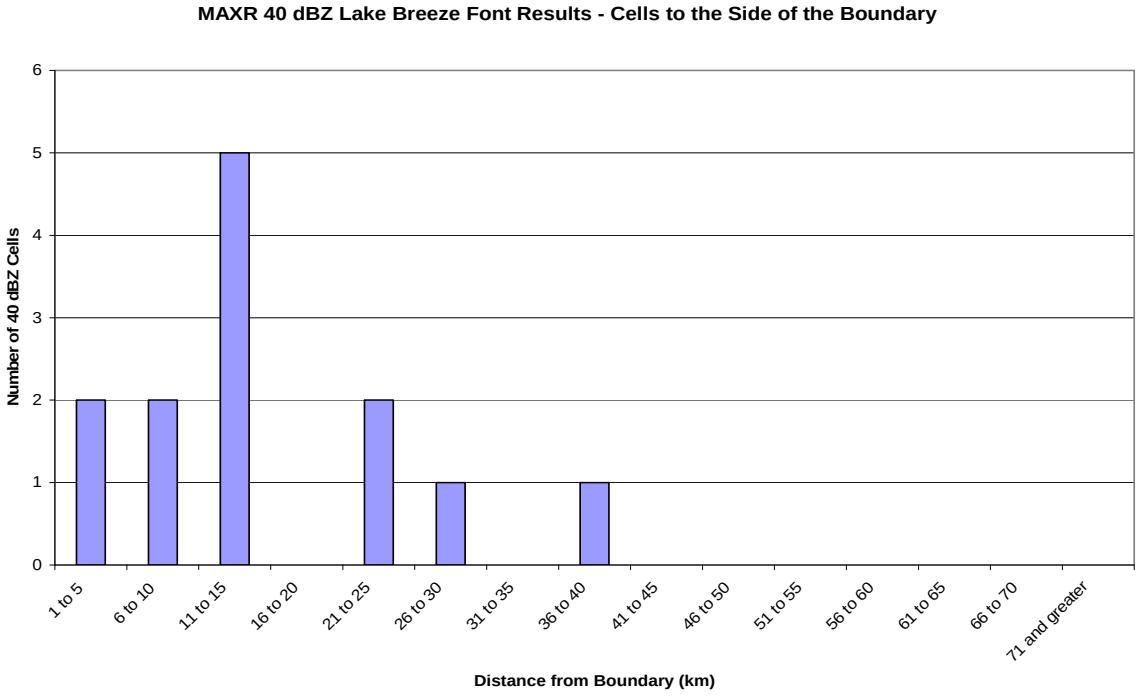

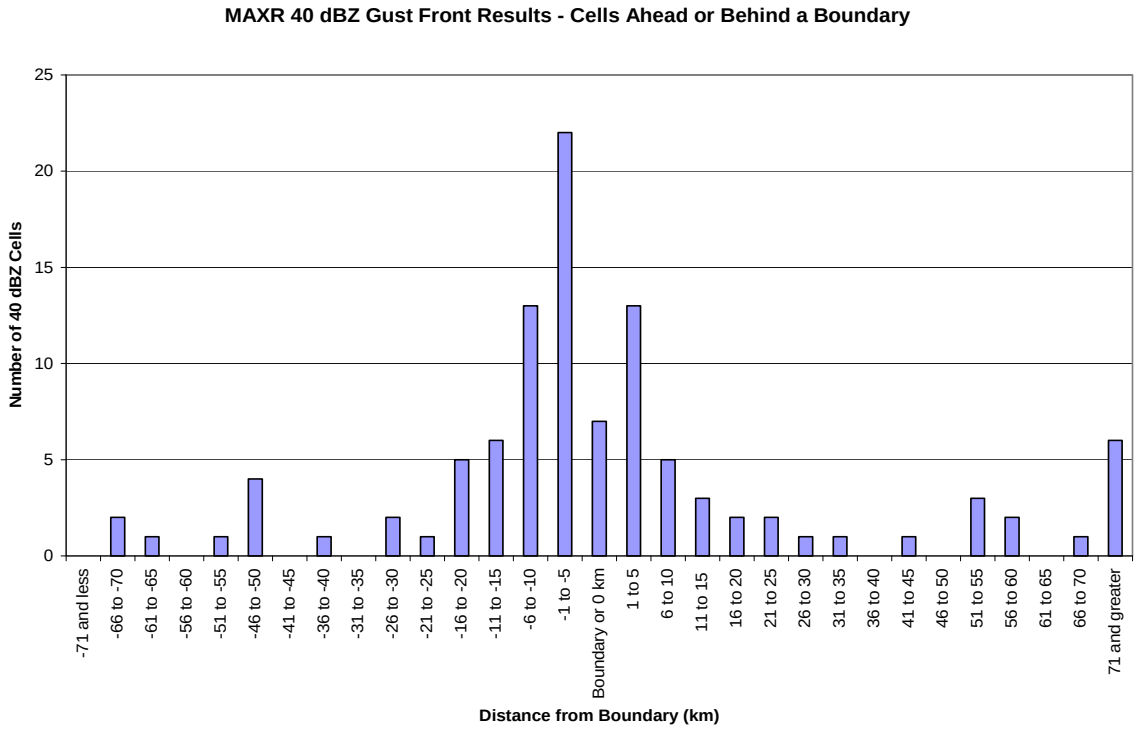

Figure 6.16a (above) and 6.16b (below). 1.0 km MAXR Gust Front Results for cells (initially reaching 40 dBZ) which occurred ahead or behind a gust front (above) and to the side of a gust front (below). Figure 6.16a negative kilometre values represent distances behind the boundary and the positive represent distances ahead.

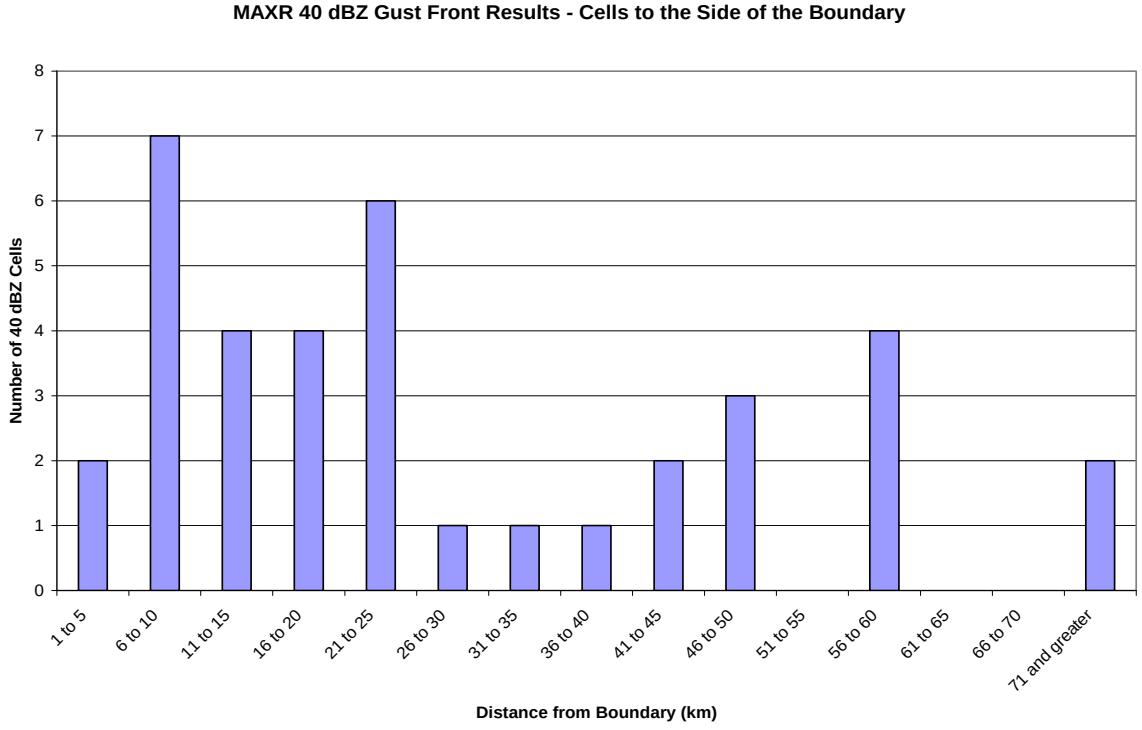

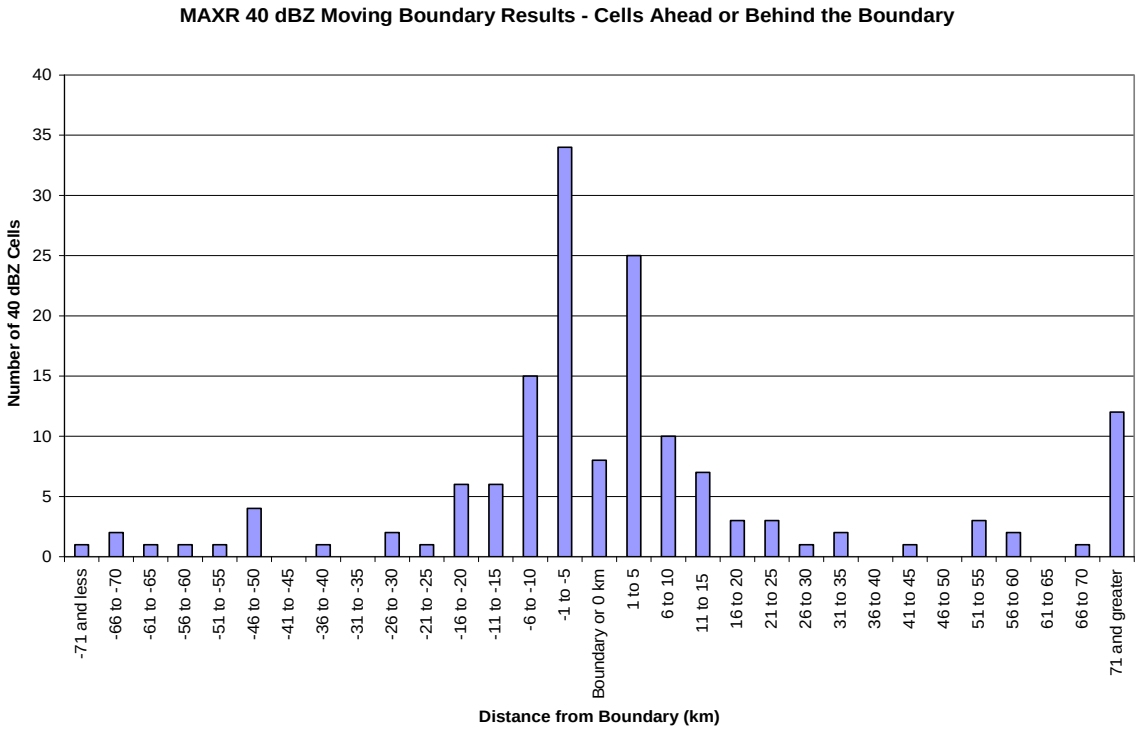

<u>Figure 6.17a (above) and 6.17b (below)</u>. 1.0 km MAXR Moving Boundary Results for cells (initially reaching 40 dBZ) which occurred ahead or behind a moving boundary (above) and to the side of a moving boundary (below). In 6.17a negative km values represent distances behind the boundary and the positive represent distances ahead.

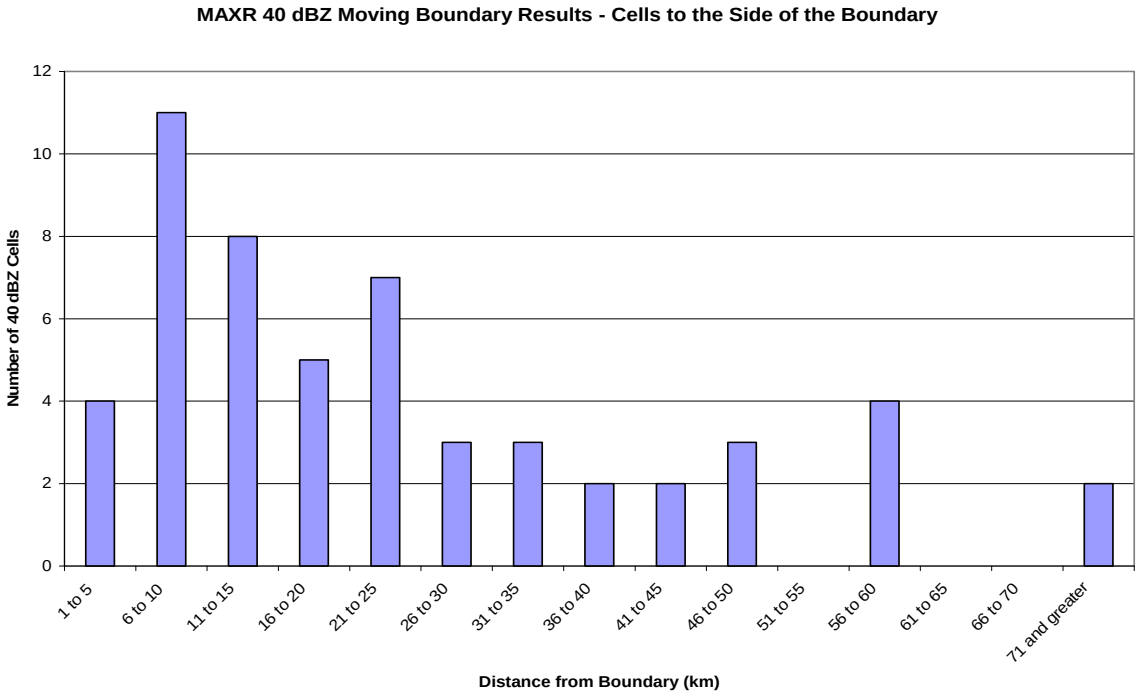

Based on the plots done for CAPPI and MAXR (Figures 6.13 to 6.17) we can see that for similar boundary results (gust front and moving), there were always two peaks occurring on the CAPPI plots (at the -1 to -5 km and 6 to 10 km intervals) and there was only one peak (-1 to -5 km) for the MAXR results. This suggests the possibility that the MAXR initiating cells are detected earlier due to the maximum reflectivity considered for 1 km and up, instead of just at a 1 km height (as in the CAPPI images).

6.4.5 40 dBZ Cell Distribution

The 40 dBZ cell initiation locations for the second analysis were mapped in AURORA. Figure 6.18 shows all the cells initially reaching 40 dBZ found from the CAPPI data. As can be seen from this plot, the points are well scattered around the 80 km range from the radar (the area considered for the second analysis). The points appear to be somewhat more sparse on the outer edges of the range. Perhaps some smaller cells do not meet the pattern vector requirements at these further distances from the radar, because the bin widths are so large. More cells may be captured close to the radar due to the bin widths being smaller; small cells easily meet pattern vector requirements. Notice the cell distribution over Lake Huron appears to be fairly sparse as well. This suggests that there are more boundaries that trigger storms over the land, or perhaps the daytime heating allows for better conditions for cells to develop over the land.

Figure 6.19 shows the 40 dBZ initiating CAPPI cells which were measured closest to a lake breeze front or a merged boundary (where two lake breeze

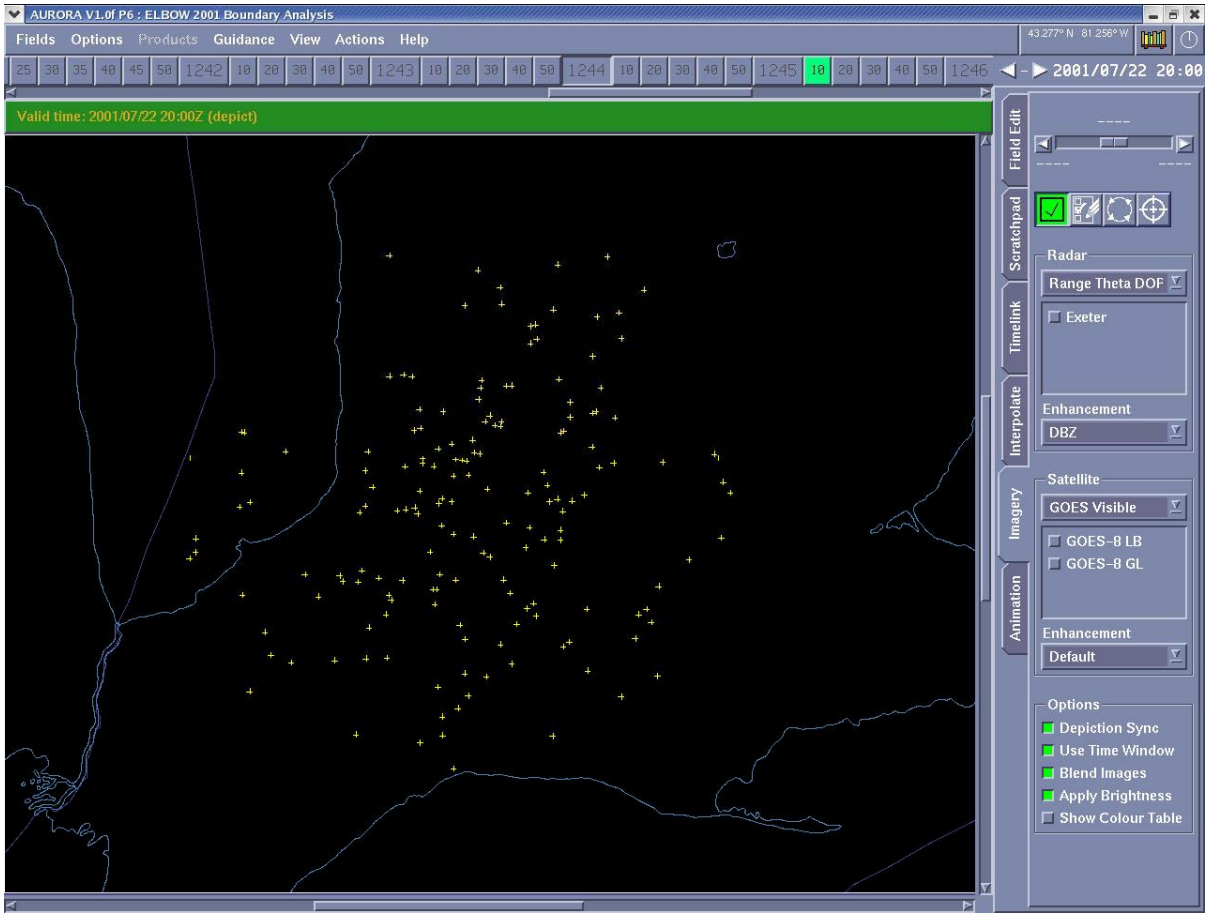

Figure 6.18. AURORA image showing the 40 dBZ cell initiation locations for the 1.0 km CAPPI data (corresponding to the second analysis with study area limited to 80 km from the radar).

fronts have merged). Notice that all the storms shown have reached 40 dBZ over land and there are no cells occurring over the water within the 80 kilometer study area for this analysis. Since lake breezes form from the temperature difference between the lake and land and penetrate inland, this is to be expected. There appear to be more cells occurring closer to Lake Erie, suggesting that perhaps the Erie lake breeze front, or an interaction of lake breeze fronts (which have travelled far inland), are triggering these cells.

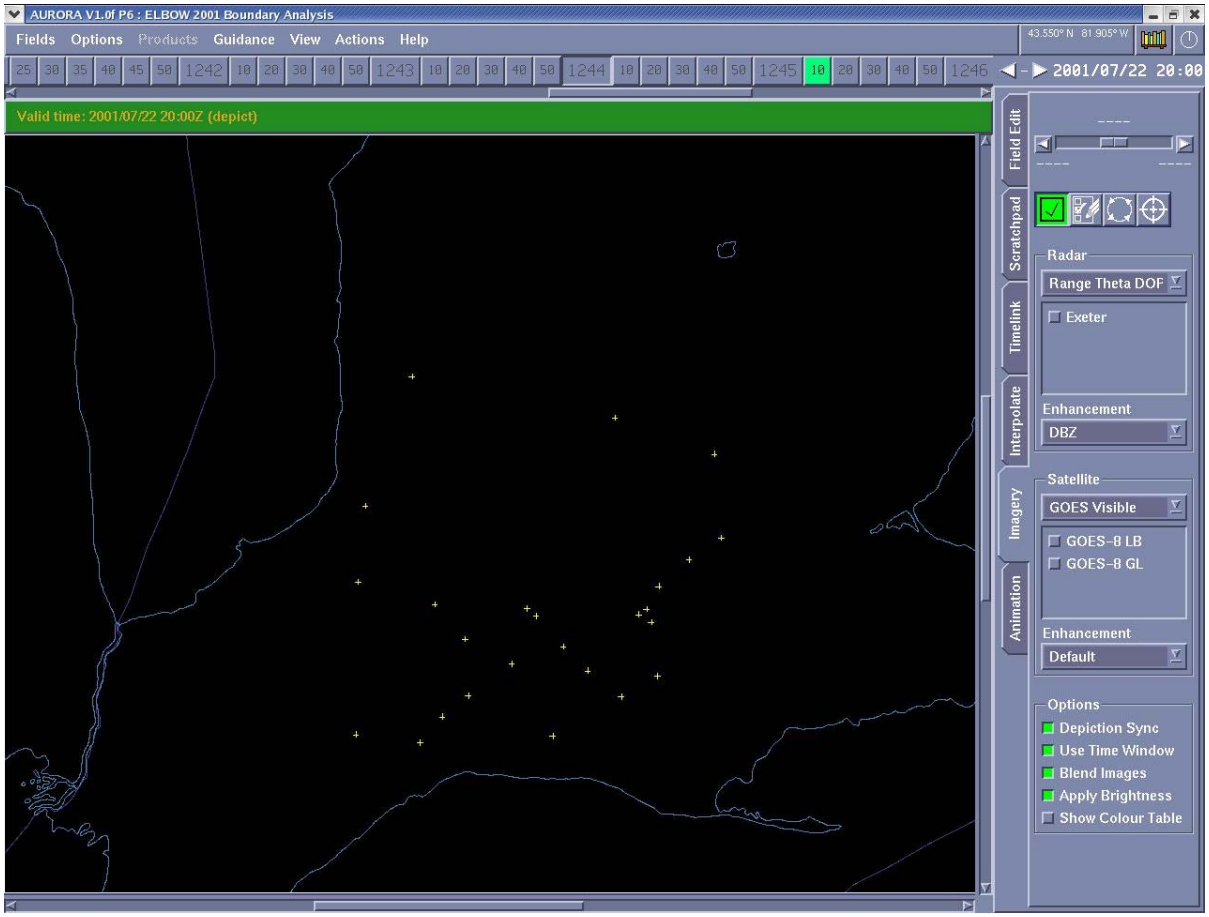

Figure 6.19. AURORA image showing the 40 dBZ cell initiation locations which measured closest to a lake breeze front or merged boundary. These data correspond to the 1.0 kilometer CAPPI analysis.

Figure 6.20 shows all the 40 dBZ cell initiation locations for the MAXR data in the second analysis (total of 260 cells). Again, this image shows sparse cell distribution over Lake Huron and the cells are again sparse toward the outer edge of the 80 kilometer distance from the radar. The distribution is most likely resulting for the same reasons given for the CAPPI distribution shown in Figure 6.18. Figure 6.21 shows the initiating MAXR cells which measured closest to a lake breeze front or merged boundary. As can be seen, most cells are occurring

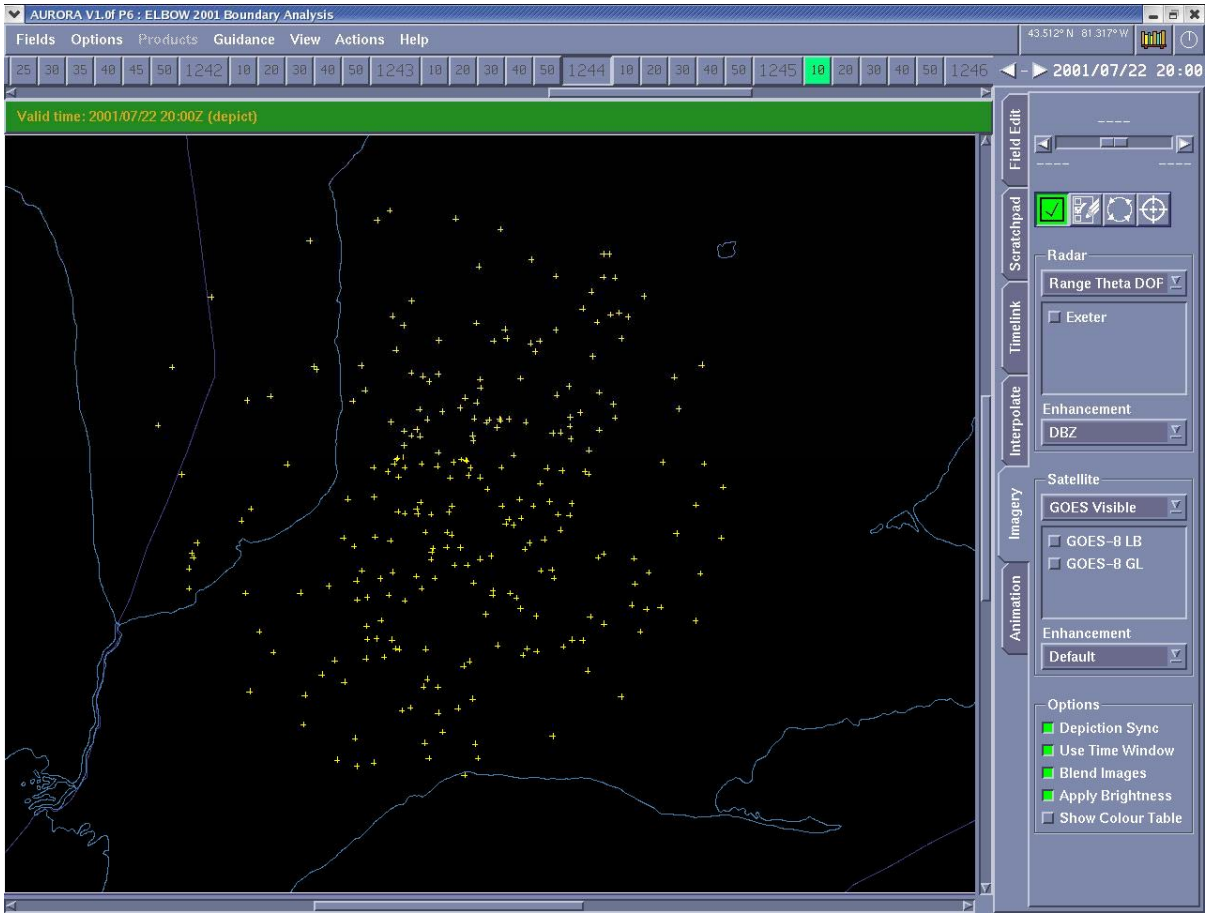

Figure 6.20. AURORA image showing the 40 dBZ cell initiation locations for the 1.0 km MAXR data (corresponding to the second analysis with study area limited to 80 km from the radar).

over land. Only 2 cells occur over Lake Huron and they are very close to shore, which is an area that could still be affected by a lake breeze front. As compared to the CAPPI plot, this MAXR plot appears to have more even distribution between the lakes (more cells are occurring closer to Lake Huron, not just close to Lake Erie). This distribution also appears to have more cells between the lakes but not as many occurring inland from the east coast of Lake Huron. This suggests that more lake breeze front interactions, triggering cell activity, occur between these two lakes. Perhaps wind conditions as compared to boundary

movement create a more favourable environment for cells to form between the lakes, as compared to those to the east of Lake Huron. ELBOW case studies, looking at storm development using current nowcasting techniques, will be considered in Chapter 7.

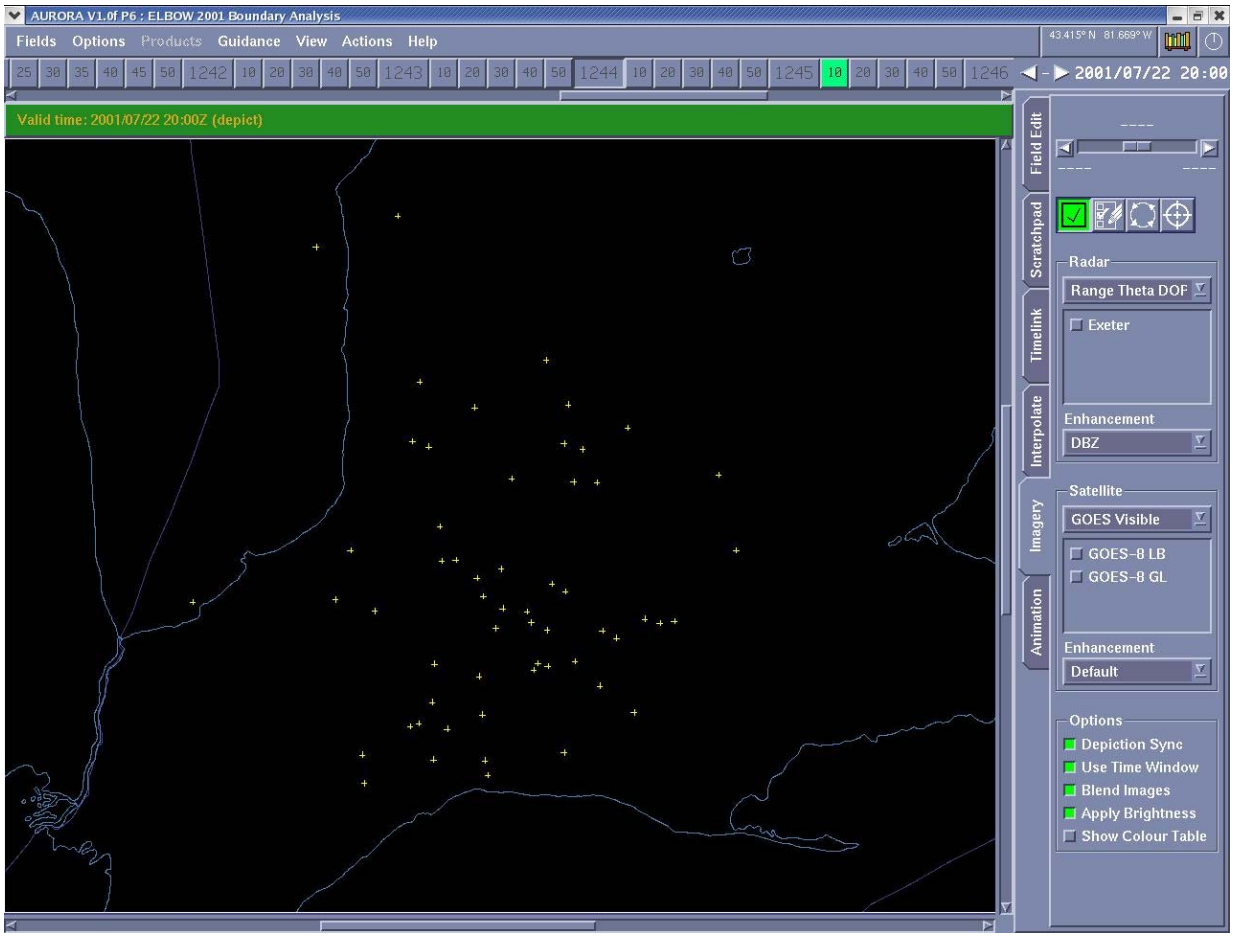

Figure 6.21. AURORA image showing the 40 dBZ cell initiation locations which measured closest to a lake breeze front or merged boundary. These data correspond to the 1.0 kilometer MAXR analysis.

6.5 Conclusion

The first 40 dBZ analysis clearly showed that many of the cells developing 100 km or greater from a boundary, or have no boundary close enough to measure to, could be eliminated from the analysis by removing days with warm

front influence. The MAXR data appeared to have many more of these cells, which suggests that these cells may be elevated from the 1.0 km level (as compared to the CAPPI), as would be expected for many cells associated with warm fronts.

The second 40 dBZ analysis was the most accurate, since there was more attention paid to visually evaluating cell tracks and gust front origins from storms. This analysis clearly showed a large number of cells reaching 40 dBZ in close proximity to a boundary. In fact, the CAPPI data showed 70.4 percent of the 40 dBZ cells initiated 20 km or less from a boundary and the MAXR results showed that 68.5 percent of the 40 dBZ cells initiated 20 km or less from a boundary.

It was also found, according to the second analysis data, that more than half of the days, which had cells detected, showed the first cell identified to be measured closest to a lake breeze front. This was found for both the CAPPI and MAXR data. This suggests that most of the time (more than 50 percent) lake breeze fronts trigger the convective activity for the day (between 1600 and 0000 UTC). Since gust fronts need a storm to create them, there must be some other factors (such as lake breeze fronts) helping to create the first storms.

By looking at the second analysis data more closely, it was observed what distribution of the initiating cells occurred ahead, behind or to the side of a boundary. For CAPPI results, it could be seen that Gust Fronts and Moving Boundaries showed 40 dBZ cells occurring ahead and behind these boundaries. From bar graphs, the peak of the cells occurred just behind the boundaries, but

there was also a second smaller peak occurring at the 6 to 10 km range, ahead of the boundary. The MAXR results for Gust Fronts and Moving Boundaries also showed a pattern of cells initiating ahead and behind the boundaries, however the cells only peaked just behind the boundary, suggesting that perhaps the cells were identified earlier with the MAXR, due to the view of the maximum reflectivity values available for 1.0 km and up. The MAXR results for Lake Breeze fronts were also very interesting, showing that 40 dBZ cell occurrence peaks just *ahead* of the boundary. Cells tended to occur from 15 km ahead to 10 km behind in the bar graph (Figure 6.15a).

The CAPPI and MAXR Moving Boundary results proved to be very interesting as compared to Wilson and Schreiber's (1986) moving boundary results. Wilson and Schreiber (1986) found the cells to generally be initiating 0 to 20 km behind a moving boundary. The ELBOW results for the Great Lakes region showed cells also initiating ahead of the moving boundaries. Some of the differences may be due to the difference in climate between Colorado and the Great Lakes region. It is also possible that these results could be due to a difference in the ratio of moving boundary types occurring, or just the presence of different types of boundaries occurring such as mountain outflows (only for Colorado) and lake breeze fronts (occurring regularly in this study). Another factor could be the difference in dBZ level being analyzed, as Wilson and Schreiber (1986) used a 30 dBZ threshold, and this analysis used a 40 dBZ threshold.

As Wilson and Schreiber (1986) noted, meteorologists used to call these “air-mass thunderstorms”; storms which were generally thought to be occurring randomly on convective summer days, without any synoptic effects. As Wilson and Schreiber (1986) showed for the Colorado area, and has been shown in this study for the Great Lakes area, these storms are showing not to be as random as was previously thought. It is clear, from the bar graphs displaying the cells in the second analysis, that many cells initiate in close proximity to a boundary. It is apparent from this study, and noted in other previous studies, that many cells may not need synoptic effects to trigger them, but a mesoscale feature (such as a lake breeze front or gust front) can serve as a trigger. Since many of the cells in this region do not occur ‘randomly’ then it should be possible to forecast where development will occur. In the following chapter, some cases will be studied using current nowcasting techniques in order to see if the reason for development can be understood.

7. Case Studies Using Recent Nowcasting Techniques

This chapter presents two sample case studies, which are considered using recent nowcasting techniques. This is done in order to see if these techniques may be useful for the Southwestern Ontario area. These nowcasting techniques have been described in detail in Chapter 1, subsection 1.4. It should be noted that other cases have been studied, besides the ones presented here, some of which showed a more clear reason for resulting development (or the lack thereof) than others.

7.1 July 22 and July 23, 2001

7.1.1 General Events

Both July 22 and July 23, 2001 had development of lake breezes on all the lakes surrounding the study region. Both days had southwesterly background flow, however, winds were somewhat stronger on July 23. We consider the peak convective hours between 1600 and 2100 UTC for both days.

On July 22, lake breezes started to set up at 1500 UTC (Lake Ontario and Lake St. Clair initially). Some cells that initiated outside the study region, before the convective part of the day, moved into the northern part of the study region during the first couple hours of the period considered. Overall, there were fewer cells which formed close to mesoscale boundaries in the study region, in comparison to July 23. Some isolated cells developed close to the Huron lake breeze front (lbf) around 1900 and 2000 UTC (as can be seen in Figures 7.1d and 7.1e). The convective activity which moved into the study region earlier was

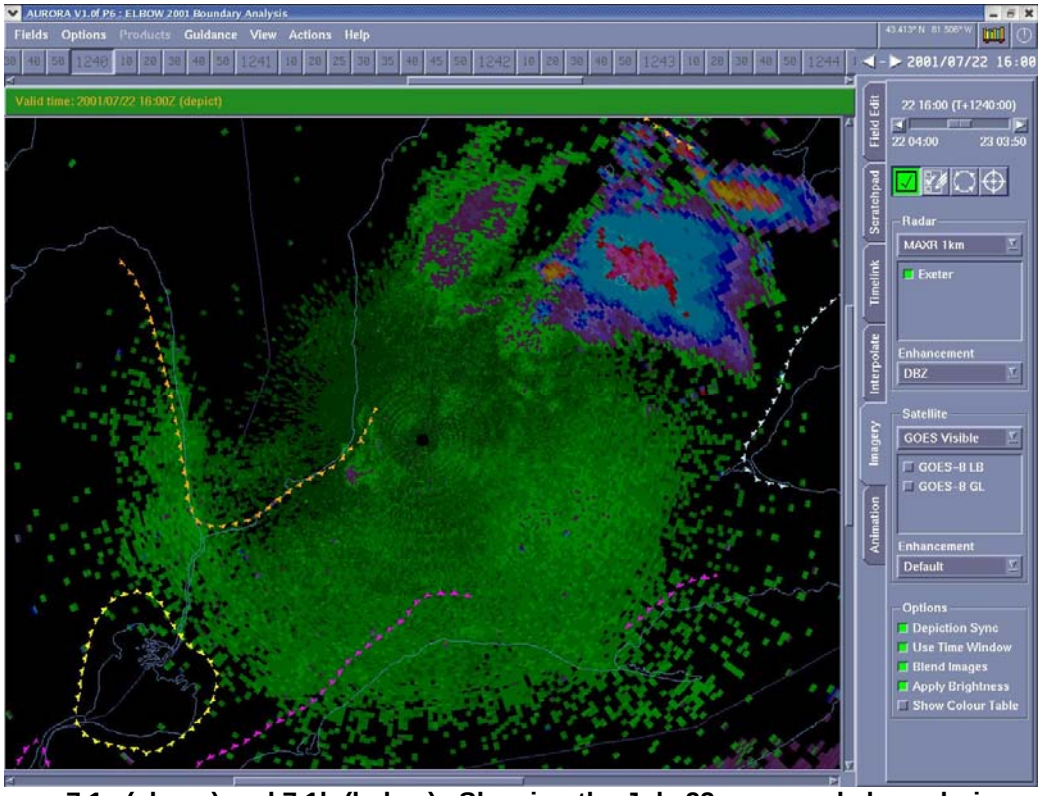

Figure 7.1a (above) and 7.1b (below). Showing the July 22 mesoscale boundaries and MAXR imagery through AURORA for (a) 1600 UTC and (b) 1700 UTC.

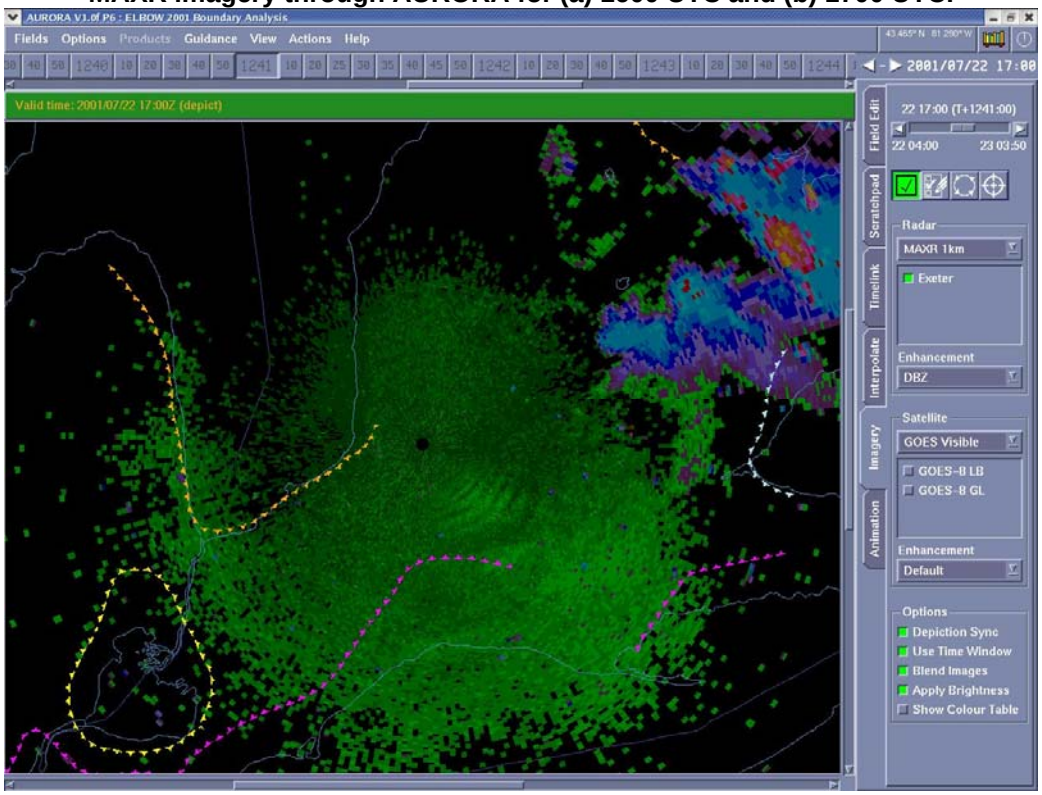

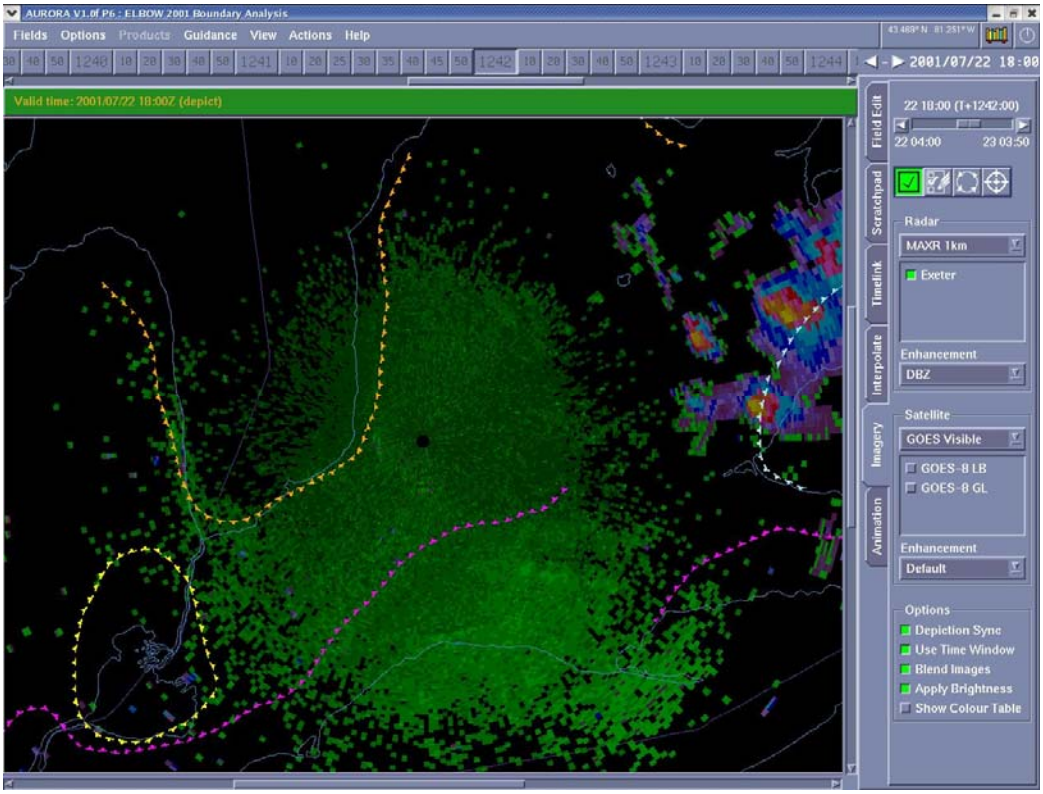

Figure 7.1c (above) and 7.1d (below). Showing the July 22 mesoscale boundaries and MAXR imagery through AURORA for (c) 1800 UTC and (d) 1900 UTC.

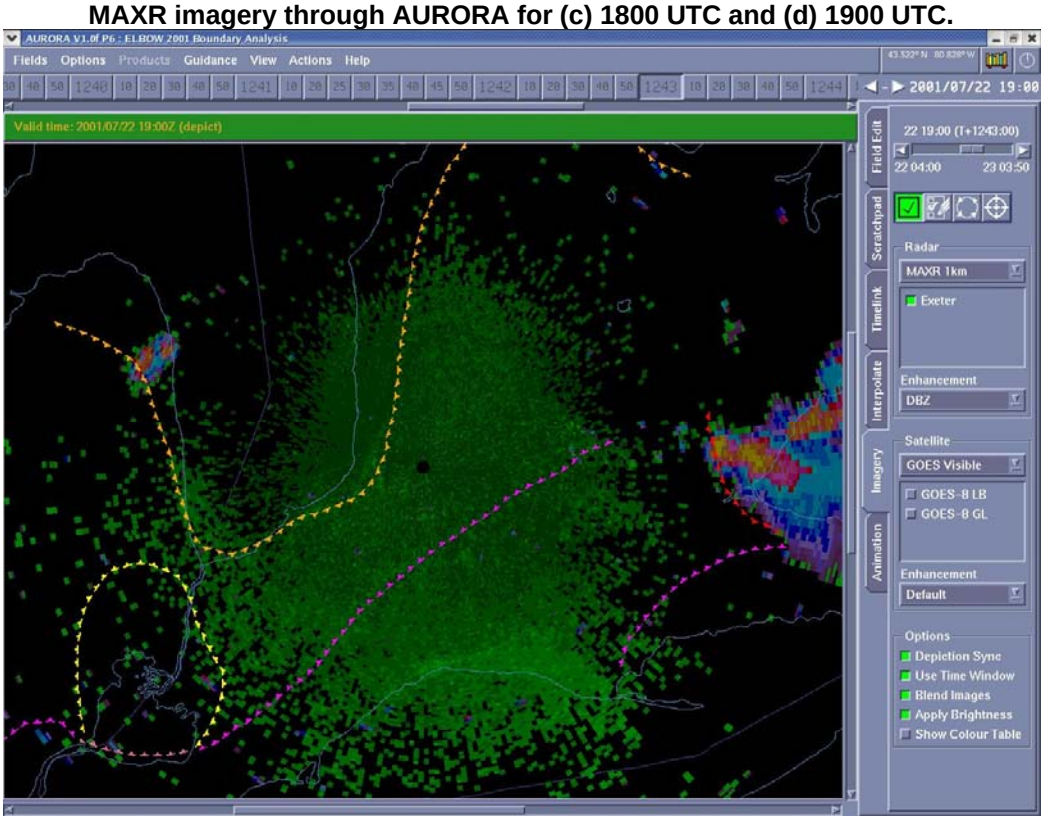

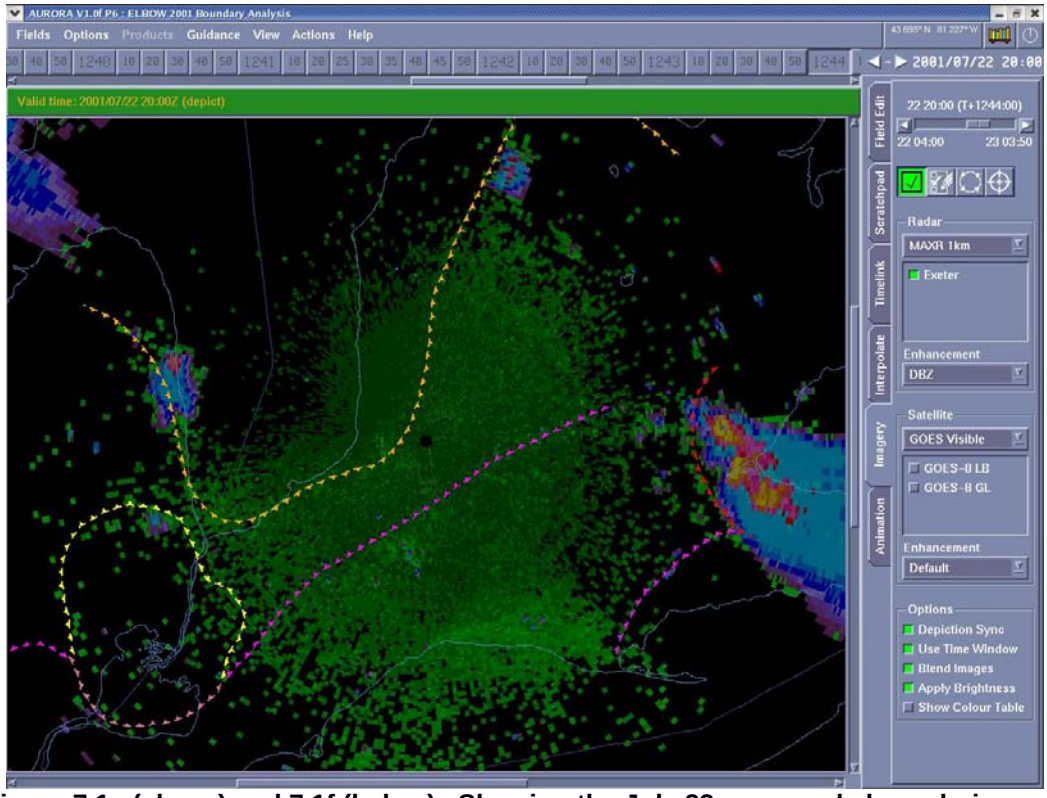

Figure 7.1e (above) and 7.1f (below). Showing the July 22 mesoscale boundaries and MAXR imagery through AURORA for (e) 2000 UTC and (f) 2100 UTC.

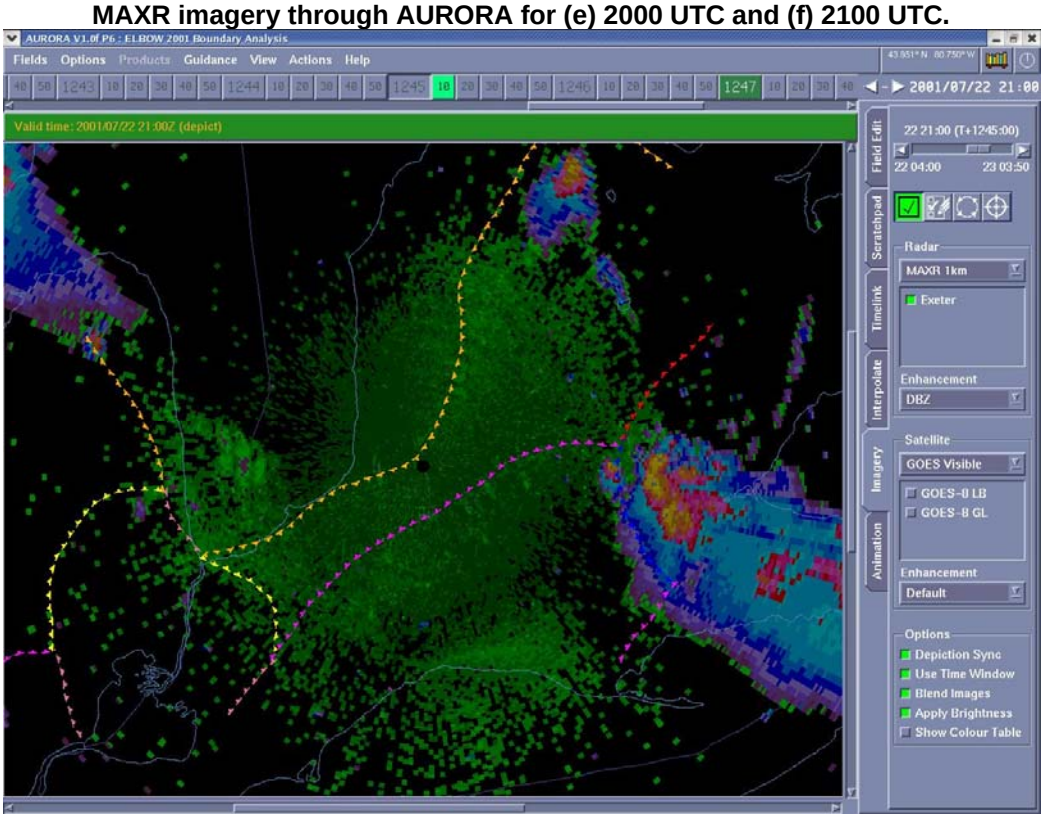

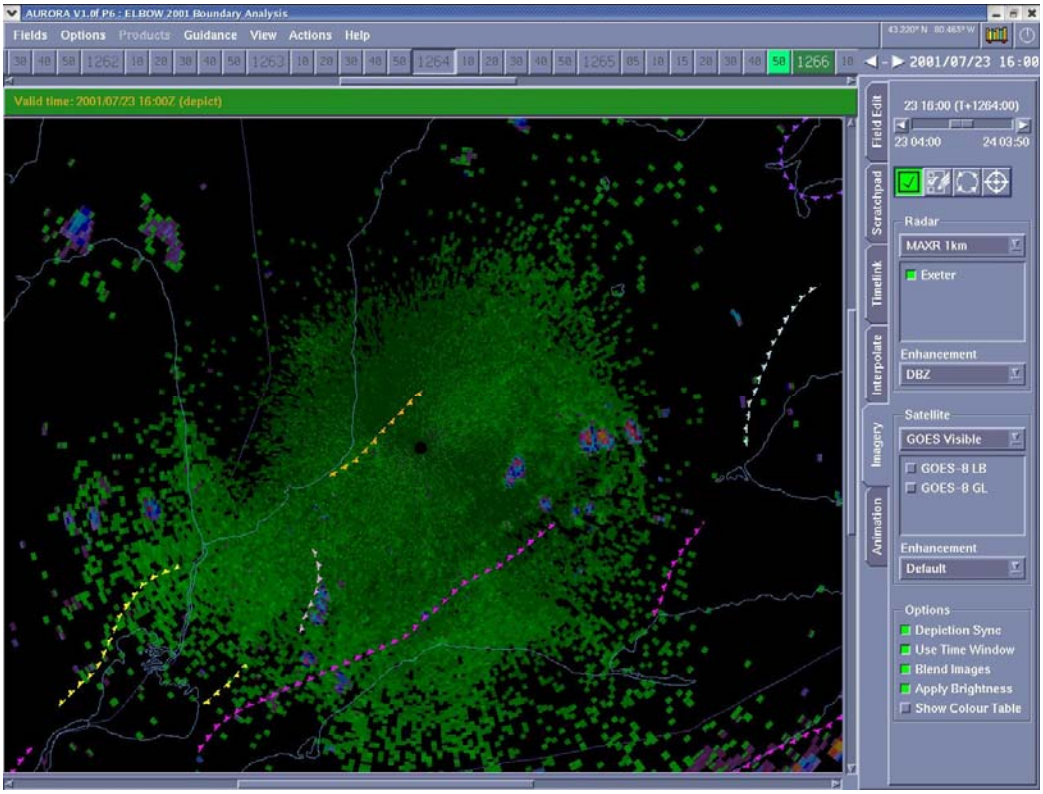

Figure 7.2a (above) and 7.2b (below). Showing the July 23 mesoscale boundaries and MAXR imagery through AURORA for (a) 1600 UTC and (b) 1700 UTC.

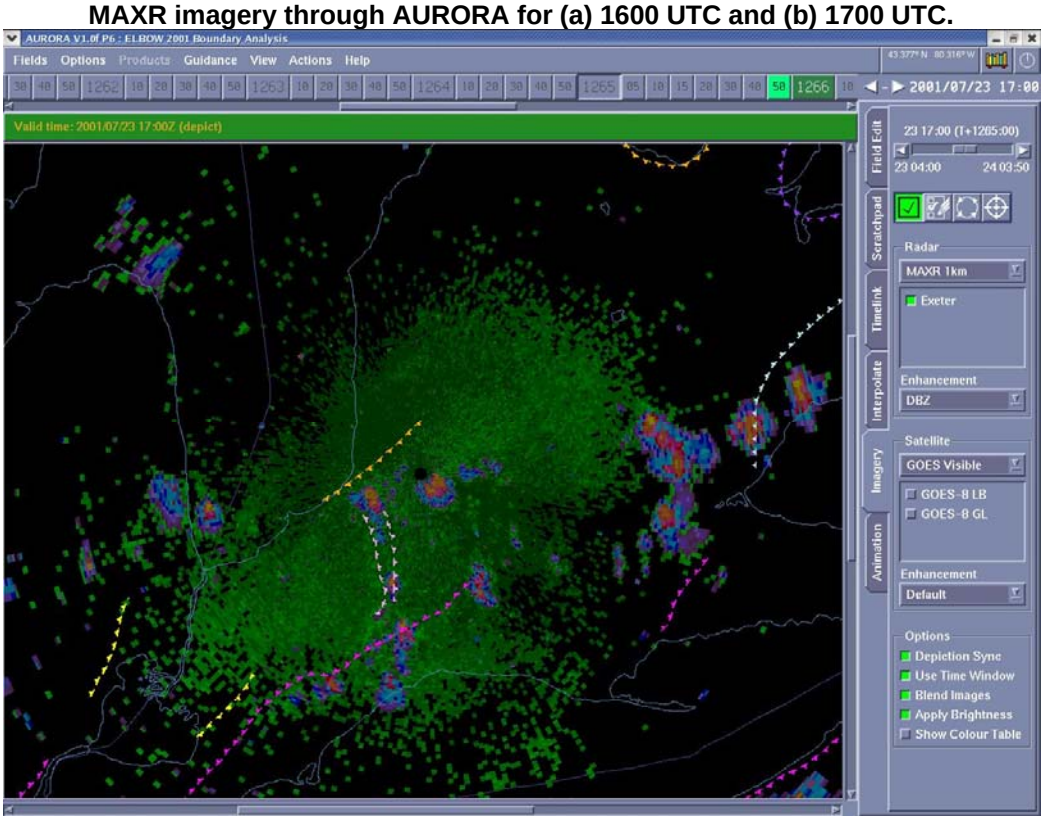

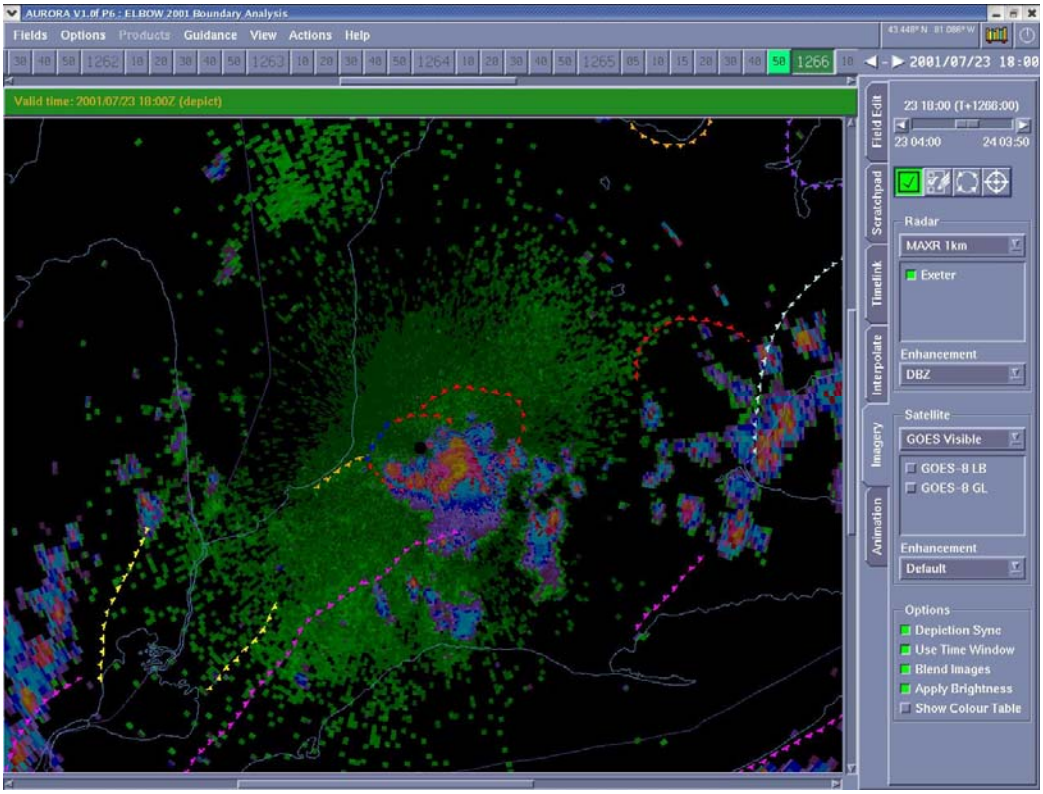

Figure 7.2c (above) and 7.2d (below). Showing the July 23 mesoscale boundaries and MAXR imagery through AURORA for (c) 1800 UTC and (d) 1900 UTC.

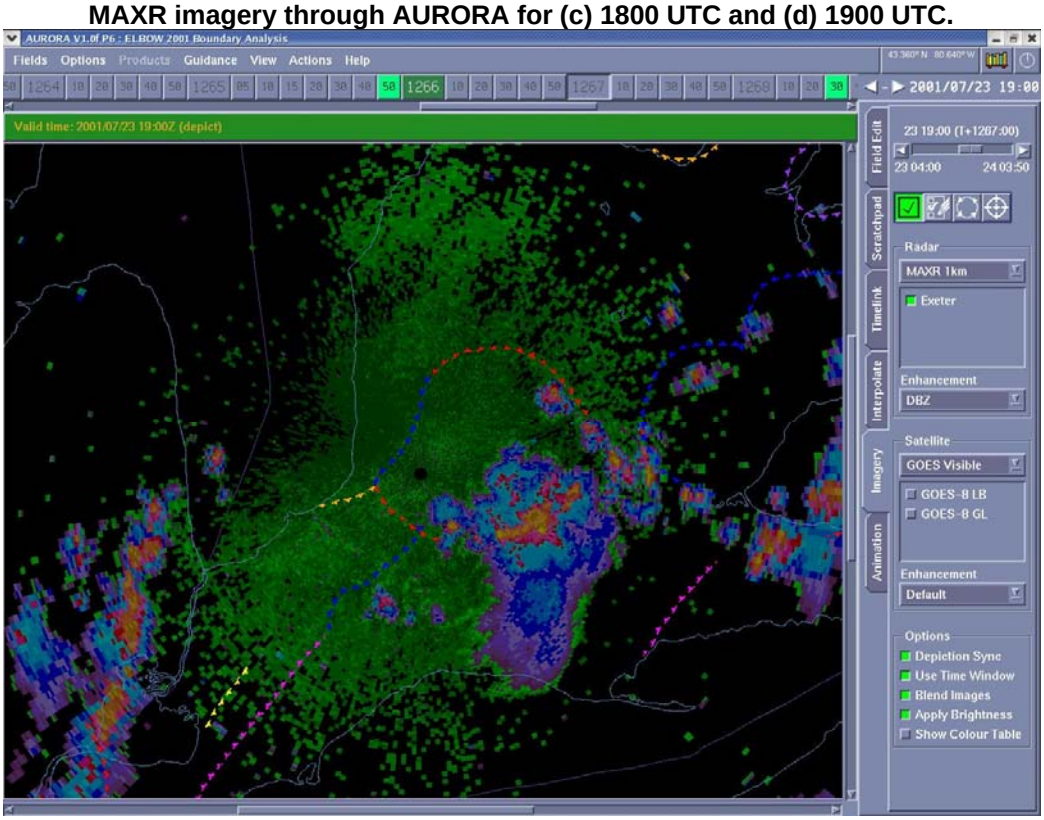

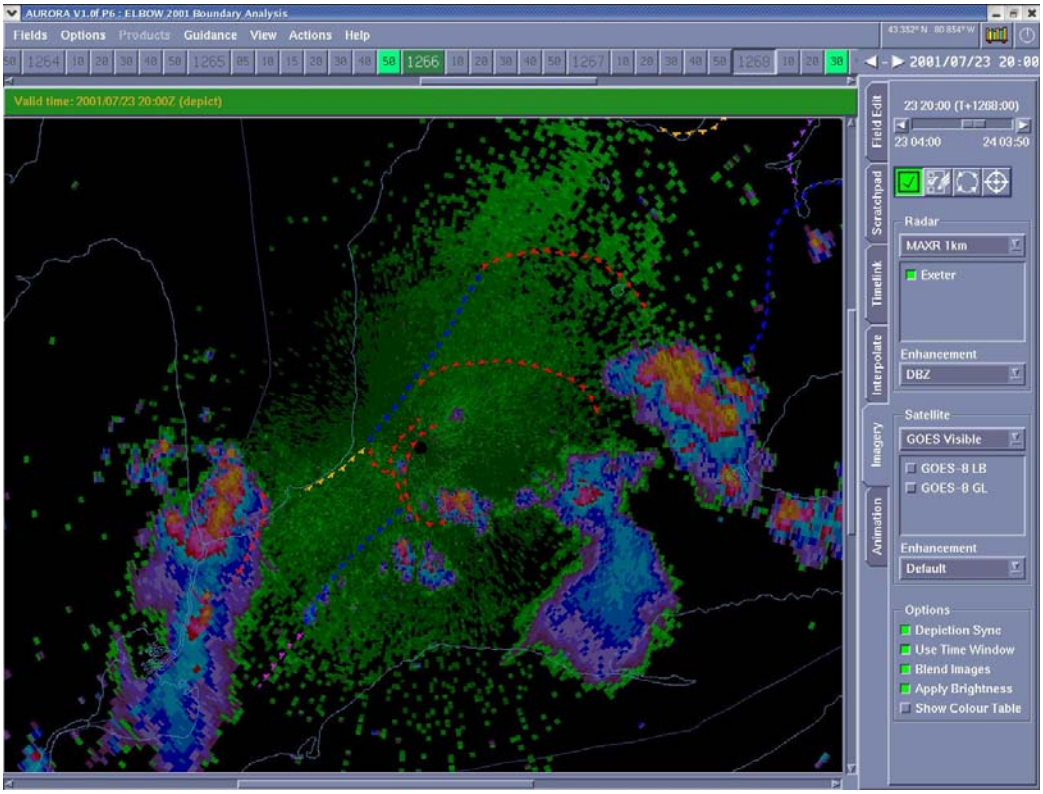

Figure 7.2e (above) and 7.2f (below). Showing the July 23 mesoscale boundaries and MAXR imagery through AURORA for (e) 2000 UTC and (f) 2100 UTC.

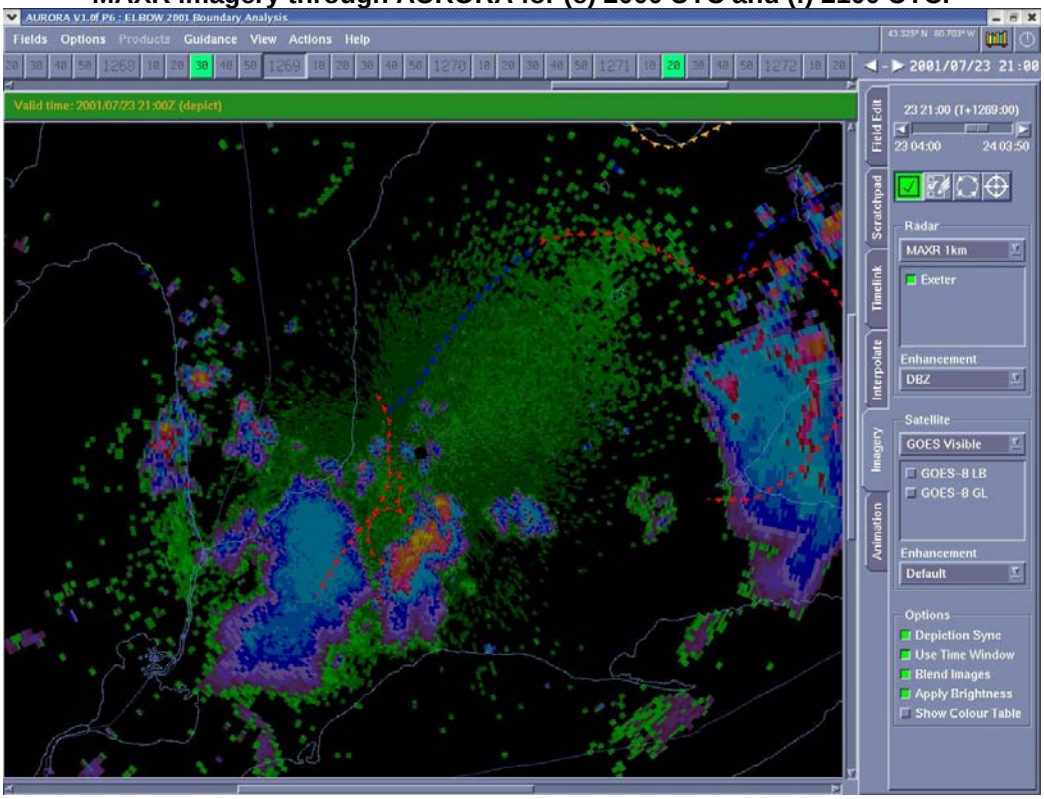

enhanced along the Lake Ontario lbf and began to backbuild into the east side of the study region at 2000 UTC. These triggered a gust front which interacted with other boundaries to form cells until late in the day. To see the development in the study region see Figures 7.1a to 7.1f.

Even though lake breeze development occurred for the same lakes and the direction of the background flow was similar to that of July 22, the development results for July 23 were quite different. Cells were triggered all through the time of concern (1600 to 2100 UTC). Cells appeared to be widely associated with the mesoscale boundaries in the study region (see Figures 7.2a to 7.2f). Many boundary interactions occurred on this day, which triggered further development. Severe storms, in the study region, were a result of this case.

Questions that arise are:

- Why did more widespread storm activity occur in the study region on July 23 between the hours of 1600 to 2100 UTC?
- Why was there so little development on July 22 along the Erie and Huron lake breeze fronts?

7.1.2 Cumulus Associated with the Lifting Zone

As discussed in Chapter 1, subsection 1.4.1, Wilson et al. (2000) note that the cumulus cloud development within the boundary's lifting zone can be a good indicator of instability in association with the boundary. The lifting zone is the area surrounding the boundary which is most likely to show storm development. Referring to the diagram in Wilson et al. (2000), here we look at the lifting zone

as the area 10 km ahead and 20 km behind these moving boundaries. Any vertical growth can indicate there is further potential for storm development.

On July 22, there was some cloud cover/development already present in the study region before the lake breeze fronts formed. Cumulus clouds started to appear in the study region, near Lake Erie, around 1400 UTC. By 1600 UTC, when lake breeze fronts had formed for all lakes, they were well defined by a cumulus cloud field, spread over the study region (see Figure 7.3a). Some vertical development of these clouds appeared to be happening by 2000 UTC along the Erie lake breeze front. However, the cloud patterns suggest that they may have been developing on an angle away from the lake breeze front.

July 23 also showed some cloud cover already present in the study region before lake breeze fronts formed. Lake breeze fronts started to form by 1400 UTC, the widespread cumulus cloud field (surrounding any pre-existing clouds) began to form by 1500 UTC (see Figure 7.4a), and cumulus clouds were outlining lake breeze front locations very well by 1540 UTC. Vertical growth in the cumulus clouds, along the low-level boundaries, could be seen almost immediately after the development of the widespread cumulus field. These vertical developments quickly evolved into storm cells along many boundaries. To see the cloud development, see Figures 7.4a to 7.4d.

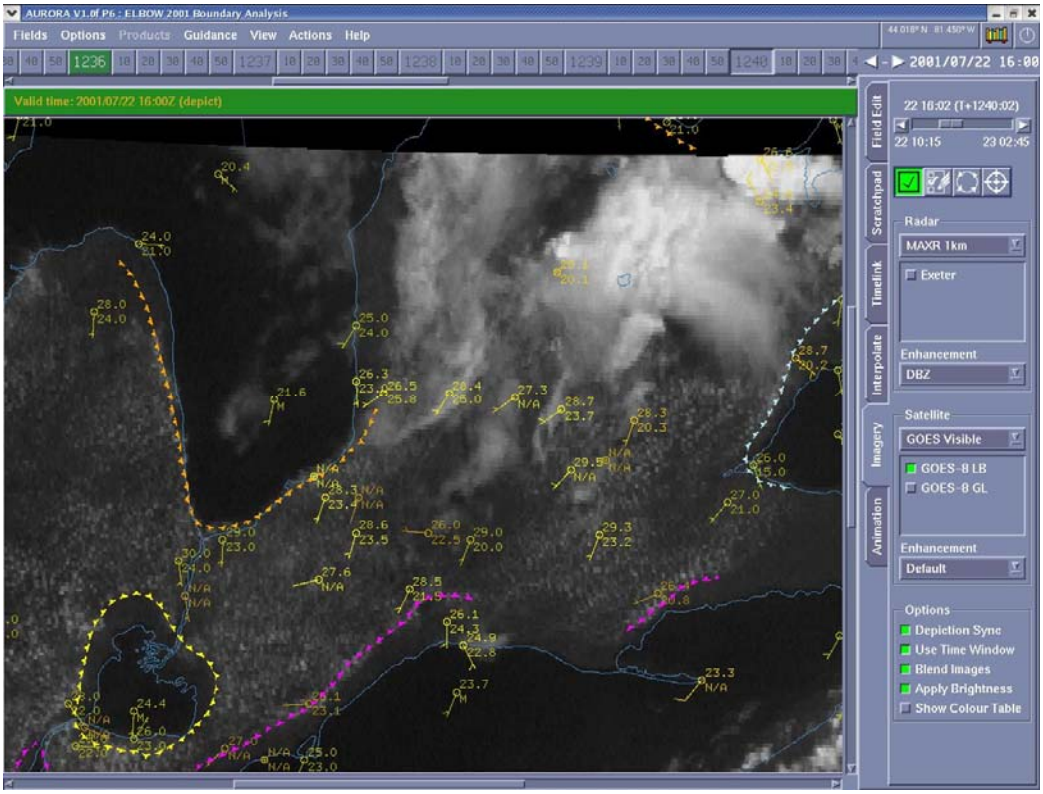

Figure 7.3a (above) and 7.3b (below). Showing the July 22 mesoscale boundaries, mesonet stations and visible satellite imagery through AURORA for (a) 1600 UTC and (b) 1700 UTC.

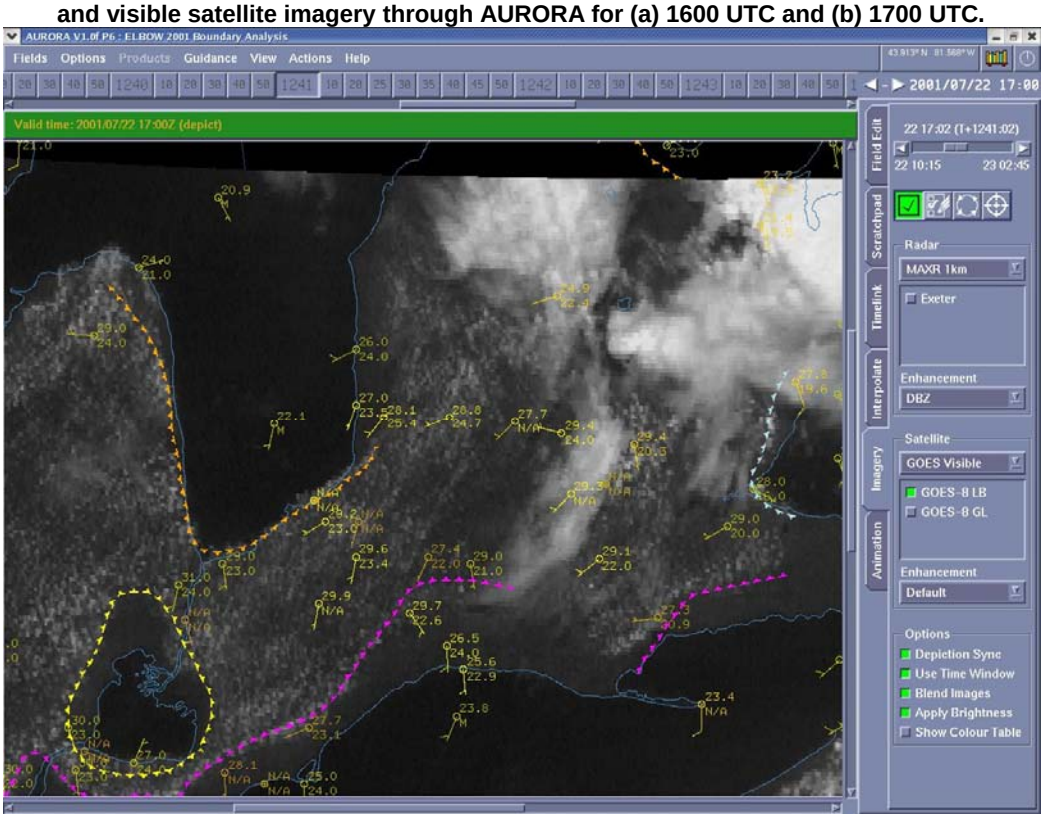

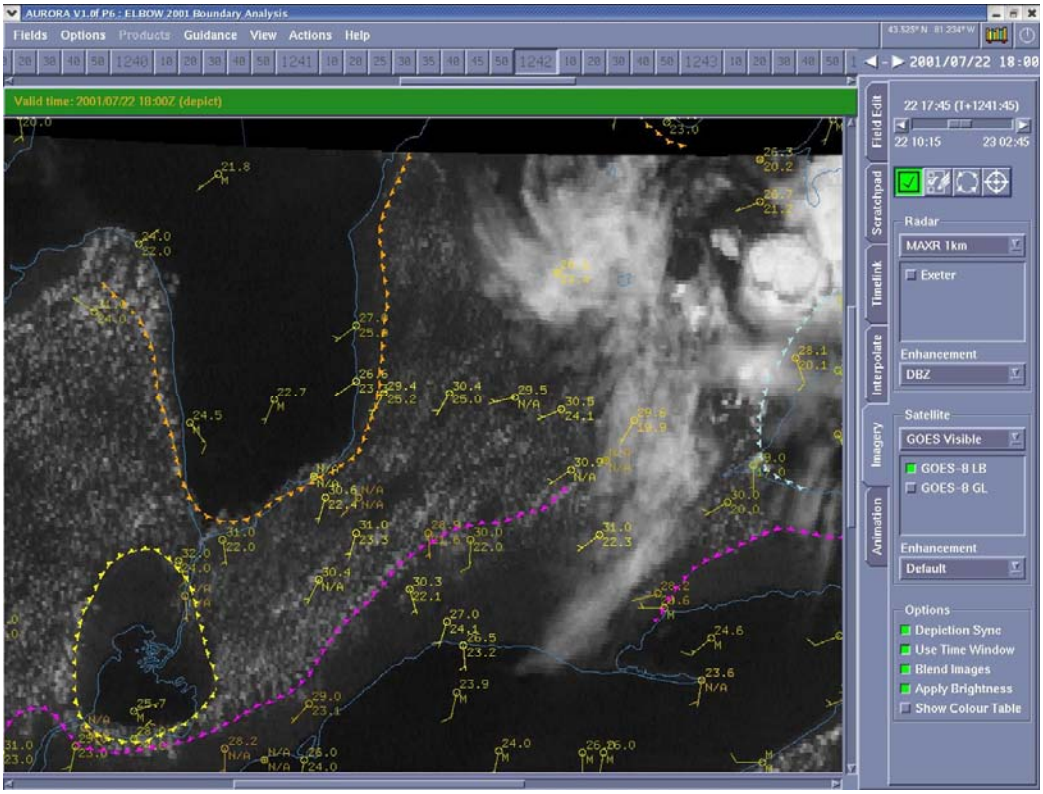

Figure 7.3c (above) and 7.3d (below). Showing the July 22 mesoscale boundaries, mesonet stations and visible satellite imagery through AURORA for (c) 1800 UTC and (d) 1900 UTC.

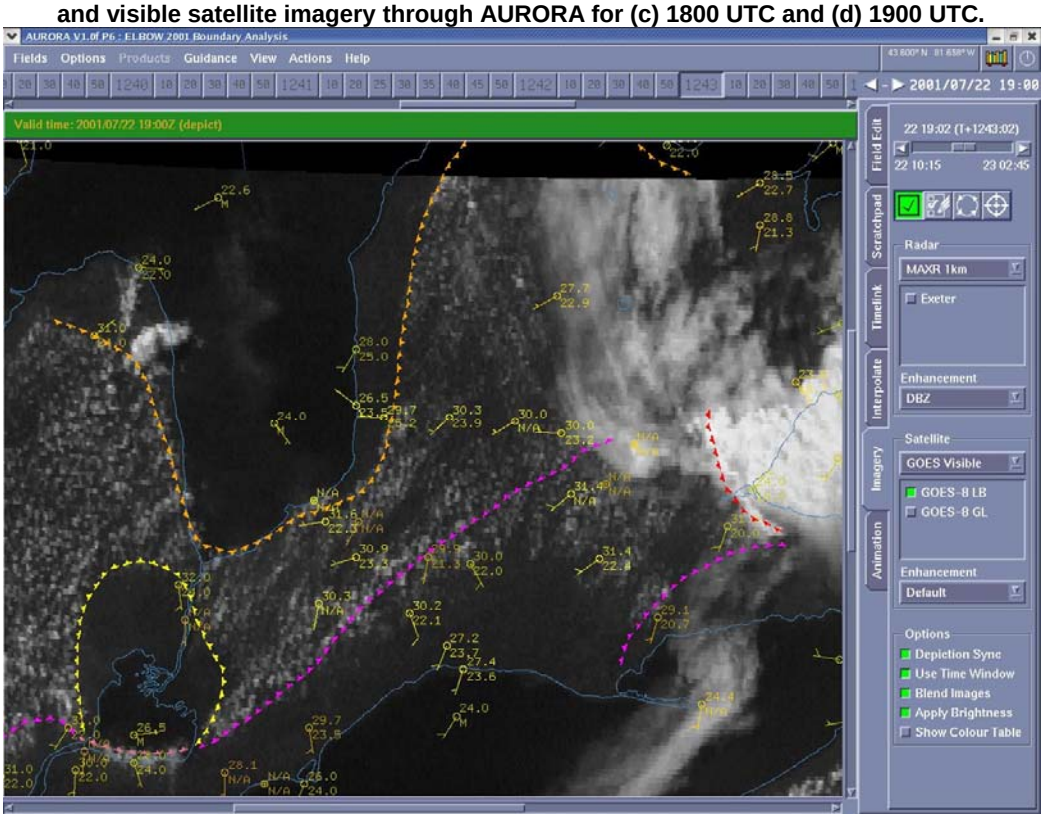

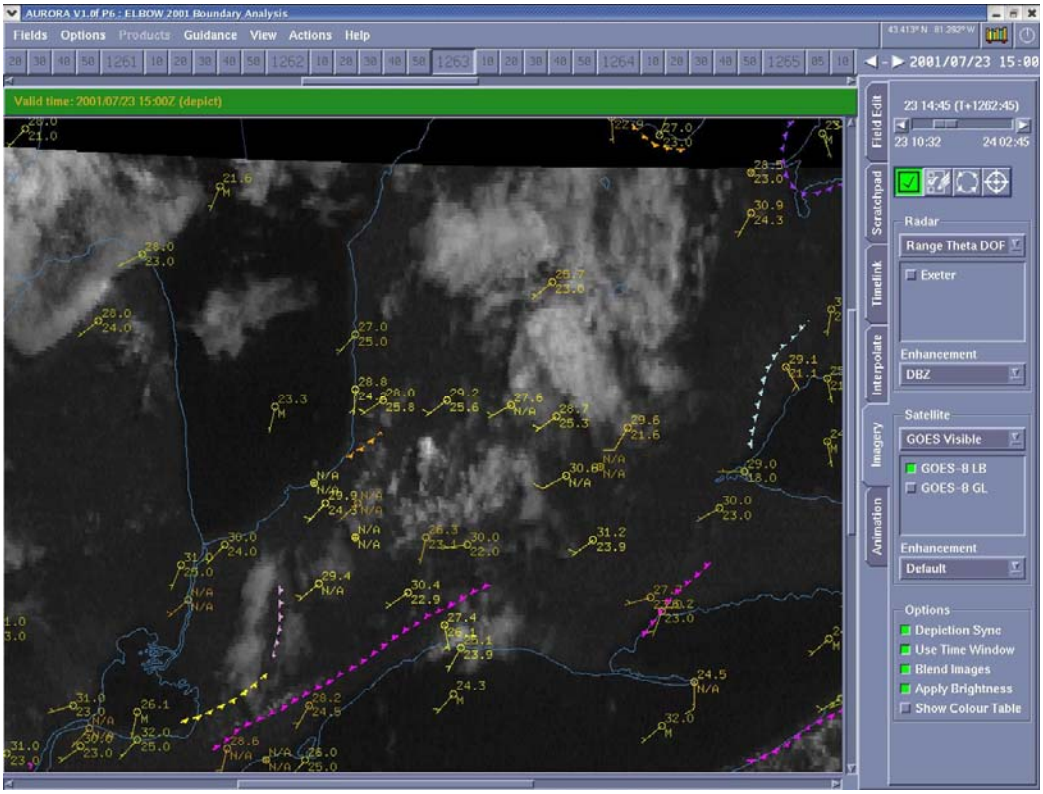

Figure 7.4a (above) and 7.4b (below). Showing the July 23 mesoscale boundaries, mesonet stations and visible satellite imagery through AURORA for (a) 1500 UTC and (b) 1600 UTC.

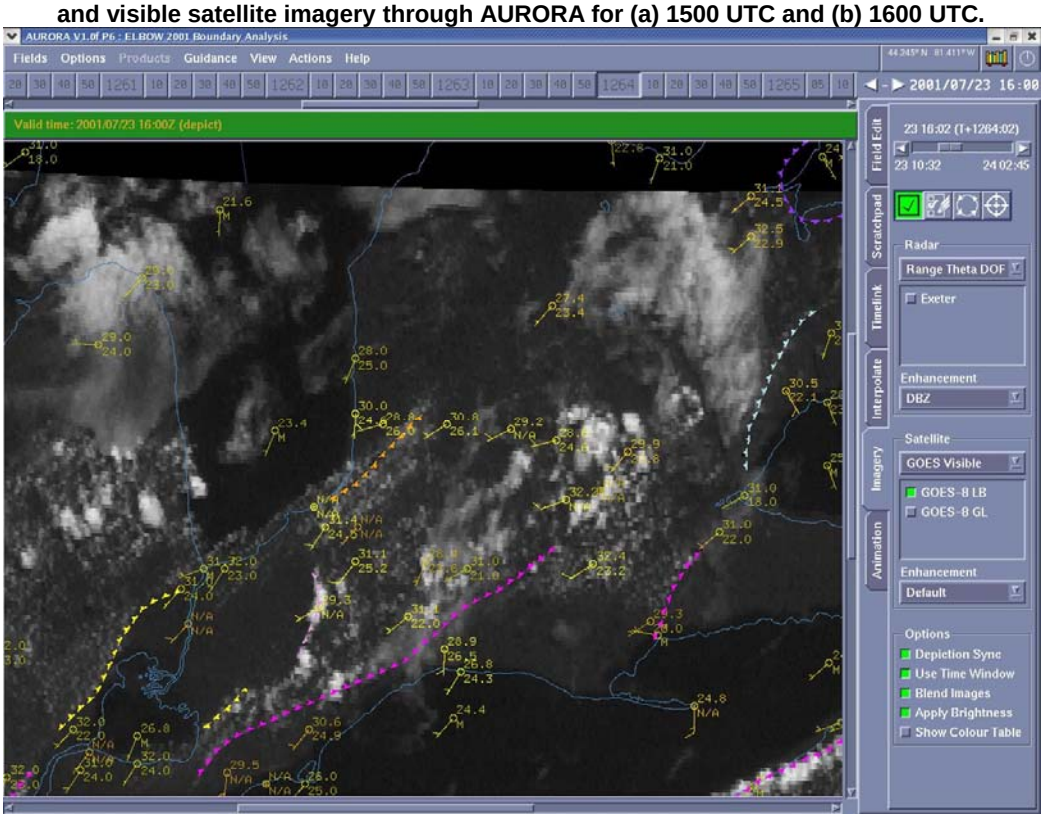

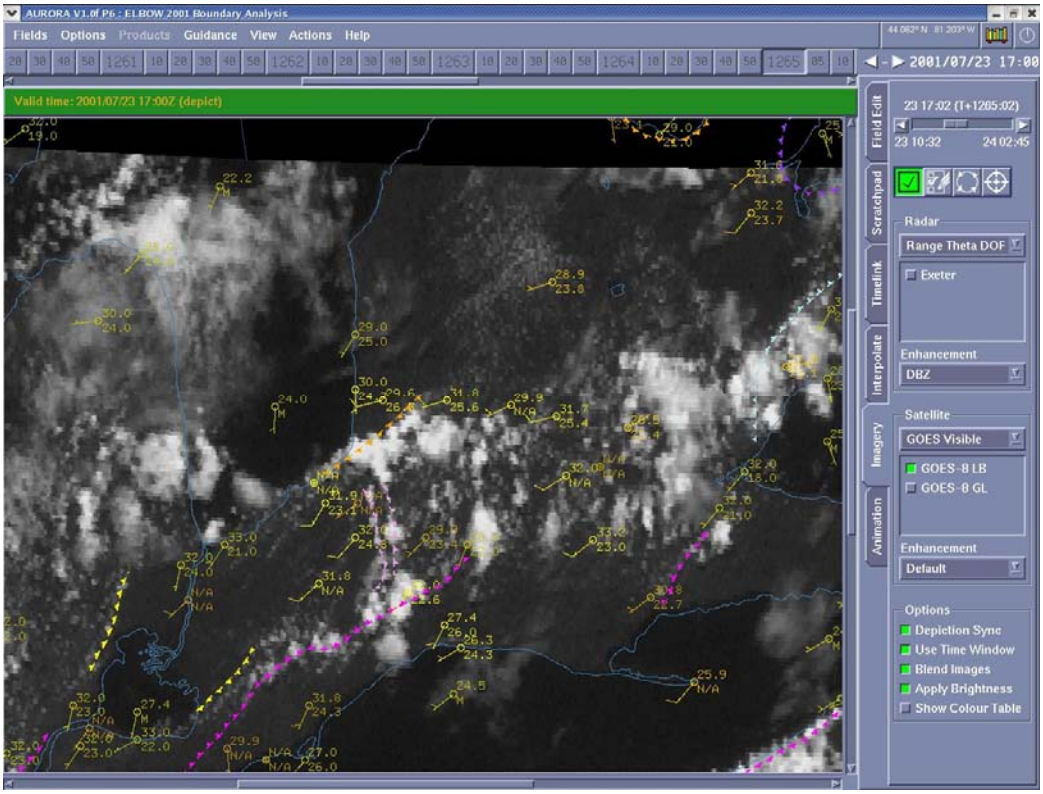

Figure 7.4c (above) and 7.4d (below). Showing the July 23 mesoscale boundaries, mesonet stations and visible satellite imagery through AURORA for (c) 1700 UTC and (d) 1800 UTC.

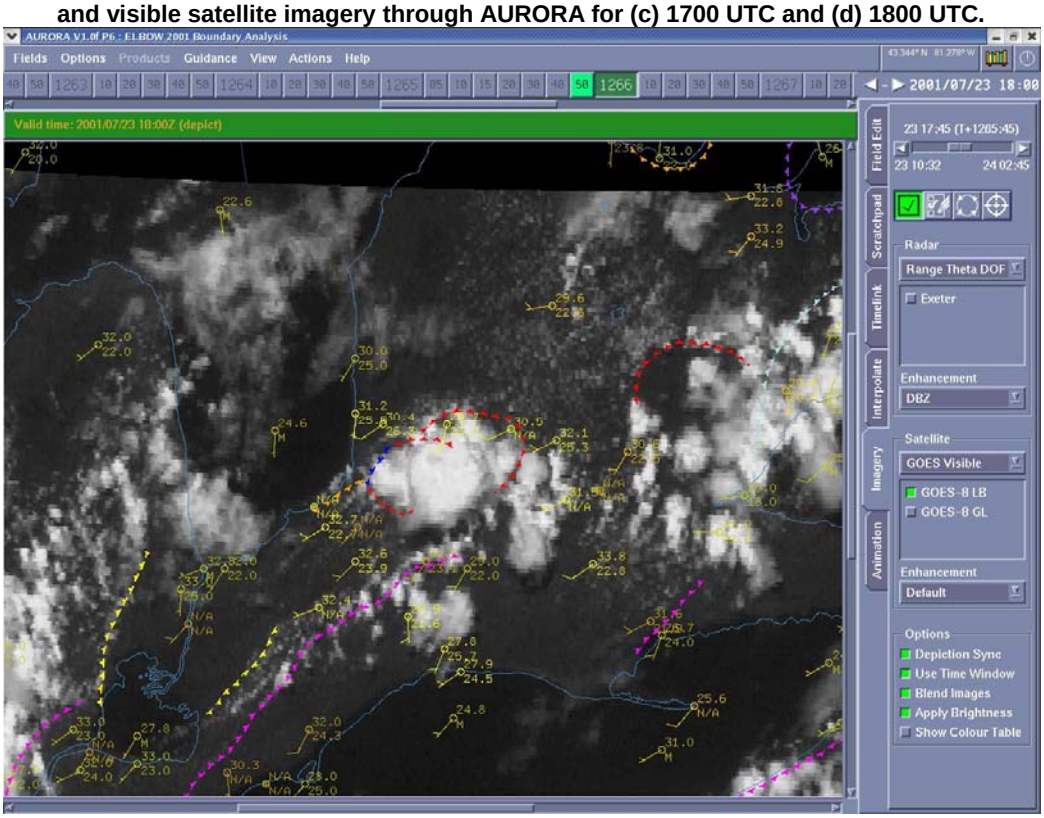

7.1.3 Lifted Index (LI) in the Lifting Zone

As covered in Chapter 1, section 1.4.2, Wilson et al. (2000) note that if the Lifted Index is shown to have a value of less than zero within a boundary's lifting zone, storm development is possible in association with that boundary.

By modifying the July 22 soundings with surface station temperature and dewpoint data, the Lifted Indices showed strong thunderstorm potential (as all values were less than -5). This was found during 1600 to 1800 UTC, for stations in the lifting zones of lake breeze fronts from Lake Huron, St. Clair, Erie and just outside the lifting zone for the Lake Ontario lake breeze front.

By modifying the July 23 soundings with surface station temperature and dewpoint data, the Lifted Indices were found to have values suggesting strong thunderstorm potential (as all values were well below -5). This was found for stations in the lifting zones of the Erie or Huron lake breeze fronts for 1500 or 1600 UTC (development was just starting at this time).

7.1.4 Convergence Strength

As covered more fully in Chapter 1, section 1.4.3, Wilson et al. (2000) note that with stronger low-level convergence in association with a boundary, the better chance there is for stronger storm development. See Figure 1.3 for a visual representation. Here we look at mesonet stations to assess the convergence strength.

July 22 shows southwesterly background flow. Concentrating on the ELBOW study area, by looking at Figure 7.3a to 7.3d it can be seen that the low

level winds associated with the Huron lake breeze circulation are similar to the background flow, on the east side of the lake, suggesting that there is very weak or no convergence. The south side of Lake Huron shows no mesonet data to confirm the winds. At 1900 UTC (Figure 7.3d) there appears to be some convergence on the east side of Huron, however, the following hour shows that the winds associated with the lake breeze adjusted back to a direction similar to the background flow. The winds depicting the Erie lake breeze circulation appear to be more southerly, and show a somewhat stronger convergence across the front at 1900 UTC. There were not many stations to show the winds associated with the lake breeze circulation to the east of Lake St. Clair. Once the lake breeze front passes the stations to the northeast of the lake, the wind direction does not change much, suggesting that the convergence is fairly weak along this lake breeze front. The winds driving the Ontario lake breeze front are very different from the background winds, suggesting stronger convergence across the front.

July 23 had somewhat stronger background flow. The convergence for this day was similar to July 22. Since the Huron and St. Clair lake breeze fronts appear to be drawn off the lakes by the background flow, there was little convergence along these fronts (as can be seen in Figures 7.4a to 7.4d). The winds associated with the Erie lake breeze circulation are seen to be somewhat more southerly than the background flow, suggesting some convergence across the Erie lake breeze front. The Ontario lake breeze winds show a strong

difference in direction from the background winds in Figures 7.4a to 7.4c. There are not many stations at the west end of the lake, however, if it is assumed that the winds are coming directly off the lake, then the convergence across the front would be strong.

The 'Other' boundary (or unknown boundary) in the study region, moving from the St. Clair lake breeze front through the centre of the study region, is showing strong movement. The mesonet winds behind the boundary have a similar direction to the environmental winds just ahead, however, they are somewhat stronger which could cause some convergence (see Figure 7.4c).

To summarize, both days showed similar convergence patterns. The mesonet stations suggest stronger convergence along the Erie and Ontario lake breeze fronts, as compared to those originating from Huron or St. Clair. The exception was the convergence across the 'Other' boundary on July 23 as it moved through the centre of the study region.

7.1.5 Updraft Orientation

As covered more fully in Chapter 1, section 1.4.4, Wilson et al. (1998) and Wilson et al. (2000) note that the tilt of the updraft associated with a boundary can help to indicate if storms will initiate along that boundary (and if pre-existing cells will mature into stronger cells). As can be seen in Figure 1.4, they looked at low-level shear in relation to a boundary to determine the resulting updraft orientation. Since it would be very time consuming to calculate the vector differences between the surface and 2.5 km winds (normal to the boundary) all

along the boundaries as well as the boundary speeds, here we simply look at the upper level environmental wind (2.5 km) orientation as compared to the winds driving the boundary in order to get an initial idea of the possible updraft orientation. Wilson et al. (1998) noted that the upper winds (steering the storms) show to be similar to the boundary movement, in an erect updraft case, so by doing this we are visually assessing if this is occurring. It would be much more accurate in future case studies to have the calculation of vector wind differences automated.

Table 7.1 shows the winds, on July 22, for each sounding at approximately 2.5 km above ground level. If there is a comparison of the 2.5 km wind, at the closest time and location, to the winds associated with each corresponding boundary, then the updraft orientation can be estimated. By comparing these against the mesonet winds in Figures 7.3a to 7.3d, it can be seen that the surface winds in the Erie lake breeze circulation are very different from the winds at the 2.5 km level. This means that updrafts will be tilted here, making the environment for storm development less favourable. The surface winds within the Huron lake breeze circulation (on the east side of the lake) are generally southwesterly. Therefore these are closer in direction to the 2.5 km winds than those for lake Erie, but are still sometimes perpendicular to them, meaning this updraft may not be erect. The northeast side of lake St. Clair has a couple stations which indicate that the lake breeze front has passed by 1900 UTC. Again these winds are very different in direction from the 2.5 km winds

Table 7.1. Showing the 2.5 km winds for each sounding performed on July 22.

Sounding Location	Time (UTC)	Height (AGL in m)	2.5 km Wind Speed (m/s)	2.5 km Wind Direction (deg)
Port Stanley	1502	2476	4.9	343
Port Stanley	1801	2497	3.4	296
Port Stanley	2101	2504	2.7	340
Port Franks	1502	2497	1.9	325
Port Franks	1801	2514	4.4	299
Port Franks	2056	2505	5.4	290
Mobile	2143	2508	4.3	299

suggesting the updraft will be tilted and less favourable for storm development. The Ontario lake breeze winds are sometimes directly opposing the 2.5 km winds which again suggests a tilt to the updraft.

Table 7.2 shows the 2.5 km winds from the soundings performed on July 23. By comparing these against the mesonet winds in Figures 7.4a to 7.4d, we can see that the orientations of the updrafts are very different in this case. The winds at 2.5 km on this day are stronger than those for July 22 (similar to the background flow on July 23). We can see that the low level winds within many of the lake breeze circulations are very similar in direction to the 2.5 km winds, especially around 1800 UTC, since the sounding is indicating southwesterly winds. Specifically, the winds driving the Huron lbf and St. Clair lbf are very similar in direction, suggesting possible erect updrafts and a more favourable storm environment. It should be mentioned however, that the fronts corresponding to these lakes are oriented in this direction as well. Another interesting feature, is that the 'Other' boundary is being driven by winds that are similar in direction to the 2.5 km winds, suggesting a possible vertical updraft. By looking at Figures 7.4a and 7.4b, we can see that the winds driving the Ontario

Table 7.2. Showing the 2.5 km winds for each sounding performed on July 23.

Sounding Location	Time (UTC)	Height (AGL in m)	2.5 km Wind Speed (m/s)	2.5 km Wind Direction (deg)
Port Stanley	1501	2487	5.2	270
Port Stanley	1800	2490	6.3	249
Port Stanley	2056	2494	7.0	240
Port Franks	1501	2500	7.2	263
Port Franks	2123	2499	6.9	249
UWO Farm	1504	2507	4.2	271
UWO Farm	1801	2501	7.9	265
UWO Farm	2137	2482	9.6	232

lbf are greater than 90 degrees different from the 2.5 km winds, suggesting a more tilted updraft. However, by 1800 UTC (Figure 7.4d), it can be seen that the winds at the most northern point of the Ontario lake breeze front are getting closer to the direction of the 2.5 km winds. Also, at this time there are many gust fronts forming which would have erect updrafts on their northeast side.

To summarize, the 2.5 km wind directions compared to the mesonet winds (within the lake breeze circulations) suggest that the updrafts were more erect on July 23 as compared to July 22, in most locations. It can also be seen that the 'Other' boundary, moving through the centre of the study area on July 23, showed a similar direction to the 2.5 km winds, therefore suggesting an erect updraft.

7.1.6 Boundary Relative Cell Speed

As covered more fully in Chapter 1, section 1.4.5, Wilson et al. (2000) note that the speed of a cell, relative to the movement of a low-level boundary can determine if the cell will continue to develop, or if it will dissipate. The equation used to calculate Boundary Relative Cell Speed is noted in section 1.4.5. In general, if a cell is moving in a similar direction and speed as the boundary, then

it will stay in proximity of it and continue to develop (from the convergence caused by the boundary). However, if it is moving in a direction away from the boundary, it will dissipate. Wilson et al. (2000) note the threshold value for Boundary Relative Cell Speed is 4 m/s; values below this threshold means the cells will stay in proximity and may develop further. However, values above this threshold will progress away from the boundary (meaning cell dissipation is probable).

Boundary Relative Cell Speeds were calculated for a number of different sample locations, by measuring the boundary speed at the particular location, and using the closest sounding (in time and location) for the steering winds (mean wind between heights of 2 and 4 km). Table 7.3 shows the boundary relative cell speeds calculated for July 22, for the locations shown in Figures 7.5a to 7.5c. Notice that many of these are greater than 4 m/s. This indicates that if cells form they are most likely to move away from the corresponding mesoscale boundary and dissipate (as noted in Chapter 1 section 1.4.5). Locations 1, 2, 6, 7, 8, 11, 12 and 14 are all below 4 m/s. If cells were to form in these locations then they would most likely stay close to the boundary and develop more fully. Most of the favourable values for further storm development are along the south and east sides of Lake Huron, and the east side of Lake St. Clair. However, no cells initiated at these locations so they did not have a chance for further development.

Table 7.4 lists the boundary relative cell speeds on July 23, for the locations shown in Figures 7.6a and 7.6b. Notice again, that many of the

Table 7.3. The boundary relative cell speeds calculated for July 22.

Location	Time (UTC)	Boundary Relative Cell Speed (m/s)
1	1700	-2.83
2	1700	-0.72
3	1700	6.03
4	1700	8.45
5	1700	5.46
6	1800	-4.35
7	1800	2.28
8	1800	-2.33
9	1800	7.08
10	1800	7.62
11	1800	-5.36
12	2000	-3.11
13	2000	6.02
14	2000	3.94
15	2000	9.34
16	2000	6.30
17	2000	4.98
18	2000	5.34

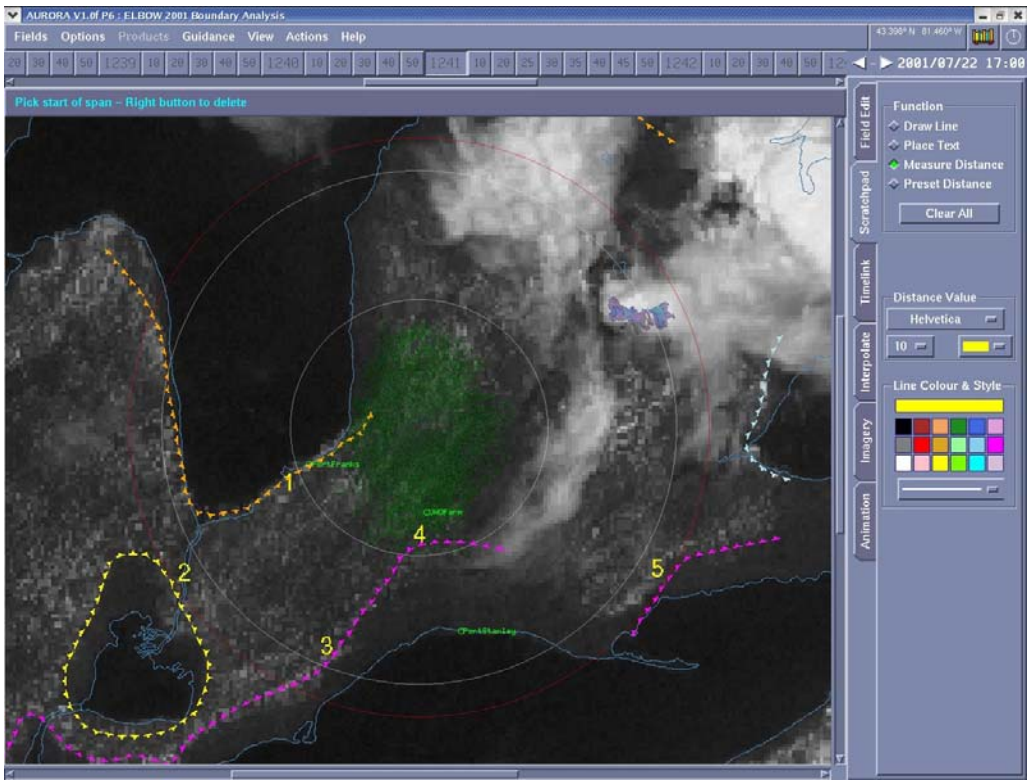

Figure 7.5a. Showing July 22 locations 1 to 5 (1700 UTC) where boundary relative cell speeds were calculated.

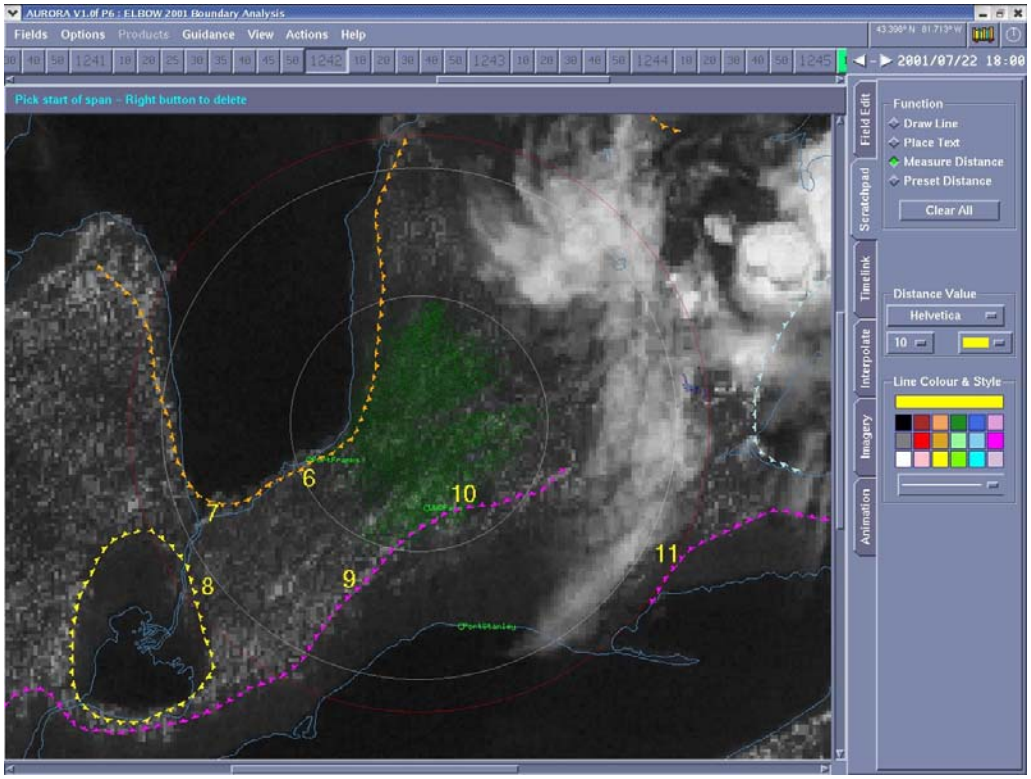

Figure 7.5b (above) and 7.5c (below). Showing July 22 locations 6 to 11 (1800 UTC) and 12 to 18 (2000 UTC) where boundary relative cell speeds were calculated.

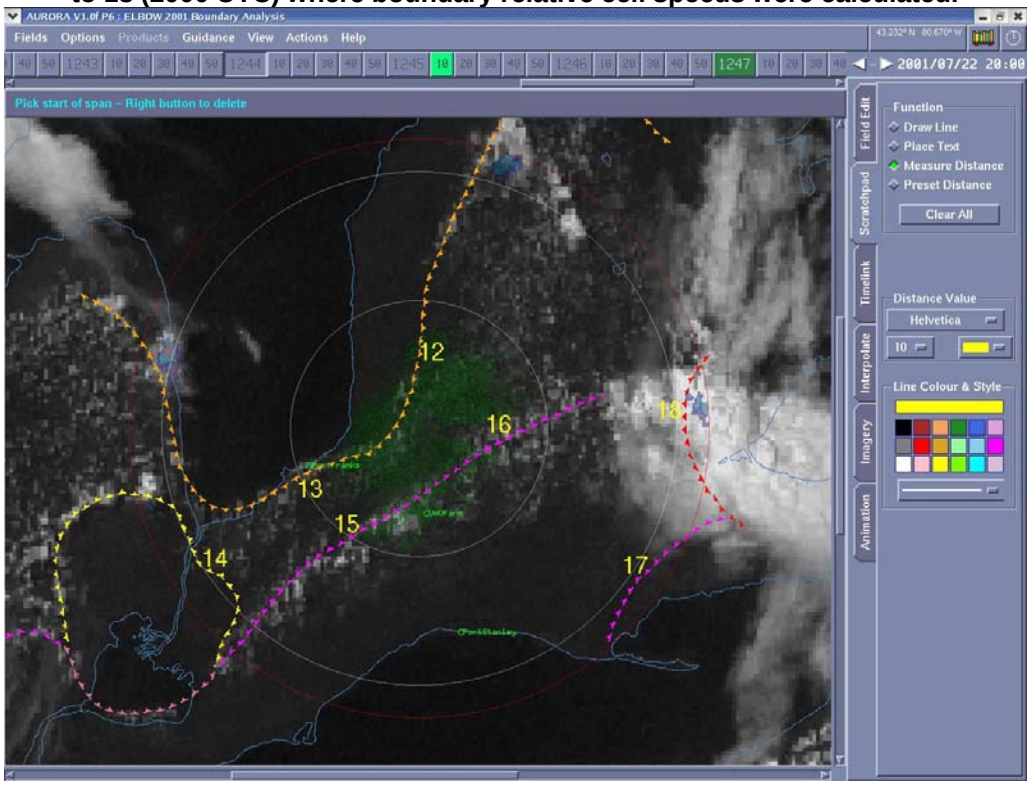

Table 7.4. The boundary relative cell speeds calculated for July 23.

Location	Time (UTC)	Boundary Relative Cell Speed (m/s)
1	1600	-6.88
2	1600	-3.29
3	1600	8.10
4	1600	5.40
5	1600	5.92
6	1600	8.41
7	1700	4.79
8	1700	-0.44
9	1700	4.60
10	1700	3.13
11	1700	7.45
12	1700	-3.76

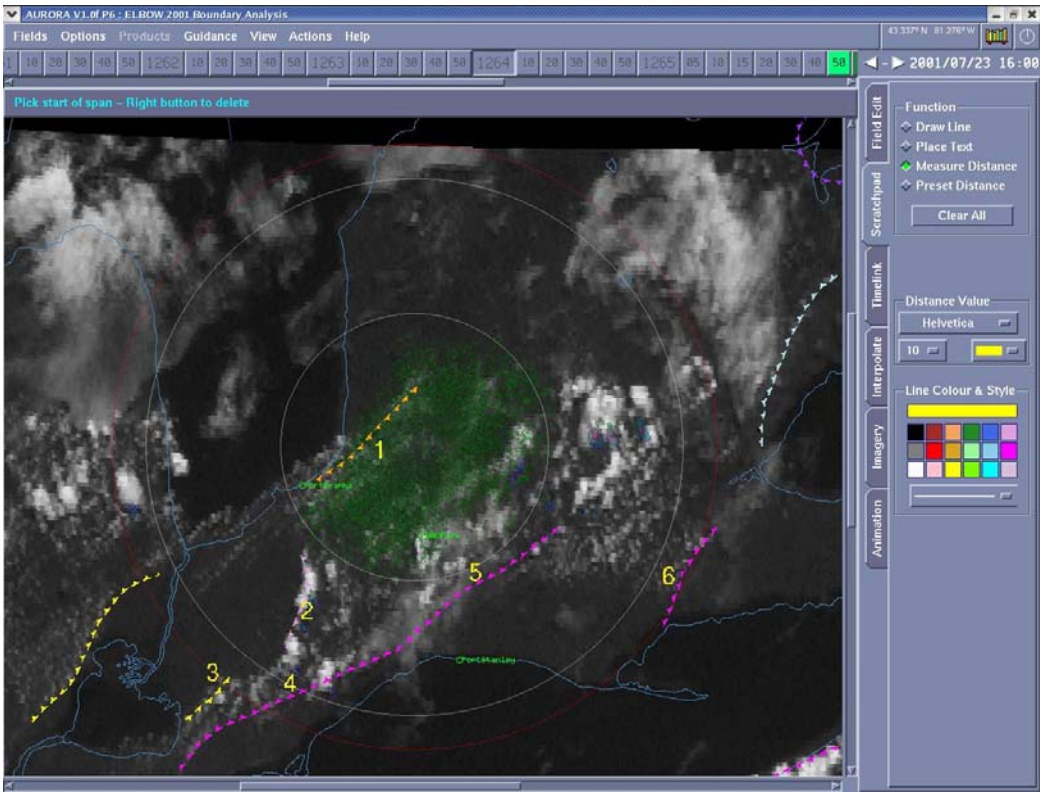

Figure 7.6a. Showing July 23 locations 1 to 6, at 1600 UTC, where boundary relative cell speeds were calculated.

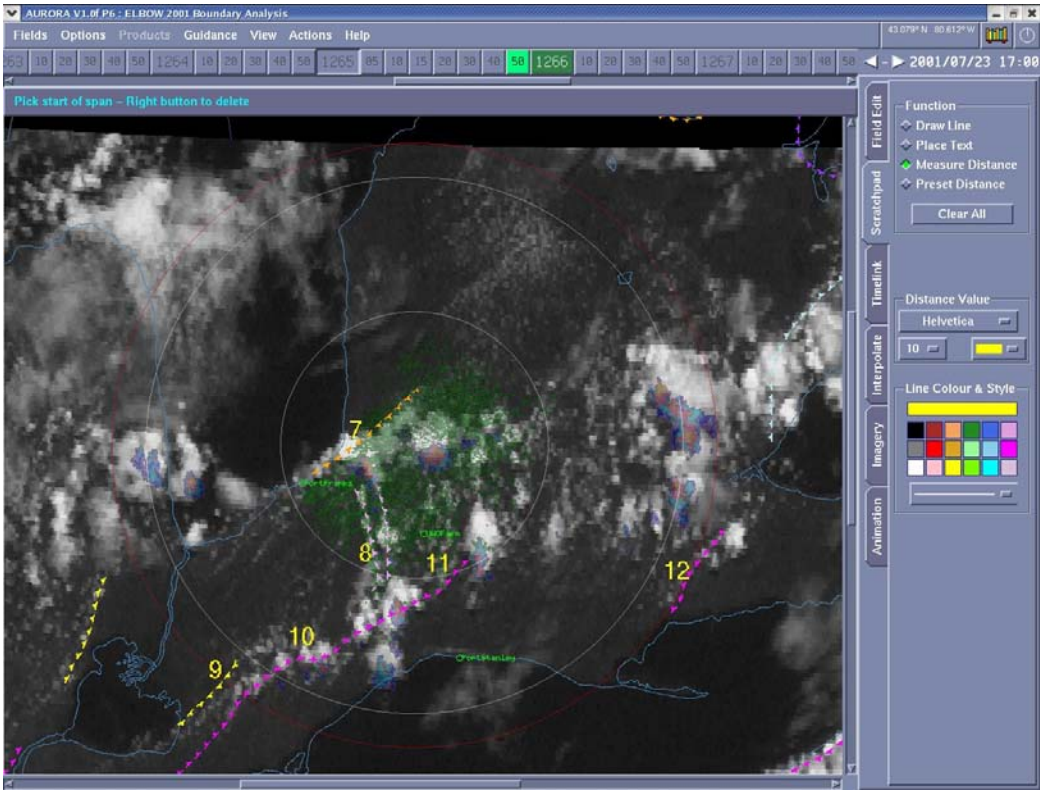

Figure 7.6b. Showing July 23 locations 7 to 12, at 1700 UTC, where boundary relative cell speeds were calculated.

locations show boundary relative cell speeds greater than 4 m/s indicating movement away from the boundary and possible dissipation. Locations 1, 2, 8, 10 and 12 are showing values less than 4 m/s. This is indicated for the 'Other' boundary (for both times indicated in Figures 7.6a and 7.6b), moving quickly through the study region between Lakes Huron and Erie. The less than 4 m/s threshold is also indicated for the Huron lake breeze front at 1600 UTC and Erie lake breeze front at 1700 UTC. As the 'Other' boundary moved closer to the Huron lbf, cells were triggered. Development intensified and many more interactions were caused, including a number of gust fronts interacting with the existing boundaries.

7.1.7 Summary

Both July 22 and July 23 had similar environmental conditions. Until looking into these cases through recent nowcasting techniques, the reason for varying development was not known. The features which were different between the two days were the vertical development of cumulus clouds. July 22 did not have nearly as much vertical development seen in the cumulus cloud field as on July 23. One reason why development was much stronger on July 23 may have been the updraft orientation. Since the 2.5 km winds for July 23 were from the southwest and those for July 22 were from the northwest, the updrafts were more erect and therefore favourable for storm development along many of the mesoscale boundaries on July 23. The mesonet winds within the lake breeze circulations showed a similar direction to the 2.5 km winds on July 23.

Another factor, that most likely contributed to the widespread development on July 23, was the 'Other' boundary (or boundary of unknown origin) which was not present on the previous day. This boundary came very close to other boundaries existing in the study region and helped to trigger cell development.

7.2 July 20, 2001

7.2.1 General Events

Cells started to form in the study region just before 1800 UTC. However, these only formed along the Huron and St. Clair lake breeze fronts. Eventually, development showed a line of cells which stretched from the southwest to the north part of the study region (see Figures 7.7a, b, c and d). This development

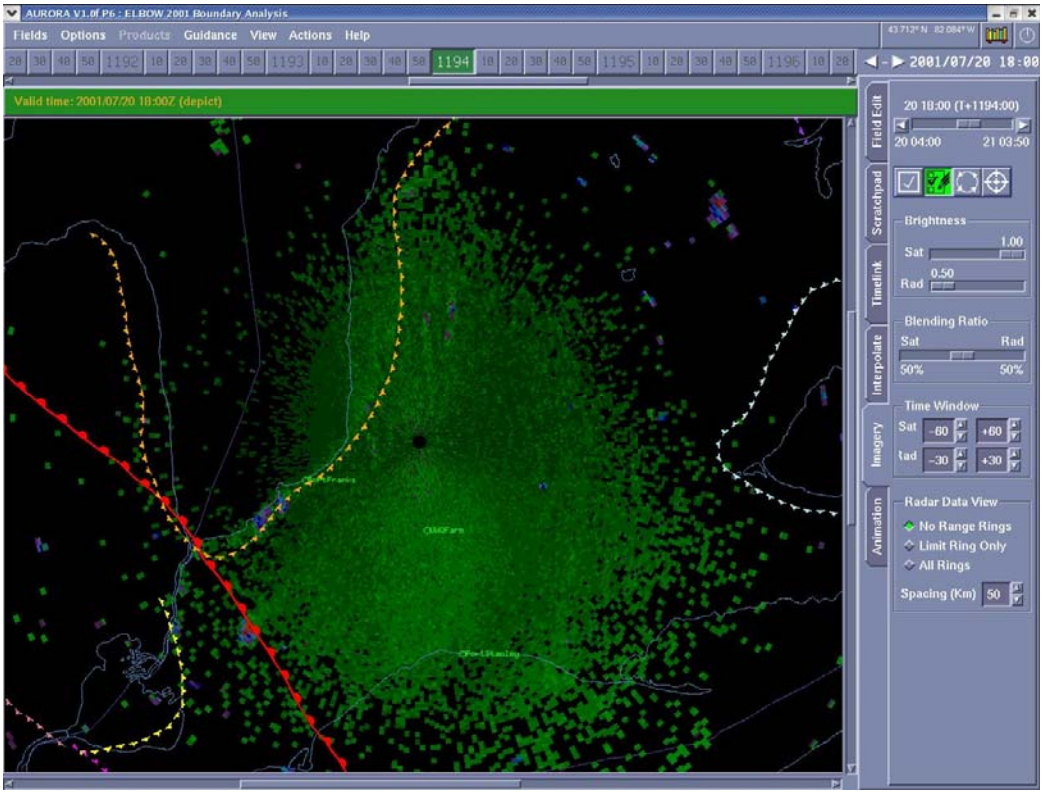

Figure 7.7a (above) and 7.7b (below). Showing the July 20, 2001 Exeter MAXR images and mesoscale boundaries, as displayed in AURORA, for (a) 1800 UTC and (b) 1900 UTC.

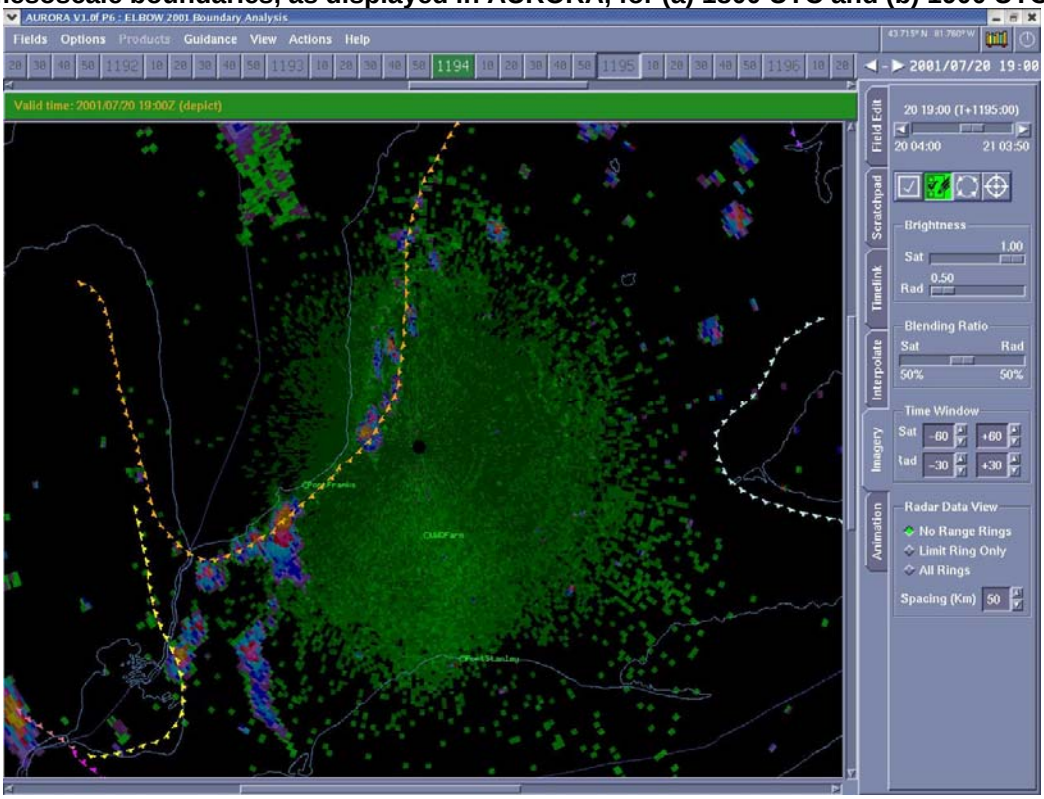

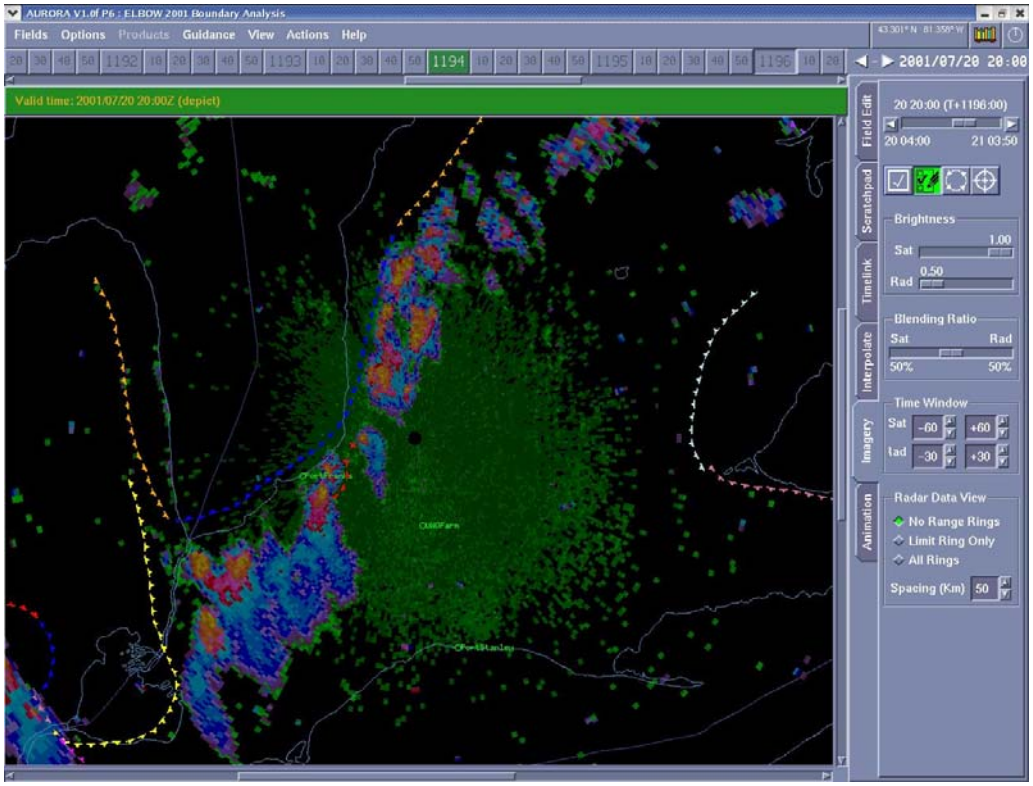

Figure 7.7c (above) and 7.7d (below). Showing the July 20, 2001 Exeter MAXR images and mesoscale boundaries, as displayed in AURORA, for (c) 2000 UTC and (d) 2100 UTC.

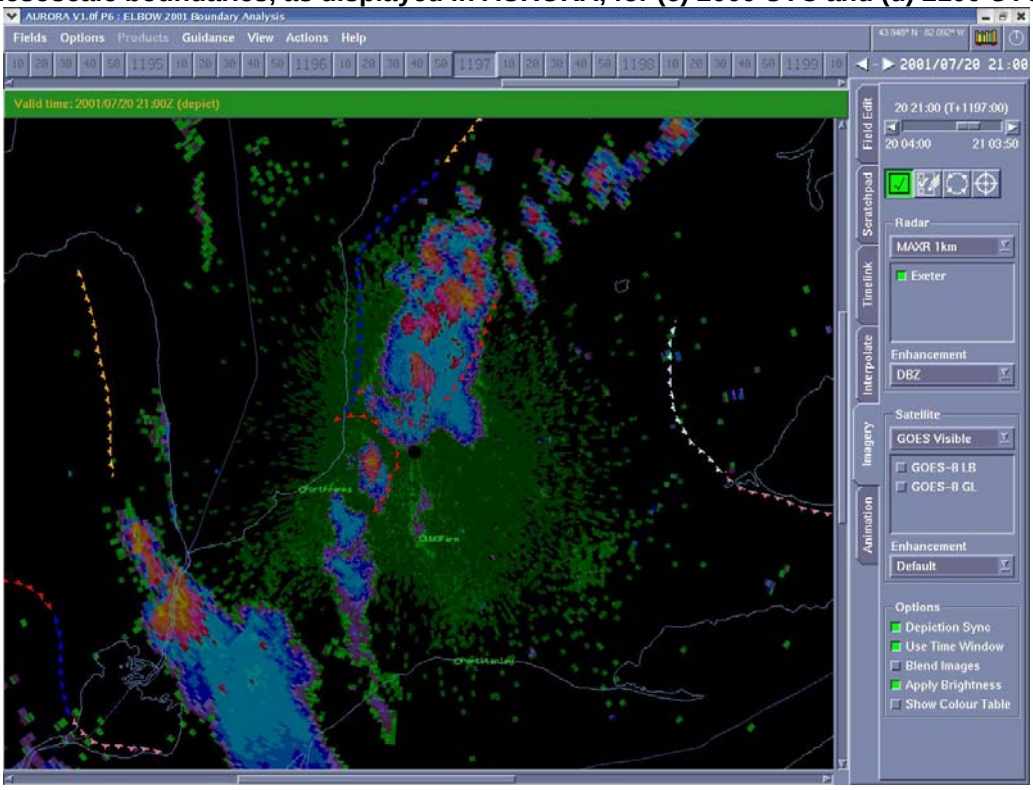

became more complex as gust fronts were triggered. The Ontario lbf and Merged (Ontario/Erie) boundaries were also affecting the study region, but no cells initiated along these boundaries. A cell (outside the study region) did form close by the Ontario lbf but it occurred at a distance (26 km) from the boundary and dissipated quickly. So, why were storms frequently initiating along the Huron and St. Clair lbf, but the same was not occurring for the Ontario lbf and Merged (Ontario/Erie) boundary?

7.2.2 Cumulus Associated with the Lifting Zone

Cumuli were occurring in the lifting zones of all lake breeze fronts by 1600 UTC, however, cumulus clouds development showed to be at a minimum around

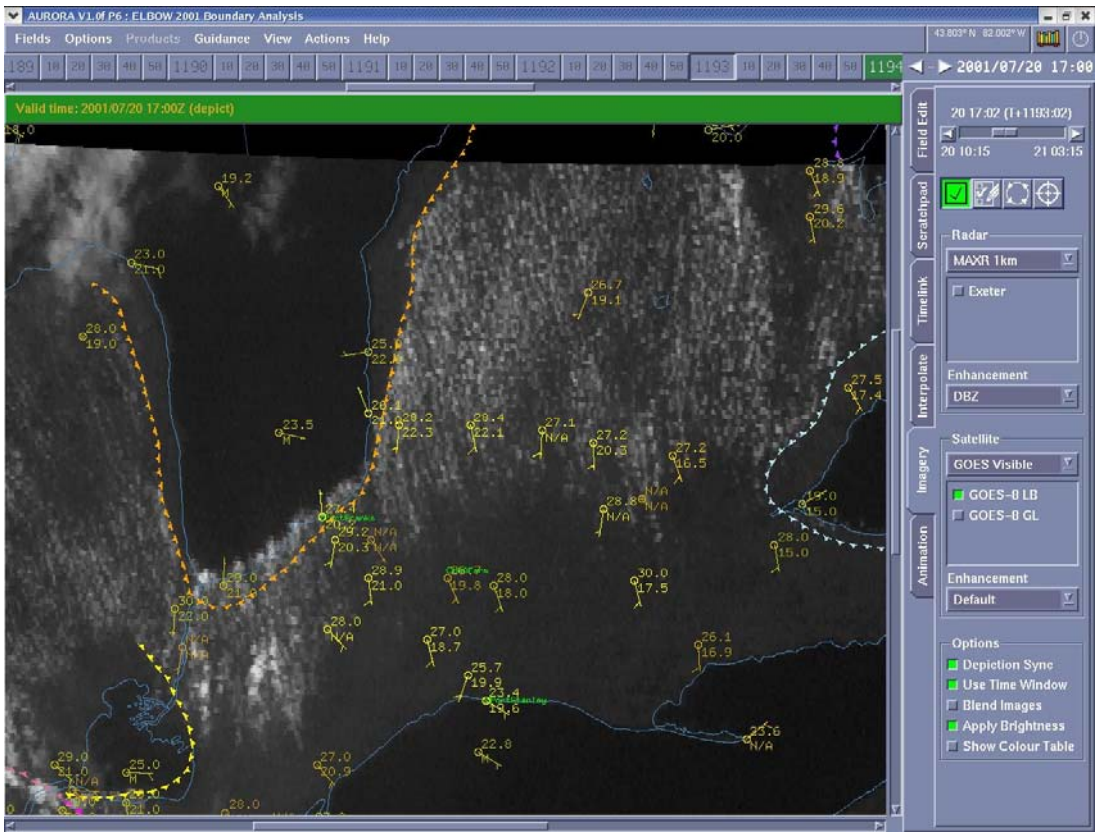

Figure 7.8a. The GOES-8 visible satellite image, mesonet stations and mesoscale boundaries, as seen in AURORA, on July 20, 2001 (1700 UTC).

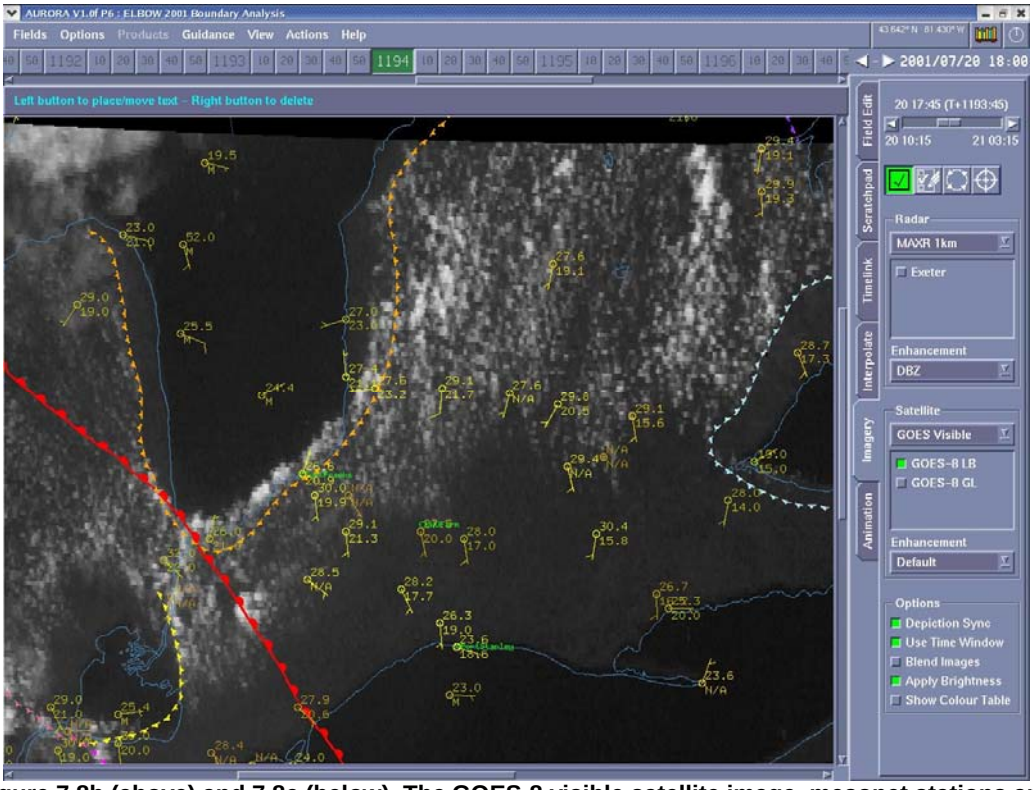

Figure 7.8b (above) and 7.8c (below). The GOES-8 visible satellite image, mesonet stations and mesoscale boundaries, as seen in AURORA, on July 20, 2001 for (b) 1800 UTC and (c) 1900 UTC.

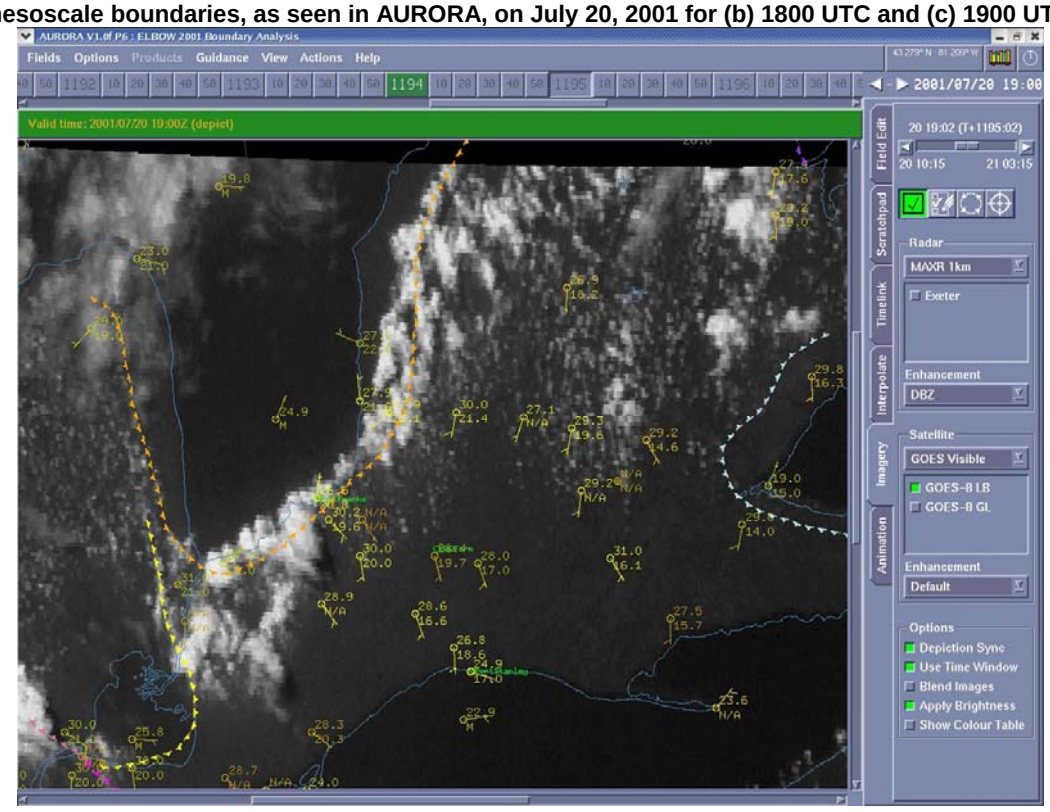

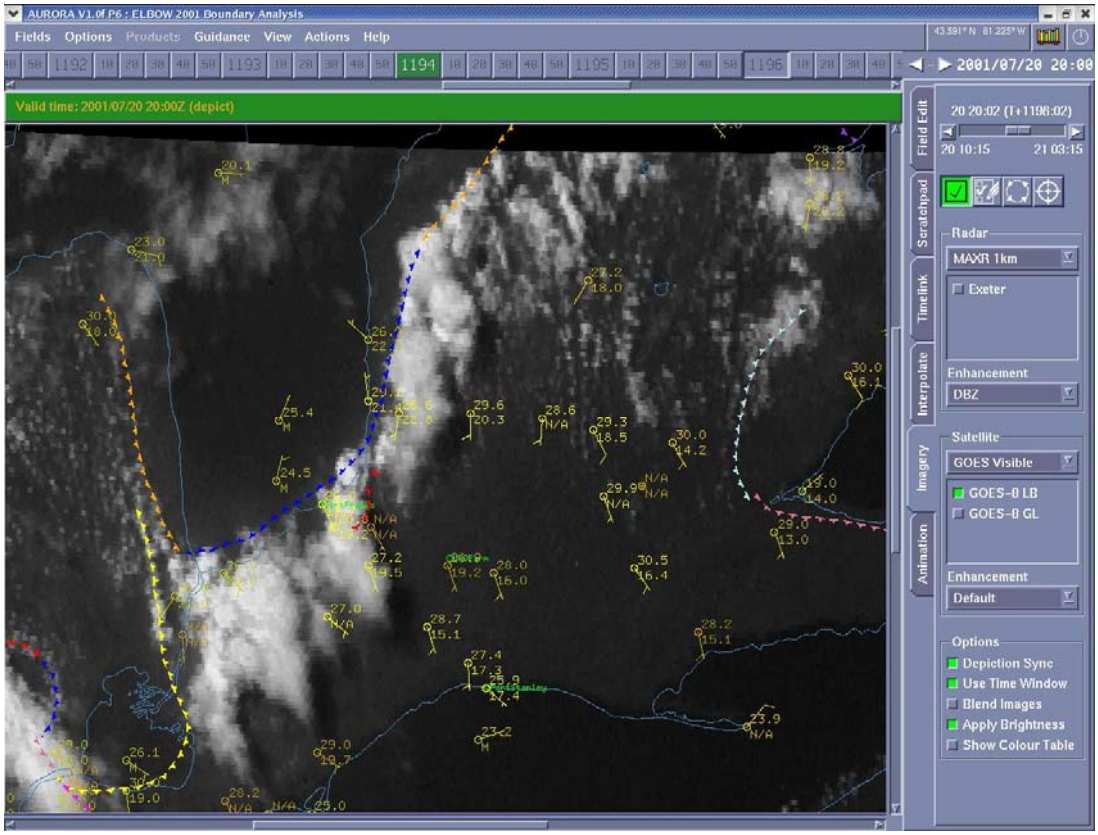

Figure 7.8d. The GOES-8 visible satellite image, mesonet stations and mesoscale boundaries, as seen in AURORA, on July 20, 2001 (2000 UTC).

the southwestern shore of Lake Ontario and southeast shore of Lake St. Clair. By 1700 UTC, the cumulus clouds were developing more fully in some of the lifting zones. Vertical growth could be seen on the south side of Lake Huron and along the St. Clair lake breeze front (see Figure 7.8a).

7.2.3 Lifted Index (LI) in the Lifting Zone

The LI for this day could not be found due to the fact that there were no substantial soundings performed. Two soundings were done at the Port Franks location on this day, but neither reached a level which was substantial enough to calculate the lifted index. Soundings from Detroit and Windsor were only available during 1200 UTC and 0000 UTC (as seen on the University of Wyoming

Website http://weather.uwyo.edu/upperair/sounding.html) which were not close enough to be representative of the time just before convective development.

7.2.4 Convergence Strength

If we look at the mesonet station winds for 1700 UTC (Figure 7.8a), we can see that there is strong convergence along the Huron lbf in the study region. In many places the winds are opposing each other. For the Ontario lbf, which is still outside the study region at this time, we can see that the southern part of the lake breeze front (corresponding to the southern shore) has fairly strong convergence. However, the northern part of the Ontario lbf appears to have weak convergence. Wind direction shown in the mesonet stations on the lake side of the lake breeze front are almost the same as the background winds around this area.

The winds represented by the station in the middle of Lake St. Clair may not be representative of the winds directly behind the lake breeze front. The lake is smaller than the others in the region, and the wind field will vary greatly from one side of the lake to the other. If we assume the winds driving the lake breeze front are coming off the lake, then the convergence strength would be significant especially for the southeast shore of the lake, yet weaker for the north shore. However, this has to be assumed, due to the lack of stations on the east side of the lake.

In looking at the mesonet winds at 1800 UTC (Figure 7.8b), we can see similar convergence results to those at 1700 UTC. Notice that the winds on the

lake and land side of the Huron lbf are opposing each other in many places, and indicate strong convergence. The Ontario lbf again has stronger convergence on the south side of the lake but weaker north of the lake. It was not possible to see the convergence strength at the eastern St. Clair lake breeze front due to a lack of stations.

7.2.5 Updraft Orientation

The 1803 UTC sounding done at Port Franks (Lake Huron) indicates 2.5 kilometer (AGL) winds of approximately 4.0 m/s coming out of the WNW (300 deg). At 1700 UTC, the winds, indicated by the mesonet stations, shown on the lake side of the Huron lbf are slower than the 2.5 km winds. However, some of the winds, especially on the east side of the lake have a similar direction to the 2.5 km winds, indicating that the updraft will be more erect and favourable for storm development. The winds at the west end of Lake Ontario show to have a very different direction than those at 2.5 km (especially those along the north shore). The updraft along this lake breeze front may be more tilted and therefore less favourable for storm development. There are no mesonet stations on the east side of Lake St. Clair to indicate wind direction.

At 1800 UTC, the winds on the lake side of the Huron lbf are showing a similar pattern to that of the winds at 1700 UTC. The winds on the east side of the lake are of similar direction to the 2.5 km winds, indicating an erect updraft. The winds to the south side of this lake are almost perpendicular to the 2.5 km winds but are weak. The winds shown on the lake side of the Lake Ontario lake

breeze front are again coming out of a very different direction than the 2.5 km winds which indicates a tilted updraft.

The Lake St. Clair winds for the east side of the lake were not available due to the lack of stations in this area. However, if we assume that the winds are coming off the lake, then the winds would have a direction close to those of the 2.5 km winds, which would also indicate a more erect updraft.

7.2.6 Boundary Relative Cell Speed

Looking at the 1803 UTC sounding, taken at Port Franks, we can see that this sounding had steering flow winds of 3.37 m/s from a direction of 323 degrees. Looking at the motion of the boundaries at 1800 UTC at given locations (assuming boundary motion is consistent and motion is occurring perpendicular to the boundary at each point), we can see that all of the boundary relative cell speeds are less than 4 meters per second for all the locations (see Table 7.5). Location maps corresponding to the values in Table 7.5 can be found in Figures 7.9a, b and c.

Table 7.5. The boundary relative cell speeds calculated for various locations on July 20, 2001

Location	Time (UTC)	Boundary Relative Cell Speed (m/s)
1	1800	-0.1
2	1800	-2.9
3	1800	3.82
4	1800	0.15
5	1800	2.74
6	1900	-2.29
7	1900	-2.26
8	1900	-2.48
9	1900	0.94
10	1900	2.7
11	2000	1.49
12	2000	2.96

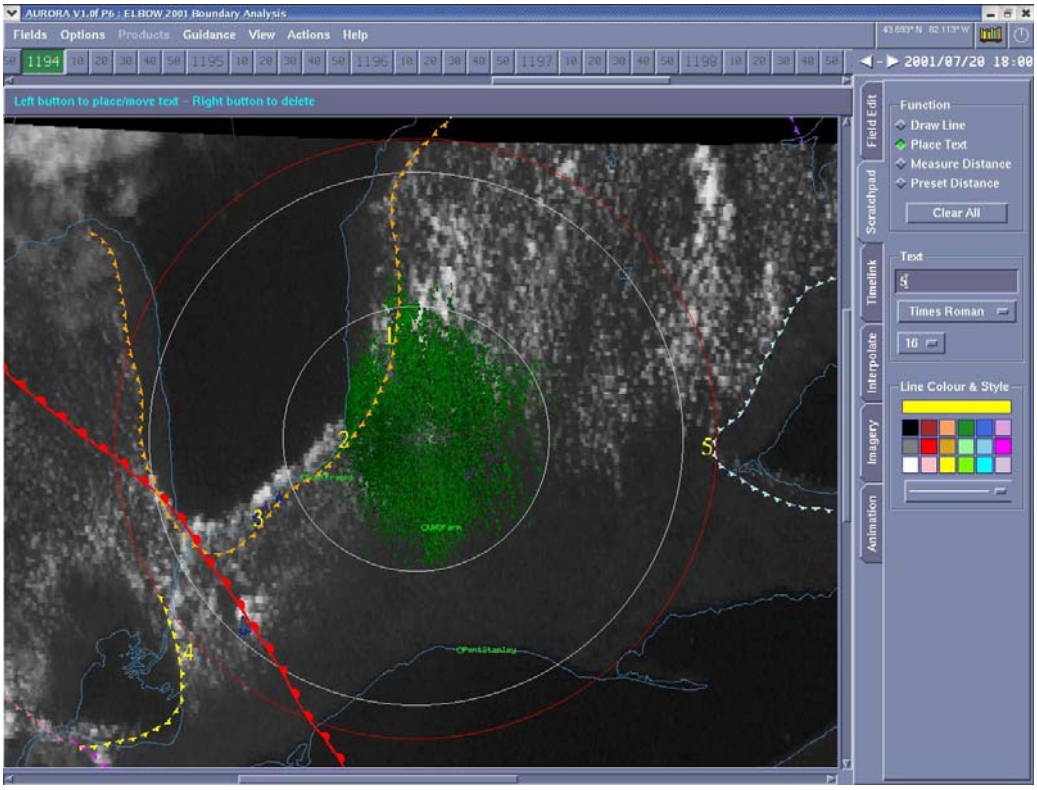

Figure 7.9a (above) and 7.9b (below). Showing the locations that boundary relative cell speeds were calculated for on July 20, 2001 at (a) 1800 UTC and (b) 1900 UTC.

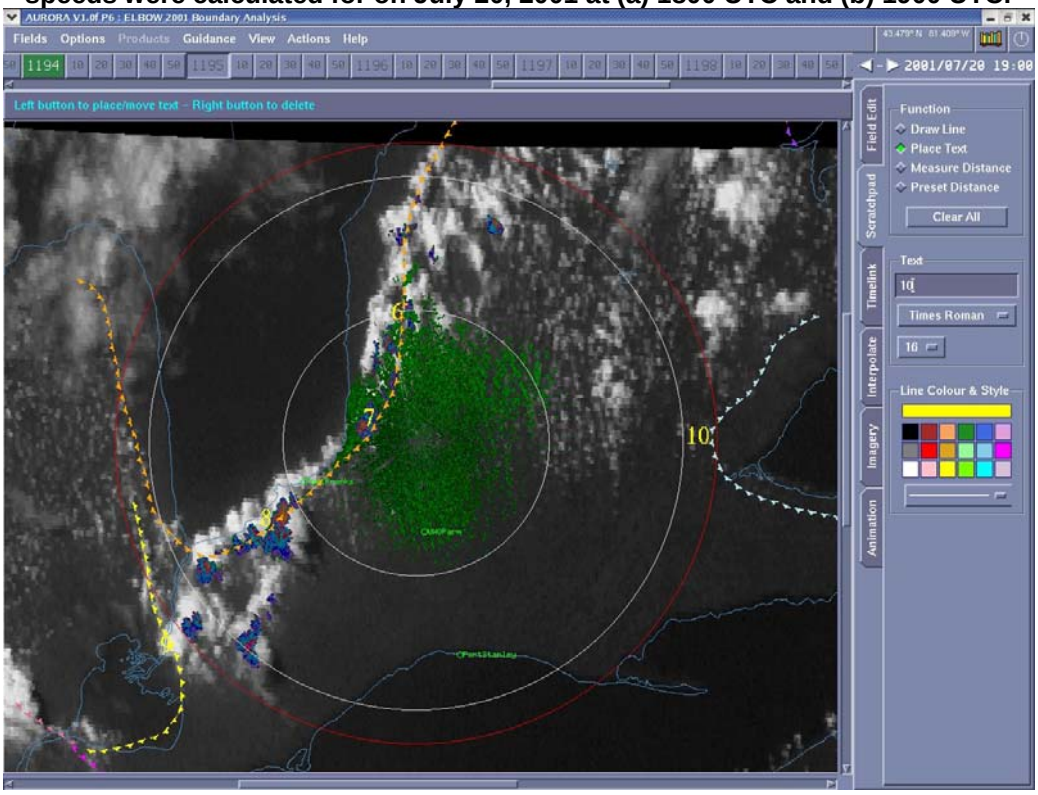

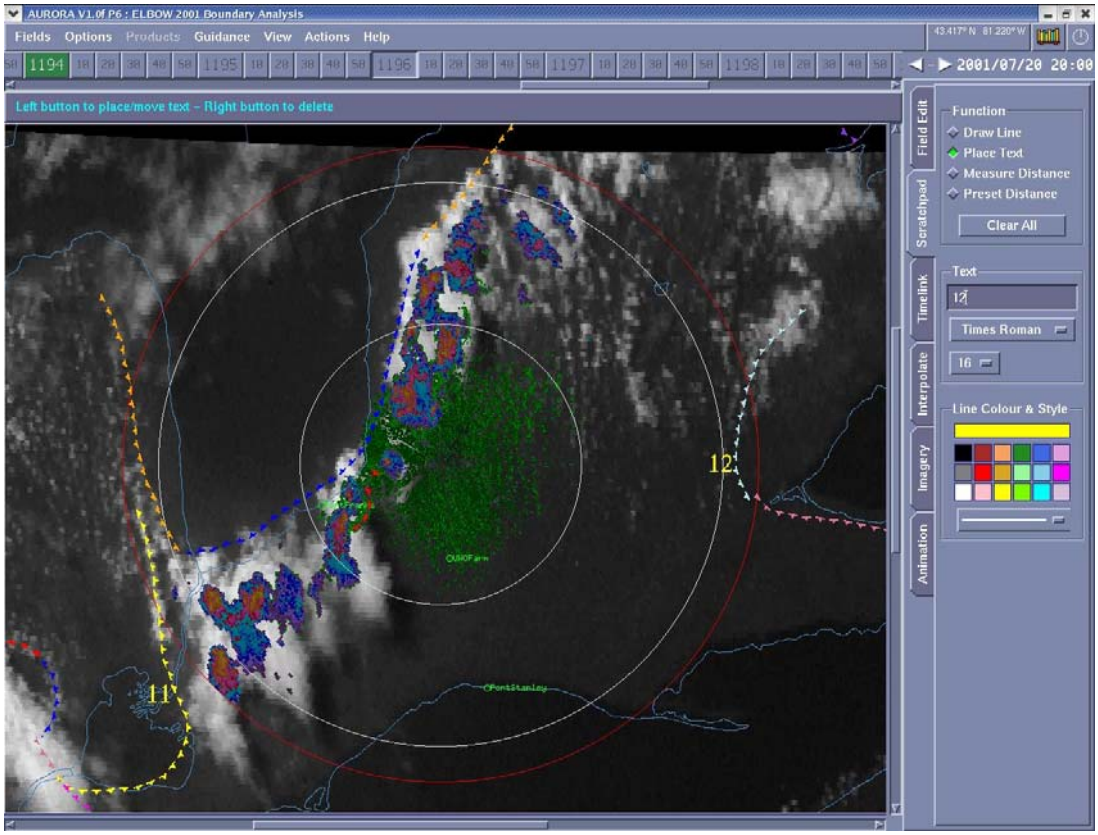

Figure 7.9c. Showing the locations that boundary relative cell speeds were calculated for on July 20, 2001 (2000 UTC).

At 1900 UTC and 2000 UTC, the boundary relative cell speed values are all below 4 m/s, suggesting that the cells may continue to develop because they will stay in proximity of the corresponding mesoscale boundary.

7.2.7 Summary

So what caused the development along the Huron and St. Clair lake breeze fronts and the lack of development along the Ontario lake breeze front? In this case a number of answers have become clear. The lack of, or little, cumulus development along the southwest shore of Lake Ontario and southeast shore of Lake St. Clair suggest unfavourable conditions for development. In both of these areas there was lack of development during the time of concern.

The Ontario lake breeze had weak convergence on the north shore, while the Huron lake breeze front showed strong convergence with the background flow. The St. Clair lake breeze front showed convergence (surface winds showed a perpendicular direction difference) on the east shore of the lake (assuming that the winds driving the lake breeze are coming from the lake, as there were a lack of stations in this area).

The 2.5 km winds suggest updraft orientation was more erect along the Huron lake breeze front than the Ontario lake breeze front (especially the north shore). Therefore the Huron lake breeze front created a more favourable storm environment. Assuming the St. Clair lbf winds were coming off the lake, the storm environment would also be favourable for the east shore.

7.3 Future Work

A reason for the development, or lack thereof, in these cases could be found using the nowcasting techniques outlined in Chapter 1. Further study of these techniques, as well as developing/researching a number of other techniques, could allow for better nowcasts in the Southwestern Ontario region. It would be useful to try to automate some of the calculations along the boundaries, as visual analysis is time consuming. Perhaps this can be done through the AURORA program or by applying the NCAR Auto-Nowcaster, developed by the National Center for Atmospheric Research (NCAR), to the area. Recently, the Research Support Desk (RSD), at Environment Canada, has been

working on operationally providing nowcasts of storm development, in association with mesoscale boundaries (Sills and Taylor, 2008).

Since these nowcasting techniques were originally utilized in locations other than the Southwestern Ontario region and looked at some different mesoscale boundary types, it would be useful to study this topic further to see if thresholds, such as that for the boundary relative cell speed and updraft orientation, are similar for this region. Further study with more dense wind fields/mesonet stations would most likely show some revealing results.

8. A Summary of Findings

This chapter provides a brief summary of the results of this study. The best method for low-level mesoscale boundary identification, the results of the cell initiation in proximity to mesoscale boundaries and the findings of the case studies using current nowcasting techniques are all covered in the following sections.

8.1 Low-Level Mesoscale Boundary Identification

As was discussed in Chapter 5, four low-level boundary identification analyses were completed. These analyses included a Mesonet analysis using only mesonet data, a Radar analysis using only Exeter radar images, a Satellite analysis using GOES-8 visible satellite images and an Integrated analysis using all mesonet, radar and satellite data (viewed simultaneously). All analyses were performed using the AURORA research tool developed by the Meteorological Service of Canada (discussed in Chapter 4).

A number of different types of boundaries were identified including: lake breeze fronts, land breeze fronts, ‘merged’ boundaries, ‘hybrid’ boundaries, ‘outflow’ boundaries and ‘other’ boundaries. All boundaries were identified using a set of specific criteria.

All of the analyses were compared to a Final ‘truth’ set of boundaries. After comparing all the analyses using a contingency table method (for lake breeze occurrence) and a Pearson and Spearman Rank correlation coefficient method

(for inland penetration distances of lake breezes) it was clear which identification analysis performed the best and which were lacking in accuracy.

The contingency table indices showed that the Integrated analysis gave the overall most accurate results as compared to the Final ‘truth’ set. The Mesonet/Radar/Satellite combination showed identification results that occasionally performed better than the Integrated analysis but were generally the second most accurate. The Integrated analysis also proved to be better in the fact that it takes much less time to perform than the Mesonet/Radar/Satellite combination (each of the Mesonet, Radar and Satellite data considered separately).

The Mesonet analysis results showed to be highly dependent on the station locations. If the stations were closer together it was easier to get a lake breeze identification, but if the stations were sparse and far between, then the identification process was more difficult.

The Radar analysis showed good lake breeze front detection as long as the lake breeze fronts occurred in the optimum area (or the clear air range of Exeter radar). This analysis showed poor results for boundaries occurring outside the clear air range. This was shown in the results for the Lake Ontario and Lake St. Clair lake breeze fronts, since these lakes actually lie outside of the radar range.

The contingency table results for the Satellite analysis showed that it performed fairly well in lake breeze front identifications. The imagery allowed for

a widespread and consistent picture of the lake breeze development, covering the whole study area, during the daylight hours. The Satellite analysis sometimes performed better than the Mesonet and Radar analyses, especially in the afternoon hours. However, it did not perform as well as the Integrated analysis or the Mesonet/Radar/Satellite combination. Identifications were easier in the peak heating hours of the day when convection was at a maximum and cumulus clouds were prevalent in order to disclose the location of the lake breeze front. Therefore the 1500 UTC results were not as good as those for 1800 and 2100 UTC.

The Pearson correlation coefficient helped to compare the inland penetration distances of lake breeze fronts for each analysis to that of the Final 'truth' set. The results proved to be very good for all the analyses, except when there were outliers where the inland penetration distances were very different. The Pearson correlation coefficient is not very resistant to outliers.

The Spearman Rank correlation coefficient, which is much more resistant to outliers, was used to compare each analysis to the Final 'truth' set. All analyses were found to have very good correlation to the Final 'truth' set, except for the Mesonet analysis later in the day (2100 UTC). This could be due to complex interactions, later in the day, between lake breeze fronts from different lakes. It was difficult to get an accurate picture of what was occurring in these situations with just mesonet station data. This could also be due to daytime heating from the surface which would heat the lake air as it moved inland,

omitting part of the indicators for lake breeze front identification. A lack of information about the location of the lake breeze front between mesonet stations could also contribute to this result.

These correlation coefficients show that the integrated, satellite and radar analyses consistently pinpoint the lake breeze front locations fairly well. In fact, either the Final ‘truth’ set versus the Radar analysis or the Final ‘truth’ set versus the Integrated analysis showed the best results.

Other interesting results included the lake breeze front frequency in the study area. It was found that 85% of the days showed lake breeze front occurrence, in the study area, originating from one or more of the lakes (for 1800 UTC).

8.2 Cell Initiation in Proximity to Low-Level Boundaries

In order to study where cell initiation occurs in relation to low-level boundaries in the Great Lakes Region, analyses were carried out similar to that of Wilson and Schreiber (1986) in Colorado. These analyses were also performed using the AURORA research tool. 1.0 km CAPPI images, 1.0 km MAXR images, URP cell tracking and cell identification were all considered. When a cell initially reached 40 dBZ the distance from the cell to the closest boundary was measured. Two analyses were done in this manner. The first analysis considered all days during summer 2001, an area within 50 km of Exeter radar and considered the URP cell tracking to be correct. The second analysis considered days without warm front influence, an area within 80 km of Exeter

radar and the cell tracking was considered more closely by the researcher. The second analysis also considered more features about the cells and the boundaries, such as if the cell reached 60 dBZ, the speed of the boundary, direction of the boundary, boundary type and classification, etc.

The first analysis showed that 62.7 percent of the 40 dBZ CAPPI cell initiations occurred at a distance of 20 kilometers or less from a boundary. 57.2 percent of the 40 dBZ MAXR cell initiations occurred at a distance of 20 kilometers or less from a boundary. This analysis clearly showed that many of the cell initiations which showed a distance of 100 kilometers or more from a boundary (or no boundary to measure to), could be eliminated by removing the incidents with warm front influence. This was the reason the second, more detailed analysis was done only on days without warm front influence.

The second analysis, which was the most accurate, showed 70.4 percent of the 40 dBZ CAPPI cell initiations occurring at a distance of 20 kilometers or less from a boundary. 68.5 percent of the 40 dBZ MAXR cell initiations occurred at a distance of 20 kilometers or less from a boundary.

By looking more closely at the data, it also suggested that lake breeze fronts may often trigger the initial convective development on many days. On the days which had cell development, it was shown that more than half of these days showed the first cell initiation (40 dBZ), of the 1600 to 0000 UTC period, to measure closest to a lake breeze front. This was true for both the CAPPI and MAXR data.

The second analysis was also studied for the orientation of the cells in relation to the boundaries. The CAPPI results showed the cell initiations occurred ahead or behind Gust Fronts and Moving Boundaries with a peak just behind the boundaries and a smaller peak 6 to 10 km ahead of the boundary. The MAXR showed similar results, as cell initiations occurred ahead and behind the Gust Fronts and Moving Boundaries, however only one peak in distribution occurred just behind these boundaries suggesting that the MAXR may show a better lead time on identification.

The MAXR results for the lake breeze fronts showed that the cell initiations occurred ahead and behind, but peaked just ahead of these boundaries. These results proved to be very interesting as Wilson and Schreiber (1986) generally found cells to initiate 0 to 20 kilometers behind a moving boundary. This could be due to the choice of a different dBZ level for analysis, or just the different specific boundary type. The Great Lakes region proves to be a very interesting and unique study region because one of the main types of boundaries occurring in this area is the lake breeze front. This shows that this boundary type helps to trigger storms, but perhaps in somewhat different proximity than the boundaries, such as mountain outflows, in the Colorado region.

As Wilson and Schreiber (1986) found for the Colorado area, these results show that the storms occur less ‘randomly’ in the Great Lakes region than previously thought. Further study may allow for better storm watches and warnings in terms of lead time and geographical precision.

8.3 Case Studies using Current Nowcasting Techniques

Case studies were broken down using recent nowcasting techniques in order to understand why and where storm development will occur in proximity to low-level mesoscale boundaries in the Great Lakes Region. These case studies were considered in terms of cumulus in the lifting zone of the boundary, Lifted Index in the lifting zone, convergence strength along the boundary, the updraft orientation along the boundary and the boundary relative cell speed (comparing the motion of the boundary to the motion of the cells triggered). All of these factors were studied in previous papers covered in Chapter 1.

By taking a look at each of these nowcasting techniques in detail for the case studies, it was found that a reason for the development, or the lack there of, could be found in these cases.

The July 22 and July 23 case was revealed to have a lack of development on July 22 and strong development on July 23, most likely due to the updraft orientation created. The winds suggest that the updrafts, on July 23, may be much more erect and therefore conducive to development. These varying conditions could also be seen in the vertical development in the cumulus cloud field for each day.

The July 20 case showed strong development along the Huron and St. Clair lake breeze fronts, but a lack of development along the Ontario lake breeze front and Merged (Ontario/Erie) boundary. The first tell-tale sign for explanation

was the lack of cumulus cloud development around the south-western shore of Lake Ontario which suggested that the conditions were not conducive to development. The Ontario lake breeze front showed weak convergence at the north shore and the Huron lake breeze front showed strong convergence. Thirdly, the winds suggested the updraft orientation may have been more erect along the Huron lake breeze front than along the Ontario lake breeze front. Overall, conditions were much more favourable for storm development along the Huron lake breeze front.

8.4 Conclusion

Overall, it was found that the best way to identify lake breeze fronts is to look at an integrated set of data (including satellite, radar and mesonet). The more data used to suggest boundary location, the better. Since this is also less time consuming than looking at each data set separately, this would be more likely to be put to use in operational forecasting.

As shown in this study, a large percentage of cells form in close proximity to mesoscale boundaries in the Great Lakes region, showing that these boundaries have a strong hand in triggering development. Lake breeze fronts appear to often trigger development just ahead of their location.

By studying cases that exhibited storm development in close proximity to low-level mesoscale boundaries, the reason for development, or the lack thereof, could be found using recent nowcasting techniques. Further study of these techniques, as well as developing/researching a number of other techniques,

could prove to be useful for nowcasts in the Great Lakes region. Future work could include developing a number of set procedures/steps for forecasters to follow in order to anticipate locations for development. Recently, the Research Support Desk (RSD), at Environment Canada, has been operationally providing nowcasts of storm development associated with mesoscale boundaries, through visual assessment of a number of data/imagery fields (Sills and Taylor, 2008).

It may also be possible to create programs to automate nowcasting techniques for the Great Lakes region, or use pre-existing software such as the NCAR Auto-nowcaster (previously used in Colorado) to make operational use even more efficient.

Convective storms tend to trigger in proximity to mesoscale boundaries in Southwestern Ontario. Establishing the best method for identifying these mesoscale boundaries and showing how current nowcasting techniques can be used to determine where conditions are conducive to development, should greatly benefit operational forecasting in the Great Lakes region.

Appendix A

This Appendix includes a list, from the ELBOW 2001 Final Data Report (Alexander et al., 2003), of the data taken during the study period. This includes the times in which mobile surveys, radiosondes and Twin Otter and Cessna flights were started. It also includes the types of scans done with the X-band radar each day, mesonet tower installation dates and dismantling dates, and damage survey locations and dates.

DAY	MAY 24	MAY 29	MAY 31	JUNE 4	JUNE 5	JUNE 7	JUNE 8	JUNE 11	JUNE 12
MOBILE SURVEYS									
Pt. Franks					1 survey: 1830 UTC	1 survey: 1756 UTC	1 survey: 1917 UTC	1 survey: 1600 UTC	2 surveys: 1525 UTC 1815 UTC
Pt. Stanley						1 survey: 1735 UTC	1 survey: 1740 UTC		1 survey: 1800 UTC
Mobile		2 surveys: 1800 UTC (Bayfield) St. Joseph							1 survey: 2030 UTC
Kippen									
RADIOSONDES									
Pt. Franks							1 sounding: 1516 UTC	1 sounding: 1758 UTC	2 soundings: 1759 UTC 2103 UTC
Pt. Stanley							1 sounding: 1737 UTC		3 soundings: 1551 UTC 1757 UTC 2100 UTC
Mobile	1 sounding: 1835 UTC		1 sounding: 2053 UTC						
UWO Farm					1 sounding: 1841 UTC		2 soundings: 1501 UTC 2025 UTC	1 sounding: 1800 UTC	3 soundings 1458 UTC 1759 UTC 2059 UTC
RADAR (X-BAND)	No	No	No	No	No	No	No	No	No
AIRCRAFT									
Twin Otter	No	No	No	No	No	No	No	No	No
Cessna	No	No	No	No	No	No	No	No	No
MESONET				Tower #4 installed	Towers #1, #2, and #3 installed	Towers #5, #6 and #7 installed			Towers #9, #11, #12 and #13 installed
DAMAGE ASSESSMENT	None	None	None	None	None	None	None	None	None

DAY	JUNE 13	JUNE 14	JUNE 15	JUNE 18	JUNE 19	JUNE 20	JUNE 21	JUNE 26
MOBILE SURVEYS								
Pt. Franks	2 surveys: 1517 UTC 1815 UTC		1 survey: 1516 UTC	1 survey: 1910 UTC	3 surveys: 1543 UTC 1956 UTC 2214 UTC	Rain gauge check: 1600 UTC		2 surveys: 1420 UTC 1928 UTC
Pt. Stanley	2 surveys: 1600 UTC 2140 UTC		2 surveys: 1457 UTC 1757 UTC	3 surveys: 1455 UTC 1757 UTC 2309 UTC	3 surveys : 1500 UTC 1800 UTC 2230 UTC			
Mobile			1 survey: 1520 UTC		1 survey : 1630 UTC			
Kippen		2 surveys: 1915 UTC 2045 UTC						2 surveys: 1400 UTC 1801 UTC
RADIOSONDES								
Pt. Franks	3 soundings: 1500 UTC 1758 UTC 2100 UTC	3 soundings: 1500 UTC 1800 UTC 2100 UTC	3 soundings: 1500 UTC 1800 UTC 2101 UTC	3 soundings: 1502 UTC 1810 UTC 2100 UTC	4 soundings: 1500 UTC 1801 UTC 1924 UTC 2101 UTC			1 sounding: 1803 UTC
Pt. Stanley	3 soundings: 1513 UTC 1801 UTC 2101 UTC	2 soundings: 1500 UTC 1800 UTC	3 soundings: 1501 UTC 1759 UTC 2100 UTC	3 soundings: 1500 UTC 1800 UTC 2100 UTC	3 soundings: 1500 UTC 1800 UTC 2100 UTC			
Mobile		1 sounding: 1953 UTC			2 soundings: 2121 UTC 2227 UTC			
UWO farm	3 soundings: 1459 UTC 1759 UTC 2059 UTC	2 soundings: 1500 UTC 1800 UTC	4 soundings: 1500 UTC 1759 UTC 2101 UTC 2113 UTC	3 soundings: 1500 UTC 1800 UTC 2100 UTC	4 soundings: 1501 UTC 1550 UTC 1905 UTC 2201 UTC		1 sounding: 1757 UTC	
RADAR (X-BAND)	No	No	Yes - Long distance Unfiltered scans - Doppler Scans	No	Yes - Long distance Unfiltered scans	No	No	No
AIRCRAFT								
Twin Otter	No	No	No	No	2 flights: 1358 UTC 1748 UTC	No	No	No
Cessna	No	No	3 flights: 1638 UTC (transit) 1811 UTC 1934 UTC (transit)	No	No	No	No	No
MESONET					Towers #10, #14 and #15 installed			
DAMAGE ASSESSME	None	None	None	None	None	None	None	None

DAY	JUNE 27	JUNE 28	JUNE 29	JUNE 30	JULY 3	JULY 4	JULY 7	JULY 9	JULY 10
MOBILE SURVEYS									
Pt. Franks	2 surveys: 1600 UTC 1851 UTC	1 survey: 1538 UTC			1 survey: 1922 UTC	3 surveys: 1530 UTC 1820 UTC 2119 UTC		2 surveys: 1554 UTC 1840 UTC	3 surveys: 1535 UTC 1900 UTC 2125 UTC
Pt. Stanley	3 surveys: 1507 UTC 1805 UTC 2205 UTC	2 surveys: 1910 UTC 2245 UTC				3 surveys : 1530 UTC 1830 UTC 2235 UTC (rain)		2 surveys: 1538 UTC 1854 UTC	3 surveys: 1545 UTC 1900 UTC 2251 UTC
Mobile	5 surveys: 1606 UTC 2105 UTC (Melb.) 1615 UTC (Kiness) 1904 UTC (Kiness)	2 surveys: 1800 UTC 1854 UTC (Walnut)			1 survey: 2202 UTC	1 survey : 1735 UTC		1 survey: 1705 UTC	2 surveys: 1842 UTC 0000 UTC (Ridgetown)
Kippen									
RADIOSONDES									
Pt. Franks	3 soundings: 1459 UTC 1759 UTC 2100 UTC	1 sounding: 2110 UTC	1 sounding: 1759 UTC		1 sounding: 2058 UTC	3 soundings: 1459 UTC 1802 UTC 2058 UTC		3 soundings: 1459 UTC 1802 UTC 2102 UTC	3 soundings: 1523 UTC 1847 UTC 2059 UTC
Pt. Stanley	3 soundings: 1501 UTC 1759 UTC 2101 UTC	1 sounding: 2100 UTC			1 sounding: 2101 UTC	3 soundings: 1501 UTC 1800 UTC 2104 UTC		3 soundings: 1501 UTC 1803 UTC 2107 UTC	3 soundings: 1500 UTC 1813 UTC 2104 UTC
Mobile	1 sounding: 1546 UTC								
UWO farm	3 soundings: 1459 UTC 1801 UTC 2101 UTC	2 soundings: 1759 UTC 2057 UTC		1 sounding: 1803 UTC	2 soundings: 1823 UTC 2101 UTC	3 soundings: 1520 UTC 1800 UTC 2101 UTC	1 sounding: 1800 UTC	3 soundings: 1502 UTC 1800 UTC 2102 UTC	1 sounding: 1500 UTC
RADAR (X-BAND)	No	No	No	Yes - Long distance unfiltered scans	No	Yes - Doppler scans - Extended donut scans - RHI's	No	No	No
AIRCRAFT									
Twin Otter	No	No	No	No	No	No	No	No	No
Cessna	2 flights: 1423 UTC 1840 UTC	No	No	No	No	No	No	No	2 flights: 1501 UTC 1751 UTC
MESONET									
DAMAGE ASSESSMENT	None	None	None	None	None	Yes – Campbellville Tornado (F0)	None	None	None

DAY	JULY 11	JULY 16	JULY 17	JULY 18	JULY 19	JULY 20	JULY 21	JULY 22
MOBILE SURVEYS								
Pt. Franks	1 survey: 1545 UTC	3 surveys: 1600 UTC 1844 UTC 2117 UTC	3 surveys: 1530 UTC 1858 UTC 2125 UTC	3 surveys: 1530 UTC 1855 UTC 2114 UTC		1 survey: 2250 UTC (rain gauge check)	2 surveys: 1530 UTC 1940 UTC	3 surveys: 1545 UTC 1818 UTC 2115 UTC
Pt. Stanley		2 surveys: 1520 UTC 1815 UTC	3 surveys: 1511 UTC 1807 UTC 2245 UTC	3 surveys: 1504 UTC 1804 UTC 2236 UTC	1 survey: 1400 UTC		1 survey: 2155 UTC	3 surveys: 1530 UTC 1810 UTC 2221 UTC
Mobile		1 survey: 1859 UTC	1 survey: 1524 UTC	1 survey: 1945 UTC	1 survey: 1635 UTC	1 survey: 1949 UTC	1 survey: 1934 UTC	1 survey: 1718 UTC
Kippen				1 survey: 1447 UTC			1 survey: 1800 UTC	
RADIOSONDES								
Pt. Franks		3 soundings: 1509 UTC 1809 UTC 2101 UTC	3 soundings: 1500 UTC 1831 UTC 2100 UTC	3 soundings: 1513 UTC 1803 UTC 2059 UTC	1 sounding: 1752 UTC	2 soundings: 1803 UTC 1847 UTC	2 soundings: 1903 UTC 2259 UTC	3 soundings: 1502 UTC 1801 UTC 2056 UTC
Pt. Stanley		3 soundings: 1501 UTC 1800 UTC 2101 UTC	3 soundings: 1501 UTC 1800 UTC 2100 UTC	3 soundings: 1500 UTC 1800 UTC 2100 UTC				3 soundings: 1502 UTC 1801 UTC 2101 UTC
Mobile			1 sounding: 2220 UTC					1 sounding: 2143 UTC
UWO farm		3 soundings: 1504 UTC 1801 UTC 2100 UTC	3 soundings: 1505 UTC 1800 UTC 2104 UTC	3 soundings: 1504 UTC 1800 UTC 2100 UTC				
RADAR (X-BAND)	No	No	No	Yes - Extended range Doppler scans - RHI's	Yes - Extended and short range Doppler scans - RHI's	Yes - Extended and short range Doppler scans - RHI's	Yes - Extended and short range scans - Ultra close range FFT scans - RHI's	No
AIRCRAFT								
Twin Otter	No	No	2 flights: 1403 UTC 1856 UTC	2 flights: 1500 UTC 1945 UTC	No	No	No	1 flight: 1652 UTC
Cessna	No	No	No	No	No	No	No	No
MESONET								
DAMAGE ASSESSMENT	None	None	None	None	None	None	None	None

DAY	JULY 23	JULY 24	JULY 25	JULY 26	AUGUST 2	AUGUST 3	SEPTEMBER 4	SEPTEMBER 5
MOBILE SURVEYS								
Pt. Franks	2 surveys: 1525 UTC 2045 UTC	2 surveys : 1525 UTC 1820 UTC		1 survey : 1510 UTC (rain gauge check)				
Pt. Stanley	3 surveys: 1504 UTC 1800 UTC 2210 UTC	3 surveys : 1505 UTC 1800 UTC 2200 UTC						
Mobile	1 survey : 1600 UTC		1 survey : 2132 UTC (rain gauge check)		1 survey : 1730 UTC			
Kippen								
RADIOSONDES								
Pt. Franks	2 soundings: 1501 UTC 2123 UTC	3 soundings: 1501 UTC 1804 UTC 2100 UTC						
Pt. Stanley	3 soundings: 1501 UTC 1800 UTC 2056 UTC	3 soundings: 1503 UTC 1802 UTC 2100 UTC			1 sounding: 1846 UTC	1 sounding: 1630 UTC		
Mobile		2 soundings: 1802 UTC 2058 UTC						
UWO farm	3 soundings: 1504 UTC 1801 UTC 2137 UTC	2 soundings: 1506 UTC 1802 UTC						
RADAR (X-BAND)	Yes - Extended and short range scans - Ultra close range FFT scans - Hyper scans - RHI's	No	No	No	No	No	No	No
AIRCRAFT								
Twin Otter	1 flight: 1526 UTC	2 flights: 1401 UTC 1830 UTC	No	No	No	No	No	No
Cessna	No	No	No	No	No	No	No	No
MESONET							Towers #1, #2, #9, #10, #11, #12, and #13 dismantled	Towers #3, #4, #5, #6, #7, #14, and #15 dismantled
DAMAGE ASSESSMENT	None	None	None	None	None	None	None	None

Appendix B

Following is the Fortran program used to quality check the CLASS radiosonde data taken at the UWO Farm. This program also formatted the data to be readable by the RAOB program.

```
      program MRS
      integer*4 i,ct,cnt,count,c,N
      real*8 t,p,temp,dpt,RH,uw,vw,ws,dir,dz,long,lat,Rng,Az,Alt
      real*8 Qp,Qt,Qh,Qu,Qv,Quv,A,salt,sws,s,press,lati,longi
      real*8 wcompu,wcompv,wdu,wdv,stemp,slat,slong,la,lo
      real*8 sdpt,cpr,sett,sd,tt,ta(1000),pa(1000),tempa(1000)
      real*8 dpta(1000),Heighta(1000),dira(1000)
      real*8 wspda(1000),t2a(1000),ar,te,Alta(1000),wsa(1000),ttt
      real*8 vct,uct,wt,ltime,lotime
c     sdata.dat is the input data, raob.txt is the outputted data
c     that has been quality checked and in RAOB format, and efile.txt
c     is the outputted data file which includes all the data levels
c     removed from the data due to quality checks
      open(unit=10,file='sdata.dat')
      open(unit=11,file='raob.txt')
      open(unit=12,file='efile.txt')
      i=1
      cnt=1
      ct=1
      c=1
      count=0
      write(12,*) "These are the p(mb)/temp(C)/dpt(C) levels"
c     the program reads the input data
  100 read(10,*) t,p,temp,dpt,RH,uw,vw,ws,dir,dz,long,lat,Rng,
     & Az,Alt,Qp,Qt,Qh,Qu,Qv,Quv
      count=count+1
       if (Alt.GT.0) then
         if (i.EQ.1) then
           stemp=temp
           press=p
           sett=t
           sdpt=dpt
c     the data immediately puts the surface level into the
c     matrix - surface data must be kept for RAOB
           ta(c)=t
           pa(c)=p
           tempa(c)=temp
           dpta(c)=dpt
           c=c+1
           i=0
c     here the program checks the data for reasonable pressure
c     temperature, and dewpoint data
         elseif (p.LT.1.0) then
         write(12,1003) p,temp,dpt
           write(12,*) "         pressure < 1mb"
           goto 133
         elseif (p.GT.1100.0) then
         write(12,1003) p,temp,dpt
```

```
            write(12,*) "         pressure > 1100mb"
            goto 100
          elseif (temp.GT.40.0) then
          write(12,1003) p,temp,dpt
            write(12,*) "         temperature is > 40 C"
            goto 100
          elseif (temp.LT.-80.0) then
          write(12,1003) p,temp,dpt
            write(12,*) "         temperature is < -80 C"
            goto 100
          elseif (dpt.GT.40.0) then
          write(12,1003) p,temp,dpt
            write(12,*) "         dew point is > 40 C"
            goto 100
          elseif (dpt.LT.-110.0) then
          write(12,1003) p,temp,dpt
            write(12,*) "         dew point is < -110 C"
            goto 100
          else
            cpr=press-p
            sd=sdpt-dpt
            tt=stemp-temp
            te=sett-t
            ar=cpr/te
c      the program checks the data for temperature/dewpoint
c      spikes that are unusual - takes the data out if these
c      spikes are greater than 3 C and temp/dpt spikes at the
c      same amount
            if (((tt.GE.3.0).OR.(tt.LE.-3.0)).AND.(sd.EQ.tt)
     & .AND.(cpr.LE.10.0)) then
                  write(12,1003) p,temp,dpt
                  write(12,*) "    large temp and dpt spike"
                  goto 100
c      the 999 level checks if the change in temp is greater
c      than 10 C in 30 mb then the level is removed
  999       elseif ((abs(tt).GT.10.0).AND.(cpr.LT.30.0)) then
             write(12,1003) p,temp,dpt
                  write(12,*) "        large jump in temperature"
                  goto 100
c      the 997 level checks the ascent rate (pressure/temp) from
c      one point to the next is not greater than 10mb/s
  997       elseif (abs(ar).GT.10.0) then
                  write(12,1003) p,temp,dpt
                  write(12,*) "        large ascent rate"
                  goto 100
c      this section checks vertical consistency
            elseif (press.LT.p) then
c      if the vert. incon. is near the surface then one level is
c      removed
              if (c.EQ.2) then
                  write(12,1003) p,temp,dpt
                  write(12,*) "        vert incon. near surface"
                  goto 100
c      if the vert. incon. is above the surface, then two levels
```

```
c      are removed
             else
                write(12,1003) pa(c-1),tempa(c-1),dpta(c-1)
                write(12,1003) p,temp,dpt
                write(12,*) "        vert. incon. - 2 levels rem"
                press=pa(c-2)
                cnt=cnt-1
                c=c-1
                goto 100
             endif
c      if pressures are equal remove one
           elseif (press.EQ.p) then
                write(12,1003) p,temp,dpt
                write(12,*) "        pressure is same as previous"
                goto 100
c     if all data has passed the previous checks, it is kept and
c     put into the matrix
           else
  222        ta(c)=t
             pa(c)=p
             tempa(c)=temp
             dpta(c)=dpt
             c=c+1
             stemp=temp
             press=p
             sett=t
             cnt=cnt+1
           endif
         endif
        goto 100
       else
  133    rewind(10)
       endif
      i=1
      N=1
      write(12,*) "These are the Alt(m)/dir(deg)/ws(m/s) levels"
c     the input file was rewound and is now read again for
c     Height, wind direction and wind speed levels
  112 read(10,*) t,p,temp,dpt,RH,uw,vw,ws,dir,dz,long,lat,Rng,
     & Az,Alt,Qp,Qt,Qh,Qu,Qv,Quv
       if (Alt.GT.0) then
c     again the first wind level is kept - surface data is
c     needed in RAOB
          if (i.EQ.1) then
            i=0
            salt=Alt
            A=Alt
            sws=ws
            sett=t
            wcompu=uw
            wcompv=vw
            slat=lat
            slong=long
            stemp=temp
```

```
            sdpt=dpt
            lati=lat
            longi=abs(long)
            t2a(N)=t
            Alta(N)=Alt
            Heighta(N)=Alt-A
            dira(N)=dir
            wsa(N)=ws
            wspda(N)=ws*1.94400
            N=N+1
c         this section check that pressure is not less than 1 mb,
c         there are realistic altitude values, wind directions,
c         and wind speeds
          elseif (p.LT.1.0) then
          write(12,1003) Alt,dir,ws
            write(12,*) "         pressure is < 1 mb"
            goto 113
          elseif (Alt.GT.31000.0) then
            write(12,1003) Alt,dir,ws
            write(12,*) "         altitude is > 31000 m"
            goto 112
          elseif (dir.GT.360.0) then
            write(12,1003) Alt,dir,ws
            write(12,*) "         wind direction is > 360 deg"
            goto 112
          elseif (dir.LT.0.0) then
            write(12,1003) Alt,dir,ws
            write(12,*) "         wind direction is < 0 deg"
            goto 112
          elseif (ws.GT.80.0) then
          write(12,1003) Alt,dir,ws
            write(12,*) "         wind speed is > 80 m/s"
            goto 112
          elseif (abs(uw).GT.ws) then
            write(12,1003) Alt,dir,ws
            write(12,*) "         u component is > wind speed"
            goto 112
          elseif (abs(vw).GT.ws) then
          write(12,1003) Alt,dir,ws
            write(12,*) "         v component is > wind speed"
            goto 112
          else
            la=slat-lat
            lo=slong-long
            s=sws-ws
            wdu=wcompu-uw
            wdv=wcompv-vw
            cpr=salt-Alt
            ttt=sett-t
            ar=cpr/ttt
            vct=wdv/ttt
            uct=wdu/ttt
            wt=s/ttt
            ltime=la/ttt
```

```
          lotime=lo/ttt
c        here abs. change in v component divided by change in time
c        must be less than 4 (from one level to the next)
             if (abs(vct).GT.4.0) then
              write(12,1003) Alt,dir,ws
              write(12,*) "         abs dv/dt > 4.0"
              goto 112
c        abs. change in u component divided by change in time must
c        be less than 4
             elseif (abs(uct).GT.4.0) then
              write(12,1003) Alt,dir,ws
              write(12,*) "         abs du/dt > 4.0"
              goto 112
c        abs. change in windspeed divided by change in time must
c        be less than 4
             elseif (abs(wt).GT.4.0) then
              write(12,1003) Alt,dir,ws
              write(12,*) "         abs dw/dt > 4.0"
              goto 112
c        abs. change in latitude divided by change in time must
c        be less than 0.0005
             elseif (abs(ltime).GT.0.0005) then
              write(12,1003) Alt,dir,ws
              write(12,*) "         abs dla/dt > 0.0005"
              goto 112
c        abs. change in longitude divided by change in time must
c        be less than 0.001
             elseif (abs(lotime).GT.0.001) then
              write(12,1003) Alt,dir,ws
              write(12,*) "         abs dlo/dt > 0.001"
              goto 112
c        abs. ascent rate (height/time) must be less than 50 m/s
             elseif (abs(ar).GT.50.0) then
              write(12,1003) Alt,dir,ws
            write(12,*) "         ascent rate is > 50 m/s"
              goto 112
c        this section checks vertical consistency
             elseif (salt.GT.Alt) then
c        if vert. incon. is next to the surface, one level is
c        removed
              if(N.EQ.2) then
                write(12,1003) Alt,dir,ws
                write(12,*) "         vert. incon. near surface"
                goto 112
c        if vert. incon. is above surface, two levels are
c        removed
              else
                write(12,1003) Alta(N-1),dira(N-1),wsa(N-1)
                write(12,1003) Alt,dir,ws
                write(12,*) "         vert. incon. - 2 levels removed"
                salt=Alta(N-2)
                N=N-1
                ct=ct-1
                goto 112
```

```
               endif
c         if alt levels are equal, remove one
               elseif (salt.EQ.Alt) then
                  write(12,1003) Alt,dir,ws
                  write(12,*) "         altitude is same as previous"
                  goto 112
c         if all the quality checks have been passed, the level
c         is added to the matrix
               else
                ct=ct+1
                sws=ws
                salt=Alt
                sett=t
                slat=lat
                slong=long
                wcompu=uw
                wcompv=vw
                stemp=temp
                sdpt=dpt
                t2a(N)=t
                Alta(N)=Alt
                Heighta(N)=Alt-A
                dira(N)=dir
                wsa(N)=ws
                wspda(N)=ws*1.94400
                N=N+1
               endif
          endif
          goto 112
         else
  113     rewind(10)
         endif
         i=1
c        this part writes the raw data format for RAOB
         write(12,*) "The number of good p/t/dp levels is ",cnt
         write(12,*) "The number of good h/ws/wd levels is ",ct
         write(12,*) "The number of levels read is ",count
         write(11,1000)  cnt,ct
         write(11,1001)  lati,longi,A
         write(11,1004)
c        the pressure, temp, and dpt levels that had been written
c        to the matrix are put into raob.txt
  599    if (i.EQ.c) then
               goto 101
         else
               write(11,1002)  pa(i),tempa(i),dpta(i)
               i=i+1
               goto 599
         endif
  101    i=1
c        the height, wind dir, wind speed levels that had been
c        written to the matrix are put into raob.txt
  598    if (i.EQ.N) then
               goto 497
```

```
      else
            write(11,1003) Heighta(i),dira(i),wspda(i)
            i=i+1
            goto 598
      endif
 497  write(*,*) cnt,ct
      write(*,*) c,N
    close(10)
    close(11)
    close(12)
    stop
1000 format (1x,10H"RAOB 5.1",14H,"SOUNDING",1,,I3,",",I3)
1001 format (1x,F6.2,",",3H"N",",",F6.2,",",3H"W",",",F6.2)
1002 format (1x,F5.1,",",F5.1,",",F5.1)
1003 format (1x,F7.1,",",F5.1,",",F5.1)
1004 format (1x,19H"AUTO",0,"NO",0,0,,)
    end
```

Appendix C

1800 UTC Correlation Charts

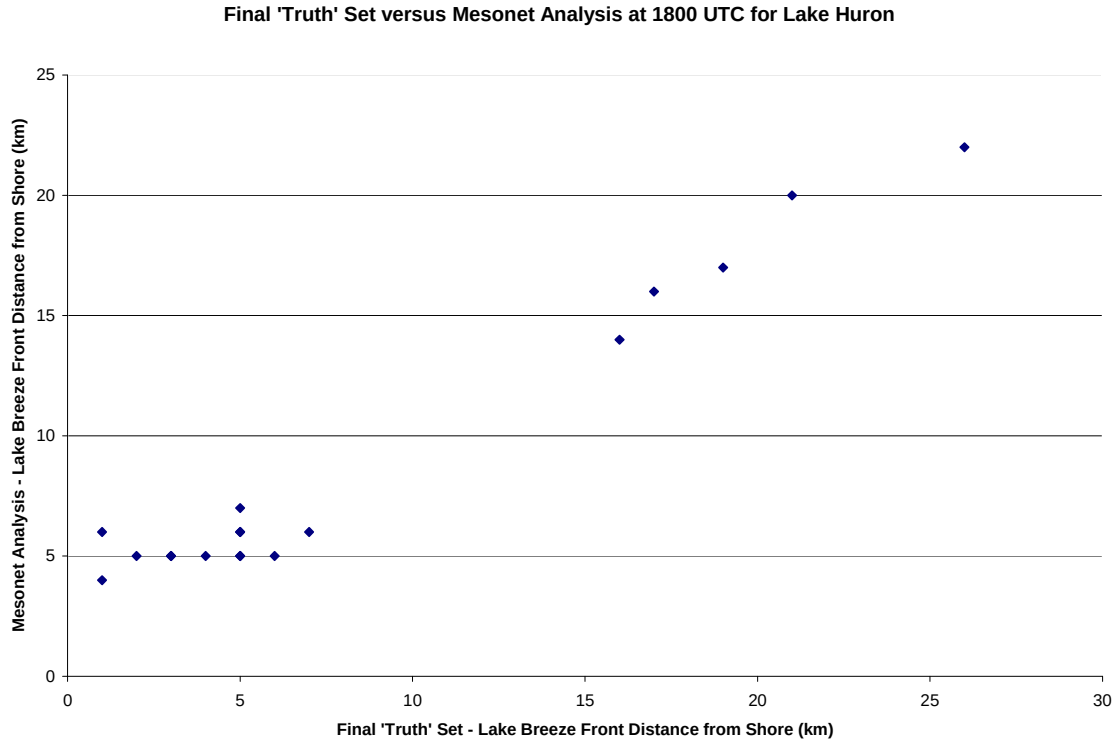

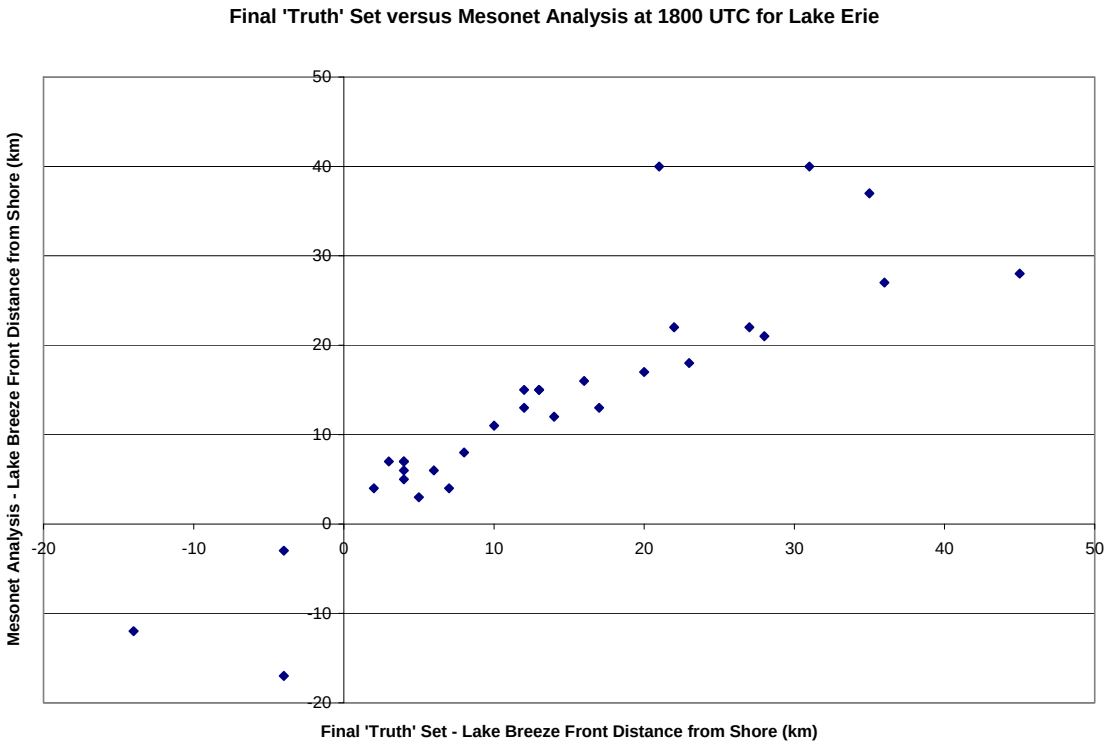
Final 'Truth' Set versus Mesonet Analysis at 1800 UTC for Lake Erie
Mesonet Analysis - Lake Breeze Front Distance from Shore (km)
50
40
30
20
10
0
-10
-20
-20
-10
0
10
20
30
40
50
Final 'Truth' Set - Lake Breeze Front Distance from Shore (km)

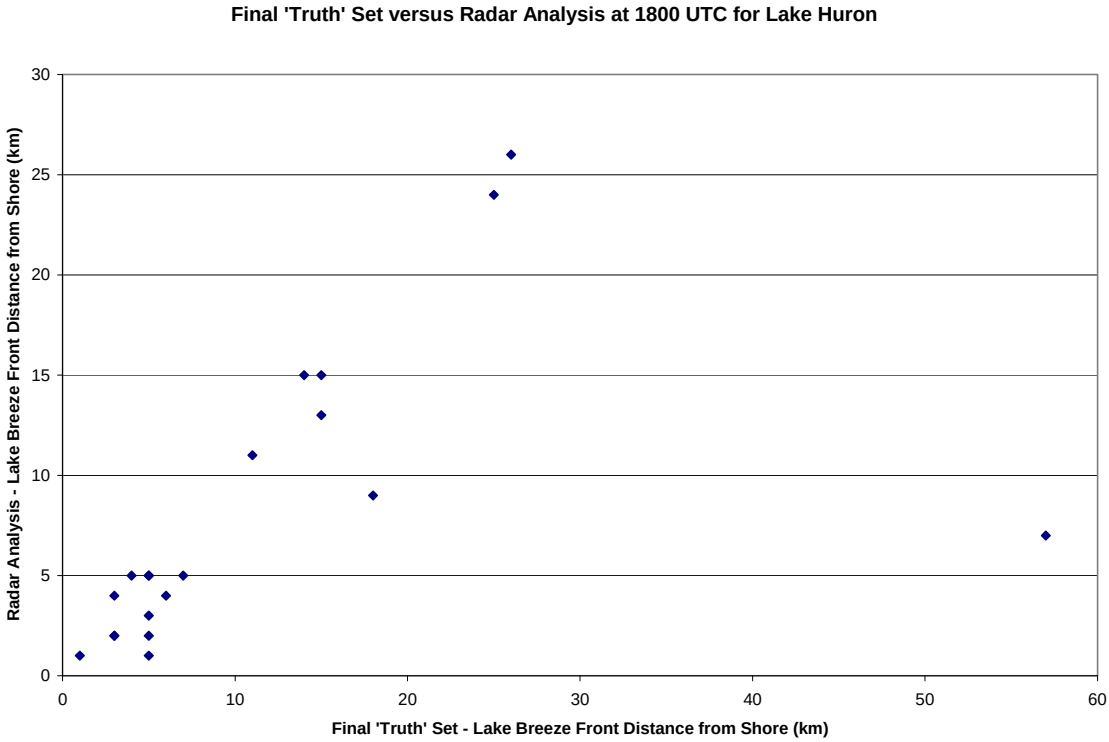
Final 'Truth' Set versus Radar Analysis at 1800 UTC for Lake Huron
Radar Analysis - Lake Breeze Front Distance from Shore (km)
30
25
20
15
10
5
0
0
10
20
30
40
50
60
Final 'Truth' Set - Lake Breeze Front Distance from Shore (km)

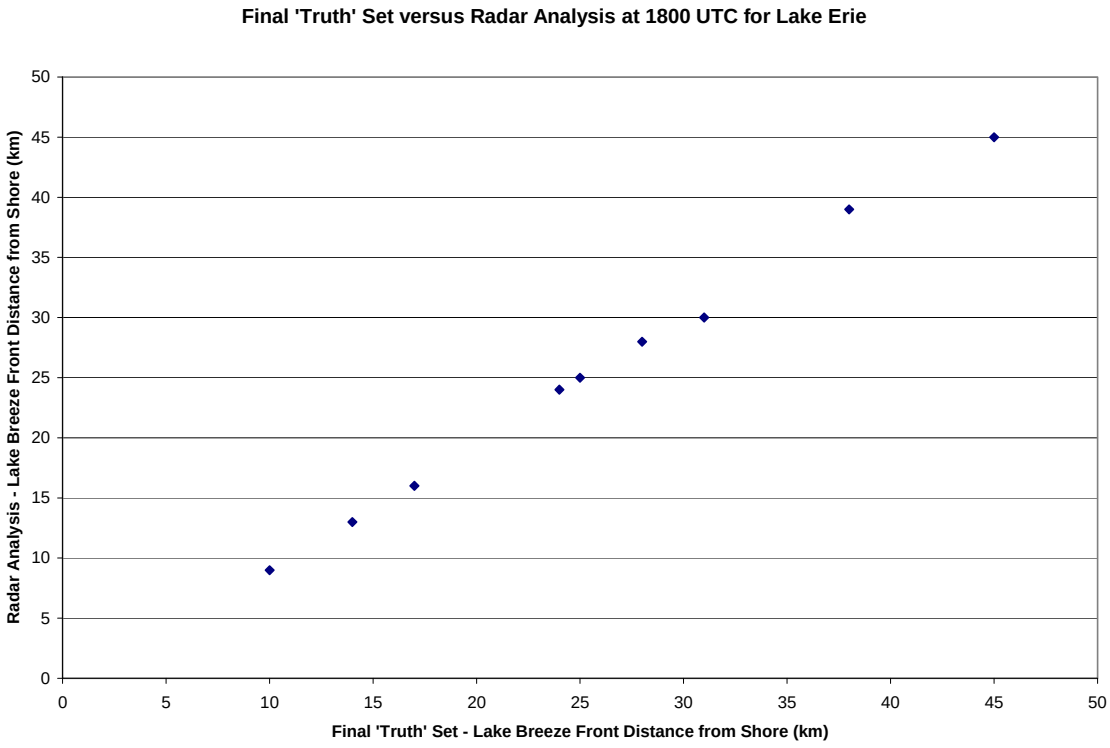
Final 'Truth' Set versus Radar Analysis at 1800 UTC for Lake Erie
Radar Analysis - Lake Breeze Front Distance from Shore (km)
Final 'Truth' Set - Lake Breeze Front Distance from Shore (km)
0
5
10
15
20
25
30
35
40
45
50

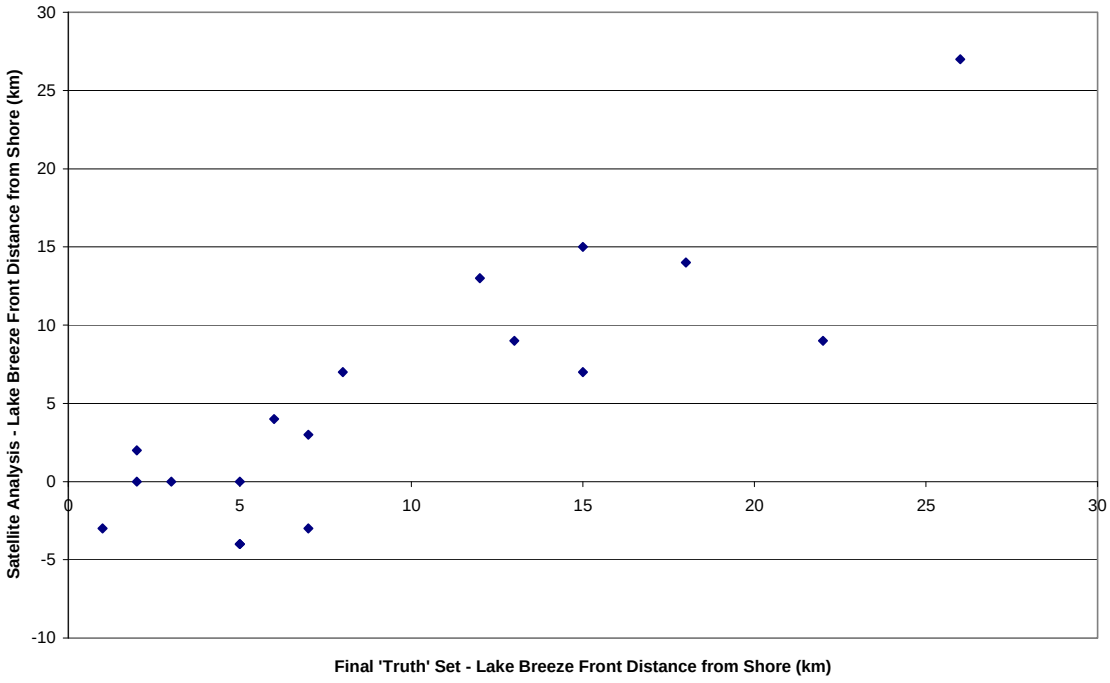
Final 'Truth' Set versus Satellite Analysis at 1800 UTC for Lake Huron
Satellite Analysis - Lake Breeze Front Distance from Shore (km)
Final 'Truth' Set - Lake Breeze Front Distance from Shore (km)
-10
-5
0
5
10
15
20
25
30

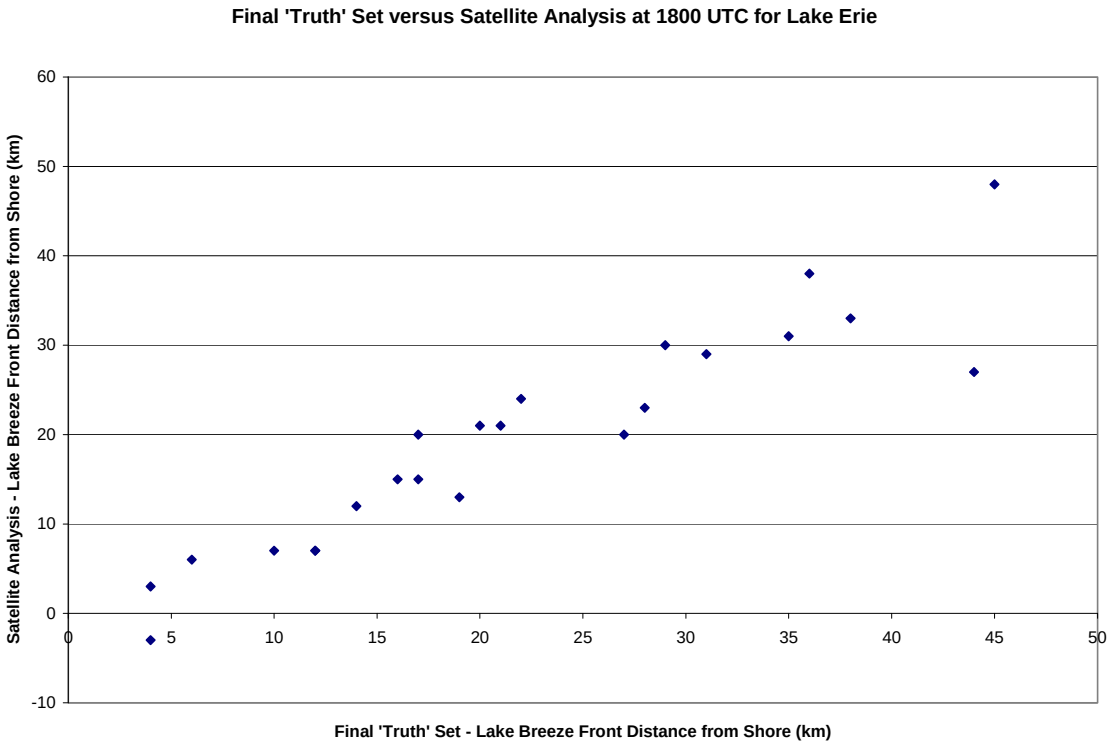
Final 'Truth' Set versus Satellite Analysis at 1800 UTC for Lake Erie
Satellite Analysis - Lake Breeze Front Distance from Shore (km)
60
50
40
30
20
10
0
-10
0
5
10
15
20
25
30
35
40
45
50
Final 'Truth' Set - Lake Breeze Front Distance from Shore (km)

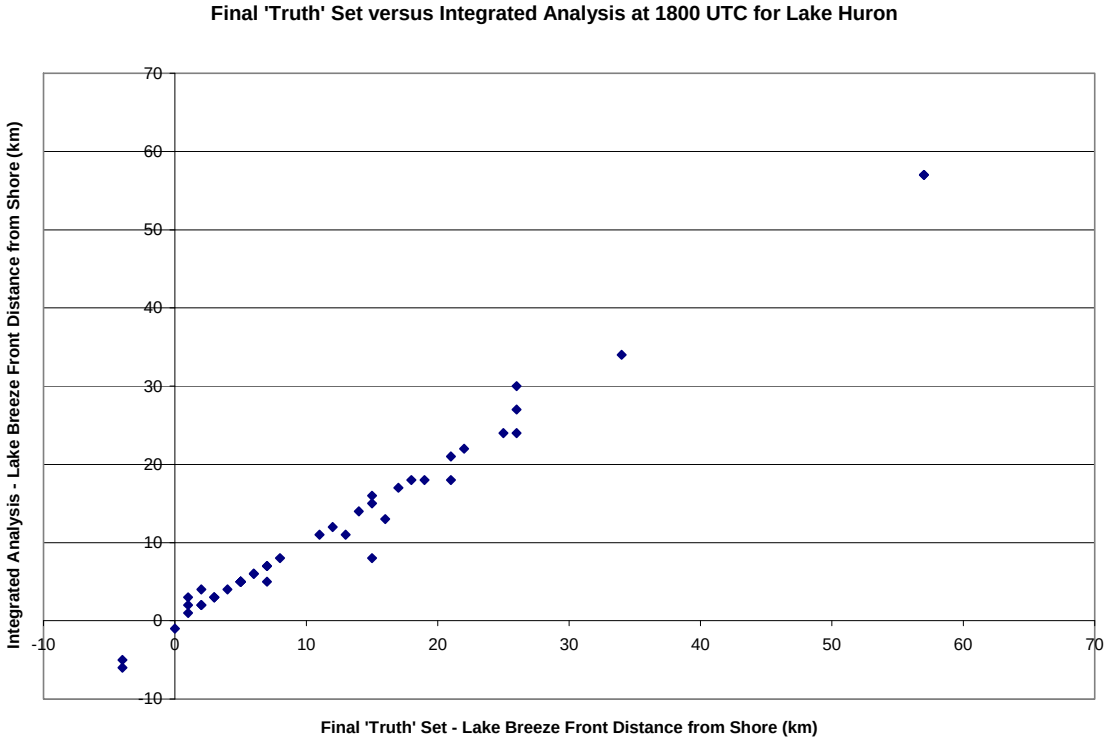
Final 'Truth' Set versus Integrated Analysis at 1800 UTC for Lake Huron
Integrated Analysis - Lake Breeze Front Distance from Shore (km)
70
60
50
40
30
20
10
0
-10
-10
0
10
20
30
40
50
60
70
Final 'Truth' Set - Lake Breeze Front Distance from Shore (km)

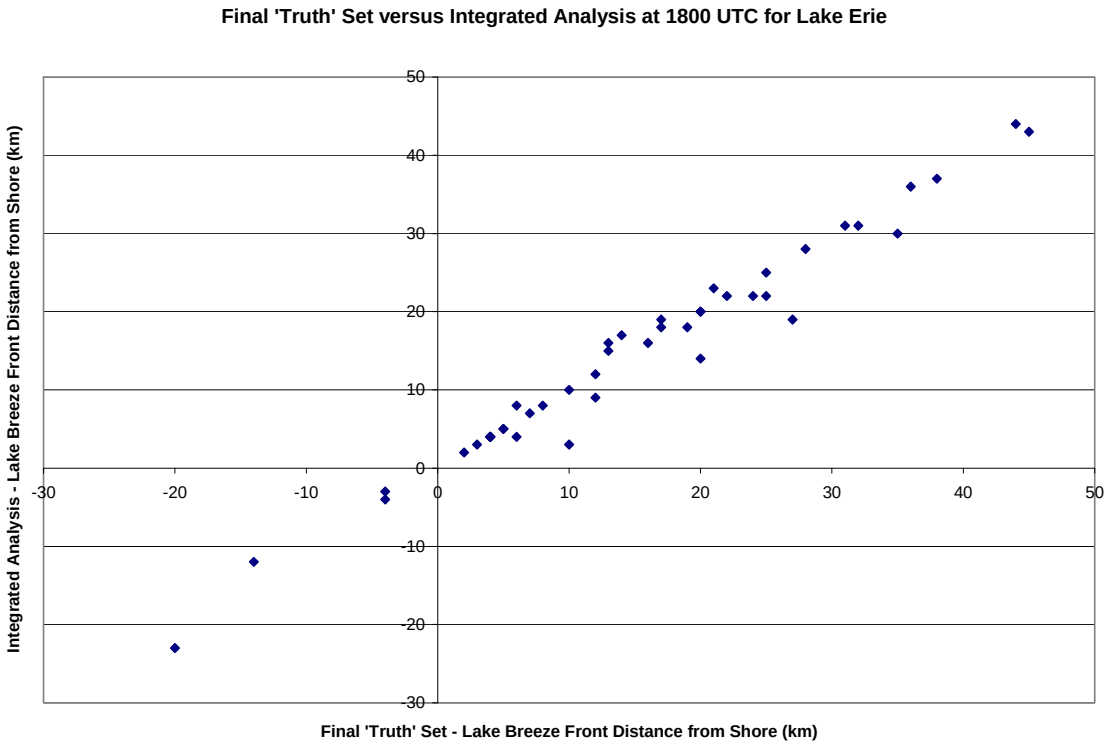

2100 UTC Correlation Charts

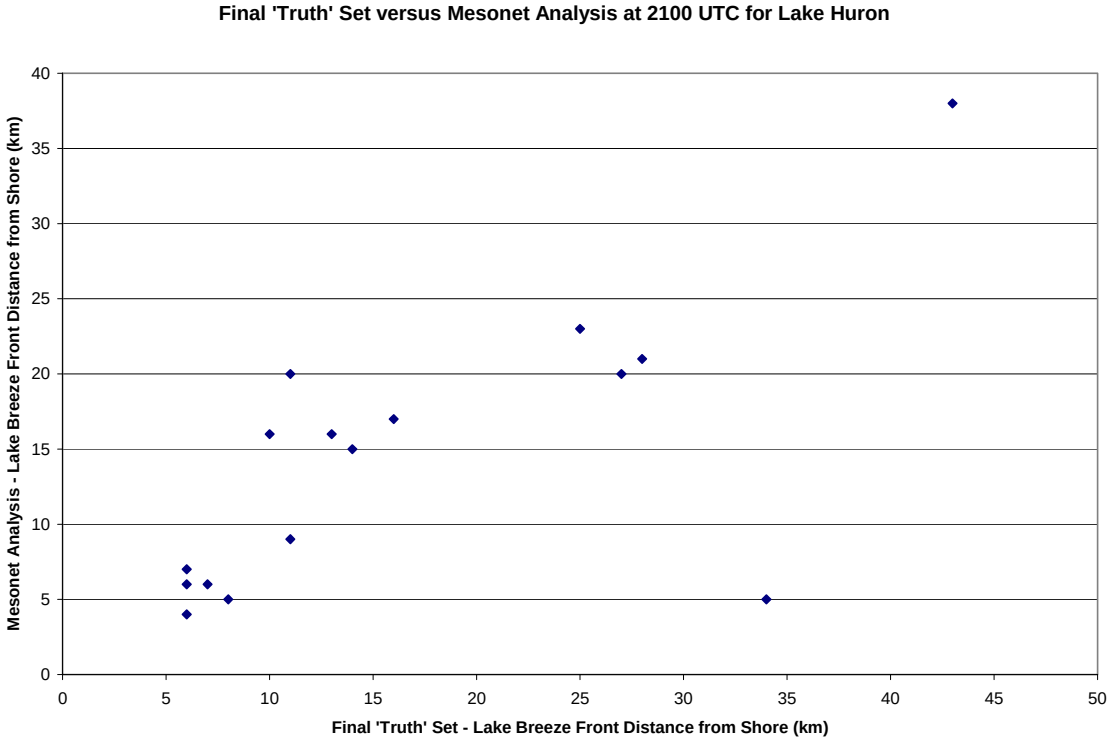

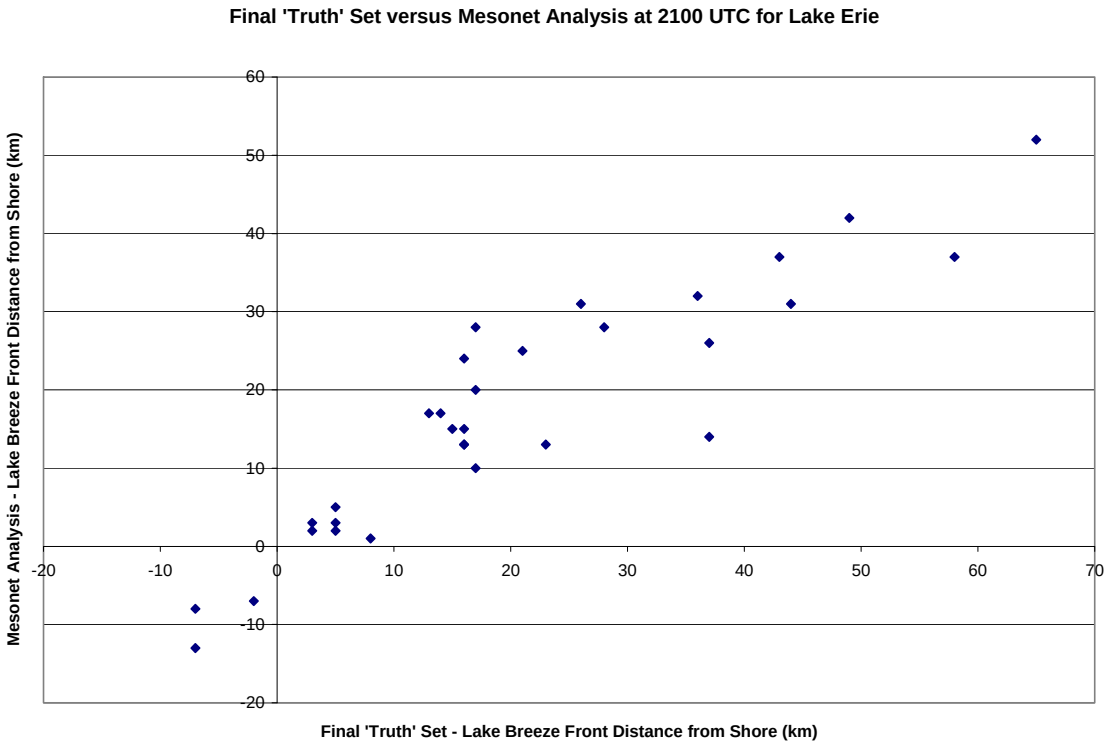
Final 'Truth' Set versus Mesonet Analysis at 2100 UTC for Lake Erie
Mesonet Analysis - Lake Breeze Front Distance from Shore (km)
Final 'Truth' Set - Lake Breeze Front Distance from Shore (km)
60
50
40
30
20
10
0
-10
-20
-20
-10
0
10
20
30
40
50
60
70

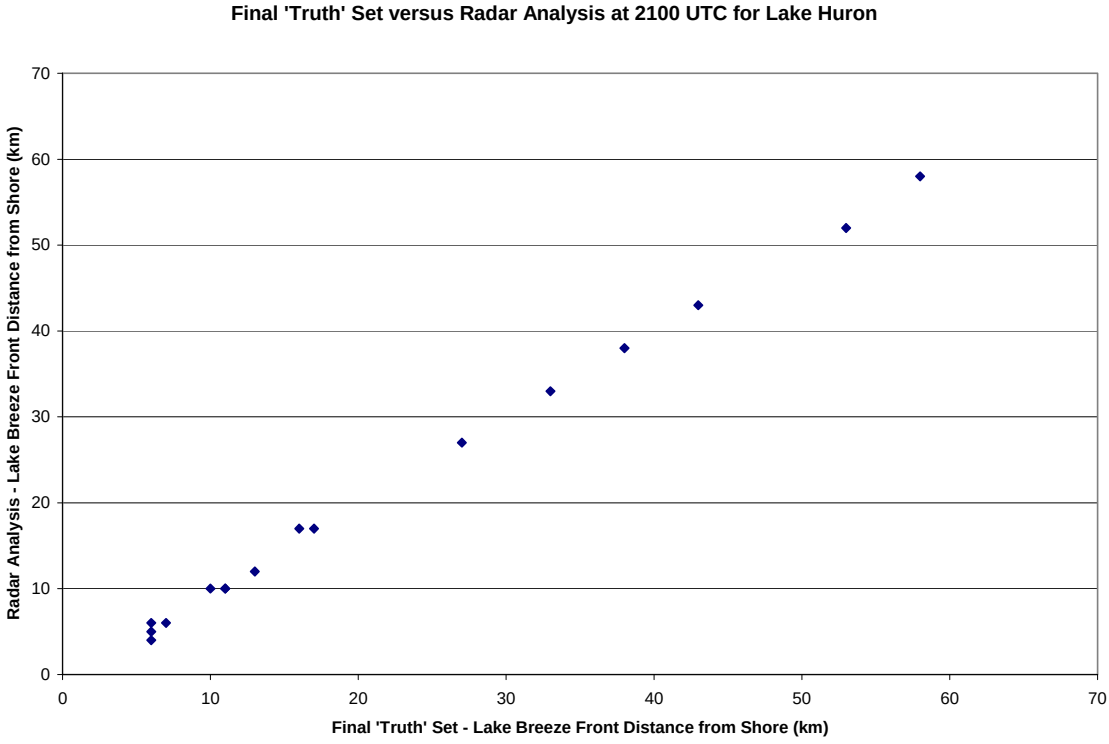
Final 'Truth' Set versus Radar Analysis at 2100 UTC for Lake Huron
Radar Analysis - Lake Breeze Front Distance from Shore (km)
Final 'Truth' Set - Lake Breeze Front Distance from Shore (km)
70
60
50
40
30
20
10
0
0
10
20
30
40
50
60
70

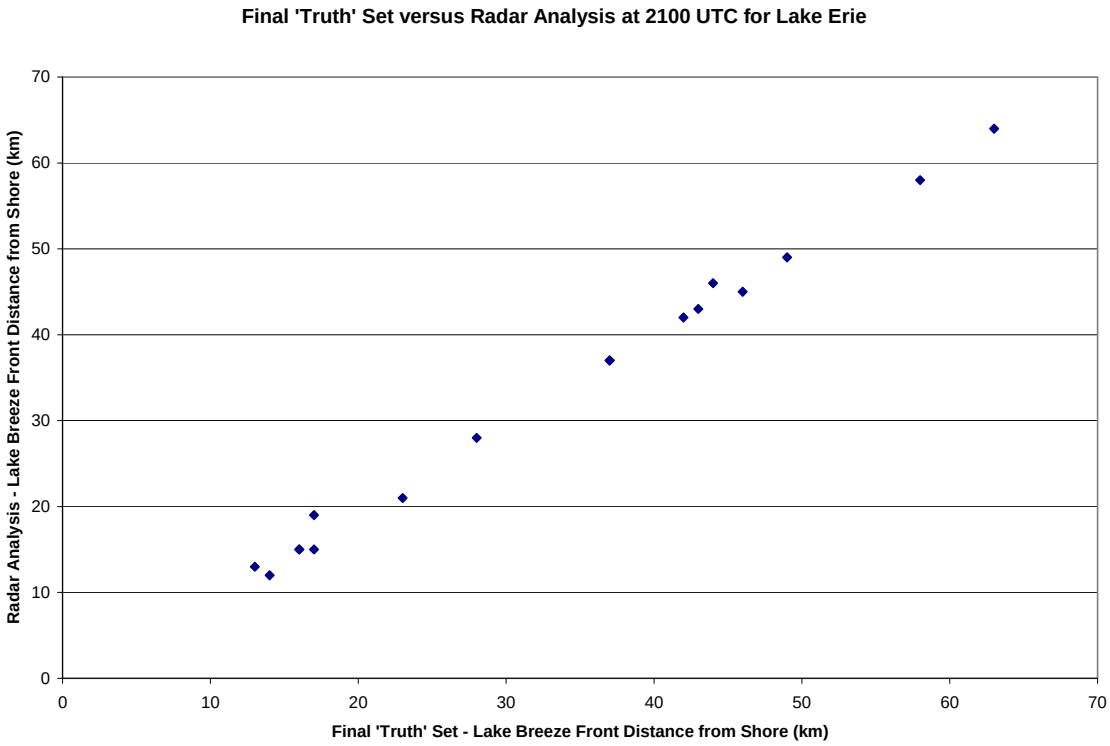
Final 'Truth' Set versus Radar Analysis at 2100 UTC for Lake Erie
Radar Analysis - Lake Breeze Front Distance from Shore (km)
Final 'Truth' Set - Lake Breeze Front Distance from Shore (km)
0
10
20
30
40
50
60
70

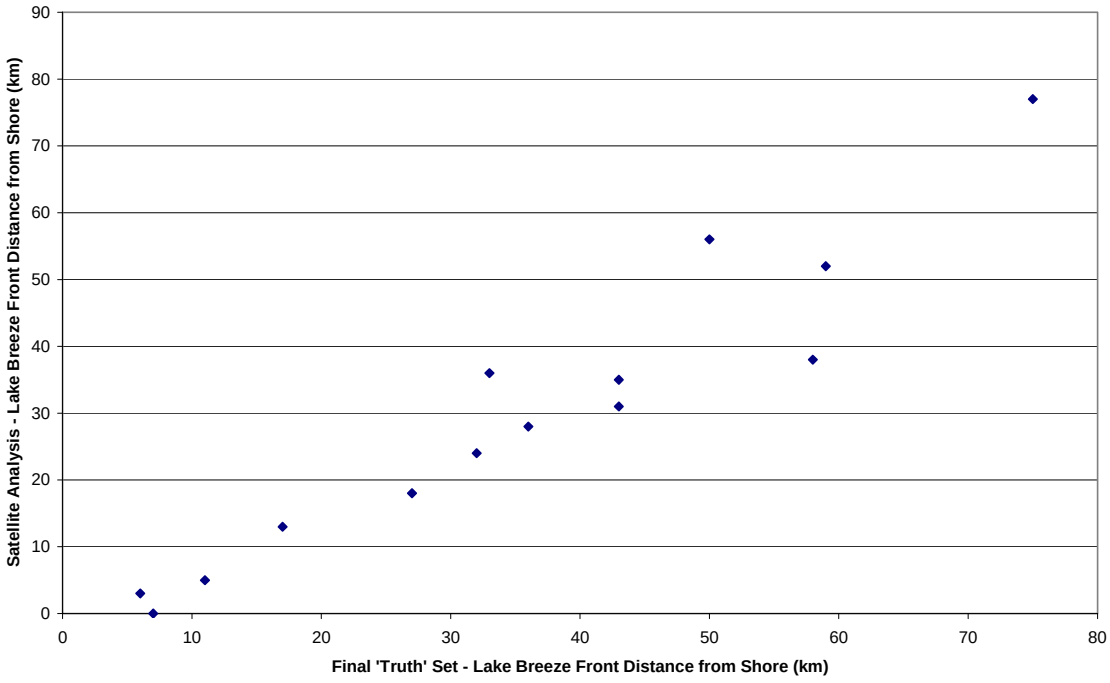
Final 'Truth' Set versus Satellite Analysis at 2100 UTC for Lake Huron
Satellite Analysis - Lake Breeze Front Distance from Shore (km)
Final 'Truth' Set - Lake Breeze Front Distance from Shore (km)
0
10
20
30
40
50
60
70
80
90

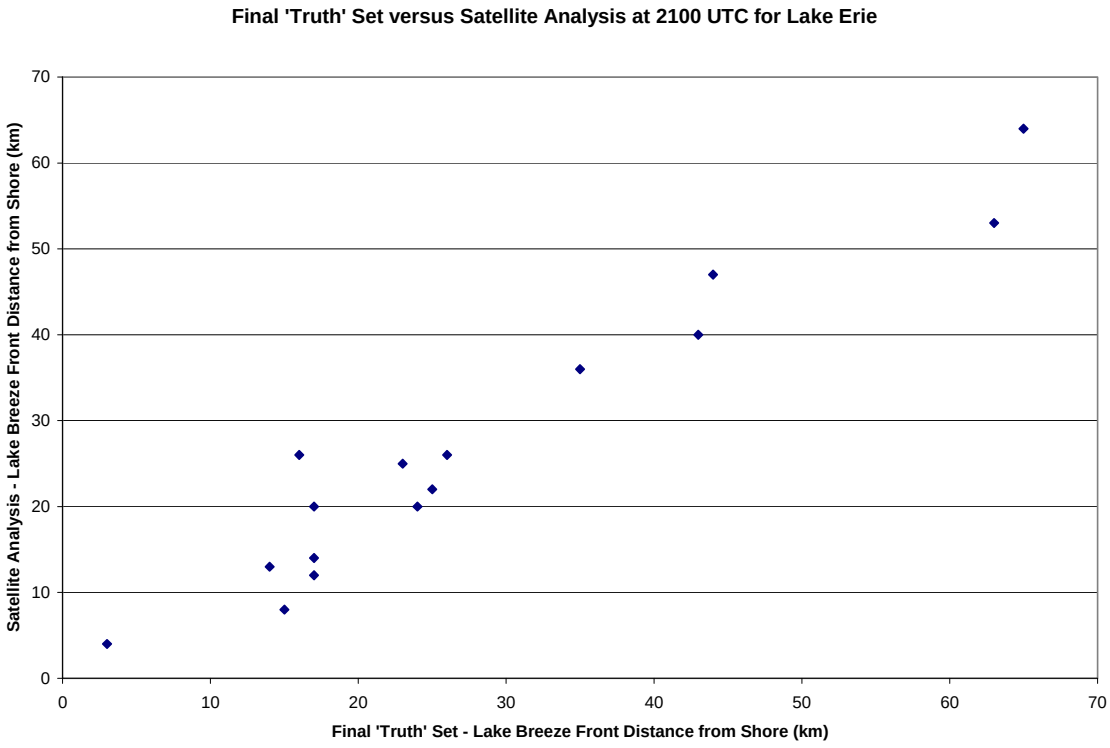
Final 'Truth' Set versus Satellite Analysis at 2100 UTC for Lake Erie
Satellite Analysis - Lake Breeze Front Distance from Shore (km)
Final 'Truth' Set - Lake Breeze Front Distance from Shore (km)
0
10
20
30
40
50
60
70

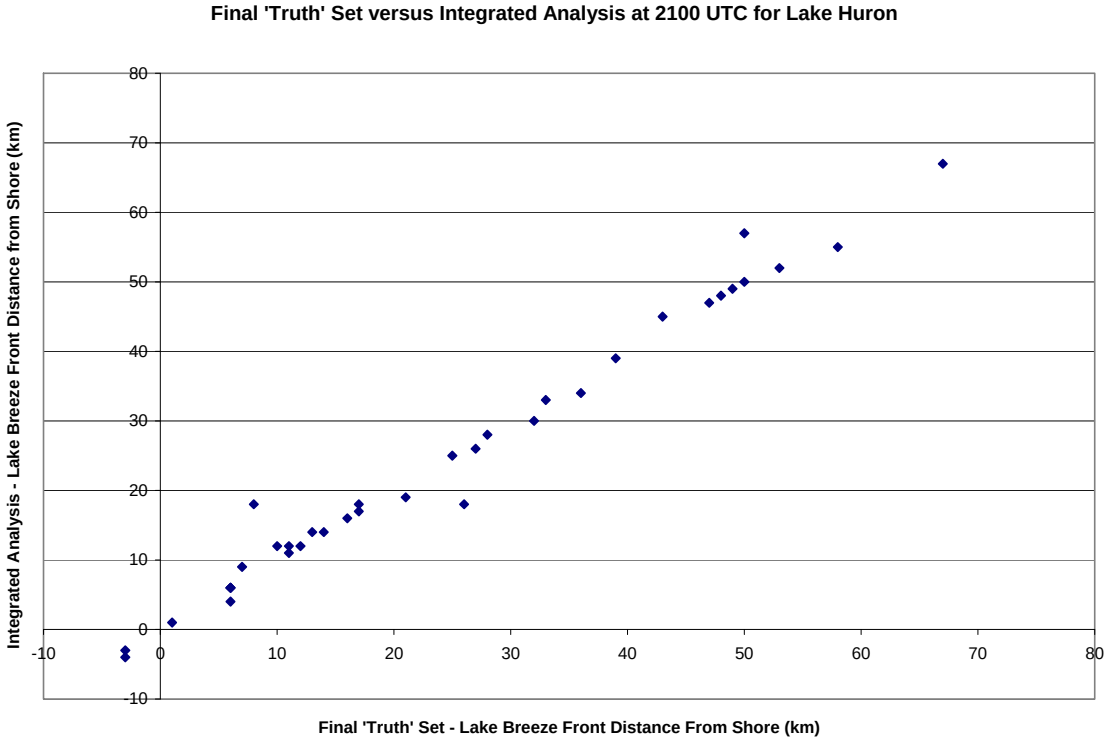
Final 'Truth' Set versus Integrated Analysis at 2100 UTC for Lake Huron
Integrated Analysis - Lake Breeze Front Distance from Shore (km)
Final 'Truth' Set - Lake Breeze Front Distance From Shore (km)
-10
0
10
20
30
40
50
60
70
80

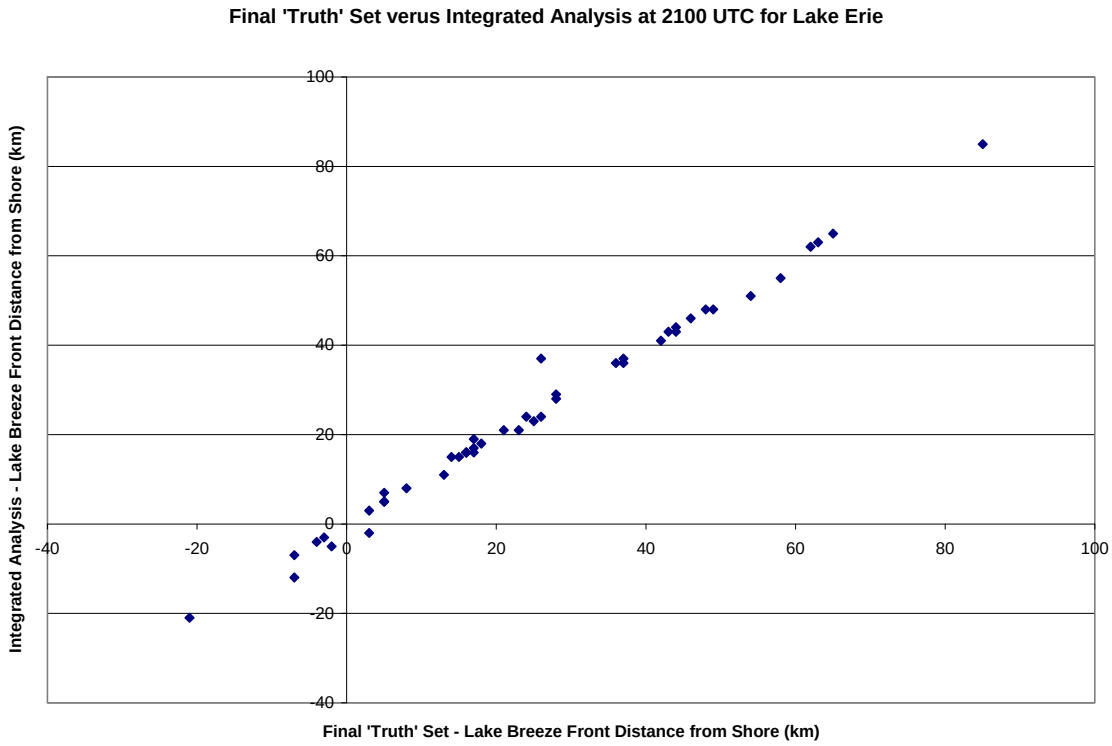
Final 'Truth' Set verus Integrated Analysis at 2100 UTC for Lake Erie
Integrated Analysis - Lake Breeze Front Distance from Shore (km)
Final 'Truth' Set - Lake Breeze Front Distance from Shore (km)
100
80
60
40
20
0
-20
-40
-40
-20
0
20
40
60
80
100

Appendix D

This appendix displays excel plots showing the values from some of the CLASS soundings taken at the UWO Farm. These have been used to determine limitation values for the 'MRS.for' quality checking program found in Appendix B.

The following graph shows the change in Longitude over the change in time (dlong/dt) plotted against the altitude. Note that the units are deg/s for dlong/dt and m for altitude.

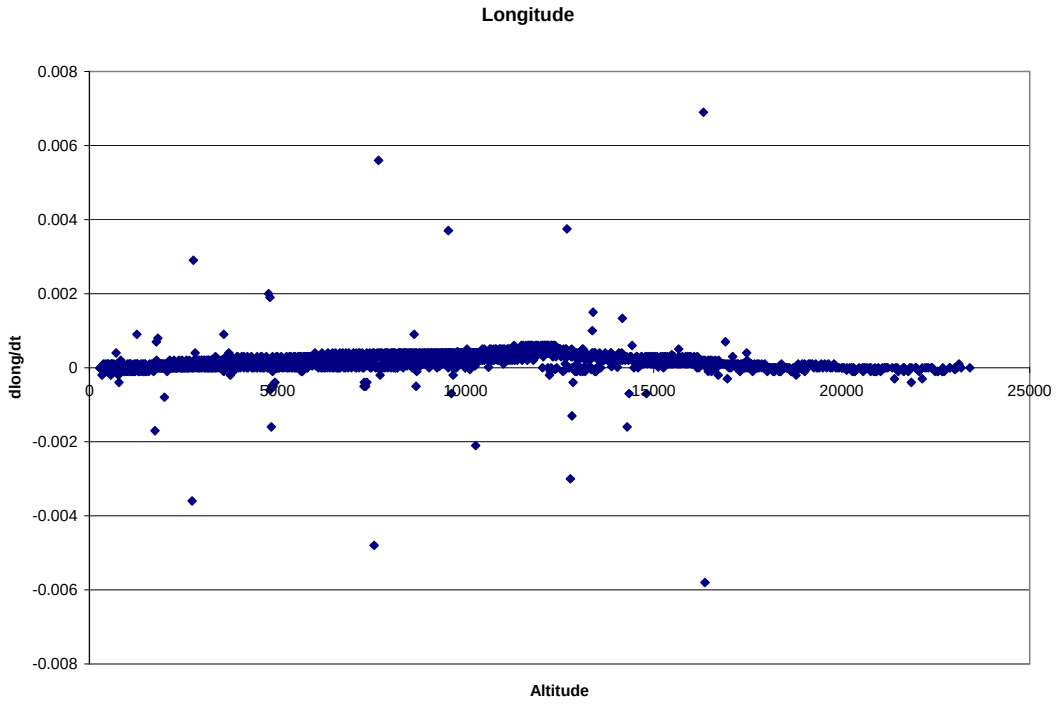

The following graph shows the change in Latitude over the change in time (dlat/dt) plotted against the altitude. Note that the units are deg/s for dlat/dt and m for altitude.

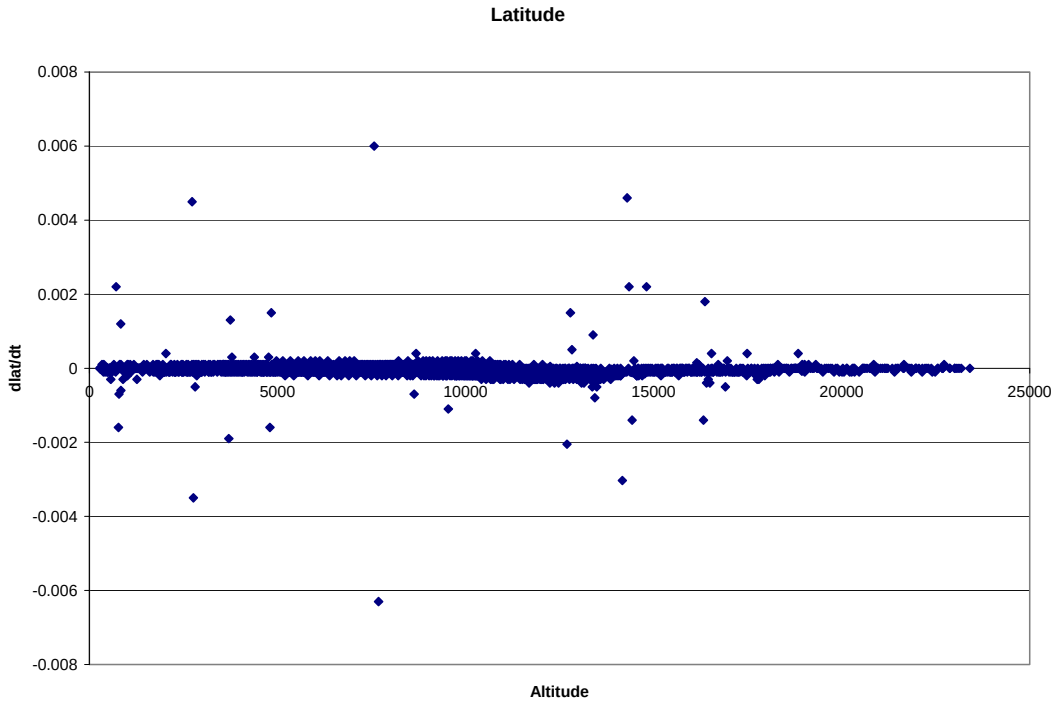

The following graph shows the change in wind speed over the change in time (dws/dt) plotted against the altitude. Note that the units are m/s^2 for dws/dt and m for altitude.

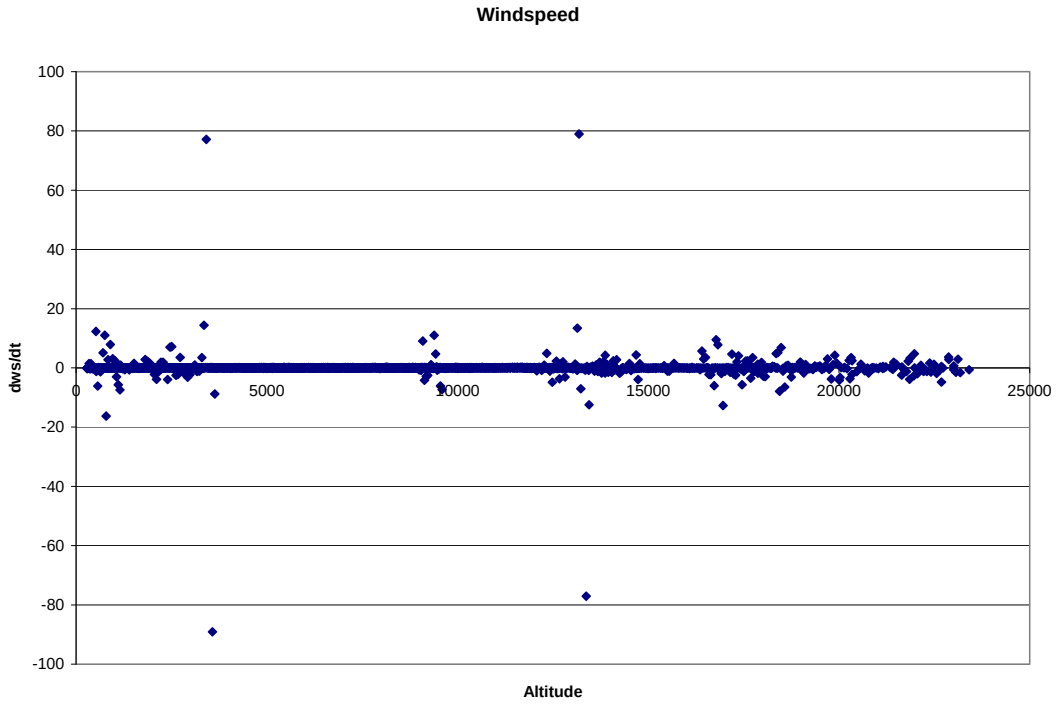

The following graph shows the change in u component wind over the change in time (du/dt) plotted against the altitude. Note that the units are m/s^2 for du/dt and m for altitude.

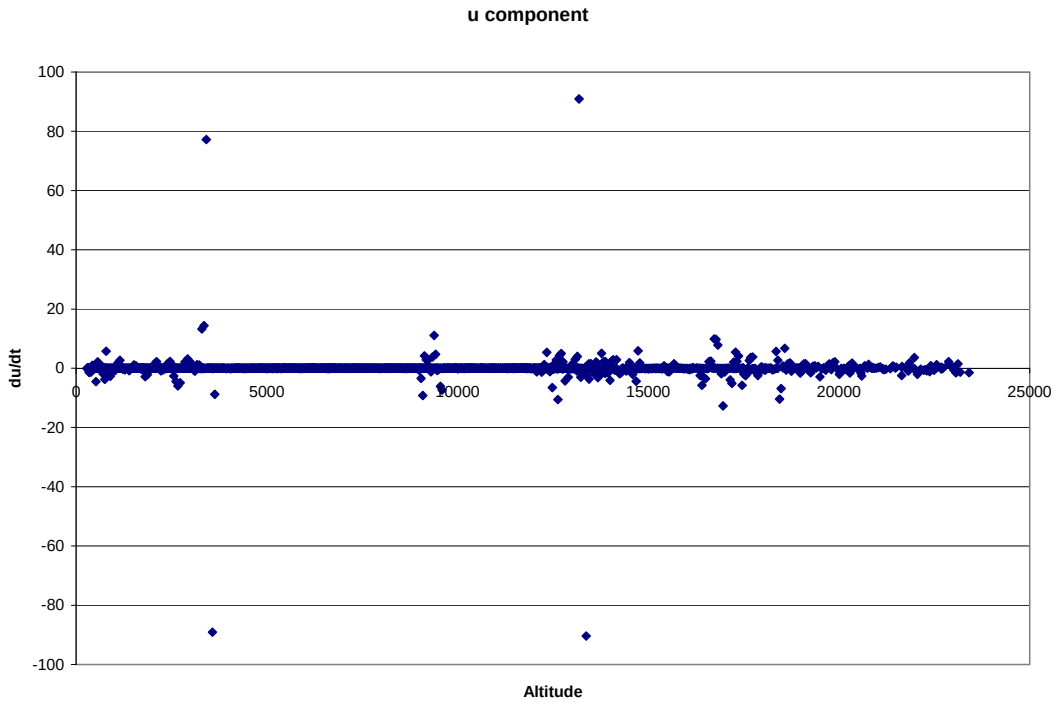

The following graph shows the change in v component wind over the change in time (dv/dt) plotted against the altitude. Note that the units are m/s^2 for dv/dt and m for altitude.

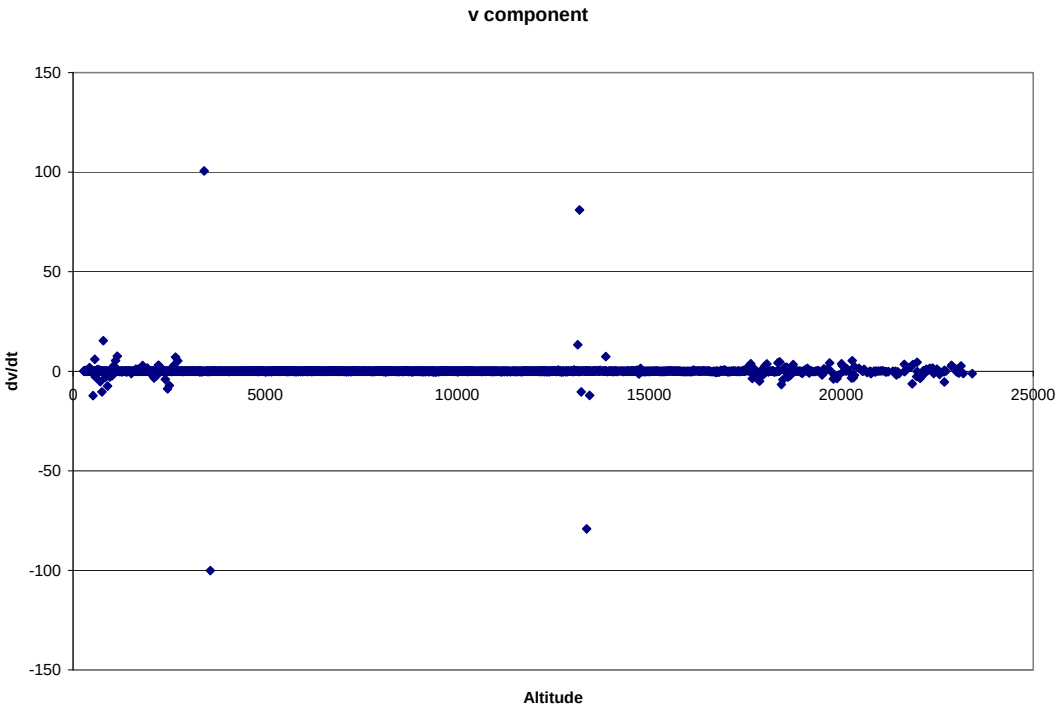

Appendix E

The fields/data that AURORA was configured for during the ELBOW 2001 project:

Map Setting Options:

Field	File Name	Description
tornado_track	TOP_database	Past tornado locations for Ontario
baqs_stations	BAQS_Stations	Border Air Quality Study stations
mobile_soundings	Mobile_Soundings	ELBOW 2001 Mobile Station Locations
PtFranksStanley	PtFranksStanley	The Port Franks and Port Stanley Radiosonde launch Locations

Note: The baqs_stations (above) were stations used for the Border Air Quality and Meteorological Study (BAQS-Met) 2007. These were plotted as a map setting in AURORA during ELBOW 2001, as AURORA was used later for the analysis of the BAQS-Met 2007 data.

Scattered Field Data:

(Note: ddd is the julian day, hh is the hour in UTC, and mm is the minutes)

Cell Identification Data

Field	File Names	Description
cellid_30_maxr	m3sfc_2001:ddd:hh:mm	For Maxr, 30dBZ threshold, minimum 2 pattern vectors
cidm_30_6vec	u5sfc_2001:ddd:hh:mm	For Maxr, 30dBZ threshold, minimum 6 pattern vectors
cellid_40_maxr	m4sfc_2001:ddd:hh:mm	For Maxr, 40dBZ threshold, minimum 2 pattern vectors
cidm_40_4vec	q1sfc_2001:ddd:hh:mm	For Maxr, 40dBZ threshold, minimum 4 pattern vectors
cellid_60_maxr	m6sfc_2001:ddd:hh:mm	For Maxr, 60dBZ threshold, minimum 2 pattern vectors
cidm_60_1vec	q2sfc_2001:ddd:hh:mm	For Maxr, 60dBZ threshold, minimum 1 pattern vector
cellid_30_cappi	i3sfc_2001:ddd:hh:mm	For Cappi, 30dBZ threshold, minimum 2 pattern vectors
cidc_30_6vec	u6sfc_2001:ddd:hh:mm	For Cappi, 30dBZ threshold, minimum 6 pattern vectors
cellid_40_cappi	i4sfc_2001:ddd:hh:mm	For Cappi, 40dBZ threshold, minimum 2 pattern vectors
cidc_40_4vec	q3sfc_2001:ddd:hh:mm	For Cappi, 40dBZ threshold, minimum 4 pattern vectors

cellid_60_cappi	i6sfc_2001:ddd:hh:mm	For Cappi, 60dBZ threshold, minimum 2 pattern vectors
cidc_60_1vec	q4sfc_2001:ddd:hh:mm	For Cappi, 60dBZ threshold, minimum 1 pattern vector

Cell Tracking Data (for all times)

Field	File Names	Description
celltrack_30_maxr	t3sfc_2001:ddd:hh:mm	For Maxr, 30dBZ threshold, minimum 2 pattern vectors
ctrm_30_6vec	u7sfc_2001:ddd:hh:mm	For Maxr, 30dBZ threshold, minimum 6 pattern vectors
celltrack_40_maxr	t4sfc_2001:ddd:hh:mm	For Maxr, 40dBZ threshold, minimum 2 pattern vectors
ctrm_40_4vec	q5sfc_2001:ddd:hh:mm	For Maxr, 40dBZ threshold, minimum 4 pattern vectors
celltrack_60_maxr	t6sfc_2001:ddd:hh:mm	For Maxr, 60dBZ threshold, minimum 2 pattern vectors
ctrm_60_1vec	q6sfc_2001:ddd:hh:mm	For Maxr, 60dBZ threshold, minimum 1 pattern vector
celltrack_30_cappi	c3sfc_2001:ddd:hh:mm	For Cappi, 30dBZ threshold, minimum 2 pattern vectors
ctrc_30_6vec	u8sfc_2001:ddd:hh:mm	For Cappi, 30dBZ threshold, minimum 6 pattern vectors
celltrack_40_cappi	c4sfc_2001:ddd:hh:mm	For Cappi, 40dBZ threshold, minimum 2 pattern vectors
ctrc_40_4vec	q7sfc_2001:ddd:hh:mm	For Cappi, 40dBZ threshold, minimum 4 pattern vectors
celltrack_60_cappi	c6sfc_2001:ddd:hh:mm	For Cappi, 60dBZ threshold, minimum 2 pattern vectors
ctrc_60_1vec	q8sfc_2001:ddd:hh:mm	For Cappi, 60dBZ threshold, minimum 1 pattern vector

Cell Tracking Data (for present time only)

Field	File Names	Description
ctpres_30_maxr	y3sfc_2001:ddd:hh:mm	For Maxr, 30dBZ threshold, minimum 2 pattern vectors
ctpresm_30_6vec	u9sfc_2001:ddd:hh:mm	For Maxr, 30dBZ threshold, minimum 6 pattern vectors
ctpres_40_maxr	y4sfc_2001:ddd:hh:mm	For Maxr, 40dBZ threshold, minimum 2 pattern vectors
ctpresm_40_4vec	u1sfc_2001:ddd:hh:mm	For Maxr, 40dBZ threshold, minimum 4 pattern vectors
ctpres_60_maxr	y6sfc_2001:ddd:hh:mm	For Maxr, 60dBZ threshold, minimum 2 pattern vectors
ctpresm_60_1vec	u2sfc_2001:ddd:hh:mm	For Maxr, 60dBZ threshold, minimum 1 pattern vector

ctpres_30_cappi	z3sfc_2001:ddd:hh:mm	For Cappi, 30dBZ threshold, minimum 2 pattern vectors
ctpresc_30_6vec	q9sfc_2001:ddd:hh:mm	For Cappi, 30dBZ threshold, minimum 6 pattern vectors
ctpres_40_cappi	z4sfc_2001:ddd:hh:mm	For Cappi, 40dBZ threshold, minimum 2 pattern vectors
ctpresc_40_4vec	u3sfc_2001:ddd:hh:mm	For Cappi, 40dBZ threshold, minimum 4 pattern vectors
ctpres_60_cappi	z6sfc_2001:ddd:hh:mm	For Cappi, 60dBZ threshold, minimum 2 pattern vectors
ctpresc_60_1vec	u4sfc_2001:ddd:hh:mm	For Cappi, 60dBZ threshold, minimum 1 pattern vector

Mesonet Station Data:

(Note: ddd is the julian day, hh is the hour in UTC, and mm is the minutes)

Field	File Names	Description
mesonet	mssfc_2001:ddd:hh:mm	York University mesonet station data
msc_data	mxsfc_2001:ddd:hh:mm	MSC mesonet station data
ome_data	omsfc_2001:ddd:hh:mm	OME mesonet station data
rtown_data	rtsfc_2001:ddd:hh:mm	Ridgetown mesonet station data
coastplot	cwsfc_2001:ddd:hh:mm	Coastwatch mesonet stations (10 minute data)
coastplot2	chsfc_2001:ddd:hh:mm	Coastwatch mesonet stations (Hourly data)

Boundaries:

(Note: ddd is the julian day, hh is the hour in UTC, and mm is the minutes)

Field	File Names	Description
mesonet_bdy	mbsfc_2001:ddd:hh:mm	Boundaries identified using the mesonet data only
satellite_bdy	sbsfc_2001:ddd:hh:mm	Boundaries identified using the satellite data only
radar_bdy	rbsfc_2001:ddd:hh:mm	Boundaries identified using the radar data only
integrated_bdy	ibsfc_2001:ddd:hh:mm	Boundaries identified using all the data sets together
final_bdy	fbsfc_2001:ddd:hh:mm	Boundaries identified using using all the boundaries from the other analyses and all of the data sets

btw_hour_bdy	fhsfc_2001:ddd:hh:mm	Final boundaries identified between the hourly depictions
lift_zone	lzsfc_2001:ddd:hh:mm	Lifting Zone corresponding to a boundary
mesonet_bdy_fg	b1sfc_2001:ddd:hh:mm	First Guess on boundary locations identified using the mesonet data
satellite_bdy_fg	b2sfc_2001:ddd:hh:mm	First Guess on boundary locations identified using the satellite data
radar_bdy_fg	b3sfc_2001:ddd:hh:mm	First Guess on boundary locations identified using the radar data

Image Configuration:
(Note: YY or YYYY is the year, MM is the month, DD is the day, hh is the hour in UTC and mm is the minute)

Satellite

Image Data	File Names	Description
LB_visible	LB.YYMMDD.hhmm.ch1	GOES-8 lake breeze sector visible satellite
great_lakes_vis	GL.YYMMDD.hhmm.ch1	GOES-8 great lakes sector visible satellite
great_lakes_ir	GL.YYMMDD.hhmm.ch4	GOES-8 great lakes sector infrared
ea_wv	EA.YYMMDD.hhmm.ch3	GOES-8 Eastern sector water vapour
ea_ir	EA.YYMMDD.hhmm.ch4	GOES-8 Eastern sector infrared

Radar

Image Data: WSO_DOPVOL_RANGE_THETA
File Names: YYMMDDhhmm,WSO,CLOGZPPI,DOPVOL1_A,18,MPRATE
Description: Exeter Doppler Radar 0.5 degree Reflectivity

Image Data: WSO_VRPPI
File Names: YYMMDDhhmm,WSO,VRPPI,DOPVOL1_A,18
Description: Exeter Doppler Radar Radial Velocity

Image Data: WSO_CAPPI_1KM
File Names: WSO_ YYYYMMDDhhmm_CONVOL,CAPPI,1.0,AGL,MPRATE$
Description: Exeter Radar 1.0 km CAPPI

Image Data: WSO_MAXR_1KM
File Names: WSO_YYYYMMDDhhmm_CONVOL,MAXR,1.0,AGL,MPRATE$
Description: Exeter Radar 1.0 km MAXR

Note: AURORA was also configured/setup to ingest RUC analysis time Grib data. A few Grib files were ingested for viewing through AURORA, however these data have not been used for further analysis.

Appendix F

Modification of the AURORA files for the CAPPI 1.0 km data

Addition to the 'Image.elbow' file:

Here we can see the colour tables are specified for the image product in AURORA

```
product wso_cappi_1
{
        label  = "CAPPI 1km"
        class  = radar
         ctable = "DBZ"                ctables RadarData_DBZ.tab
         ctable = "RAIN MM/HR"   ctables RadarData_MMHR.tab
         ctable = "cell"               ctables RadarData_cellDBZ.tab
         ctable = "30DBZ cell"   ctables RadarData_30DBZ.tab
         ctable = "40DBZ cell"   ctables RadarData_40DBZ.tab
         ctable = "60DBZ cell"   ctables RadarData_60DBZ.tab
}
```

Here the data are declared, specifying how the metafiles are named

```
image   WSO_CAPPI_1KM
        {
        directory      = radar1
        fname_mask     = WSO_............_CONVOL,CAPPI,1.0,AGL,MPRATE$
        fname_time     = WSO_%4d%2d%2d%2d%2d YYYY MM DD hh mm
        site           = Exeter
        product_tag    = wso_cappi_1
         encode        = urp_polar
        projection     = radar
         mapdef         = none
        }
```

Addition to the Setup files:

Here the imagery directories are declared. Notice 'radar1' which specifies the location of the CAPPI 1.0 km data. Location of the colour tables corresponding to the imagery data are also declared beside 'ctables'. See the text highlighted in blue.

```
##      Imagery directories
        ElbowImages           $HOME/ELBOW_data/ELBOW_sat
        radar                 $HOME/ELBOW_data/ELBOW_rad
         radar1                 $HOME/ELBOW_data/ELBOW_capp
         radar2                 $HOME/ELBOW_data/ELBOW_maxr
        ctables               $HOME/config/Ctables
        #       im_ctables            $HOME/Elbow/IM/ctables
```

Colour Table sample:

This simple colour table highlights the 40 dBZ data. Any bins that are below 40 dBZ are displayed in grey. Any bins that are 40 dBZ or higher are displayed in blue. Here the lower limit and upper limit for dBZ are declared and then the colour is declared in RGB values.

```
RadarDataLUT
PrecipitationRate-Reflectivity DBZ
-32.0   40.0    105 105 105
40.0    100.0   175 238 238
```

Appendix G

Modification of the AURORA files for the present time Celltracking files corresponding to the CAPPI 1.0 km data for a 40 dBZ threshold and a minimum pattern vector setting of 4.

Addition to the 'Config.elbow' file:

This has been added to the 'Fields' block:

```
ctpresc_40_4vec              surface
               {
               label                  = <*default*> "1.0km 40dBZ Cappi CT present cell
4vec"
               short_label            = <*default*> "Cappi CT pres 40 4vec"
               }
```

This has been added to the 'Elements' block:

Notice that all of the data available from the cell tracking are declared under attributes

```
ctpresc_40_4vec
                {
                label                   = <*default*> "1.0km 40dBZ Cappi CT present cell
4vec"
                short_label             = <*default*> "Cappi CT pres 40 4vec"
                element_group           = Miscellaneous
                field_group             = Surface
                level_type              = Surface
                alias                   = cctp404v
                file_id                 = u3
                precision               = .01  none

                time_dependence = Normal
                field_type      = Scattered
                wind_class      = None

                attributes      =
                        {
                        TRACKNUM
                                {
                                attribute_label         = <*default*> "Track Number"
                                attribute_short_label   = <*default*> "Track No"
                                }
                        TRACK_STAT
                                {
                                attribute_label         = <*default*> "Track Stat"
                                attribute_short_label   = <*default*> "Track Stat"
                                }
                        TIME_STEP
                                {
                                attribute_label         = <*default*> "Time Step"
                                attribute_short_label   = <*default*> "Time Step"
                                }
                        OBJ_SPEED
                                {
                                attribute_label         = <*default*> "Object Speed (m/s)"
                                attribute_short_label   = <*default*> "Speed"
                                }
                        OBJ_BEARING
                                {
```

```
                        attribute_label         = <*default*> "Object Bearing
(deg)"
                        attribute_short_label   = <*default*> "Bearing"
                        }
                DELTA_AREA
                        {
                        attribute_label         = <*default*> "Delta Area
(km^2/s)"
                        attribute_short_label   = <*default*> "Delta Area"
                        }
                INDEX
                        {
                        attribute_label         = <*default*> "Index"
                        attribute_short_label   = <*default*> "Index"
                        }
                VALIDTIME
                        {
                        attribute_label         = <*default*> "Valid Time
(YYMMDDHHmm)"
                        attribute_short_label   = <*default*> "Time"
                        }
                HHMM
                        {
                        attribute_label         = <*default*> "Hours/Minutes"
                        attribute_short_label   = <*default*> "hhmm"
                        }
               SITEID
                        {
                        attribute_label         = <*default*> "Site ID"
                        attribute_short_label   = <*default*> "Site ID"
                        }
                ID
                        {
                        attribute_label         = <*default*> "ID"
                        attribute_short_label   = <*default*> "ID"
                        }
                ELLIPSE_XN
                        {
                        attribute_label         = <*default*> "Ellipse XN (km)"
                        attribute_short_label   = <*default*> "exn"
                        }
                ELLIPSE_YN
                        {
                        attribute_label         = <*default*> "Ellipse YN (km)"
                        attribute_short_label   = <*default*> "eyn"
                        }
                DIAMX
                        {
                        attribute_label         = <*default*> "Diameter X (km)"
                        attribute_short_label   = <*default*> "Diam X"
                        }
                DIAMY
                        {
                        attribute_label         = <*default*> "Diameter Y (km)"
                        attribute_short_label   = <*default*> "Diam Y"
                        }
                DIAM_RATIO
                        {
                        attribute_label         = <*default*> "Diameter Ratio"
                        attribute_short_label   = <*default*> "Diam Ratio"
                        }
                ELLIPSE_AREA
                        {
                        attribute_label         = <*default*> "Ellipse Area
(km^2)"
                        attribute_short_label   = <*default*> "earea"
                        }
```

```
                        ELLIPSE_ORIEN
                                {
                                attribute_label         = <*default*> "Ellipse Orientation
(deg)"
                                attribute_short_label   = <*default*> "eorien"
                                }
                        AVE_VALUE
                                {
                                attribute_label         = <*default*> "Average Value
(DBZ)"
                                attribute_short_label   = <*default*> "Ave Value"
                                }
                        MAX_VALUE
                                {
                                attribute_label         = <*default*> "Maximum Value
(DBZ)"
                                attribute_short_label   = <*default*> "Max Value"
                                }
                        XCENTRE
                                {
                                attribute_label         = <*default*> "X Centre (Range in
km)"
                                attribute_short_label   = <*default*> "X Cen"
                                }
                        YCENTRE
                                {
                                attribute_label         = <*default*> "Y Centre (Theta in
deg)"
                                attribute_short_label   = <*default*> "Y Cen"
                                }
                         NUMPV
                                {
                                attribute_label         = <*default*> "numpv"
                                attribute_short_label   = <*default*> "numpv"
                                }
                        ELLIPSE_A
                                {
                                attribute_label         = <*default*> "Ellipse A (km)"
                                attribute_short_label   = <*default*> "Ellipse A"
                                }
                        ELLIPSE_B
                                {
                                attribute_label         = <*default*> "Ellipse B (km)"
                                attribute_short_label   = <*default*> "Ellipse B"
                                }
                        RADAR_LAT
                                {
                                attribute_label         = <*default*> "Radar Latitude
(deg)"
                                attribute_short_label   = <*default*> "Radar Lat"
                                }
                        RADAR_LONG
                                {
                                attribute_label         = <*default*> "Radar Longitude
(deg)"
                                attribute_short_label   = <*default*> "Radar Long"
                                }
                        LAT
                                {
                                attribute_label         = <*default*> "Latitude (deg)"
                                attribute_short_label   = <*default*> "Lat"
                                }
                        LONG
                                {
                                attribute_label         = <*default*> "Longitude (deg)"
                                attribute_short_label   = <*default*> "Long"
                                }
```

```
                }



        editor                  =
                {
                modify_file                             = cctp404_entry
                }
        sample                  = Default
        }
```

This has been added to the ‘Sources’ block:
All the cell identification and cell tracking data, for the CAPPI 1.0 km radar data, are located in the same directory and considered to be the same ‘source’.

```
ctc_cells
                {
                label                           = "Cappi Cell ID/Tracking"
                short_label                     = "Cappi CID/CT"
                source_type                     = Depiction

                directory_tag                   = ctc_Data
                directory_path                  = None

                subsources                      = None
                minutes_required                = True
                }
```

<u>Addition to the ‘Presentation.elbow’ file</u>:

Here, the track number is set to be displayed beside the cell marker which is displayed as a ‘plus’ symbol. Both are to be displayed in the colour magenta.

```
field   ctpresc_40_4vec  sfc     ALL

        member  spot
                class   plot
                        class_member    label   TrackNo         TRACKNUM
                                default
                                        offset  5 10
                                        hjust   left
                                        vjust   bottom
                                        size    15
                                        colour  Magenta
                                        font    simplex
                        class_member    mark    marker
                                default
                                        size    5
                                        colour  Magenta
                                        marker  plus
                class   legend
                        class_member    label   value
                                default
                                        size    legend
                                        colour  Magenta
                                        font    simplex
                                        hjust   left
```

Addition to the Setup file:

This has been added to the Directories Setup:
The data are located under the ctc_Data with the rest of the cell tracking and identification data for the CAPPI 1.0 km radar data (see the text highlighted in blue)

```
##      Surface Station Data
        Station_Data          $HOME/ELBOW_data/ELBOW_sfc
        ctm_Data              $HOME/ELBOW_data/ELBOW_ctm
        ctc_Data              $HOME/ELBOW_data/ELBOW_ctc
        Mesonet_Data          $HOME/ELBOW_data/ELBOW_sfc
         OME_Data               $HOME/ELBOW_data/ELBOW_sfc
         MSC_Data               $HOME/ELBOW_data/ELBOW_sfc
         Ridgetown_Data         $HOME/ELBOW_data/ELBOW_sfc
         Coastwatch_Data10min   $HOME/ELBOW_data/ELBOW_sfc
         Coastwatch_Data1hr     $HOME/ELBOW_data/ELBOW_sfc
```

This has been added to the Interface Setup:
Again, these data are included under the ctc_cells (see the text highlighted in blue)

```
[depiction.external]
        #!      Optional access to external FPA databases for comparison/import
        #!      (where sources must be defined in Config files) (examples):
                #       aviation_desk
                #       atlantic_office
                #       elbow_synoptic
                          surface_stns
                        ctm_cells
                        ctc_cells
                        mesonet_stns
                        coastwatch_stns
                          coastwatch_stnsH
                        coastwatch_stnsX
                        rtown_data
                        ome_data
                        msc_data
```

This has been added to the Depiction Setup:
These data are declared under the surface fields as ctpresc_40_4vec (see the text highlighted in blue)

```
#!      Surface fields:
         #      field   pressure              msl
        #       field   temperature           surface
        #       field   weather_system        surface
        #       field   wind                  surface
                field   fronts                surface
                field   mesonet               surface
                field    cellid_30_maxr       surface
                field    cidm_30_6vec         surface
                field    cellid_40_maxr       surface
                field    cidm_40_4vec         surface
                field    cellid_60_maxr       surface
                field    cidm_60_1vec         surface
                field    cellid_30_cappi              surface
                field    cidc_30_6vec         surface
                field    cellid_40_cappi              surface
                field    cidc_40_4vec         surface
                field    cellid_60_cappi              surface
                field    cidc_60_1vec         surface
```

```
        field   celltrack_30_maxr       surface
        field    ctrm_30_6vec          surface
        field    celltrack_40_maxr       surface
        field    ctrm_40_4vec          surface
        field    celltrack_60_maxr       surface
        field   ctrm_60_1vec           surface
        field    celltrack_30_cappi      surface
        field    ctrc_30_6vec          surface
        field    celltrack_40_cappi      surface
        field    ctrc_40_4vec          surface
        field    celltrack_60_cappi      surface
        field    ctrc_60_1vec          surface
        field    ctpres_30_maxr        surface
        field    ctpresm_30_6vec         surface
        field    ctpres_40_maxr          surface
        field    ctpresm_40_4vec               surface
        field    ctpres_60_maxr          surface
        field    ctpresm_60_1vec               surface
        field   ctpres_30_cappi         surface
        field    ctpresc_30_6vec         surface
        field    ctpres_40_cappi         surface
        field    ctpresc_40_4vec         surface
        field    ctpres_60_cappi         surface
        field    ctpresc_60_1vec         surface
        field    msc_data              surface
        field   ome_data               surface
        field   rtown_data             surface
        field   coastplot              surface
         field    coastplot2           surface
#       field   vertical_vel           850mb
```

Appendix H

A sample of a cell tracking metafile

Notice the variables declared in the subfield list which corresponds to the data in the 'plot' points following:

```
* MSC/MRB Metafile Standard
 rev 2.0
 units latlon

 field scattered ctpresc_40_4vec sfc
 subfields 29
   TRACKNUM      label
   TRACK_STAT    label
   TIME_STEP     label
   OBJ_SPEED     label
   OBJ_BEARING   label
   DELTA_AREA    label
   INDEX         label
   VALIDTIME     label
   HHMM          label
   SITEID        label
   ID            label
   ELLIPSE_XN    label
   ELLIPSE_YN    label
   DIAMX         label
   DIAMY         label
   DIAM_RATIO    label
   ELLIPSE_AREA  label
   ELLIPSE_ORIEN label
   AVE_VALUE     label
   MAX_VALUE     label
   XCENTRE       label
   YCENTRE       label
   NUMPV         label
   ELLIPSE_A     label
   ELLIPSE_B     label
   RADAR_LAT     label
   RADAR_LONG    label
   LAT           label
   LONG          label
 plot 42.56984 -81.75816 634 -1 0 8.9 264.407349 -0.087883 1
200106301130 1130 WSO 3 -28.54 -90.9 17.00 18.43 0.92 91.59 13.16 44.37
55.50 96.00 198.00 11 8.1 3.6 43.37030 -81.38420 42.54808 -81.74657
 plot 42.41444 -81.98690 635 -4 0 N/A N/A N/A 6 200106301130 1130 WSO 6
-50.25 -106.2 13.00 10.04 1.30 45.13 -60.55 42.82 50.50 115.00 205.00 5
4.2 3.4 43.37030 -81.38420 42.43080 -81.97675
* End
```

Appendix I

Following is the low-level mesoscale boundary identification criteria used to identify all boundaries in the ELBOW study area during the summer of 2001. Criteria were laid out by Dr. David Sills (Cloud Physics and Severe Weather Research Section, Environment Canada) with some input/modifications from the author:

Semi-Objective Analysis Criteria

v050121

The attached criteria, together with a basic knowledge of mesoscale circulations and boundary behaviour, should be used to identify lake breeze fronts, land breeze fronts, outflow boundaries, 'merged' boundaries, 'hybrid' boundaries and 'other' boundaries in the ELBOW 2001 dataset. This detection method is semi-objective.

Positive factors are platform-specific indicators that signal the presence of a boundary. Negative factors can be used to dismiss the possibility of a boundary existing. For lake breezes, there are a number of factors that can prevent the development of or lead to the dissipation of a lake breeze circulation. However, gust fronts can exist in many types of weather situations.

The location of a boundary for drawing in the front should be the best estimate based on the observation platform being used. For instance, with mesonet data, one might only know that a boundary is located between two stations or two sets of stations. The best estimate of the position of the boundary can be made by assuming a quasi-continuous motion between time intervals. For satellite and radar, it is typically much easier to identify the exact position of boundaries using fine lines (radar) and/or lines of cumulus cloud (satellite).

For each day during the study, a series of depictions at hourly intervals or less will be analyzed. For the purposes of this study, a boundary must be detected at more than one time interval and, in the case of surface data, at more than one station to be entered into the database. The area to be analysed using the boundary criteria includes that within the Exeter radar range ring.

Synoptic-scale boundaries such as warm fronts, cold fronts, troughs, etc. also need to be identified and entered into the database. Before mesoanalysis begins, the positions of synoptic-scale boundaries in the study region (if any) must be established for each day using analyzed surface maps. An attempt must be made to relate these boundaries to observed features in radar, satellite and surface data. Synoptic-scale boundary information is then entered into the database if necessary.

Lake Breeze Front

A lake breeze frontal boundary typically forms along the leading edge of a lake breeze and separates relatively warm air over land from relatively cool marine air.

Platform	Positive Factors	Negative Factors	Ambiguous
Satellite (visible)	► line of cumulus clouds or sharp gradient in cumulus cloudiness quasi-parallel to shoreline ► gradual inland penetration of above	► persistent thick cloudiness over most or all of lake ► gradual change in the depth of cumulus clouds inland from lake (gradually deepening CBL)	► no cloud visible ► thin cirrostratus or broken mid-level clouds prevents seeing cumulus clouds
Radar (LogZ, Vr)	► fine line or sharp gradient in clear air reflectivity quasi-parallel to shoreline ► shift in radial velocity along fine line ► gradual inland penetration of above	► large area of persistent precipitation over region	► no clear air echoes ► fine line or gradient in clear air echoes not well defined
Surface (Stn plots, Time series)	► rapid shift in wind direction to onshore wind (may be accompanied by rapid change in wind speed, sharp decrease in temperature and dew point within ~20 km of shore), ► gradual inland penetration of onshore winds ► elongated area of convergence quasi-parallel to shoreline Note: an area of broad divergence over the lake and the adjacent lake shore indicates a lake breeze circulation is present and may be used to support the presence of a lake breeze front	► no onshore winds	► often very subtle surface gradients at boundaries in moderate / high low-level wind regimes

Land Breeze Front

A land breeze frontal boundary typically forms along the leading edge of a land breeze and separates relatively warm air over water from relatively cool night time land air.

Platform	Positive Factors	Negative Factors	Ambiguous
Satellite (visible)	► single line of cumuliform clouds over lake quasi-parallel to shoreline	► persistent, thick cloudiness over the region	► no cloud visible ► no visible images available (in dark hours) ► thin cirrostratus or broken mid-level clouds prevents seeing cumuliform clouds
Radar (LogZ, Vr)	► single fine line or sharp gradient in clear air reflectivity quasi-parallel to shoreline ► shift in radial velocity along fine line	► large area of persistent precipitation over the area	► no clear air echoes ► fine line or clear air echoes not well defined
Surface (Stn plots, Time series)	► rapid shift in wind direction to offshore wind (may be accompanied by rapid change in wind speed, sharp decrease in temperature and dew point close to the shore) Note: an area of broad convergence over the lake and the adjacent lake shore indicates a land breeze circulation is present and may be used to support the presence of a land breeze front	► no offshore winds	► winds light and variable

Merged Lake Breeze Boundary

This boundary forms when two lake breeze fronts collide and merge into a single convergence line. The two boundaries that make up this 'merged' boundary must be positively identified prior to merger. This boundary is typically quasi-stationary but may move slowly away from the position of the initial merger.

Platform	Positive Factors	Negative Factors	Ambiguous
Satellite (visible)	► line of cumulus clouds quasi-parallel to both shorelines	► persistent thick cloudiness over most or all of either lake	► no cloud visible ► thin cirrostratus or broken mid-level clouds prevents seeing cumulus clouds
Radar (LogZ, Vr)	► fine line in clear air reflectivity quasi-parallel to both shorelines ► shift in radial velocity along fine line	► large area of persistent precipitation over region	► no clear air echoes ► fine line or gradient in clear air echoes not well defined
Surface (Stn plots, time series)	► rapid shift in wind direction (may be accompanied by rapid change in wind speed, temperature, dew point) ► elongated area of convergence quasi-parallel to both shorelines	► no onshore winds	► often very subtle surface gradients at boundaries in moderate / high low-level wind regimes

Outflow Boundary

An outflow boundary separates relatively warm air from the relatively cool air associated with outflow from a shower or thunderstorm. This boundary is typically fast moving initially, but may become slow moving or quasi-stationary.

Platform	Positive Factors	Negative Factors	Ambiguous
Satellite (visible, infrared)	► line of cumulus clouds or sharp gradient in cumulus cloudiness quasi-concentric around area of convection or in a line ahead of a linear convective system ► gradual movement of above away from area of convection	► none	► no cloud visible ► thin cirrostratus or broken mid-level clouds prevents seeing cumulus clouds
Radar (LogZ, Vr)	► fine line or sharp gradient in clear air reflectivity quasi-concentric around area of convection or in a line ahead of a linear convective system ► shift in radial velocity quasi-concentric around area of convection or in a line ahead of a linear convective system ► gradual movement of above away from area of convection	► none	► no clear air echoes ► fine line or gradient in clear air echoes not well defined
Surface (Stn plots, time series)	► a rapid shift in wind direction (may also be accompanied by a decrease in temperature, a sharp increase in wind speed and an increase in dew point) for at least two neighbouring stations resulting in a pattern of winds diverging from a small area (that is not a lake)	► none	► often subtle surface gradients with old outflow boundaries ► outflow boundary may take on a linear formation, making it difficult to distinguish from an unknown boundary

Hybrid Boundary

This is a boundary that is formed when a lake breeze front merges with a gust front or another low-level boundary which is not a lake breeze. The two boundaries that make up this 'hybrid' boundary must be positively identified prior to merger. The hybrid boundary may be quasi-stationary or continue to move.

Platform	Positive Factors	Negative Factors	Ambiguous
Satellite (visible)	► line of cumulus clouds or sharp gradient in cumulus cloudiness quasi-parallel to shoreline and area of convection	► persistent thick cloudiness over most or all of lake	► no cloud visible ► thin cirrostratus or broken mid-level clouds prevents seeing cumuliform clouds
Radar (LogZ, Vr)	► fine line or sharp gradient in clear air reflectivity quasi-parallel to shoreline and area of convection ► shift in radial velocity along fine line	► large area of persistent precipitation over region	► no clear air echoes ► fine line or gradient in clear air echoes not well defined
Surface (Stn plots, time series)	► rapid shift in wind direction (may be accompanied by rapid change in wind speed, temperature, dew point) ► elongated area of convergence quasi-parallel to shoreline	► no onshore winds	► often very subtle surface gradients at boundaries in moderate / high low-level wind regimes

Other Boundary

This category includes boundaries generated by boundary-layer processes not described above, such as strong horizontal convective rolls, temperature gradients at the interface between clear and cloudy skies, changes in friction or terrain, etc. In addition, it includes boundaries whose source cannot be identified. Boundaries in this category may be quasi-stationary or moving.

Platform	Positive Factors	Negative Factors	Ambiguous
Satellite (visible)	► line of cumulus clouds or sharp cloudiness gradient	► none	► no cloud visible ► thin cirrostratus or broken mid-level clouds prevents seeing cumuliform clouds
Radar (LogZ, Vr)	► fine line or sharp gradient in clear air reflectivity ► shift in radial velocity along fine line	► none	► no clear air echoes ► fine line or gradient in clear air echoes not well defined
Surface (Stn plots, time series)	► rapid shift in wind direction (may be accompanied by rapid change in wind speed, temperature, dew point) ► elongated area of persistent convergence between surface stations	► none	► often very subtle surface gradients at boundaries in moderate / high wind regimes

Appendix J

The following are the results for lake breeze front occurrence corresponding to Lake Huron and Lake Erie. Results are shown for 1500 UTC, 1800 UTC and 2100 UTC. A 'Y' indicates a 'yes' for lake breeze occurrence for the time in question. A blank space indicates that the lake breeze front did not occur for the corresponding lake during the time in question. Note that days highlighted in blue have at least one of the data sets missing for the time of analysis. Therefore when statistical comparison is done between data sets, this entry must be disregarded.

1500 UTC Results											
		MESONET		**RADAR**		**SATELLITE**		**INTEGRATED**		**FINAL**	
Month	**Day**	**Huron**	**Erie**	**Huron**	**Erie**	**Huron**	**Erie**	**Huron**	**Erie**	**Huron**	**Erie**
June	1										
	2										
	3										
	4	Y						Y		Y	
	5	Y								Y	
	6	Y						Y		Y	
	7		Y	Y				Y		Y	Y
	8		Y								Y
	9	Y	Y	Y				Y	Y	Y	Y
	10	Y	Y			Y		Y	Y	Y	Y
	11	Y				Y		Y	Y	Y	Y
	12										
	13	Y					Y	Y		Y	Y
	14	Y								Y	
	15										
	16					Y				Y	
	17					Y		Y		Y	Y
	18										
	19								Y		Y
	20										
	21		Y						Y		Y
	22										
	23	Y		Y				Y		Y	
	24	Y	Y	Y				Y	Y	Y	Y
	25							Y		Y	
	26	Y						Y		Y	Y
	27		Y					Y	Y	Y	Y
	28	Y						Y	Y	Y	Y
	29		Y					Y		Y	Y
	30						Y		Y		Y
July	1										

	2					Y				Y	
	3										
	4										
	5					Y		Y		Y	
	6										Y
	7										
	8										
	9		Y						Y		Y
	10		Y					Y	Y	Y	Y
	11					Y				Y	
	12					Y				Y	
	13										
	14										
	15	Y						Y		Y	
	16							Y		Y	
	17										
	18		Y						Y	Y	Y
	19							Y		Y	
	20		Y								
	21										
	22		Y				Y				
	23		Y	Y			Y		Y	Y	Y
	24	Y	Y			Y	Y	Y		Y	Y
	25		Y						Y		Y
	26										
	27						Y				
	28										
	29										
	30						Y				Y
	31	Y						Y		Y	
August	1							Y	Y	Y	Y
	2									Y	Y
	3										
	4			Y				Y		Y	
	5	Y	Y					Y	Y	Y	Y
	6		Y								
	7										Y
	8										Y
	9		Y						Y		Y
	10										
	11	Y	Y			Y		Y	Y	Y	Y
	12	Y						Y		Y	
	13					Y		Y		Y	
	14										
	15						Y				
	16	Y									

	17			Y			Y				Y
	18		Y								Y
	19										
	20										
	21										
	22										Y
	23										
	24		Y								Y
	25										
	26						Y				Y
	27			Y				Y	Y	Y	Y
	28										
	29	Y	Y					Y		Y	Y
	30										
	31										

*1500 UTC days marked in blue:
No radar images available – June 20, July 5, and August 13, 14, 15, 23
No satellite images available – August 1, 2

1800 UTC Results											
		MESONET		**RADAR**		**SATELLITE**		**INTEGRATED**		**FINAL**	
Month	**Day**	**Huron**	**Erie**	**Huron**	**Erie**	**Huron**	**Erie**	**Huron**	**Erie**	**Huron**	**Erie**
June	1										
	2										
	3										
	4	Y	Y					Y	Y	Y	Y
	5	Y	Y			Y		Y	Y	Y	Y
	6	Y				Y		Y		Y	
	7		Y	Y			Y	Y	Y	Y	Y
	8		Y			Y	Y	Y	Y	Y	Y
	9	Y	Y	Y		Y	Y	Y	Y	Y	Y
	10	Y	Y		Y	Y	Y	Y	Y	Y	Y
	11	Y				Y		Y	Y	Y	Y
	12	Y								Y	
	13	Y		Y	Y	Y	Y	Y	Y	Y	Y
	14	Y		Y		Y		Y		Y	
	15					Y		Y		Y	
	16							Y	Y	Y	Y
	17					Y	Y	Y		Y	Y
	18										
	19			Y				Y	Y	Y	Y
	20	Y						Y	Y	Y	Y
	21	Y	Y					Y	Y	Y	Y
	22					Y		Y		Y	
	23	Y	Y			Y	Y	Y	Y	Y	Y
	24	Y	Y	Y		Y	Y	Y	Y	Y	Y

	25		Y	Y	Y	Y	Y	Y	Y	Y	Y
	26	Y		Y		Y		Y		Y	Y
	27	Y	Y	Y		Y	Y	Y	Y	Y	Y
	28	Y	Y			Y	Y	Y	Y	Y	Y
	29		Y			Y	Y	Y	Y	Y	Y
	30					Y	Y	Y	Y	Y	Y
July	1					Y					
	2					Y		Y	Y	Y	Y
	3										
	4					Y				Y	
	5					Y		Y		Y	
	6	Y	Y					Y	Y	Y	Y
	7										
	8							Y	Y	Y	
	9	Y	Y					Y	Y	Y	Y
	10	Y	Y			Y		Y	Y	Y	Y
	11	Y				Y		Y		Y	
	12					Y		Y		Y	
	13					Y		Y		Y	
	14	Y	Y			Y		Y	Y	Y	Y
	15	Y	Y	Y	Y	Y	Y	Y	Y	Y	Y
	16			Y			Y	Y	Y	Y	Y
	17	Y		Y				Y		Y	
	18	Y	Y	Y		Y	Y	Y	Y	Y	Y
	19	Y	Y	Y		Y	Y	Y	Y	Y	Y
	20	Y	Y	Y		Y		Y		Y	
	21						Y		Y		Y
	22	Y	Y	Y		Y	Y	Y	Y	Y	Y
	23		Y		Y	Y	Y	Y	Y	Y	Y
	24	Y	Y		Y	Y	Y	Y	Y	Y	Y
	25										
	26			Y		Y	Y	Y	Y	Y	Y
	27	Y	Y	Y			Y	Y	Y	Y	
	28										Y
	29	Y		Y		Y	Y	Y		Y	Y
	30	Y		Y		Y	Y	Y	Y	Y	Y
	31	Y	Y	Y			Y	Y	Y	Y	Y
August	1	Y		Y				Y	Y	Y	Y
	2								Y		Y
	3		Y			Y		Y	Y	Y	Y
	4		Y	Y			Y	Y	Y	Y	Y
	5	Y	Y				Y	Y	Y	Y	Y
	6			Y	Y			Y	Y	Y	Y
	7	Y				Y	Y	Y	Y	Y	Y
	8		Y	Y				Y	Y	Y	Y
	9		Y		Y	Y	Y	Y	Y	Y	Y

	10	Y	Y			Y	Y	Y	Y	Y	Y
	11	Y	Y			Y		Y	Y	Y	Y
	12	Y		Y		Y		Y		Y	
	13					Y	Y	Y	Y	Y	Y
	14	Y				Y	Y	Y	Y	Y	Y
	15			Y	Y		Y	Y	Y	Y	Y
	16										
	17			Y							
	18	Y	Y	Y				Y		Y	Y
	19										
	20						Y		Y		Y
	21	Y	Y	Y			Y	Y	Y	Y	Y
	22										Y
	23		Y	Y		Y	Y	Y	Y	Y	Y
	24	Y	Y	Y		Y	Y	Y	Y	Y	Y
	25					Y	Y	Y	Y	Y	
	26										
	27			Y	Y		Y	Y	Y	Y	Y
	28	Y				Y		Y		Y	
	29	Y	Y		Y	Y	Y	Y	Y	Y	Y
	30								Y		Y
	31										

*1800 UTC days marked in blue:
No radar images available – June 4, July 5, and August 13, 14
No satellite images available – August 1, 2

2100 UTC Results											
		MESONET		**RADAR**		**SATELLITE**		**INTEGRATED**		**FINAL**	
Month	**Day**	**Huron**	**Erie**	**Huron**	**Erie**	**Huron**	**Erie**	**Huron**	**Erie**	**Huron**	**Erie**
June	1										
	2					Y					
	3										
	4	Y	Y				Y	Y	Y	Y	Y
	5	Y	Y					Y			Y
	6	Y		Y				Y		Y	
	7		Y	Y	Y	Y	Y	Y	Y	Y	Y
	8		Y			Y	Y	Y	Y	Y	Y
	9	Y	Y	Y	Y	Y		Y	Y	Y	Y
	10				Y		Y	Y	Y	Y	Y
	11	Y				Y		Y	Y	Y	Y
	12		Y			Y	Y	Y	Y	Y	Y
	13	Y		Y		Y	Y	Y	Y	Y	Y
	14	Y		Y		Y		Y		Y	
	15							Y		Y	
	16		Y					Y	Y	Y	Y
	17		Y			Y		Y	Y	Y	Y

	18										
	19			Y		Y	Y	Y	Y	Y	Y
	20	Y		Y				Y		Y	
	21	Y									
	22					Y		Y		Y	
	23	Y	Y	Y		Y		Y	Y	Y	Y
	24	Y	Y		Y	Y	Y	Y	Y	Y	Y
	25		Y	Y	Y	Y	Y	Y	Y	Y	Y
	26	Y		Y		Y	Y	Y	Y	Y	Y
	27	Y	Y	Y		Y	Y	Y	Y	Y	Y
	28		Y		Y	Y	Y	Y	Y	Y	Y
	29		Y	Y	Y	Y	Y	Y	Y	Y	Y
	30					Y	Y	Y	Y	Y	Y
July	1										
	2		Y						Y		Y
	3										
	4					Y					Y
	5										
	6		Y					Y	Y	Y	Y
	7										
	8								Y	Y	Y
	9		Y			Y	Y	Y	Y	Y	Y
	10	Y	Y				Y	Y	Y	Y	Y
	11							Y		Y	
	12	Y								Y	
	13							Y		Y	
	14		Y				Y		Y		Y
	15		Y		Y	Y	Y	Y	Y	Y	Y
	16							Y	Y	Y	Y
	17	Y						Y		Y	
	18	Y	Y	Y		Y	Y	Y	Y	Y	Y
	19	Y	Y	Y		Y	Y	Y	Y	Y	Y
	20	Y	Y			Y		Y		Y	
	21										
	22		Y		Y	Y	Y	Y	Y	Y	Y
	23			Y				Y		Y	
	24	Y	Y				Y	Y	Y	Y	Y
	25							Y			
	26		Y	Y		Y	Y	Y	Y	Y	Y
	27	Y	Y	Y	Y			Y	Y	Y	Y
	28										Y
	29	Y					Y	Y		Y	Y
	30	Y		Y		Y	Y	Y	Y	Y	Y
	31	Y		Y	Y		Y	Y	Y	Y	Y
August	1	Y			Y			Y	Y	Y	Y
	2								Y		Y

	3		Y			Y		Y	Y	Y	Y
	4	Y	Y	Y	Y		Y	Y	Y	Y	Y
	5	Y						Y	Y	Y	Y
	6		Y	Y	Y			Y	Y	Y	Y
	7	Y					Y		Y	Y	Y
	8		Y	Y	Y		Y		Y	Y	Y
	9				Y	Y	Y	Y	Y	Y	Y
	10					Y		Y		Y	Y
	11		Y		Y	Y		Y	Y	Y	Y
	12	Y		Y		Y		Y		Y	Y
	13							Y		Y	
	14		Y					Y	Y	Y	Y
	15			Y				Y	Y	Y	Y
	16										
	17										
	18	Y		Y	Y	Y		Y	Y	Y	Y
	19										
	20										
	21		Y	Y	Y		Y	Y	Y	Y	Y
	22										Y
	23		Y	Y		Y	Y	Y	Y	Y	Y
	24	Y	Y	Y	Y	Y	Y	Y	Y	Y	Y
	25						Y	Y	Y	Y	Y
	26										
	27			Y	Y			Y	Y		Y
	28					Y		Y		Y	
	29		Y		Y			Y	Y	Y	Y
	30										
	31										

*2100 UTC days marked in blue:
No radar images available – July 9, and August 13, 14
No satellite images available – August 1, 2

Appendix K

The following Appendix shows the results found for the distances of the lake breeze fronts from their corresponding shoreline. Distances are noted to the nearest kilometer. Positive distances indicate lake breeze fronts on the land side of the shoreline and negative distances indicate lake breeze fronts on the lake side of the shoreline. A distance of zero kilometers would indicate fronts lying directly over the shoreline of their corresponding lake.

Results for 1800 UTC and 2100 UTC are shown. Each analysis is compared to the Final 'truth' Set by comparing the lake breeze fronts that exist for both analyses at the corresponding time. This is shown for both Lake Erie and Lake Huron. Note that Port Stanley was the shore reference location for Lake Erie and Port Franks was the shore reference location for Lake Huron. Distances were measured perpendicular to the shoreline, at the shoreline location closest to these stations.

1800 UTC Results

ERIE LAKE BREEZE 1800 UTC			
		Distances from the Lake Shore (km)	
MONTH	**DAY**	**FINAL**	**MESONET**
June	7	6	6
	8	2	4
	9	36	27
	10	28	21
	21	20	17
	23	4	7
	24	13	15
	25	31	40
	27	27	22
	28	17	13
	29	22	22
July	6	-4	-3
	9	8	8
	10	3	7
	14	-14	-12
	15	16	16
	18	12	15
	19	35	37
	23	45	28
	24	14	12
	31	21	40
August	3	5	3
	4	4	6

	8	13	15
	10	-4	-17
	11	7	4
	18	23	18
	21	4	5
	23	4	7
	24	12	13
	29	10	11

		HURON LAKE BREEZE 1800 UTC	
		Distances from the Lake Shore (km)	
MONTH	**DAY**	**FINAL**	**MESONET**
June	5	26	22
	9	21	20
	13	5	5
	14	5	7
	21	16	14
	24	19	17
	26	5	6
	27	1	6
July	18	6	5
	19	5	6
	20	2	5
	27	1	4
	30	3	5
	31	5	5
August	5	17	16
	12	3	5
	18	4	5
	24	7	6

		ERIE LAKE BREEZE 1800 UTC	
		Distances from the Lake Shore (km)	
MONTH	**DAY**	**FINAL**	**RADAR**
June	10	28	28
	13	38	39
	25	31	30
July	23	45	45
	24	14	13
August	6	25	25
	9	24	24
	27	17	16
	29	10	9

HURON LAKE BREEZE 1800 UTC			
		Distances from the Lake Shore (km)	
MONTH	**DAY**	**FINAL**	**RADAR**
June	13	5	5
	14	5	1
	19	14	15
	25	18	9
	26	5	3
July	15	25	24
	16	3	4
	18	6	4
	19	5	5
	26	15	13
	27	1	1
	30	3	2
	31	5	2
August	4	26	26
	6	15	15
	8	57	7
	12	3	2
	18	4	5
	24	7	5
	27	11	11

ERIE LAKE BREEZE 1800 UTC			
		Distances from the Lake Shore (km)	
MONTH	**DAY**	**FINAL**	**SATELLITE**
June	9	36	38
	10	28	23
	13	38	33
	25	31	29
	27	27	20
	28	17	20
	29	22	24
	30	20	21
July	15	16	15
	18	12	7
	19	35	31
	22	44	27
	23	45	48
	24	14	12
	29	29	30
	30	19	13
	31	21	21
August	4	4	-3
	7	6	6

	21	4	3
	24	12	7
	27	17	15
	29	10	7

HURON LAKE BREEZE 1800 UTC			
		Distances from the Lake Shore (km)	
MONTH	**DAY**	**FINAL**	**SATELLITE**
June	13	5	0
	25	18	14
	26	5	-4
	28	12	13
	29	8	7
	30	13	9
July	18	6	4
	19	5	-4
	20	2	0
	22	1	-3
	24	2	2
	24	26	27
	26	15	7
August	9	7	3
	11	15	15
	12	3	0
	24	7	-3
	29	22	9

ERIE LAKE BREEZE 1800 UTC			
		Distances from the Lake Shore (km)	
MONTH	**DAY**	**FINAL**	**INTEGRATED**
June	7	6	4
	8	2	2
	9	36	36
	10	28	28
	13	38	37
	16	-20	-23
	19	25	22
	20	5	5
	21	20	14
	23	4	4
	24	13	16
	25	31	31
	27	27	19
	28	17	19
	29	22	22

	30	20	20
July	6	-4	-4
	9	8	8
	10	3	3
	14	-14	-12
	15	16	16
	18	12	12
	19	35	30
	22	44	44
	23	45	43
	24	14	17
	30	19	18
	31	21	23
August	3	5	5
	4	4	4
	5	20	20
	6	25	25
	7	6	8
	8	13	15
	9	24	22
	10	-4	-3
	11	7	7
	15	32	31
	20	10	3
	21	4	4
	23	4	4
	24	12	9
	27	17	18
	29	10	10

HURON LAKE BREEZE 1800 UTC			
		Distances from the Lake Shore (km)	
MONTH	**DAY**	**FINAL**	**INTEGRATED**
June	5	26	24
	9	21	21
	10	6	6
	13	5	5
	14	5	5
	19	14	14
	20	-4	-5
	21	16	13
	23	34	34
	24	19	18
	25	18	18
	26	5	5
	27	1	3

	27	21	18
	28	12	12
	29	8	8
	30	13	11
July	15	25	24
	16	3	3
	17	0	-1
	18	6	6
	19	5	5
	20	2	2
	22	1	2
	23	2	2
	24	2	4
	24	26	30
	26	15	8
	27	1	1
	29	-4	-6
	30	3	3
	31	5	5
August	4	26	27
	5	17	17
	6	15	16
	7	57	57
	8	57	57
	9	7	5
	11	15	15
	12	3	3
	15	5	5
	18	4	4
	23	7	7
	24	7	7
	27	11	11
	29	22	22

2100 UTC Results

ERIE LAKE BREEZE 2100 UTC			
		Distances from the Lake Shore (km)	
MONTH	**DAY**	**FINAL**	**MESONET**
June	4	3	2
	7	16	13
	8	3	3
	9	49	42
	12	5	2
	16	-2	-7

	17	-7	-13
	23	16	13
	24	21	25
	25	43	37
	27	44	31
	28	37	26
	29	58	37
July	2	8	1
	6	5	3
	10	15	15
	14	-7	-8
	15	28	28
	18	36	32
	22	65	52
	24	17	10
	27	26	31
August	3	5	5
	4	17	20
	6	37	14
	8	23	13
	11	13	17
	21	14	17
	23	16	15
	24	17	28
	29	16	24

		HURON LAKE BREEZE 2100 UTC	
		Distances from the Lake Shore (km)	
MONTH	**DAY**	**FINAL**	**MESONET**
June	6	28	21
	9	43	38
	13	6	4
	20	6	7
	26	7	6
	27	11	9
July	10	34	5
	17	8	5
	18	16	17
	27	14	15
	30	11	20
	31	10	16
August	5	25	23
	12	6	6
	18	13	16
	24	27	20

ERIE LAKE BREEZE 2100 UTC			
		Distances from the Lake Shore (km)	
MONTH	**DAY**	**FINAL**	**RADAR**
June	7	16	15
	9	49	49
	10	63	64
	25	43	43
	28	37	37
	29	58	58
July	15	28	28
	31	44	46
August	4	17	15
	6	37	37
	8	23	21
	11	13	13
	18	42	42
	21	14	12
	24	17	19
	27	46	45
	29	16	15

HURON LAKE BREEZE 2100 UTC			
		Distances from the Lake Shore (km)	
MONTH	**DAY**	**FINAL**	**RADAR**
June	9	43	43
	13	6	4
	25	33	33
	26	7	6
	27	11	10
July	18	16	17
	19	6	6
	30	11	10
	31	10	10
August	4	53	52
	6	17	17
	8	38	38
	12	6	5
	18	13	12
	23	58	58
	24	27	27

ERIE LAKE BREEZE 2100 UTC			
		Distances from the Lake Shore (km)	
MONTH	**DAY**	**FINAL**	**SATELLITE**
June	7	16	26

	8	3	4
	10	63	53
	13	35	36
	19	24	20
	25	43	40
	30	26	26
July	10	15	8
	22	65	64
	24	17	14
	31	44	47
August	4	17	12
	7	25	22
	8	23	25
	21	14	13
	24	17	20

		HURON LAKE BREEZE 2100 UTC	
		Distances from the Lake Shore (km)	
MONTH	**DAY**	**FINAL**	**SATELLITE**
June	8	75	77
	9	43	35
	19	32	24
	23	59	52
	24	50	56
	25	33	36
	26	7	0
	28	43	31
	30	17	13
July	26	36	28
	30	11	5
August	12	6	3
	23	58	38
	24	27	18

		ERIE LAKE BREEZE 2100 UTC	
		Distances from the Lake Shore (km)	
MONTH	**DAY**	**FINAL**	**INTEGRATED**
June	4	3	-2
	7	16	16
	8	3	3
	9	49	48
	10	63	63
	11	-3	-3
	12	5	5
	16	-2	-5
	17	-7	-7

	19	24	24
	23	16	16
	24	21	21
	25	43	43
	27	44	44
	28	37	37
	29	58	55
	30	26	24
July	2	8	8
	6	5	5
	8	-21	-21
	10	15	15
	14	-7	-12
	15	28	28
	16	48	48
	18	36	36
	19	85	85
	22	65	65
	24	17	17
	26	-4	-4
	27	26	37
	30	28	29
	31	44	43
August	3	5	7
	4	17	16
	5	18	18
	6	37	36
	7	25	23
	8	23	21
	9	54	51
	11	13	11
	15	62	62
	18	42	41
	21	14	15
	23	16	16
	24	17	19
	27	46	46
	29	16	16

		HURON LAKE BREEZE 2100 UTC	
		Distances from the Lake Shore (km)	
MONTH	**DAY**	**FINAL**	**INTEGRATED**
June	4	47	47
	6	28	28
	10	21	19
	13	6	6

	19	32	30
	20	6	4
	24	50	57
	25	33	33
	26	7	9
	27	11	12
	28	43	45
	29	12	12
	30	17	17
July	15	49	49
	16	26	18
	17	8	18
	18	16	16
	19	6	6
	22	1	1
	24	39	39
	26	36	34
	27	14	14
	29	-3	-4
	30	11	11
	31	10	12
August	4	53	52
	5	25	25
	6	17	18
	11	50	50
	12	6	6
	15	-3	-3
	18	13	14
	21	67	67
	23	58	55
	24	27	26
	29	48	48

Appendix L

The following is a sample calculation (done through Excel) for the Pearson Correlation Coefficient. This example uses the Radar versus Final 'truth' Set results for Lake Erie for 1800 UTC. (Note: some values may be rounded due to column widths).

ERIE LAKE BREEZE 1800 UTC									
		Distance (km)			km-kmmean		(km-kmmean)^2		
MONTH	DAY	FINAL	RADAR		FINAL	RADAR	FINAL	RADAR	FINAL(km-kmmean) *RADAR(km-kmmean)
June	10	28	28		2.22222	2.5556	4.9383	6.5309	5.67901235
	13	38	39		12.2222	13.556	149.38	183.75	165.6790124
	25	31	30		5.22222	4.5556	27.272	20.753	23.79012347
July	23	45	45		19.2222	19.556	369.49	382.42	375.9012346
	24	14	13		-11.778	-12.444	138.72	154.86	146.5679012
August	6	25	25		-0.7778	-0.4444	0.6049	0.1975	0.34567901
	9	24	24		-1.7778	-1.4444	3.1605	2.0864	2.56790123
	27	17	16		-8.7778	-9.4444	77.049	89.198	82.90123455
	29	10	9		-15.778	-16.444	248.94	270.42	259.4567901
	MEAN	**25.78**	**25.444**			**SUM**	**1019.6**	**1110.2**	**1062.888889**

$$r_{xy} = (\sum_{i=1}^{n}[x_i' y_i']) / ([\sum_{i=1}^{n}(x_i')^2]^{1/2}[\sum_{i=1}^{n}(y_i')^2]^{1/2})$$

= (1062.889)/((SQRT(1019.556))*(SQRT(1110.222)))

= 0.999

Appendix M

Shown below are the first analysis CAPPI and MAXR results of 40 dBZ cells which initiated at a distance of 50 km or less from Exeter radar. These include cells which initiated between 1600 and 0000 UTC.

CAPPI					
40dBZ Cell Initiation Information - 1600 to 0000 UTC					
Cells considered within radius of 50 km from Radar					
Month	**Day**	**Cell #**	**Time**	**Distance to Closest Boundary (km)**	**Boundary Type**
June	1	None			
	2	61	2200	25	Gust Front
		80	2300	18	Gust Front
		83	2310	27	Gust Front
		84	2310	28	Gust Front
		85	2310	36	Gust Front
	3	None			
	4	None			
	5	None			
	6	None			
	7	None			
	8	None			
	9	None			
	10	256	2300	1	Gust Front
		257	2300	6	Gust Front
		258	2300	10	Gust Front
		259	2300	14	L Erie lbf
		260	2310	32	Gust Front
	11	None			
	12	None			
	13	None			
	14	None			
	15	None			
	16	None			
	17	None			
	18	None			
	19	None			
	20	None			
	21	98	2210	None	
		115	10	None	
	22	None			
	23	252	1810	6	L Huron lbf
		261	2010	13	Gust Front
		262	2010	2	L Huron lbf
		264	2110	6	Gust Front

		269	2210	0	Hybrid
		274	2300	4	Hybrid
		275	2300	10	Hybrid
		279	0	16	Gust Front
	24	None			
	25	None			
	26	None			
	27	None			
	28	553	2100	3	Hybrid
	29	None			
	30	654	1910	5	L Huron lbf
		765	10	55	Gust Front
		766	10	53	Gust Front
		767	10	44	Gust Front
July	1	None			
	2	None			
	3	None			
	4	1056	1910	21	L Huron lbf
		1068	2000	28	Gust Front
		1070	2000	23	Gust Front
		1073	2010	34	Gust Front
		1074	2010	11	L Erie lbf
		1075	2010	9	Gust Front
	5	None			
	6	None			
	7	None			
	8	None			
	9	None			
	10	None			
	11	None			
	12	None			
	13	None			
	14	None			
	15	None			
	16	None			
	17	1	2310	3	Other
	18	8	2300	10	L Erie lbf
		9	2300	8	Hybrid
		10	0	8	Gust Front
		11	0	4	Gust Front
	19	46	1900	10	Hybrid
		57	2010	14	Hybrid
		58	2010	17	Hybrid
		59	2010	2	Hybrid
		60	2010	5	Merged
		62	2010	4	L Huron lbf

		71	2100	11	Hybrid
		81	2210	9	Hybrid
	20	97	1900	5	L Huron lbf
		113	2000	6	Gust Front
		114	2000	4	Hybrid
		115	2000	5	Hybrid
		117	2010	17	Hybrid
		118	2010	20	Hybrid
	21	223	1810	31	Gust Front
		250	1900	21	Gust Front
		252	1900	47	Gust Front
		253	1900	35	Gust Front
		255	1900	5	Gust Front
		257	1910	31	Gust Front
		258	1910	30	Gust Front
		285	2000	22	Gust Front
		288	2010	32	Gust Front
		289	2010	29	Gust Front
		290	2010	9	Gust Front
		304	2100	69	Gust Front
		305	2100	32	Gust Front
		306	2100	42	Gust Front
		307	2100	38	Gust Front
		308	2100	31	Gust Front
		312	2110	57	Gust Front
		322	2200	123	Gust Front
	22	None			
	23	11	1700	21	L Huron lbf
		12	1700	8	L Huron lbf
		14	1710	10	L Erie lbf
		17	1710	8	Other
		14	1800	3	Gust Front
		15	1800	5	Gust Front
		18	1810	7	L Erie lbf
		19	1810	6	Gust Front
		44	1900	8	Gust Front
		62	2000	9	Gust Front
		82	2110	2	Gust Front
		95	2210	9	Gust Front
	24	None			
	25	None			
	26	None			
	27	None			
	28	None			
	29	None			
	30	None			

	31	None			
August	1	None			
	2	1	1710	16	L Huron lbf
		5	1810	35	L Erie lbf
		21	2200	6	Gust Front
		22	2210	6	Other
		29	2300	6	Gust Front
		30	2300	6	Gust Front
		38	0	6	Gust Front
	3	None			
	4	None			
	5	None			
	6	None			
	7	None			
	8	None			
	9	None			
	10	None			
	11	None			
	12	None			
	13	None	Note: Radar imagery is missing during this day		
	14	None	Note: Radar imagery is missing during this day		
	15	None	Note: some Radar imagery is missing during this day		
	16	27	1600	4	Gust Front
		28	1600	7	Gust Front
		29	1600	5	Gust Front
		31	1610	1	Gust Front
		32	1610	3	Gust Front
		42	1710	4	Gust Front
		46	1800	125	L Ont lbf
		47	1800	127	L Ont lbf
		48	1800	127	L Ont lbf
		55	2000	None	
		56	2000	None	
		58	2000	None	
		59	2000	None	
		60	2000	None	
		61	2010	None	
		62	2010	None	
	17	None			
	18	111	2200	8	L Huron lbf
	19	385	1610	None	
		386	1610	None	
		387	1610	None	

		398	1700	59	Gust Front
		399	1700	54	Gust Front
		400	1700	54	Gust Front
		401	1700	52	Gust Front
		404	1700	54	Gust Front
		405	1700	45	Gust Front
		407	1700	56	Gust Front
		408	1700	59	Gust Front
		410	1710	15	Gust Front
		428	1800	8	Gust Front
		433	1810	22	Gust Front
		434	1810	16	Gust Front
		456	1900	30	Gust Front
		458	1900	4	Gust Front
		459	1910	2	Gust Front
		477	2000	12	Gust Front
		478	2000	22	Gust Front
		483	2010	27	Gust Front
		506	2110	9	Gust Front
		507	2110	1	Gust Front
		508	2110	4	Gust Front
		526	2200	2	Gust Front
		529	2210	16	Gust Front
		531	2210	5	Gust Front
		534	2210	10	Gust Front
		551	2300	8	Gust Front
		554	2300	6	Gust Front
		555	2300	6	Gust Front
		556	2300	6	Gust Front
		557	2300	3	Gust Front
		558	2300	5	Gust Front
		561	2310	3	Gust Front
		563	2310	12	Gust Front
		586	0	1	Gust Front
		591	10	4	Gust Front
	20	727	1710	1	Other
		749	1800	0	Other
		751	1810	1	Gust Front
		754	1810	13	Gust Front
		772	1900	3	Other
		774	1910	1	Other
		775	1910	1	Other
		788	2000	1	Gust Front
		803	2100	11	Other
		805	2100	16	Other
	21	None			

	22	None			
	23	None			
	24	None			
	25	None			
	26	160	1900	11	Other
	27	None			
	28	None			
	29	None			
	30	None			
	31	None			

MAXR					
40dBZ Cell Initiation Information -1600 to 0000 UTC					
Cells considered within radius of 50 km from Radar					
Month	**Day**	**Cell #**	**Time**	**Distance to Closest Boundary (km)**	**Boundary Type**
June	1	None			
	2	110	2200	35	Gust Front
		137	2300	17	Gust Front
		138	2300	17	Gust Front
		140	2300	32	Gust Front
		142	2300	46	Gust Front
		143	2310	21	Gust Front
		145	2310	26	Gust Front
		163	0	98	L Ont lbf
		165	10	97	L Ont lbf
		166	10	97	L Ont lbf
		167	10	86	L Ont lbf
	3	None			
	4	None			
	5	None			
	6	None			
	7	None			
	8	None			
	9	118	2300	29	Merged
		119	2300	31	Merged
	10	264	2200	1	Gust Front
		265	2200	7	Gust Front
		266	2200	16	Gust Front
		271	2200	10	Gust Front
		272	2210	0	Gust Front
		291	2300	6	Gust Front
		292	2300	3	Gust Front
		293	2300	10	Gust Front
		294	2300	17	Gust Front
		295	2300	295	L Erie lbf

		297	2300	16	L Erie lbf
		298	2300	29	L Erie lbf
		299	2310	34	L Erie lbf
		300	2310	20	Gust Front
	11	None			
	12	None			
	13	None			
	14	None			
	15	None			
	16	None			
	17	None			
	18	None			
	19	1240	2110	27	Other
		1246	2210	9	L Huron lbf
	20	None			
	21	97	2100	100	L Huron lbf
		122	2310	None	
		123	2310	None	
		124	2310	None	
		138	0	None	
	22	None			
	23	406	1800	4	L Huron lbf
		423	2010	13	Gust Front
		425	2110	7	Gust Front
		428	2200	4	Gust Front
		429	2200	3	Hybrid
		430	2200	5	Gust Front
		431	2210	4	Hybrid
		438	2300	3	Hybrid
		439	2300	9	Gust Front
		441	2310	13	Hybrid
	24	None			
	25	None			
	26	None			
	27	None			
	28	None			
	29	723	2300	1	L Erie lbf
	30	778	1810	3	L Huron lbf
		787	1900	10	L Huron lbf
		789	1900	5	L Huron lbf
		805	2000	9	Hybrid
		809	2010	3	L Erie lbf
		810	2010	6	L Erie lbf
		899	2300	8	L Huron lbf
		931	0	38	Gust Front
		933	10	32	Gust Front

July	1	1185	1600	None	
	2	None			
	3	None			
	4	1383	1910	21	L Huron lbf
		1404	2000	36	L Erie lbf
		1408	2010	36	L Erie lbf
		1409	2010	2	L Erie lbf
		1410	2010	9	Gust Front
	5	None			
	6	None			
	7	135	1600	104	L Ont lbf
	8	None			
	9	None			
	10	None			
	11	None			
	12	None			
	13	None			
	14	None			
	15	None			
	16	None			
	17	1	2310	3	Other
	18	12	2300	10	L Erie lbf
		13	0	4	Gust Front
		14	10	8	Gust Front
	19	51	1900	10	Hybrid
		52	1910	3	Hybrid
		67	2010	13	Hybrid
		68	2010	2	Hybrid
		79	2110	10	Hybrid
		88	2200	8	Hybrid
		89	2200	9	Hybrid
	20	108	1900	5	L Huron lbf
		120	2000	7	Gust Front
		121	2000	5	Gust Front
		122	2000	7	Hybrid
		123	2000	5	Hybrid
		124	2000	18	Hybrid
		125	2010	16	Hybrid
		149	2200	6	Hybrid
	21	225	1710	34	Lake Erie lbf
		255	1810	29	Gust Front
		285	1900	13	Gust Front
		287	1900	46	Gust Front
		288	1900	33	Gust Front
		289	1900	47	Gust Front
		321	2000	8	Gust Front

		322	2000	34	Gust Front
		352	2100	60	Gust Front
		353	2100	31	Gust Front
		354	2100	32	Gust Front
		355	2100	36	Gust Front
		357	2110	37	Gust Front
		371	2200	111	Gust Front
		378	2210	92	Gust Front
		379	2210	129	Gust Front
		387	2300	103	Gust Front
	22	None			
	23	14	1700	1	Other
		15	1710	21	Other
		17	1710	2	Other
		18	1710	7	Other
		17	1800	5	Gust Front
		18	1800	11	Gust Front
		19	1800	3	Gust Front
		20	1800	7	Gust Front
		21	1800	9	Gust Front
		22	1800	3	Gust Front
		25	1810	2	Gust Front
		28	1810	6	L Erie lbf
		29	1810	2	L Erie lbf
		68	2010	1	Gust Front
		83	2100	13	Gust Front
		84	2100	10	Gust Front
		85	2110	10	Hybrid
		86	2110	1	Gust Front
		87	2110	9	Gust Front
		97	2210	0	Gust Front
		98	2210	28	Gust Front
	24	None			
	25	196	1710	168	Other
		197	1710	167	Other
		198	1710	160	Other
		203	1710	175	Other
		217	1800	157	L Huron lbf
		245	1900	176	L Huron lbf
		246	1900	139	L Huron lbf
		247	1900	136	L Huron lbf
		248	1900	132	L Huron lbf
		273	2000	None	
		281	2010	None	
		296	2100	47	Other
		297	2100	41	Other

	26	None			
	27	None			
	28	None			
	29	None			
	30	None			
	31	None			
August	1	None			
	2	1	1700	15	L Huron lbf
		2	1710	10	L Huron lbf
		25	2200	16	Other
		27	2210	9	Gust Front
		34	2300	3	Gust Front
		35	2300	11	Gust Front
		36	2300	11	Gust Front
	3	None			
	4	None			
	5	None			
	6	None			
	7	None			
	8	243	2200	27	Gust Front
		265	2300	57	Gust Front
	9	353	1910	2	L Huron lbf
	10	None			
	11	None			
	12	None			
	13	None	Note: Radar imagery is missing during this day		
	14	None	Note: Radar imagery is missing during this day		
	15	None	Note: Some Radar imagery is missing during this day		
	16	63	1600	29	Gust Front
		64	1600	14	Gust Front
		67	1600	33	Gust Front
		68	1600	42	Gust Front
		71	1600	5	Gust Front
		72	1610	8	Gust Front
		73	1610	2	Gust Front
		91	1700	12	Gust Front
		93	1710	4	Gust Front
		94	1710	33	Gust Front
		95	1710	13	Gust Front
		120	1810	123	L Ont lbf
		121	1810	118	L Ont lbf
		122	1810	124	L Ont lbf
		125	1810	158	L Ont lbf

		126	1810	130	L Ont lbf
		127	1810	131	L Ont lbf
		163	1900	None	
		164	1900	None	
		165	1900	None	
		166	1900	None	
		167	1900	None	
		168	1900	None	
		169	1900	None	
		170	1900	None	
		171	1900	None	
		172	1910	None	
		174	1910	None	
		176	1910	None	
		177	1910	None	
		216	2000	None	
		217	2000	None	
		219	2000	None	
		220	2000	None	
		221	2000	None	
		222	2000	None	
		223	2010	None	
		225	2010	None	
		226	2010	None	
		227	2010	None	
		228	2010	None	
		230	2010	None	
		257	2100	None	
		259	2110	None	
		274	2210	None	
		283	2310	45	Gust Front
		285	2310	37	Gust Front
		286	2310	37	Gust Front
		287	2310	41	Gust Front
		293	0	8	Other
	17	None			
	18	341	2200	8	L Huron lbf
	19	763	1600	None	
		764	1600	None	
		767	1610	None	
		768	1610	None	
		786	1700	60	Gust Front
		791	1700	58	Gust Front
		792	1700	58	Gust Front
		793	1710	77	Gust Front
		794	1710	44	Gust Front

		795	1710	44	Gust Front
		815	1800	9	Gust Front
		818	1810	13	Gust Front
		819	1810	25	Gust Front
		847	1900	7	Gust Front
		853	1900	4	Gust Front
		854	1900	7	Gust Front
		881	2010	11	Gust Front
		882	2010	16	Gust Front
		884	2010	10	Gust Front
		885	2010	13	Gust Front
		886	2010	15	Gust Front
		905	2110	13	Gust Front
		906	2110	3	Gust Front
		907	2110	0	Gust Front
		909	2110	0	Gust Front
		910	2110	13	Gust Front
		937	2200	2	Gust Front
		938	2200	8	Gust Front
		941	2200	0	Gust Front
		944	2210	15	Gust Front
		946	2210	5	Gust Front
		949	2210	15	Gust Front
		950	2210	1	Gust Front
		976	2300	8	Gust Front
		980	2300	0	Gust Front
		982	2300	1	Gust Front
		983	2300	6	Gust Front
		984	2300	6	Gust Front
		985	2300	13	Gust Front
		986	2300	11	Gust Front
		988	2310	4	Gust Front
		992	2310	18	Gust Front
		1013	0	3	Gust Front
		1015	0	2	Gust Front
		1016	0	10	Gust Front
	20	1174	1700	4	Gust Front
		1177	1710	1	Other
		1179	1710	1	Gust Front
		1180	1710	0	Gust Front
		1182	1710	3	Gust Front
		1183	1710	3	Gust Front
		1206	1800	1	Gust Front
		1207	1800	11	Other
		1208	1800	1	Gust Front
		1211	1810	9	Gust Front

		1212	1810	4	Gust Front
		1213	1810	0	Gust Front
		1232	1900	2	Other
		1234	1910	1	Other
		1235	1910	22	Gust Front
		1249	2000	4	Gust front
		1267	2100	11	Other
		1270	2100	16	Other
		1271	2110	1	Other
		1294	2300	2	Gust Front
		1300	10	15	Gust Front
	21	None			
	22	None			
	23	8	2010	4	L Huron lbf
		17	2100	2	L Huron lbf
	24	None			
	25	None			
	26	140	1600	18	Other
		141	1610	16	Other
		155	1810	1	Other
		162	1900	9	Other
	27	None			
	28	None			
	29	None			
	30	None			
	31	None			

Appendix N

This Appendix includes data collected from the second cell initiation analysis for the 1.0 km CAPPI and 1.0 km MAXR images, respectively. 40 dBZ cell initiations considered are within 80 km of Exeter radar. The data listed below includes the month, day, cell number, time, distance to the closest boundary (km), direction from the cell to the boundary, in front/behind/to the side, boundary type, boundary classification, latitude and longitude.

40 dBZ CAPPI Cells (manually corrected any errors that were visible in the cell tracking)										
Range: 80km from Exeter radar										
Time: 1600 to 0000 UTC										
Month	**Day**	**Cell #**	**Time**	**Distance to Closest Boundary (km)**	**Direction from the Cell to the Boundary**	**In front/ behind/ to the side (tts)?**	**Boundary Type**	**Boundary Classification**	**Latitude**	**Longitude**
June	2	46	2100	88	238	Ahead	Gust Front	Moving	43.165	-82.1896
		47	2100	92	237	Ahead	Gust Front	Moving	43.2143	-82.171
		59	2200	112	178	To the side	Gust Front	Moving	43.4087	-82.2002
		61	2200	35	345	To the side	Gust Front	Moving	43.0137	-81.5912
		62	2200	46	14	To the side	Gust Front	Moving	42.9239	-81.8425
		63	2200	100	186	To the side	Gust Front	Moving	43.2936	-82.0309
		70	2300	40	90	Behind	Gust Front	Moving	43.44	-81.612
		80	2300	17	145	To the side	Gust Front	Moving	43.572	-81.2482
		83/84	2310	28	68	Behind	Gust Front	Moving	43.3458	-81.4361
		65	0	80	105	Ahead	Ontario lbf	Moving	43.5331	-80.7932
	3	None								
	4	None								
	7	None								
	8	None								
	13	None								
	14	None								
	15	None								
	16	None								
	17	None								
	19	883	2110	7	163	Behind	Other	Synoptic	43.8438	-80.7018
		887	2210	5	336	Not tts	Merged (Huron/Erie)	Collision	43.2447	-80.4352

		893	2310	8	330	Not tts	Merged (Huron/Erie)	Collision	43.0584	-80.7054
		894	2310	3	319	Not tts	Merged (Huron/Erie)	Collision	42.9779	-80.9512
	22	None								
	23	252	1810	6	266	Ahead	L Huron lbf	Moving	43.6236	-81.4716
		255	1900	3	253	Not tts	Hybrid (Huron lbf/Gust Front)	Collision	43.424	-81.4298
		258	1900	5	268	Not tts	Hybrid (Huron lbf/Gust Front)	Collision	43.4995	-81.4392
		252/253	1910	6	277	Ahead for Huron - Not tts for Hybrid	Joint - Huron lbf and Hybrid joint (Huron lbf/gust front)	Collision	43.2437	-81.321
		261	2010	16	277	Ahead (Huron lbf) To the side (Hybrid)	Joint - Huron lbf/Hybrid Joint	Intersection	43.1045	-81.1298
		262	2010	2	229	To the side (Huron lbf and Hybrid)	Joint - Huron lbf/Hybrid Joint	Intersection	43.1334	-81.3097
		264	2110	6	359	Behind	Gust Front	Moving	43.5335	-81.2089
		267	2200	3	252	Not tts	Hybrid (Huron lbf/Gust Front)	Collision	43.4222	-81.2987
		269	2210	0	248	Not tts	Hybrid (Huron lbf/Gust Front)	Collision	43.4623	-81.3336
		272	2300	8	314	Behind	Gust Front	Moving	43.5102	-81.1914
		274	2300	4	268	Not tts	Hybrid (Huron lbf/Gust Front)	Collision	43.444	-81.259
		272	2310	6	316	Behind	Gust Front	Moving	43.5195	-81.2242
		279	0	15	326	Behind	Gust Front	Moving	43.5203	-81.1703
	24	None								
	25	None								
	26	None								
	27	None								
	28	551	2010	9	342	Not tts	Hybrid (Erie lbf/Gust Front)	Merger	42.8254	-81.2935
		553	2100	3	344	Not tts	Hybrid (Erie lbf/Gust Front)	Merger	42.9808	-81.1586
	29	None								
	30	637	1710	8	158	Ahead	Erie lbf	Moving	42.9343	-81.1197
		642	1810	2	200	Ahead	Erie lbf	Moving	42.9213	-80.8702
		654	1910	5	352	Ahead	Huron lbf	Stationary	43.1225	-81.6309
		683	2100	28	263	To the side	Erie lbf	Moving	43.0708	-80.68
		689	2110	19	288	To the side	Hybrid (Huron/GF)	Collision	43.3537	-80.4062
		743	2300	40	138	Behind	Gust Front	Moving	43.9141	-81.558
		739	2310	13	169	Behind	Gust Front	Moving	43.9226	-80.8257

		763	0	10	342	Behind	Erie lbf	Moving	43.0393	-80.664
		765	10	55	143	Behind	Gust Front	Moving	43.623	-81.547
		766	10	53	147	Behind	Gust Front	Moving	43.6271	-81.4999
July	1	None								
	2	None								
	5	No radar from 1600 to 1910								
		None								
	6	None								
	8	None								
	9	Radar data are missing for 1900 on								
		None								
	10	4	2110	13	149	Ahead	Erie lbf	Moving	42.7561	-81.6245
		21	0	8	9	Not tts	Hybrid (Erie/GFs)	Merger	42.9031	-81.2018
		22	0	8	12	Not tts	Hybrid (Erie/GFs)	Merger	42.9093	-81.2729
		24	0	13	345	Not tts	Hybrid (Erie/GFs)	Merger	42.8754	-81.3603
		25	0	10	133	Not tts	Hybrid (Erie/GFs)	Merger	42.9327	-81.7011
		24	10	24	310	Not tts	Hybrid (Erie/GFs)	Merger	42.759	-81.3411
	11	None								
	12	None								
	13	None								
	14	None								
	18	5	2010	10	164	Ahead	Erie lbf	Moving	42.856	-81.2602
		6	2010	10	113	To the side	Erie lbf	Moving	42.8043	-81.3436
		8	2300	10	120	To the side	Erie lbf	Moving	43.073	-81.3767
		9	2300	8	270	To the side	Hybrid (Erie/GF)	Merger	43.1455	-81.3624
		8	2310	8	298	To the side	Hybrid (Erie/GF)	Merger	43.1096	-81.3713
		10	0	8	269	Behind (GF Closest) ahead (GF Furthest)	Joint (where two gust fronts are coming together)	Intersection	43.1336	-81.5635
		11	0	4	239	Behind	Gust Front	Moving	43.1504	-81.6198
	22	404	2110	2	270	Not tts	Hybrid (Erie/GF)	Merger	43.3788	-80.431
	23	3	1610	42	209	To the side	Erie lbf	Moving	43.4486	-80.4609
		7	1700	21	236	Ahead(in terms of movement)	Other	Moving	43.3216	-81.3291
		12	1700	8	326	Ahead	Huron lbf	Stationary	43.3057	-81.6146
		12	1710	8	198	Ahead (in terms of movement)	Other	Moving	43.2899	-81.633
		14	1710	10	226	To the side	Erie lbf	Moving	43.0505	-81.0428
		16	1710	8	329	Behind	Erie lbf	Moving	42.7407	-81.4144
		6	1800	10	18	Behind	Gust Front	Moving	43.3843	-81.3255
		10	1800	13	269	Ahead	Gust Front	Moving	43.2391	-81.2539
		14	1800	3	309	Ahead	Gust Front	Moving	43.329	-80.9302

		6	1810	2	50	Behind	Gust Front	Moving	43.4411	-81.2398
		10	1810	9	334	Ahead	Gust Front	Moving	43.2342	-80.9671
		11	1810	5	254	Ahead	Gust Front	Moving	43.2634	-81.3607
		14	1810	3	314	Ahead	Gust Front	Moving	43.3042	-80.9609
		18	1810	7	271	To the side	Huron lbf	Moving	43.068	-81.0732
		25	1900	24	261	To the side	Gust Front	Moving	43.1731	-80.9857
		42	1900	14	65	Not tts	Hybrid (GF/Ont)	Merger	43.4381	-80.4473
		44	1900	8	212	Behind	Gust Front	Moving	43.2006	-81.2215
		62	2000	8	209	To the side	Gust Front	Moving	43.1904	-81.199
		82	2110	2	287	To the side	Gust Front	Moving	43.1094	-81.3846
		94	2210	2	337	Not tts	Hybrid(Huron/GF)	Collision	43.9019	-80.9919
		95	2210	9	178	Ahead	Gust Front	Moving	43.6071	-81.1379
	24	None								
	26	None								
	27	None								
	29	None								
	30	None								
	31	None								
August	3	None								
	4	None								
	5	None								
	6	None								
	7	None								
	9	None								
	10	None								
	11	None								
	13	No radar available for the whole period								
	14	No radar or satellite available for the whole period								
	15	None								
	17	None								
	19	382	1600	None	N/A	N/A	N/A	N/A	42.9999	-80.7155
		385	1610	None	N/A	N/A	N/A	N/A	43.1295	-81.4854
		386	1610	None	N/A	N/A	N/A	N/A	43.0465	-81.5369
		387	1610	None	N/A	N/A	N/A	N/A	43.3056	-81.4515
		390	1700	51	194	To the side	Gust Front	Moving	43.3911	-81.6179
		394	1700	58	208	To the side	Gust Front	Moving	43.4126	-81.4294
		395	1700	53	218	To the side	Gust Front	Moving	43.3284	-81.3617
		400	1700	54	248	Ahead	Gust Front	Moving	43.1367	-81.1518
		401	1700	52	218	To the side	Gust Front	Moving	43.3168	-81.3714
		408	1700	59	211	To the side	Gust Front	Moving	43.406	-81.3911
		410	1710	15	181	To the side	Gust Front	Moving	43.0848	-81.7606

		430	1800	45	91	Behind	Gust Front	Moving	43.181	-82.1703
		431	1800	37	103	Behind	Gust Front	Moving	43.3767	-82.0283
		424	1810	20	66	Ahead	Gust Front	Moving	43.3517	-81.5929
		433	1810	23	258	Ahead	Gust Front	Moving	43.4995	-80.9621
		434	1810	16	75	To the side	Gust Front	Moving	43.1365	-81.8073
		456	1900	30	33	Ahead	Gust Front	Moving	43.1228	-81.6812
		457	1900	54	40	Ahead	Gust Front	Moving	42.9947	-81.9332
		458	1900	4	221	Behind	Gust Front	Moving	43.4034	-81.4862
		437	1910	13	150	Ahead	Gust Front	Moving	43.7979	-81.3014
		453	1910	7	20	Ahead	Gust Front	Moving	43.2964	-81.5092
		459	2000	15	199	Ahead	Gust Front	Moving	43.8438	-81.184
		464	2000	52	54	Ahead	Gust Front	Moving	43.0828	-82.0107
		478	2000	22	267	Ahead	Gust Front	Moving	43.5697	-80.9423
		480	2000	11	185	To the side	Gust Front	Moving	43.3059	-81.9969
		463	2010	69	35	Ahead	Gust Front	Moving	42.8517	-81.9764
		468	2010	11	115	Behind	Gust Front	Moving	43.5408	-81.3642
		471	2010	57	36	Ahead	Gust Front	Moving	42.9409	-81.9108
		477	2010	12	192	To the side	Gust Front	Moving	43.4935	-81.4603
		483	2010	27	202	To the side	Gust Front	Moving	43.4332	-81.8841
		502	2100	14	102	To the side	Gust Front	Moving	43.4774	-82.0336
		468	2110	4	107	Behind	Gust Front	Moving	43.7514	-81.0786
		486	2110	3	107	Behind	Gust Front	Moving	43.1366	-81.6927
		501	2110	12	102	To the side	Gust Front	Moving	43.4761	-82.0241
		506	2110	10	124	Behind	Gust Front	Moving	43.6006	-81.2423
		515	2200	4	72	Behind	Gust Front	Moving	43.5451	-81.4441
		517	2200	1	116	Behind	Gust Front	Moving	42.942	-81.5297
		522	2200	26	287	Ahead	Gust Front	Moving	42.6804	-81.3023
		526	2210	2	179	Behind	Gust Front	Moving	43.451	-81.378
		527	2210	24	88	Behind	Gust Front	Moving	43.8039	-81.1772
		529	2210	16	111	Behind	Gust Front	Moving	43.7207	-81.0575
		531	2210	5	135	Behind	Gust Front	Moving	43.3002	-81.4803
		499	2300	1	177	Ahead	Gust Front	Moving	43.3544	-81.2126
		550	2300	24	161	To the side	Gust Front	Moving	43.8843	-81.2588
		551	2300	8	68	Behind	Gust Front	Moving	43.6186	-81.2384
		553	2300	0	190	Slightly behind	Gust Front	Moving	43.474	-81.2644
		554	2300	6	13	Ahead	Gust Front	Moving	43.4243	-81.3189
		555	2300	6	359	Ahead	Gust Front	Moving	43.4216	-81.283
		556	2300	6	138	Ahead	Gust Front	Moving	43.3868	-81.2752
		536	2310	10	117	Behind	Gust Front	Moving	43.7557	-81.0629
		547	2310	1	54	Behind	Gust Front	Moving	43.2638	-81.0705
		560	2310	8	129	Behind	Gust Front	Moving	43.7924	-81.0039

		561	2310	3	88	Behind	Gust Front	Moving	43.2149	-81.0804
		563	2310	37	15	To the side	Gust Front	Moving	43.0257	-81.293
		563	0	2	56	Behind	Gust Front	Moving	43.4631	-80.867
		581	0	3	51	Behind	Gust Front	Moving	43.4105	-80.8424
		585	0	3	272	Ahead	Gust Front	Moving	43.6051	-80.8407
		586	0	16	139	Behind	Gust Front	Moving	43.0805	-81.0513
		563	10	3	277	Ahead	Joint (where two gust fronts are interacting)	Merger	43.5479	-80.8553
		576	10	0	26	Slightly behind	Gust Front	Moving	43.4216	-80.7944
		585	10	1	132	Behind	Gust Front	Moving	43.6814	-80.8693
		586	10	14	142	Behind	Gust Front	Moving	43.0302	-81.1056
	20	725	1700	14	165	Ahead	Erie lbf	Moving	42.9105	-80.6409
		727	1710	1	138	Behind (only in movement)	Other	Moving	43.3264	-81.005
		728	1710	21	12	To the side	Gust Front	Moving	42.939	-81.5983
		739	1800	10	211	To the side	Other	Moving	43.3441	-80.8903
		749	1800	0	109	Slightly behind (only in movement)	Other	Moving	43.3466	-81.0771
		743	1810	9	289	Behind	Gust Front	Moving	43.1993	-81.3965
		749	1810	0	331	Slightly ahead (only in movement)	Other	Moving	43.2586	-80.9666
		751	1810	1	87	Behind	Gust Front	Moving	43.5088	-81.1722
		754	1810	4	50	Ahead	Gust Front	Moving	43.0929	-81.5297
		769	1900	5	359	Behind	Erie lbf	Moving	42.7628	-80.9817
		772	1900	3	127	Behind (only in movement)	Other	Moving	43.5331	-80.9415
		763	1910	6	198	Ahead	Gust Front	Moving	43.0688	-80.8766
		774	1910	1	88	Behind (only in movement)	Other	Moving	43.3969	-81.0269
		775	1910	1	17	To the side	Other	Moving	43.3654	-81.0127
		779	2000	29	187	Ahead	Erie lbf	Moving	43.1263	-80.6409
		786	2000	69	232	Behind	Gust Front	Moving	43.7875	-80.7834
		787	2000	38	198	Ahead	Erie lbf	Moving	43.1912	-80.5416
		788	2000	1	269	Behind	Gust Front	Moving	43.2904	-81.4409
		786	2010	66	237	Behind	Gust Front	Moving	43.7256	-80.7743
		790	2010	1	179	Ahead	Erie lbf	Moving	42.86	-80.7595
		795	2100	5	111	Behind (only in movement)	Other	Moving	43.606	-81.1559
		803	2100	11	267	Ahead (only in movement)	Other	Moving	43.4961	-80.9732
		805	2100	16	333	To the side	Other	Moving	43.2352	-81.0207
		805	2110	10	17	To the side	Other	Moving	43.2741	-81.1467

		795	2200	38	9	Ahead	Gust Front	Moving	43.3333	-80.9795
		815	2200	8	34	Ahead	Gust Front	Moving	43.6239	-80.9807
		807	2210	15	358	Ahead	Gust Front	Moving	43.5437	-80.8664
		808	2210	N/A	N/A	N/A	N/A	N/A	43.777	-80.8567
		808	2300	2	254	Behind	Gust Front	Moving	43.7098	-81.0786
		823	2300	N/A	N/A	N/A	N/A	N/A	43.4255	-80.6321
	21	None								
	23	None								
	24	None								
	26	133	1610	14	143	Ahead	Erie lbf	Moving	42.992	-81.2743
		139	1700	66	327	Ahead	Other	Synoptic	42.9895	-80.9326
		160	1900	11	137	Behind	Other	Synoptic	43.0809	-81.5204
	28	None								
	29	None								
	31	None								

40 dBZ MAXR Cells (manually corrected any errors that were visible in the cell tracking)

Range: 80km from Exeter radar

Time: 1600 to 0000 UTC

Month	Day	Cell #	Time	Distance to Closest Boundary (km)	Direction from the Cell to the Boundary	In front/behind/to the side (tts)?	Boundary Type	Boundary Classification	Latitude	Longitude
June	2	82	2100	88	240	Ahead	Gust Front	Moving	43.1686	-82.1775
		90	2100	91	238	Ahead	Gust Front	Moving	43.2038	-82.1671
		100	2200	100	188	To the side	Gust Front	Moving	43.2905	-81.9928
		106	2200	38	79	Behind	Gust Front	Moving	43.4853	-82.312
		109	2200	58	237	Ahead	Gust Front	Moving	42.6901	-81.5635
		110	2200	34	346	To the side	Gust Front	Moving	43.0168	-81.5991
		111	2200	47	4	To the side	Gust Front	Moving	42.8978	-81.7417
		118	2300	95	215	Ahead	Gust Front	Moving	43.2116	-81.2966
		130	2300	58	111	To the side	Gust Front	Moving	43.6341	-81.7908
		137	2300	17	142	To the side	Gust Front	Moving	43.5646	-81.2536
		140	2300	104	201	Ahead	Gust Front	Moving	43.3778	-81.5077
		142	2300	46	107	To the side	Gust Front	Moving	43.5603	-81.6661
		110	2310	30	135	To the side	Gust Front	Moving	43.6309	-81.384
		143	2310	114	205	Ahead	Gust Front	Moving	43.442	-81.3777
		145	2310	25	110	To the side	Gust Front	Moving	43.5211	-81.4174
		147	0	91	94	Ahead	L Ont lbf	Moving	43.4018	-80.9654

		148	0	96	101	Ahead	L Ont lbf	Moving	43.4941	-80.999
		164	0	80	105	Ahead	L Ont lbf	Moving	43.5331	-80.7932
		163	10	90	100	Ahead	L Ont lbf	Moving	43.481	-80.9381
		166	10	97	106	Ahead	L Ont lbf	Moving	43.5863	-80.9877
		167	10	85	94	Ahead	L Ont lbf	Moving	43.401	-80.8904
	3	None								
	4	None								
	7	None								
	8	None								
	13	None								
	14	None								
	15	None								
	16	None								
	17	None								
	19	1234	2100	9	154	Behind	Other	Synoptic	43.7146	-81.2018
		1240	2110	27	155	Behind	Other	Synoptic	43.7683	-81.5423
		1238	2110	6	166	Behind	Other	Synoptic	43.8283	-80.7004
		1245	2210	5	335	Not tts	Merged (Huron/Erie)	Collision	43.2447	-80.4352
		1246	2210	9	156	Behind	Huron lbf	Moving	43.1279	-81.2506
		1252	2300	4	330	Not tts	Merged (Huron/Erie)	Collision	43.0345	-80.8193
		1252	2310	3	328	Not tts	Merged (Huron/Erie)	Collision	42.9779	-80.9512
		1254	2310	2	141	Not tts	Merged (Huron/Erie)	Collision	42.9723	-81.0708
	22	None								
	23	406	1800	4	267	Ahead	Huron lbf	Moving	43.4912	-81.4928
		405	1810	6	266	Ahead	Huron lbf	Moving	43.6325	-81.4742
		406	1810	8	268	Ahead	Huron lbf	Moving	43.48	-81.4396
		406	1900	14	256	Not tts	Hybrid (Huron/GF)	Collision	43.404	-81.269
		413	1900	5	181	To the side	Huron lbf (at Joint with Hybrid which is not considered)	Moving	43.2895	-81.3973
		415	1900	3	269	Not tts	Hybrid (Huron/GF)	Collision	43.4961	-81.4514
		408	1910	6	279	Ahead of Huron lbf – Not tts for Hybrid	Joint - Huron lbf and Hybrid joint (Huron lbf/gust front)	Collision	43.242	-81.3265
		416	2000	4	225	Not tts	Hybrid (Huron/GF)	Intersection	43.1691	-81.3153

		423	2010	16	277	Ahead of Huron lbf - To the side for Hybrid	Joint - Huron lbf and Hybrid joint (Huron lbf/gust front)	Intersection	43.1045	-81.1298
		425	2110	7	12	Behind	Gust Front	Moving	43.5262	-81.2603
		428	2200	3	0	Behind	Gust Front	Moving	43.5237	-81.212
		429	2200	2	255	Not tts	Hybrid (Huron/GF)	Collision	43.4254	-81.3021
		430	2200	5	346	Behind	Gust Front	Moving	43.5198	-81.0894
		431	2210	4	273	Not tts	Hybrid (Huron/GF)	Collision	43.386	-81.2751
		432	2210	10	20	Not tts	Hybrid (Erie/GF)	Intersection	42.6648	-81.2666
		438	2300	3	267	Not tts	Hybrid (Huron/GF)	Collision	43.4854	-81.2647
		439	2300	9	314	Behind	Gust Front	Moving	43.5054	-81.1845
		428	2310	6	314	Behind	Gust Front	Moving	43.5171	-81.2196
		441	2310	13	274	Not tts	Hybrid	Collision	43.2708	-81.1488
		444	0	15	329	Behind	Gust Front	Moving	43.5227	-81.1738
	24	None								
	25	None								
	26	None								
	27	None								
	28	679	2010	9	344	Not tts	Hybrid (Erie/GF)	Merger	42.8254	-81.2935
		680	2100	3	356	Not tts	Hybrid (Erie/GF)	Merger	42.9782	-81.1674
		682	2110	9	345	Not tts	Hybrid (Erie/GF)	Merger	42.8754	-81.3603
		686	2210	13	350	Not tts	Hybrid (Hybrid(Erie/GF)/Huron) - more than one interaction	Collision	42.8934	-81.3952
	29	723	2300	1	138	Ahead	Erie lbf	Moving	43.2084	-81.3879
	30	769	1710	8	154	Ahead	Erie lbf	Moving	42.9654	-81.0385
		770	1710	4	316	Behind	Erie lbf	Moving	42.7406	-81.2336
		776	1810	1	200	Ahead	Erie lbf	Moving	42.9213	-80.8702
		778	1810	3	345	Ahead	Huron lbf	Stationary	43.2117	-81.3423
		787	1900	9	349	Ahead	Huron lbf	Stationary	43.1698	-81.273
		789	1900	4	336	Ahead	Huron lbf	Stationary	43.1107	-81.7272
		805	2000	14	271	To the side	Huron lbf	Stationary	43.0866	-81.5995
		789	2010	4	149	Ahead	Erie lbf	Moving	43.0935	-81.1095
		809	2010	4	153	Ahead	Erie lbf	Moving	43.1422	-80.9861
		826	2100	29	261	To the side	Erie lbf	Moving	43.0708	-80.68
		830	2100	13	317	Not tts	Hybrid (Huron/GF)	Collision	43.323	-80.5199
		820	2110	24	259	To the side	Erie lbf	Moving	43.0809	-80.7291
		835	2110	13	263	To the side	Erie lbf	Moving	43.0511	-80.8652
		859	2200	12	299	To the side	Erie lbf	Moving	43.076	-80.6335
		860	2200	86	164	Behind	Huron lbf	Moving	43.9443	-81.827

		866	2210	6	144	Behind	Gust Front	Moving	43.7998	-82.1509
		868	2210	0	335	Slightly Ahead	Gust Front	Moving	43.999	-81.6021
		881	2300	19	170	Behind	Gust Front	Moving	43.5537	-82.0178
		887	2300	10	134	Behind	Gust Front	Moving	43.7561	-81.2606
		890	2300	28	157	Behind	Gust Front	Moving	43.9842	-81.1869
		899	2300	8	356	Ahead	Huron lbf	Moving	43.0996	-81.1875
		874	2310	14	176	Behind	Gust Front	Moving	43.929	-80.8394
		904	0	50	151	Behind	Gust Front	Moving	43.6248	-81.4346
		911	0	1	336	Behind	Erie lbf	Moving	42.9387	-81.2593
		923	0	60	153	Behind	Huron lbf	Moving	43.6905	-81.0623
		926	0	54	161	Behind	Gust Front	Moving	43.5872	-81.6267
		928	0	61	161	Behind	Gust Front	Moving	43.6464	-81.6414
		929	10	48	145	Behind	Gust Front	Moving	43.6124	-81.4138
July	1	1170	1600	N/A	N/A	N/A	N/A	N/A	43.1934	-80.8425
		1187	1610	N/A	N/A	N/A	N/A	N/A	42.8816	-81.6669
	2	None								
	5	No radar from 1600 to 1910								
		None								
	6	None								
	8	None								
	9	Radar data are missing for 1900 on								
		None								
	10	5	2110	13	150	Ahead	Erie lbf	Moving	42.7471	-81.6274
		23	0	7	12	Not tts	Hybrid (Erie/GFs)	Merger	42.927	-81.2778
		24	0	11	133	Not tts	Hybrid (Erie/GFs)	Merger	42.9327	-81.7011
		23	10	23	312	Not tts	Hybrid (Erie/GFs)	Merger	42.7679	-81.3414
	11	None								
	12	None								
	13	None								
	14	None								
	18	5	2000	12	115	To the side	Erie lbf	Moving	42.813	-81.3572
		7	2010	9	169	Ahead	Erie lbf	Moving	42.8489	-81.2456
		10	2300	7	278	To the side	Hybrid (Erie/GF)	Moving	43.1363	-81.3788
		13	0	4	239	Behind	Gust Front	Moving	43.1504	-81.6198
		14	10	8	194	To the side (GF Furthest and Closest)	Joint - two Gust Fronts	Intersection	43.2083	-81.6488
	22	479	2110	2	274	Not tts	Hybrid (Erie/GF)	Merged	43.3666	-80.4309
	23	3	1600	38	207	To the side	Erie lbf	Moving	43.4232	-80.4953
		7	1700	5	310	Behind	Erie lbf	Moving	42.9567	-81.0837
		13	1700	1	156	Ahead	Erie lbf	Moving	42.8235	-81.4492

		14	1700	1	87	Behind (in terms of movement)	Other	Moving	42.986	-81.5147
		7	1710	10	226	To the side	Erie lbf	Moving	43.0505	-81.0428
		13	1710	9	335	Behind	Erie lbf	Moving	42.7402	-81.3989
		17	1710	1	227	Ahead (in terms of movement)	Other	Moving	43.2245	-81.5289
		7	1800	10	228	Ahead	Gust Front	Moving	43.3111	-81.3276
		9	1800	30	312	Ahead	Gust Front	Moving	43.1313	-80.7188
		17	1800	5	14	Behind	Gust Front	Moving	43.424	-81.2853
		18	1800	11	1	Behind	Gust Front	Moving	43.3792	-81.3365
		19	1800	3	311	Ahead	Gust Front	Moving	43.3233	-80.9312
		20	1800	7	76	To the side	Gust Front	Moving	43.2853	-81.0978
		21	1800	9	27	To the side	Gust Front	Moving	43.2264	-81.0695
		15	1810	8	7	Behind	Gust Front	Moving	43.3817	-81.2369
		19	1810	3	315	Ahead	Gust Front	Moving	43.2959	-80.9764
		20	1810	14	178	Ahead	Erie lbf	Moving	43.1929	-81.1946
		21	1810	15	226	To the side	Erie lbf	Moving	43.1603	-81.03
		26	1810	31	299	Ahead	Gust Front	Moving	43.2543	-80.5837
		28	1810	5	271	To the side	Erie lbf	Moving	43.0677	-81.0944
		29	1810	2	357	Behind	Erie lbf	Moving	43.053	-81.2084
		19	1900	6	215	Behind	Gust Front	Moving	43.185	-81.2311
		20	1900	23	264	To the side	Gust Front	Moving	43.1632	-80.9944
		45	1900	4	3	To the side	Gust Front	Moving	43.5569	-80.5812
		20	1910	48	9	To the side	Gust Front	Moving	43.1593	-80.6748
		48	1910	2	242	Ahead	Gust Front	Moving	43.6334	-80.5958
		67	2010	3	303	Not tts	Hybrid (Erie/GF)	Merger	42.8471	-81.7949
		68	2010	1	296	Behind	Gust Front	Moving	43.3182	-81.4329
		69	2010	22	57	To the side	Huron lbf	Stationary	43.0935	-82.1881
		84	2100	11	75	Behind	Gust Front	Moving	43.3216	-81.6734
		72	2110	2	273	To the side	Gust Front	Moving	42.9638	-81.4917
		84	2110	2	270	Ahead	Gust Front	Moving	43.4092	-81.5234
		85	2110	10	313	Not tts	Hybrid(Huron/GFs)	Collision	43.5507	-81.3083
		86	2110	1	39	Behind	Gust Front	Moving	43.1104	-81.4213
		87	2110	9	271	To the side	Gust Front	Moving	43.2482	-81.3423
		83	2200	20	36	Behind	Gust Front	Moving	43.3308	-81.1046
		96	2200	4	336	Not tts	Hybrid(Huron/GFs)	Collision	43.8733	-80.9968
		95	2210	20	22	Behind	Gust Front	Moving	43.3152	-81.0584
		97	2210	0	179	Slightly Ahead	Gust Front	Moving	43.5263	-81.1446
		98	2210	27	28	Behind	Gust Front	Moving	43.2687	-81.122
	24	None								
	26	None								

	27	None								
	29	347	2010	1	104	Behind	Huron lbf	Moving	44.0236	-81.561
	30	None								
	31	None								
August	3	None								
	4	None								
	5	None								
	6	None								
	7	None								
	9	353	1910	2	357	Ahead	Huron lbf	Moving	43.2278	-81.6841
		361	2000	3	333	Ahead (Huron) Not tts(Hybrid)	Joint (Huron lbf and Hybrid(Huron/GF))	Intersection	43.2971	-81.3372
		366	2010	18	312	Behind	Erie lbf	Moving	42.7059	-81.2248
		357	2010	8	62	To the side	Erie lbf	Moving	42.6801	-81.6182
	10	None								
	11	None								
	13	No radar available for the whole period								
	14	No radar or satellite available for the whole period								
	15	None								
	17	None								
	19	750	1600	N/A	N/A	N/A	N/A	N/A	42.9875	-81.5647
		761	1600	N/A	N/A	N/A	N/A	N/A	43.017	-80.6991
		763	1600	N/A	N/A	N/A	N/A	N/A	43.0809	-81.4759
		764	1600	N/A	N/A	N/A	N/A	N/A	43.1256	-81.6366
		767	1610	N/A	N/A	N/A	N/A	N/A	42.9652	-81.5018
		768	1610	N/A	N/A	N/A	N/A	N/A	43.3025	-81.4446
		786	1700	60	212	To the side	Gust Front	Moving	43.4062	-81.3799
		791	1700	57	202	To the side	Gust Front	Moving	43.4268	-81.496
		792	1700	58	208	To the side	Gust Front	Moving	43.4118	-81.4316
		793	1710	77	240	Ahead	Gust Front	Moving	43.2947	-80.9383
		794	1710	44	221	To the side	Gust Front	Moving	43.2462	-81.4137
		795	1710	44	211	To the side	Gust Front	Moving	43.2904	-81.4833
		798	1800	19	61	To the side	Gust Front	Moving	43.0924	-81.821
		816	1800	46	90	Behind	Gust Front	Moving	43.1782	-82.1825
		799	1810	11	179	To the side	Gust Front	Moving	43.3989	-81.5914
		819	1810	24	256	Ahead	Gust Front	Moving	43.5119	-80.9421
		820	1810	47	85	Behind	Gust Front	Moving	43.1414	-82.1906
		835	1900	8	141	To the side	Gust Front	Moving	43.8062	-81.4793
		850	1900	55	39	Ahead	Gust Front	Moving	42.9959	-81.951
		853	1900	4	229	Behind	Gust Front	Moving	43.401	-81.4873
		854	1900	7	100	Behind	Gust Front	Moving	43.457	-81.4915

		799	1910	16	30	Ahead	Gust Front	Moving	43.2324	-81.5794
		853	1910	7	18	Ahead	Gust Front	Moving	43.2948	-81.507
		849	2000	51	54	Ahead	Gust Front	Moving	43.0872	-82.0009
		878	2000	6	170	To the side	Gust Front	Moving	43.2613	-82.0227
		861	2010	69	35	Ahead	Gust Front	Moving	42.8517	-81.9764
		866	2010	56	37	Ahead	Gust Front	Moving	42.9476	-81.9023
		881	2010	11	114	Behind	Gust Front	Moving	43.5407	-81.3675
		882	2010	24	206	To the side	Gust Front	Moving	43.4008	-81.8782
		884	2010	10	190	To the side	Gust Front	Moving	43.4803	-81.4688
		886	2010	15	123	Ahead	Gust Front	Moving	43.747	-81.5042
		878	2100	13	118	Ahead	Gust Front	Moving	43.5662	-81.9419
		898	2100	1	123	Behind	Gust Front	Moving	43.6254	-81.1091
		900	2100	1	292	Ahead	Gust Front	Moving	42.7758	-81.7963
		898	2110	9	133	Behind	Gust Front	Moving	43.6006	-81.2423
		899	2200	18	297	Ahead	Gust Front	Moving	42.704	-81.3845
		909	2200	41	16	Ahead	Gust Front	Moving	43.0803	-81.6326
		927	2200	2	122	Behind	Gust Front	Moving	42.9442	-81.5398
		931	2200	24	71	Behind	Gust Front	Moving	43.7429	-81.1653
		933	2200	4	78	Behind	Gust Front	Moving	43.5451	-81.4441
		921	2210	5	116	Behind	Gust Front	Moving	43.1321	-81.5578
		929	2210	18	143	To the side	Gust Front	Moving	43.687	-81.5269
		941	2210	2	19	Ahead	Gust Front	Moving	43.4241	-81.5128
		944	2210	15	112	Behind	Gust Front	Moving	43.716	-81.0483
		949	2210	15	140	To the side	Gust Front	Moving	43.6405	-81.8001
		969	2300	6	358	Ahead	Gust Front	Moving	43.4216	-81.283
		970	2300	6	17	Ahead	Gust Front	Moving	43.4169	-81.3265
		975	2300	25	163	To the side	Gust Front	Moving	43.8933	-81.2568
		976	2300	8	69	Behind	Gust Front	Moving	43.6202	-81.2441
		978	2300	1	238	Ahead	Gust Front	Moving	43.8723	-80.7986
		979	2300	5	120	Behind	Gust Front	Moving	43.7436	-80.9948
		980	2300	0	359	Slightly Ahead	Gust Front	Moving	43.4724	-81.2621
		982	2300	1	179	Ahead	Gust Front	Moving	43.3544	-81.2126
		944	2310	10	117	Behind	Gust Front	Moving	43.7557	-81.0629
		959	2310	4	88	Behind	Gust Front	Moving	43.2116	-81.0847
		967	2310	40	159	To the side	Gust Front	Moving	44.008	-81.3376
		981	2310	4	102	Behind	Gust Front	Moving	43.8372	-80.8771
		986	2310	21	39	To the side	Gust Front	Moving	43.1401	-81.4402
		992	2310	18	103	Behind	Gust Front	Moving	43.7124	-81.3845
		983	0	3	68	Behind	Gust Front	Moving	43.4541	-80.8769
		1009	0	20	141	To the side	Gust Front	Moving	43.721	-81.1579
		1013	0	3	290	Ahead	Gust Front	Moving	43.5936	-80.8461

		1014	0	7	267	Ahead	Gust Front	Moving	43.5664	-80.7983
		1015	0	2	263	Ahead	Gust Front	Moving	43.5041	-80.8443
		1017	0	101	76	To the side	Gust Front	Moving	43.3673	-82.226
		1013	10	1	132	Behind	Gust Front	Moving	43.6814	-80.8693
	20	1160	1610	34	307	Ahead (only in movement)	Other	Moving	43.1581	-80.5044
		1174	1700	15	15	To the side	Gust Front	Moving	42.9861	-81.5957
		1175	1700	54	95	Ahead	Gust Front	Moving	43.6267	-82.2715
		1162	1710	0	18	Slightly ahead	Gust Front	Moving	43.5124	-81.5373
		1174	1710	21	12	To the side	Gust Front	Moving	42.939	-81.5983
		1176	1710	35	232	To the side	Other	Moving	43.6634	-80.505
		1177	1710	1	134	Behind (only in movement)	Other	Moving	43.3264	-81.005
		1178	1710	22	142	Ahead	Erie lbf	Moving	42.8165	-81.4766
		1179	1710	10	3	To the side	Gust Front	Moving	43.0316	-81.553
		1180	1710	0	154	Behind	Gust Front	Moving	43.1483	-81.5195
		1182	1710	4	136	Ahead	Gust Front	Moving	43.3282	-81.5864
		1183	1710	3	115	Ahead	Gust Front	Moving	43.3901	-81.5429
		1206	1800	1	88	Behind	Gust Front	Moving	43.5259	-81.1772
		1208	1800	1	87	Behind	Gust Front	Moving	43.3145	-81.1623
		1190	1810	0	337	Slightly ahead (only in movement)	Other	Moving	43.2586	-80.9666
		1191	1810	0	321	Ahead	Gust Front	Moving	43.1102	-81.1867
		1199	1810	1	16	Ahead (only in movement)	Other	Moving	43.608	-80.9477
		1211	1810	9	286	Behind	Gust Front	Moving	43.1994	-81.392
		1212	1810	4	60	Ahead	Gust Front	Moving	43.0929	-81.5297
		1213	1810	0	80	Slightly ahead	Gust Front	Moving	43.4208	-81.516
		1224	1900	3	124	Behind (only in movement)	Other	Moving	43.5331	-80.9415
		1228	1900	5	358	Behind	Erie lbf	Moving	42.7628	-80.9817
		1232	1900	2	84	Behind (only in movement)	Other	Moving	43.3699	-81.0374
		1234	1910	1	116	Behind (only in movement)	Other	Moving	43.4076	-81.0159
		1235	1910	22	197	Ahead	Gust Front	Moving	43.2034	-80.8237
		1236	1910	1	40	Behind	Gust Front	Moving	42.994	-80.8884
		1238	2000	4	247	Behind	Gust Front	Moving	43.1815	-81.3937
		1243	2000	69	232	Behind	Gust Front	Moving	43.7875	-80.7834
		1246	2000	1	167	Behind	Gust Front	Moving	43.2904	-81.4409
		1243	2010	66	237	Behind	Gust Front	Moving	43.7256	-80.7743
		1252	2010	1	179	Ahead	Erie lbf	Moving	42.86	-80.7595

		1243	2100	27	224	To the side	Other	Moving	43.7639	-80.8564
		1267	2100	11	268	Ahead (only in movement)	Other	Moving	43.4961	-80.9732
		1270	2100	16	333	To the side	Other	Moving	43.2352	-81.0207
		1243	2110	31	227	To the side	Other	Moving	43.7824	-80.8116
		1270	2110	6	34	To the side	Other	Moving	43.2831	-81.1402
		1271	2110	1	87	Behind (only in movement)	Other	Moving	43.4379	-81.1276
		1273	2210	N/A	N/A	N/A	N/A	N/A	43.778	-80.7538
		1274	2210	14	3	Ahead	Gust Front	Moving	43.5449	-80.9081
		1287	2210	6	255	Behind	Gust Front	Moving	43.9122	-81.0805
		1288	2210	19	242	Behind	Gust Front	Moving	43.8727	-80.8382
		1284	2300	N/A	N/A	N/A	N/A	N/A	43.193	-80.7232
		1294	2300	2	250	Behind	Gust Front	Moving	43.7098	-81.0786
		1295	2300	N/A	N/A	N/A	N/A	N/A	43.4255	-80.6321
		1297	2310	N/A	N/A	N/A	N/A	N/A	43.796	-80.9057
		1300	10	15	303	To the side	Gust Front	Moving	43.3946	-80.8779
	21	None								
	23	8	2010	4	207	Ahead	Huron lbf	Moving	43.5754	-81.2922
		17	2100	2	194	Ahead	Huron lbf	Moving	43.4063	-81.1671
	24	None								
	26	140	1600	18	145	Ahead	Erie lbf	Moving	42.9654	-81.4031
		140	1610	11	145	Ahead	Erie lbf	Moving	42.8753	-81.4079
		147	1700	66	326	Ahead	Other	Synoptic	42.9953	-80.9228
		155	1810	1	155	Behind	Other	Synoptic	43.0924	-81.821
		175	2000	5	139	Behind	Other	Synoptic	42.6941	-81.6826
	28	None								
	29	None								
	31	273	1800	1	134	Behind	Other	Synoptic	43.9292	-80.819
		275	1800	95	335	Ahead	Other	Synoptic	43.0444	-80.5175

References

Alexander, L., D. Sills, and P. Taylor, 2003: ELBOW 2001: Final Data Report. York University, 74 pp, available from the authors.

Atlas, D., 1960: Radar Detection of the Sea Breeze. *J. Appl. Meteorol.*, **17**, 244 – 258.

Biggs, W.G., and M.E. Graves, 1962: A Lake Breeze Index. *J. Appl. Meteorol.*, **1**, 474 – 480.

Byers, H.R., and R.R. Braham, 1948: Thunderstorm Structure and Circulation. *J. Meteorol.*, **5**, 71 – 86.

Byers, H.R., and H.R. Rodebush, 1948: Causes of Thunderstorms of the Florida Peninsula. *J. Meteorol.,* **5**, 275 – 280.

Comer, N.T., and I.G. McKendry, 1993: Observations and Numerical Modelling of Lake Ontario Breezes. *Atmos.-Ocean*, **31**, 481 – 499.

Cotton, W.R., 1990: Storms: First Edition. *ASTeR Press, Fort Collins, CO, 158 pp.

Curry, M., 2012: Lake Effects in Southern Manitoba. Honours Thesis, Department of Environment and Geography, University of Manitoba, Winnipeg, Manitoba, 65 pp.

Dixon, M., and G. Wiener, 1993: TITAN: Thunderstorm Identification, Tracking, Analysis, and Nowcasting – A Radar-based Methodology. *J. Atmos. Oceanic Technol.*, **10**, 785-797.

Environmental Research Services, 2002: RAOB The Complete RAwinsonde Observation Program: User Guide & Technical Manual, 53 pp.

Estoque, M.A., J. Gross and H.W. Lai, 1976: A Lake Breeze over Southern Lake Ontario. *Mon. Wea. Rev.*, **104**, 386 – 396.

Firanski, B., 2002: Radar Observations of Lake Breeze Induced Summer Convective Storms. Master of Science Thesis, CRESS, York University, Toronto, Ontario, 228 pp.

Galway, J.G., 1956: The Lifted Index as a Predictor of Latent Instability. *Bull. Amer. Meteorol. Soc.*, **37**, 528 – 529.

Greaves, B., R. Trafford, N. Driedger, R. Paterson, D. Sills, D. Hudak, and N. Donaldson, 2001: The AURORA Nowcasting Platform – Extending the Concept of a Modifiable Database for Short Range Forecasting. Preprints, *17th International Conference on Interactive Information and Processing Systems <IIPS> for Meteorology, Oceanography, and Hydrology*, Albuquerque, NM, Amer. Meteorol. Soc., 236-239.

King, P.W.S, M.J. Leduc, D.M.L. Sills, N.R. Donaldson, D.R. Hudak, P. Joe and B.P. Murphy, 2003: Lake Breezes in Southern Ontario and Their Relation to Tornado Climatology. *Wea. Forecast.*, **18**, 795 – 807.

Mueller, C., T. Saxen, R. Roberts, J. Wilson, T. Betancourt, S. Dettling, N. Oien and J. Yee, 2003: NCAR Auto-Nowcast System. *Wea. Forecast.*, **18**, 545 – 561.

Lyons, W.A., 1972: The Climatology and Prediction of the Chicago Lake Breeze. *J. Appl. Meteorol.*, **11**, 1259 – 1270.

Paterson, R., B. de Lorenzis, N. Driedger, E. Goldberg, B. Greaves, and R. Trafford, 1993: The Forecast Production Assistant. Preprints*, Ninth International Conference on Interactive Information and Processing Systems for Meteorology, Oceanography and Hydrology*, Anaheim, CA, Amer. Meteorol. Soc., 129-133.

Pearce, R.P., 1955: The calculation of a sea-breeze circulation in terms of the the differential heating across the coastline. *Q. J. R. Meteorol. Soc.,* **81**, 351 – 381.

Pearce, R.P., 1956: Discussions: The calculation of a sea-breeze circulation in terms of the differential heating across the coast line. *Q. J. R. Meteorol. Soc.,* **82**, 235 – 241.

Purdom, J.F.W., 1976: Some Uses of High-Resolution GOES Imagery in the Mesoscale Forecasting of Convection and Its Behavior. *Mon. Wea. Rev.,* **104**, 1474 – 1483.

Rotunno, R., J.B. Klemp, and M.L. Weisman, 1988: A Theory for Strong, Long-Lived Squall Lines. *J. Atmos. Sci.*, **45**, 463 – 485.

Ryznar, E., and J.S. Touma, 1981: Characteristics of True Lake Breezes Along the Eastern Shore of Lake Michigan. *Atmos. Env.*, **15**, 1201 – 1205.

Sills, D. M. L., 1998: Lake and Land Breezes in Southwestern Ontario: Observations, Analyses and Numerical Modelling. PhD dissertation, CRESS, York University, Toronto, Ontario, 338 pp.

Sills, D.M.L., J.R. Brook, I. Levy, P.A. Makar, J. Zhang, and P.A. Taylor, 2011: Lake breezes in the southern Great Lakes region and their influence during BAQS-Met 2007. *Atmos. Chem. Phys.,* **11**, 7955-7973.

Sills, D. M. L., and N.M. Taylor, 2008: The Research Support Desk (RSD) Initiative at Environment Canada: Linking Severe Weather Researchers and Forecasters in a Real-Time Operational Setting. Preprints, *24th AMS Conference on Severe Local Storms,* Savannah, GA, Amer. Meteorol. Soc., Paper 9A.1.

Simpson, J. E., 1994: Sea Breeze and Local Wind. Cambridge University Press, Cambridge, 234 pp.

University of Wyoming, College of Engineering, Department of Atmospheric Science. Upper Air Data, http://weather.uwyo.edu/upperair/sounding.html, accessed January 23, 2008.

Vaisala, 1996: DIGICORA II MW15 FOR AES: User's Guide, 50 pp.

Weisman, M.L; and J.B. Klemp, 1986: Characteristics of Isolated Convective Storms. Chapter 15. *Meso. Meteorol. Forecast.*, P.S. Ray, Ed., Amer. Meteorol. Soc., 793 pp.

Wexler, R., 1946: Theory and Observations of Land and Sea Breezes. *Bull. Amer. Meteorol. Soc.,* **27**, p. 272 – 287.

Wilks, D. S., 1995: Statistical Methods in the Atmospheric Sciences. Academic Press, San Diego, California, 467 pp.

Wilson, J. W., N. A. Crook, C. K. Mueller, J. Sun, and M. Dixon, 1998: Nowcasting Thunderstorms: A Status Report. *Bull. Amer. Meteorol. Soc.,* **79**, 2079-2099.

Wilson, J. W., and D. L. Megenhardt, 1997: Thunderstorm Initiation, Organization, and Lifetime Associated with Florida Boundary Layer Convergence Lines. *Mon. Wea. Rev.,* **125**, p. 1507-1525.

Wilson, J., R. Roberts, C. Mueller and T. Saxen, 2000: NCAR Auto-nowcaster (powerpoint presentation). *Prepared for the WMO Nowcasting Workshop in conjunction with the World Weather Research Program Sydney 2000 Field Demonstration Program (Oct. 30 to Nov. 10).* National Center for Atmospheric Research, Boulder, Colorado, USA

Wilson, J. W.; and W.E. Schreiber, 1986: Initiation of Convective Storms at Radar–Observed Boundary-Layer Convergence Lines. *Mon. Wea. Rev.,* **114**, 2516-2536.